NUMERICAL MODELLING OF MULTIPLE STANDING COLUMN WELLS APPLIED TO GEOTHERMAL HEATING AND COOLING IN UK BUILDINGS

BOBO MINGSUM NG

A thesis submitted in partial fulfilment
of the requirements of the
University of Northumbria at Newcastle
for the degree of
Doctor of Philosophy

Research undertaken in the
School of Built and Natural Environment
October 2011

Abstract

Standing column wells (SCWs) have the potential to deliver much higher rates of heat transfer to geothermal heating and cooling systems in buildings via heat pumps than conventional vertical borehole heat exchange arrays. Its open-end column design with porous casing along the borehole (depending on the formation) encourages the flow of groundwater from the rock's porous matrix into the well or the opposite way according to the hydraulic gradients. This approach induces a further heat transfer mechanism in addition to the conduction: it is advection. Advection induced by the groundwater movement due to the hydraulic gradient and the action of the well pump causes warmer water (in winter) and cooler (in summer) to be drawn into the well thus increasing heat transfer capacity. This is beneficial for SCWs to offer much higher heat transfer performance than other conventional approaches.

The development of a numerical model for clusters of standing column wells is described in this thesis. The model is three-dimensional, dynamic and solves the governing equations using a finite volume discretisation scheme with a fully implicit algorithm. The slower acting field equations are solved using a wider time interval than that used for the faster acting well equations and the two sets of equations are coupled through the field equation source terms. A groundwater bleed feature is incorporated. The model has been validated thermally and hydraulically using existing field data. Two test cases have been applied to reveal the advantages of using SCWs in UK conditions, competing with the conventional closed-loop system of vertical borehole heat exchangers. The results of the applications suggest that SCWs can deliver substantially higher rates of heat transfer than conventional closed-loop borehole heat exchanger arrays, typically up to 250Wm^{-1}, especially when groundwater bleed is operational. The results also confirm that a bleeding operation can offer up to 2.2K improvement (reduction) in the outlet well water temperature in summer and (increase) in the well water temperature in winter. Investigation results on borehole diameter confirm that

a larger well borehole diameter would offer improved heat transfer performance in some cases, according to the relative change of the heat transfer coefficient. Analysis of borehole to borehole spacing seems to suggest that 5m is the most effective spacing of the three different spacing choices for this type of application. The results also show that SCW installation in London Clay performs less well than Magnesian Limestone and Old Red Sandstone; the latter two seem to be appropriate formation types to work with this type of application. The advantage of adopting multiple well arrangements (SCW clusters) over the use of single wells has also been confirmed. The important practical consequence of this is that far less geotechnical drilling is needed as the required borehole depth reduces substantially under multiple well arrangements. The results gathered from three different buildings also reveal that the balance between heating and cooling demands appears to have less impact on the mean formation temperature change than the large cooling application, which is beneficial to maintain a steady system performance over a long period of time. The results also suggest that the impact on the rock formation was very dominant in the first few years but it declined towards the end of the 5 year analysis period used in this work. The results from the CO_2 emission analysis demonstrate that an annual carbon emission reduction of up to 46% can be achieved by using the geothermal system with SCWs instead of the conventional system consisting of a gas-fired condensing boiler and a conventional air-cooled chiller. They also confirm that the balance between heating and cooling demands has a substantial impact on the carbon saving delivered by this technology.

Contents

Figures

Tables

Acknowledgements

I owe my deepest gratitude to my principal supervisor Prof. Chris Underwood. He has been very patient and supportive throughout the last four years. His enthusiasm and immense knowledge on the geothermal area enabled me to develop many useful skills to carry out my research, such as program writing, problem solving and discretisation techniques. He also inspired and motivated throughout the research and writing of this thesis; this work could not have been done without his support. In addition, I would like to thank my second supervisor Dr. Sara Walker as well. She has been very supportive and has given me a lot of insightful comments on my research.

I would like to extend my appreciation to Prof. Brian Agnew. He offered a lot of useful advice when I came across problems in the CFD modelling work and interpreting the model results.

I am indebted to Professor Jeff Spitler at Oklahoma State University for providing valuable data on the standing column well installations at Haverhill Library, in Massachusetts.

I am indebted to my many colleagues in the SBES subject group and to SCRI for giving me help and support all the time.

I would also like to thank Mr. John Woody from Alistair Harvey Foundation Scholarship for offering me financial support to finish my first degree in the UK, and Mr William W.K. Lai (from IVE HK) for encouraging me to continue my studies.

I wish to thank my mum, dad and brother for all their love and emotional support all these years.

Lastly, and most importantly, I wish to thank my boyfriend Lars Mai. Thanks for taking care of me and helping me to get through the difficult times over the past few years.

Author’s declaration

I declare that the work contained in this thesis has not been submitted for any other award and that it is all my own work. I also confirm that this work fully acknowledges opinions, ideas and contributions from the work of others.

Any ethical clearance for the research presented in this thesis has been approved. Approval has been sought and granted by the School Ethics Committee / University Ethics Committee / external committee.

Name:

Bobo M Ng

Signature:

Date:

1. Introduction

1.1 Background and rationale for this research

Geothermal energy is a reliable and stable source for providing space heating and cooling with relatively low electricity consumption and high energy efficiency, in comparison to conventional heating and cooling systems.

The performance of a geothermal system with heat pump is usually described by coefficient of performance (*CoP*), which is defined as amount of heat (or refrigerating effect) produced by the heat pump divided by the compressor absorbed power. A typical *CoP* of an air source heat pump (ASHP) system is about 2.5 and varies in accordance with the external air temperature, while the *CoP* of a vertical type geothermal heating and cooling system (GHCS) is not directly influenced by the weather; hence a more stable and higher figure can be achieved, in general about 3.5-4.0. In this work, only vertical ground heat exchanger will be examined. Figure 1.1 indicates the *CoP* of a typical commercial water source heat pump operating at conditions applicable to typical mean UK ground conditions (GSHP) and a typical commercial air source heat pump (ASHP) operating according to varying external air temperatures. (The maximum theoretically possible performance line on this graph illustrates the Carnot *CoP*.) The typical UK design point illustrated in this figure assumes an external air temperature for the heating system of -3^{o}C, whereas the equilibrium point represents the typical threshold in external air temperature above which heating is no longer required. It is clear from this illustration that a well-configured GSHP is capable of out-performing an ASHP across the entire heating season.

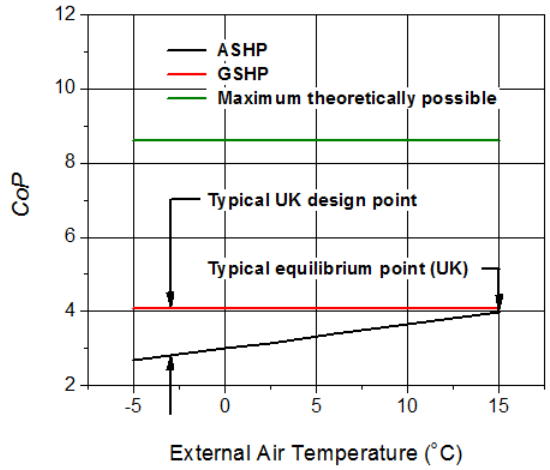

Figure 1.1 Comparison of commercial ground source and air source heat pump

In the UK, mild winters with typical mean annual air temperatures of 8 to 11°C coupled with many sites bearing reasonably high water tables create a good opportunity to exploit groundwater for use in geothermal systems for both heating and cooling buildings. Geothermal energy is expected to make a significant contribution to the European Union's target of 80% carbon reduction by 2050 (DTI, 2007).

The world capacity of geothermal energy utilisation reported by Lund (2010) was 48.49GW, an increase of 58% over the previous five years (Lund, Freeston & Boyd, 2005), with an annual growth rate of 11.4%. Geothermal system utilising ground source heat pumps is the largest application of geothermal energy, amounting to 68.3% of the current world total (Lund, 2010), with the remainder being taken up by direct (natural) geothermal 'hot rocks'. The UK is reported to be one of the fastest growing countries in the use of indirect geothermal energy, having increased its installed capacity from 10.2MW in 2005 to 186.2MW in 2010 (Lund, 2010). Thus, continuing rapid growth in this technology in the UK is expected to continue in the coming years.

1.2 Typical types of ground source heating and cooling systems

Though the abbreviation GSHP (ground source heat pump) has been used previously, from this point on reference will be made to geothermal heating and cooling systems (abbreviated: GHCS) to signify a wider range of possibilities for ground source heat pumps that covers the following:

- Ground source heating in winter (heat is extracted from the ground and elevated in grade by a heat pump for use in building heating systems)
- Ground sink cooling in summer (heat is absorbed from a building by means of the heat pump operating as a refrigerator and the heat rejected by the refrigerator is, in turn, transferred to the ground)
- Direct cooling – heat is rejected directly from the building into the ground (the refrigerator is switched off)

Geothermal heating and cooling systems can be categorised into two general types: closed-loop systems (Figure 1.2) and open-loop systems (Figure 1.3). There is a clear distinction between closed and open-loop systems when comparing water circulation through the system. A closed loop system operates independently of any ground water presence (though heat transfer can be enhanced due to advective heat transfer to the closed loop from the moving groundwater).

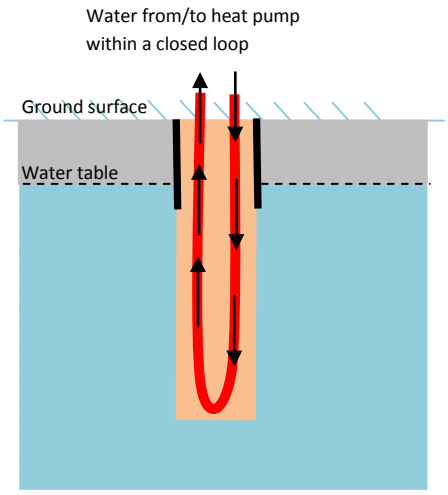

Figure 1.2 Closed-loop system (vertical)

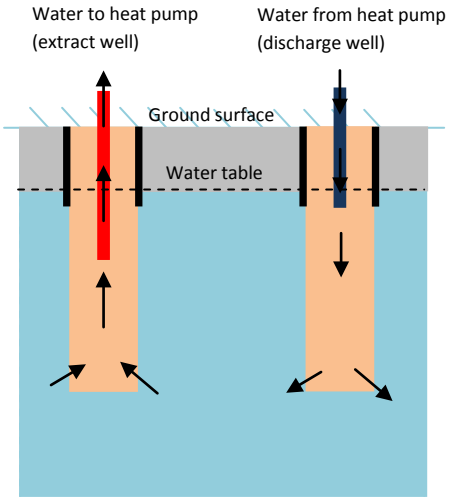

Figure 1.3 Open-loop system

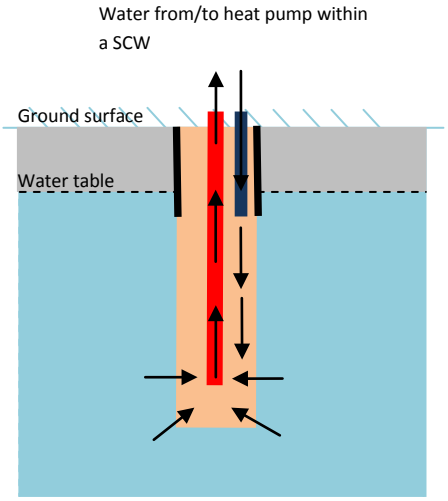

Figure 1.4 Standing column well

In the UK, the most common approach to harvesting geothermal energy for buildings is by means of closed-loop vertical borehole heat exchange arrays embedded at depths of typically 100m. This is a reliable but expensive method. An alternative is to directly pump groundwater from an abstraction well to the surface and exchange heat directly from it prior

to returning it by means of a reinjection well – the open-loop method. However, this method is only applicable in areas where groundwater yields are high and static water levels are close to the surface. A hybrid approach, the standing column well (SCW) (Figure 1.5), is a combination of the two.

In this approach, water is recirculated within a well and limited quantities of groundwater can conditionally be abstracted from the formation. The open-end column design with porous borehole walls encourages the flow of groundwater into and out of the SCW; the groundwater movement facilitates advective heat transfer to the SCW in conjunction with the conductive heat transfer that is usually found in conventional closed-loop systems. Thus, the SCW approach can possibly offer higher heat transfer rates than the closed-loop method and potentially requires less geotechnical drilling operations (resulting in a reduction in cost). The water recirculation design (from SCW) also overcomes the uncertainties inherent in the open-loop method and introduces the application of this technology to a wider context. However, fouling and corrosion is an issue for SCW according to the quality of the groundwater, as is the case with open-loop systems.

1.3 Construction of standing column wells (SCWs)

Typically, the SCW borehole is from a hundred to several hundred metres deep and penetrates into a saturated aquifer. The borehole wall is cased above the water table and uncased below (in the consolidated layer) to allow groundwater abstraction. Where the rock interface is unsound, the well below the casing may be screened with a perforated liner. Water is drawn from the bottom of the well using a submersible pump and returned at the top. The water may be drawn from the bottom of the well either by locating the submersible pump there or by locating it higher in the well and using a suction pipe connected to the suction port of the pump and running down to the bottom of the well. An even better approach is to place the submersible pump towards the top of a larger diameter suction pipe 'sleeve', which extends to the bottom of the well from which intake water is drawn. The suction pipe in this case offers very low frictional resistance to the flowing water. This work focuses on this latter combination. The basic structure of the SCW is shown in Figures 1.3 and 1.5.

The diameter of the borehole/well is usually small (about 0.1 to 0.2m) to enhance the turbulent flow and the mixing of the returning water and local groundwater in a narrow annulus (where a suction pipe sleeve is used) for better heat transfer.

The groundwater is recirculated from the well to the building through two open-end columns: the discharge pipe and the suction pipe. The discharge pipe returns the water to the well just below the water table level, while the suction pipe is extended through the entire depth of the well and intakes the water at the bottom of the suction pipe (often through perforations around the lower circumference of the suction pipe).

Bleeding part of the system water instead of fully returning to the well could initiate a significantly groundwater flows into the well from the surrounding rock. Bleed operation allows the well temperature to approach that of the far-field temperature to and thus increase heat transfer rates during peak load demands.

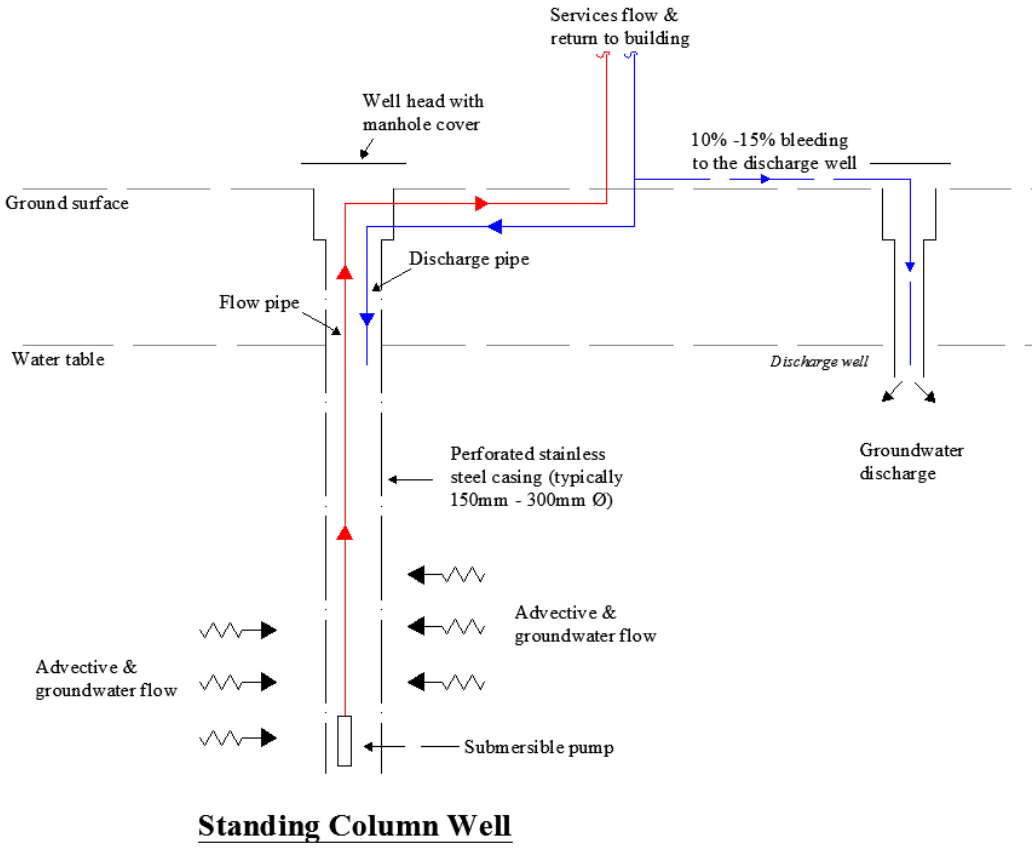

Figure 1.5 Construction of standing column well (SCW) systems

2. Literature review

2.1. History of using ground source

The history of using ground sources began with a steady underground temperature being scientifically confirmed by the famous French chemist and physicist Lavoisier. He did this by installing a mercury thermometer at a depth of 27m below street level in Paris at the end of the 17th century and this was exactly measured at the Royal Edinburgh Observatory in 1838 (Sanner, 2001). Utilising available underground energy was a question until Zölly suggested in 1912 in Switzerland using the ground as a heat source (Rawlings, 1999). The first ground source heat pump operation documented in the literature was record by Crandall in 1946 in respect of a direct expansion ground coil system installed in a house in Indianapolis (USA) in 1945 (Sanner, 2001).

In the late 1940s, Ingersoll introduced heat transport in the ground to the new ground source heat technology through mathematical methods (Ingersoll, 1954). Utilisation of the ground as a heat source/sink was widely adopted in commercial premises after the first oil crisis in 1973. By the end of the 1970s, over a thousand ground source heat pumps were installed in Sweden (Rawlings, 1999), which is now one of the leading countries in the world for geothermal heat pump applications. Besides Sweden, geothermal heat pump technology has been well established in other European countries such as Germany, Switzerland and Austria (Lund *et al.*, 2004).

The relatively high temperature from the earth and relatively low electricity input (to run the heat pump compressor) are two of the main reasons for the use of ground source heat pumps to deliver heating or cooling to buildings. The strength of this argument is highlighted by comparing the performance of the simpler air source heat pump with a geothermal source heat pump: the coefficient of performance (*CoP*) of the geothermal (ground source) remains consistent and high across external temperatures from -5°C to 10°C, whereas the *CoP* of the

air source heat pump is very sensitive to external temperature variations and falls with decreasing external temperatures (Figure 1.1). A comparative study between a geothermal heat pump and an air to water heat pump for heating and cooling systems demonstrated significant energy saving by the geothermal system; this has become the justification for the rapid growth in the capacity of this technology in recent years (Romero *et al.*, 2005). Lund's (2010) latest worldwide direct geothermal utilisation review reported that the world installed capacity of this technology (geothermal heat pumps) has grown 2.15 times at a compound annual rate of 16.6%.

The open-loop system is the oldest method to utilise the ground source (used since the late 1940s) and the closed-loop system (i.e. the ground coupling method) was not widely adopted until the mid-1980s (Rafferty, 1997).

However, the relatively poor performance of the closed-loop system and the uncertainty of the open-loop system subject to the hydraulic properties of the aquifer eventually led to the birth of the SCW system.

2.2. SCW development

The development of SCWs began in the 1980s: earlier research mainly focusing on the effect of the design and physical construction, while recent work has concentrated more on the numerical modelling of SCWs and heat transfer analysis. Regarding the physical construction, earlier SCW work such as Oliver and Braud's design (1981) had an impermeable outer casing and a suction pipe 'sleeve'; hence the groundwater movement surrounding the borehole wall was ignored in the energy transfer analysis. The temperature distribution in the pipes was solved analytically based on the pure conduction heat transfer theory, involving the temperature gradient across the earth, the annulus and the inner pipe (suction pipe). Their analytical solutions unveiled that the length of the ground heat exchangers can be reduced by increasing the thermal resistance (pipe insulation) of the inner 'sleeve' pipe wall, due to the reduction of short-circuiting heat transfer between the inner pipe and the annulus.

Yuill and Mikler (1995) investigated the influence of the groundwater movement on the performance of a SCW (referred to as a 'thermal well' in their text) with an open well cased construction enhancing the flow of groundwater into and out of the well. The heat transfer mechanism under this casing design involved not only pure conduction through the rocks and the well surface, but also advection in the surrounding rock and convection along the dip tubes and borehole walls. A dimensionless term called the groundwater factor (GF) was used to represent the ratio of heat transfer to the SCW by conduction or convection (due to the groundwater movement). The outward and inward groundwater flow rates to the SCW were determined from the hydraulic gradient across the SCW and GF, according to the Darcy equation in cylindrical coordinates. A numerical model using an explicit finite difference (FD) scheme was constructed, with reference to the cylindrical coordinates to simulate the excitation response from the aquifer due to SCW operation. A small time step (t=0.0004s) was required to achieve an accurate approximation from this numerical model. The

hydraulic head distributions along the SCW could only be measured experimentally; thus an 'equivalent thermal conductivity' was introduced to consider the impact of groundwater motion in an approximation of the water temperature inside the SCW. Therefore, the usability of this model is limited without drilling a test borehole to collect the hydraulic head conditions in advance.

Rees, *et al*. (2004) and Deng (2004) proposed a finite volume (FV) numerical model of SCWs to cope with the induced groundwater flow movement artificially under different groundwater abstraction schemes, known as ‘bleed’ operation. A range of 5% to 15% bleeding rate (with respect to the nominal recirculating pump flow rate) was suggested to be the most effective range to enhance SCW performance. Regarding the groundwater flow analysis, the resistances of the groundwater flow along the borehole, suction pipe and the rocks were analysed by a nodal network. The borehole flux was calculated by the well borehole model according to thermal resistances and thermal mass analysis from the nodal network, being passed onto a finite volume model (coupled by Darcy's flow equation and Bear’s (1972) porous medium energy equation) to simulate the aquifer responses surrounding the SCW.

With reference to the computation power efficiency of the numerical model, a one-dimensional numerical SCW model was developed by Deng, Rees and Spitler (2005) in order to accelerate the equation solving speed of their previous model (Deng, 2004; Rees *et al.*, 2004). A tri-diagonal matrix algorithm (TDMA) method was adopted in the finite difference model to speed up the simulation time. The water inside the SCW was assumed to be a perfectly mixed single zone to calculate the mean water temperature in the well. The leaving water temperature from the well can be estimated from this mean value and corrected by a short-circuit correction to account for short-circuit phenomena inside the well. The groundwater movement caused by pumping and buoyancy was taken into account in this model through the improved value of thermal conductivity, referred to as ‘enhanced thermal conductivity’, similar to the ‘equivalent thermal conductivity’ in Yuill and Mikler’s

model (1995). Enhanced thermal conductivity can be worked out either from in-situ experiments (numerically or physically) or the correlations based on the actual hydraulic and thermal properties of the rock from the site.

In addition to numerical SCW design, a survey (Orio *et al.*, 2005) of SCW installations was conducted in North America that offers practical suggestions for the construction, operation strategies and characteristics of SCW design according to the data collected from 34 standing column wells in 21 different locations. Table 2.1 summarises the construction and modelling development of SCW design from the literature mentioned above.

Table 2.1 Summary of the SCW model development

	Well design	Analytical/ Numerical model scheme	Key features of the model
Oliver and Braud (1981)	Impermeable concentric outer casing (2 in or 5.08cm) with a suction pipe 'sleeve'. Typical well depth: 137m – 231m	Analytical solutions	The temperature distribution in the pipes was solved analytically based on the pure conduction heat transfer theory
Yuill and Mikler (1995)	A open well cased through unconsolidated formation only, with a perforated end section suction pipe for water intake Typical well depth: up to 400m	Finite difference	A dimensionless term called the groundwater factor (GF) was developed to represent the ratio of heat transfer to the SCW by conduction or convection due to the groundwater movement
Rees, *et al*. (2004)		Finite volume	The borehole flux was calculated by the well borehole model according to thermal resistances and thermal mass analysis from the nodal network, being passed onto a finite volume model
Deng, Rees and Spitler (2005)		A tri-diagonal matrix algorithm (TDMA) with finite difference scheme	This is a computation power efficiency model in which the water inside the SCW was assumed to be a perfectly mixed single zone to calculate the mean water temperature in the well.

2.3. Benefits of using SCWs

Recent studies (Norris, 1971; Yavuzturk & Chiasson, 2002; Lund *et al.*, 2004; Lund, Freeston & Boyd, 2005; Deng, Spitler & Rees, 2006; Lu & Wang, 2008) in the USA have confirmed that SCWs allow a significant reduction in borehole depth requirement when compared with the conventional closed-loop system of a single U-tube heat exchanger, as a result of the enhancement in the flow of groundwater into and out of the well by adopting open-end columns.

The performance of SCWs is further improved by 'bleeding', i.e. part of the water from the system being bled (discharged) instead of fully recirculated to the annulus of the SCW to induce a flow of groundwater and increase far-field temperature communication with the well. A parametric study by Rees, *et al.* (2004) showed that the bleed rate was one of the most significant parameters to affect SCW performance and offer reductions in borehole depth, capital cost and life cycle cost compared with the non-bleed case.

Orio, Johnson and Poor (2006) studied ten years of the performance of a SCW application in a New England school in the USA, which achieved a considerable saving in electricity use (about 1300MWh per year) after replacing the electric heating system with a geothermal heating and cooling system (ten heat pumps coupled to six SCWs). The supply water temperature from the SCWs was measured after ten years of operation and the data demonstrated that it remained fairly constant throughout this period. This is the key benefit of adopting a ground source rather than an air source as a heat transfer medium to the heat pump, justifying the reliable and stable performance of geothermal systems.

Even though the merits of SCWs have been revealed, only a few studies (Oliver & Braud, 1981; Yuill & Mikler, 1995; Deng, 2004; Rees *et al.*, 2004; Deng, Rees & Spitler, 2005) have focused on SCW design. Most of these have only considered either heating or cooling applications based on a single well applicable to North American applications; little attention has been paid to UK applications. Multiple borehole arrangements are commonly

used for large applications in conventional closed-loop systems but not often in SCW design. All existing SCW numerical models are only capable of dealing with single well construction, even though several multiple SCW arrangements have already appeared in North American non-residential building applications (Orio *et al.*, 2005). The mild winters and cool summers experienced in the UK mean that it should be possible to extract heat from the ground during winter and reject it during summer to enhance the seasonal performance of SCWs. These are the key elements of novelty that form the basis of this work.

2.4. Related analytical solutions study

i. Thermal response

Earlier analytical approaches to solving earth heat exchange problems with a buried vertical pipe were mainly based on the Kelvin's line source concept and only considered the heat transfer mechanism as pure conduction.

Based on Kelvin's line source theory, the excitations from the ground pipe can be treated as a single finite line placed in an infinite medium. If only conductive heat transfer is concerned (i.e. no groundwater movement), the problem can be solved by a simple conductive heat transfer equation.

Equation 2.1

$$Q = kA\,\frac{\partial T}{\partial x}$$

The cylindrical coordinate solution that satisfies the conduction equation to determine the temperature distribution is:

Equation 2.2

$$\frac{\partial^2 T}{\partial r^2} + \frac{\partial^2 T}{\partial z^2} + \frac{1}{r}\frac{\partial T}{\partial r} + \frac{Q}{k} = \frac{1}{\alpha}\frac{\partial T}{\partial t}$$

for the domain $r > r_b$ and $t > 0$ and $0 > z > \infty$.

Ingersoll, *et al.* (1948) introduced Kelvin's concept into this field, considering the earth heat exchanger as a single 'line' disturbance (known as line source theory) in a homogenous aquifer to determine the temperature in the surrounding field.

T_∞ = far-field temperature (°C) (= T_u)

r_∞ = far-field distance (m)

T_b = borehole wall temperature (°C)

Q = heat transfer rate to the ground (Wm^{-1})

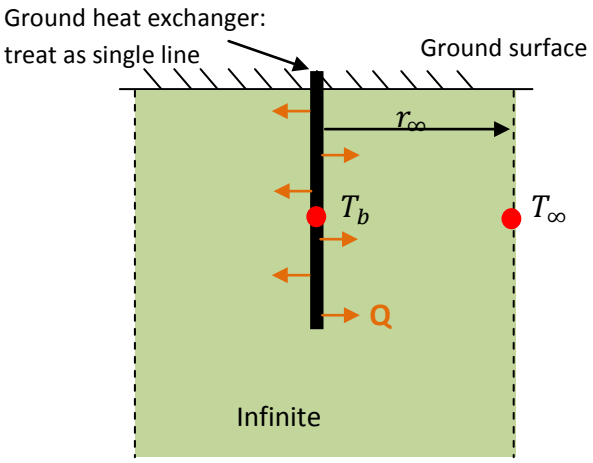

Figure 2.1 Line source theory concept

Equation 2.3

$$T - T_u = \frac{Q}{2\pi k}\int_x^\infty \frac{e^{-\beta^2}}{\beta} d\beta = \frac{Q}{2\pi k} I(X)$$

where:

$$IX = \frac{r}{2\sqrt{\alpha t}}$$

T = temperature in the soil at any selected distance from the pipe (°C)

T_u = uniform initial temperature of the soil (°C)

Q = heat emission of the pipe (negative for absorption) (Wm^{-1})

r = distance from the centre line of the pipe (m)

k = thermal conductivity of the soil ($Wm^{-1}K^{-1}$)

α = thermal diffusivity of the soil ($m^2\ s^{-1}$)

t = time since start of operation (hours)

β = variable of integration

After expanding the exponential term with power series, Equation 2.3 can be written as:

Equation 2.4

$$T - T_u = \frac{Q_b}{4\pi k}\left[\ln\left(\frac{4\alpha t}{{r_b}^2}\right) - \gamma + c\right]$$

where:

γ = Euler's constant

For a large heat exchanger application (more than four inches (or 100mm) in diameter) or concerning a short period of time, the line source theory could yield significant errors (Ingersoll & Plass, 1948). Carlaws and Jaegar (1959) suggested the following cylindrical source concept solution for a hollow cylinder with a constant heat flux *Q* generated on its surface.

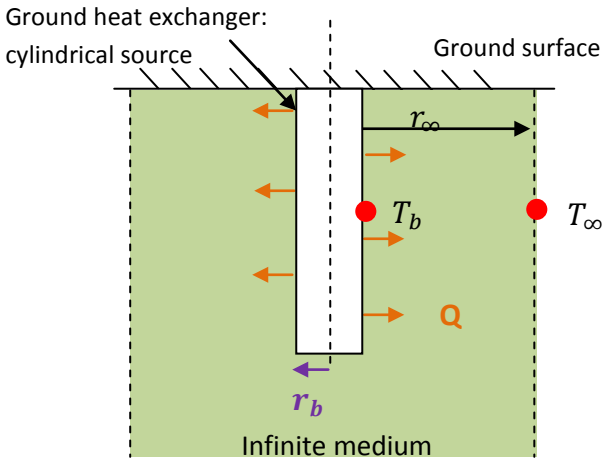

Figure 2.2 Cylindrical source theory

Equation 2.5

$$\Delta T_{r-b}(r,t) = \frac{2Q}{\pi k}\int_0^\infty (1-e^{-ku^2t})\frac{J_0(ur)Y_1(ur_b)-Y_0(ur)J_1(ur_b)}{u^2\left[{J_1}^2(ur_b)+{Y_1}^2(ur_b)\right]}du$$

at $r = r_b$

where:

ΔT_{r-b}= variation of the ground temperature at radial distance r (K)

= Bessel function

Y = Bessel function

Q = constant heat flux (Wm^{-2})

r = distance from the centre line of the pipe (m)

r_b = radius of the heat exchanger (m)

k = thermal conductivity of the soil ($Wm^{-1}K^{-1}$)

u = integration variable

If the domain of the problem is sufficiently large ($r/r_b > 10$), the temperature response derived from the line heat source theory should be very similar to those applying the cylindrical heat source concept. The size of boreholes of SCWs is normally very small, about 75mm to 200mm; thus it is possible to treat the heat extraction and injection via the pipe to the earth as a line source in the numerical model if the domain is large enough

ii. Hydraulic response

Regarding the hydraulic response, the most well-known equation to describe hydraulic characteristics underground in a transient state associated with a fixed value of excitation is the Theis equation (Theis, 1935). The Theis equation is based on Carslaw's heat conduction theory, imposing a constant source term, initial condition and the boundary condition to achieve the first hydraulic equation coping with the unsteady state condition.

Equation 2.6

$$h_o - h\,(r,t) = \frac{Q}{4\pi T}\int_U^{\infty}\frac{e^{-u}du}{u}$$

where:

$$u = \frac{r^2 S}{4Tt}$$

h_o = hydraulic head before pumping (m)

$h(r,t)$ = hydraulic head at a radial distance (r) at any time (t) after pumping (m)

Q = pumping rate (m^3s^{-1})

T = transmissivity of the aquifer (m^2s^{-1})

S = storativity of the aquifer

Nevertheless, the 'infinite areal extent' assumption in the Theis equation may sometimes restrict the application of it, especially if there is a problem with special boundary conditions or concerning the flow in a very small domain. Thus, Todd (1980) introduced the image method to cope with special boundary conditions such as impermeable and rechargeable boundaries. In this modelling work, no special boundary conditions are initially considered but can be handled by the model as a leakage term.

Furthermore, Maddock (1972) considered the management problem of variable pumping loads, which cannot be solved by the Theis equation due to the fixed constant source term. He proposed another equation simply based on a similar concept to Theis', but the source term is described as a discrete time term instead of a single continuous source. His equation allows seasonal pumping and lifting to be taken into account and hence achieve more practical pumping loads, i.e. a reduction in cost. From his equation, the drawdown at well a at time t due to the pumping at well j at a rate of $Q(j,\tau)$ is:

Equation 2.7

$$s(a,t) = \frac{1}{4\pi T}\sum_{j=1}^{M}\int_{0}^{t} Q(j,\tau)\ exp\left(\frac{-{R_{ja}}^2\, S}{4T(t-\tau)}\right)d\tau$$

where:

s = drawdown (m)

S = storativity of the aquifer

Q = pumping rate (m^3s^{-1})

T = transmissivity of the aquifer (m^2s^{-1})

R_{ja} = distance between well k and j if $a \neq$ j. Otherwise it is the radius of a. (m)

τ = unit time period

M = number of wells

t = time (s)

Morel-Seytoux and Daly (1975) improved Maddock's equation by introducing a more efficient way to determine the coefficient. The function in this equation is known as a discrete kernel function.

This function is used as an analytical model to evaluate the performances of various numerical approaches in this work. The principle of the discrete kernel generator is actually the same as the Theis recovery function (Freeze & Cherry, 1979), apart from the use of imaginary source types (Figure 2.3). A pulse imaginary source is adopted in the discrete kernel function but a continuous imaginary source is used in the Theis recovery function, which is used to counteract the original source for the purpose of dealing with variable loads.

Equation 2.8

$$U = \frac{1}{4\pi T}\left\{E_1\left(\frac{r^2 S}{4Tt}\right) - E_1\left(\frac{r^2 S}{4T(t-\tau)}\right)\right\}$$

where:

U = drawdown (m)

E_1 = exponential integral/well function

T = transmissivity (ms^{-1})

S = storativity

t = time (s)

τ = unit time period

r = distance from the well (m)

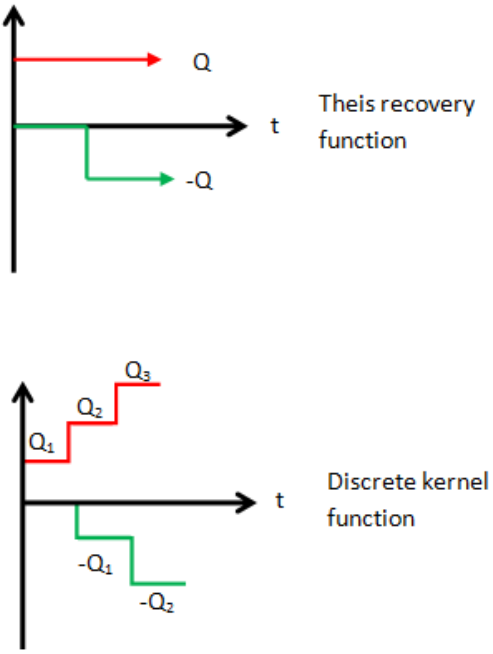

Figure 2.3 Application of the imaginary source of the Theis recovery and discrete kernel functions

Summary of the literature review:

- The history of the discovery and utilisation of ground sources has been reviewed: the relatively stable and high performance of using the ‘ground’ as a source (in comparison with ‘air’ sources) have led to the rapid growth in GHCS technology.
- The development of SCWs, including their physical construction and numerical modelling, has been reviewed.
- A number of research efforts have confirmed the benefit of using SCW over conventional closed-loop designs in terms of reduction in borehole depth requirement and hence lowering the drilling cost.
- Relevant analytical solutions in relation to the responses from the ground due to the thermal and hydraulic excitations have been studied; one of these approaches might form the concept of the model in this work.

3. Research aims and objectives

The aim of this research is to develop, test and apply a three-dimension numerical performance model of a standing column well field for UK application to building heating and cooling, with consideration for multiple well applications.

The objectives of this work are:

- To develop a three-dimensional dynamic thermofluid model of the geological field and superimpose one or more detailed SCW well models onto the field model.
- To evaluate and implement suitable discretisation and solution schemes for the model equations.
- To conduct simple verification tests on the completed model using existing field data derived from pumping tests and thermal response tests conducted at various UK sites.
- To apply the model to a range of typical UK commercial building applications involving winter heating and summer cooling and compare the results with those from a conventional closed-loop geothermal array design.
- To quantify the energy and carbon saving due to the use of an SCW array compared with conventional closed-loop systems.
- To develop simple procedures and recommendations for the practical design of SCW arrays for UK applications.

The model is expected to contribute better understanding of standing column well system performance by:

- Predicting geothermal heat transfer rates compared with conventional closed-loop methods.
- Predicting the interaction between individual wells in multiple well arrays.
- Quantifying the performance of multiple well arrays for rock formations and building energy demand characteristics applicable to the UK.
- Providing a tool for designing standing column well networks for operation over extended time periods.

4. SCW model development

4.1 Structure of the model

For the purpose of managing certain operations (such as bleed flow) and installation arrangements in the numerical model in a more flexible way, a field model of the background geology is first developed and then a detailed well model is developed separately so that it can be superimposed on the field model.

The field problem consisting of the heat and groundwater flow in the rock formation was considered a ‘parent model’ to that of the standing column well cluster. Thus a ‘child model’ (i.e. the well model) was coupled to the field model equations through the source terms and solved using a smaller time interval than that used to solve the field equations. In effect, each well was treated by the field equations as a line source/sink of finite depth. This decoupling means that the field equations could be solved independent of the standing column wells at the coarser time step appropriate to the field variables. The well equations were then solved iteratively at shorter series of time steps within the coarser field time step and the source terms were then updated in the field equations. An advantage of this approach (this has not been done in the present work but remains an area of future interest) is that standing column wells of different types can be applied with other source types (e.g. closed-loop heat exchangers) to form a fully flexible hybrid scheme if desired. The graphic representation of the concept is shown in Figure 4.1.

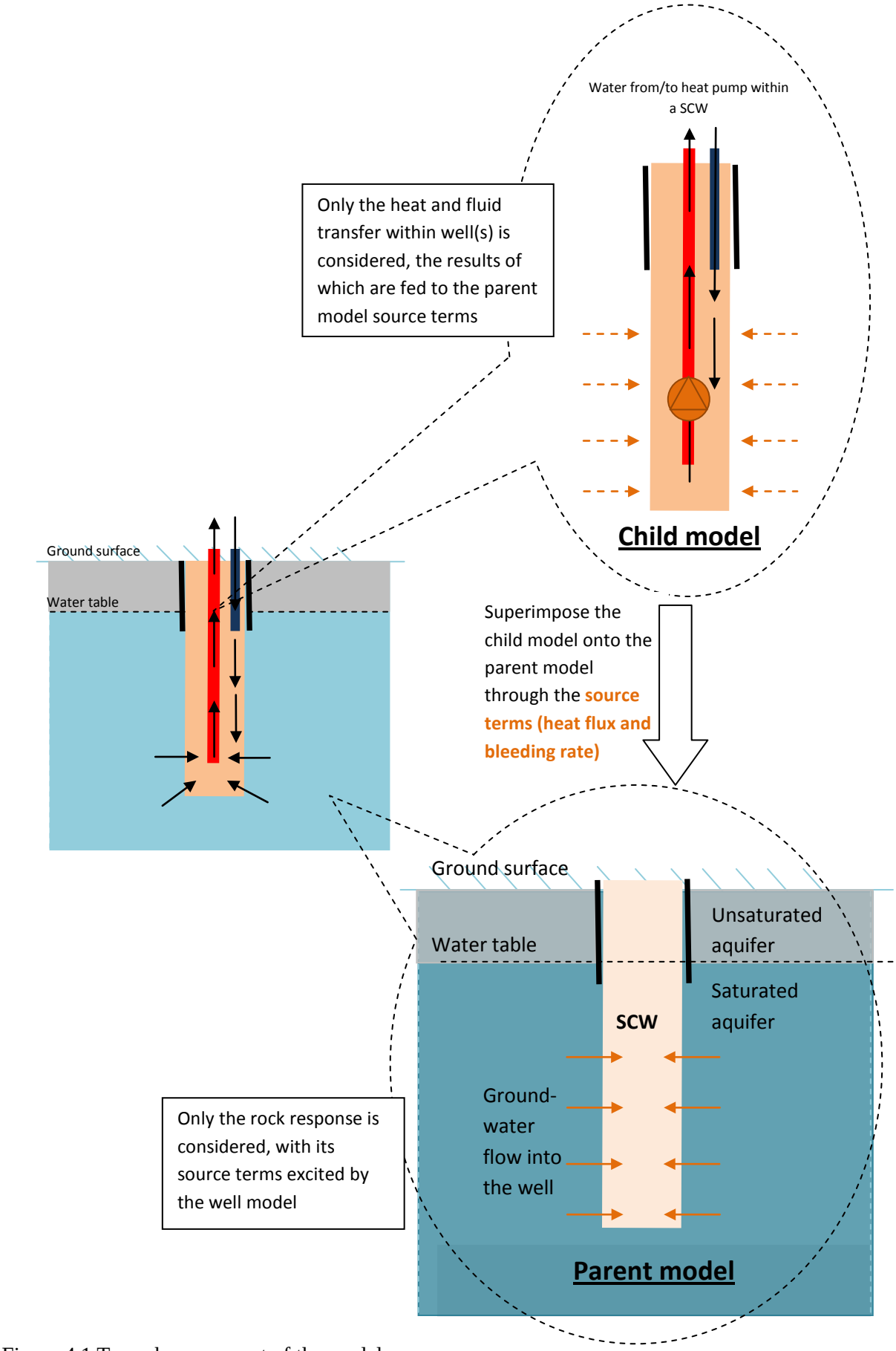

Figure 4.1 Two-phase concept of the model

4.2 Field model development

The field model consists of two sets of partial differential equations (PDEs): the head diffusion equation in saturated flow conditions and the energy equation in the porous medium (Bear, 1972) to handle the thermal and hydraulic energy transport in the aquifer. These two equations are coupled using Darcy's equation, which relates flow velocity to head via the hydraulic conductivity properties of the rock. Homogeneity and isotropy are assumed throughout the field domain.

SCW systems require relatively low discharge and suction flow rate to balance the pumping cost and heat transfer performance, which imposes a low velocity flow profile of water surrounding the well(s). Hence, it is sufficient to apply Darcy's law in this work to predict the fluid flow in the rock.

Equation 4.1 Head diffusion equation

$$\frac{S_s}{K}\frac{\partial h}{\partial t} - \frac{F}{K} = \nabla^2 h$$

where:

K = hydraulic conductivity (ms^{-1})

S_s = specific storage (m^{-1})

F = source term (s^{-1})

h = hydraulic head (m)

t = time (s)

Equation 4.2 Darcy flow equation

$$u_x = -\frac{K}{n}\frac{\partial h}{\partial x}$$

where:

u_x = the velocity in the *x* direction (ms^{-1})

n = rock porosity

(and, likewise, u_y & u_z).

Equation 4.3 Energy equation

$$\left[n\rho_{\mathrm{w}}c_{\mathrm{pw}} + (1+n)\rho_s c_{ps}\right]\frac{\partial T}{\partial t} - n\rho_{\mathrm{w}}c_{\mathrm{pw}}\nabla uT - k_{\mathrm{eff}}\nabla^2 T = Q$$

where:

ρ = density, subscripts: w = water, s = solid (i.e. rock, etc.) (kgm^{-3})

c_{pw} = specific heat capacity, subscripts as above ($Jkg^{-1}K^{-1}$)

T = temperature (K)

k_{eff} = effective thermal conductivity ($Wm^{-1}K^{-1}$)

Q = source term (Wm^{-3})

4.2.1 Numerical approaches analysis

There are many different types of numerical techniques that are capable of dealing with the PDEs governing groundwater flow problems. Each of them have different algebraic equation structures, element shapes, nodal point arrangements, time derivative approximations, etc. to obtain the values of various variables in a finite domain of interest. The selection of the appropriate numerical approach is a critical task to ensure the objectives of the work and the problems of the field are depicted by the model efficiently.

The finite difference (FD) method is one of the most common techniques used in this field due to its simplicity. Programs such as MODFLOW or GMS are constructed by this approach. For problems involving complex geometries or boundary conditions, other approaches such as the finite volume (FV) or finite element approaches are usually employed.

Most of the existing SCW models nowadays either employ the FD or FV methods; however, the computational efficiency of these two numerical techniques, particularly with regards to handling GHCS problems, is not that clear. With the intention of selecting the most computationally efficient and accurate approach to solve a three-dimensional flow problem in an aquifer in conjunction with well abstraction and reinjection activities, the performance of several numerical solution schemes with different combinations of numerical approaches were investigated. The best combination was identified and used as a basis for superimposing a 'child model' of the standing column well cluster. The best combination was largely governed by accuracy and computational efficiency considerations.

Two discretisation techniques (finite-difference (FD) and finite-volume (FV)) and two time-derivative solution schemes (implicit and explicit approaches) were examined (Figure 4.2). Furthermore, a two-dimensional finite element (FE) approach based on commercial software (Matlab PDE toolbox (Little & Moler, 1984)) was investigated.

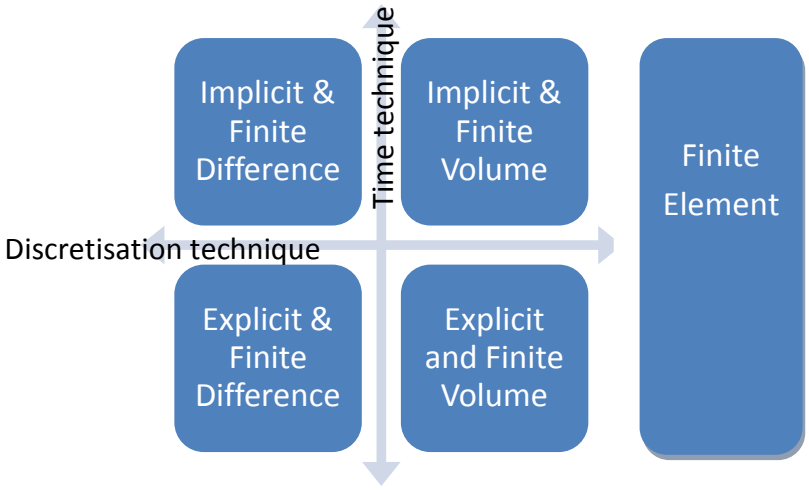

Figure 4.2 Combination of numerical approaches

4.2.2 Assumptions

In order to compare the various numerical options described above, one layer confined aquifer cuboids, 100m x 100m x 100m in three dimensions and 100m x 100m in two dimensions, was considered with a fully penetrated line source located in the middle of the domain. All boundaries were considered as no flow boundaries (i.e. general groundwater flow is not considered – only that caused by pumping is considered). The line source concept was utilised to describe the pumping action from the well, i.e. the structure of the SCW was omitted. A control case was generated using the line source theory-based method of Barry, *et al*. (2000), applied to the practical hydrogeology test case of Morel-Seytoux and Daly (1975). The response of the various model formulations was compared with the control case based on a unit pulse alternatively applied to heat input and pumped water flow rate, each of 10h duration.

4.2.3 Comparison of implicit and explicit approaches

Figure 4.3 shows that an explicit approach consumes much more computational power to solve the same problem, as is the case with the implicit approach, caused by the use of a relatively small time step to limit the magnitude of truncation errors associated with this approach. An explicit FV (EFV) scheme also requires more time than the explicit FD (EFD) scheme to solve the problem. This might be due to its relatively complex discretisation structure.

The preliminary results suggest that the computation costs of both explicit model formulations are substantially higher than all other implicit options. These model formulations were therefore discarded from the following studies.

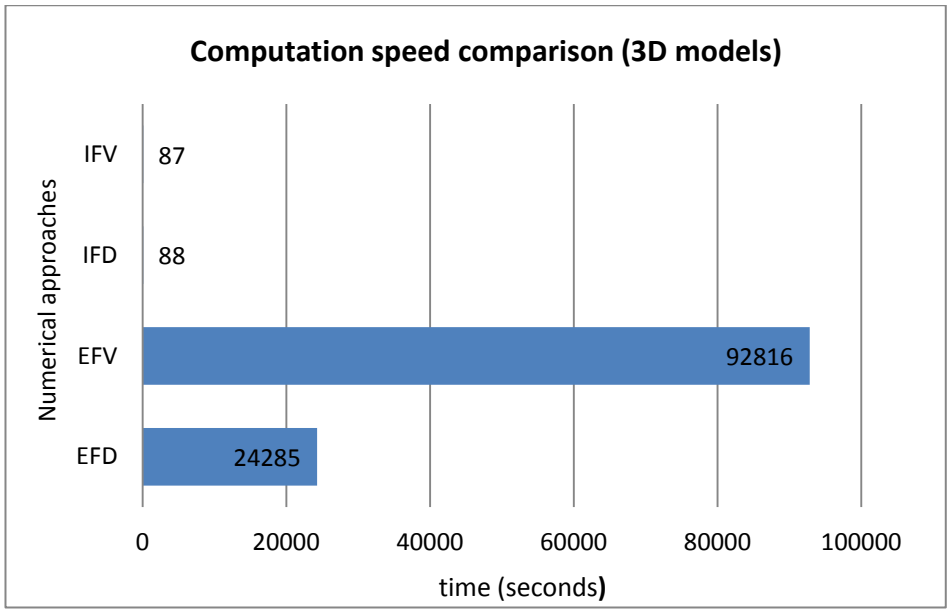

Figure 4.3 Computation speed comparison (3D models)

4.2.4 Comparison of IFD, IFV and commercial FE approaches

The IFD and IFV models from the previous analysis were reconstructed into two dimensions, with the aim of generating compatible results to the 2D FE model. The head and energy balance equations were handled separately as well to facilitate comparison with the analytical solution (Morel-Seytoux & Daly, 1975). The drawdown and temperature variations 1m away from the well caused by a 10 hour unit pulse disturbance were calculated and the deviations between the various numerical methods (IFD, IFV & FE) and analytical solution were compared.

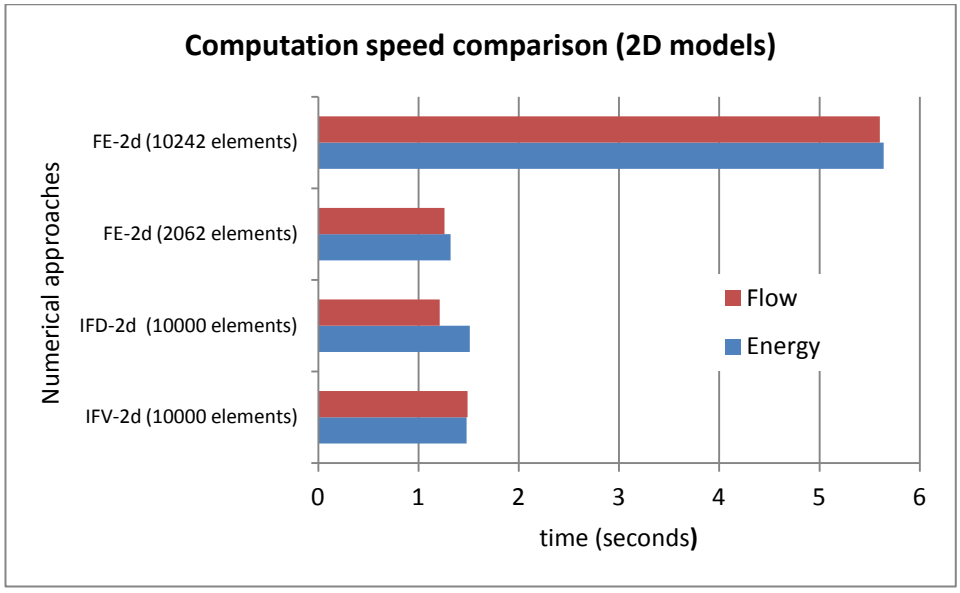

Figure 4.4 Computation speed comparison (2D models)

Figure 4.4 shows that the IFV, IFD (both with 10000 elements) and low resolution FE model (with 2062 elements) consumed similar amounts of computation time (about 1.5 seconds) to solve the same problem, but the higher resolution FE model (which contained 10242) elements took about three times longer than its low resolution counterpart to solve the problems.

The rock temperature responses at a distance of 1m from the centre of the well under a unit pulse disturbance, predicted by the FE (low resolution), IFD and IFV models, are shown in Figure 4.5. The FE model (low resolution) appeared to have the best agreement with the analytical solution, with standard errors (root mean square errors) of 0.029, whereas the IFD and IFV models generated significantly higher values of standard errors of 0.039 and 0.040 (respectively) under the initial grid spacing of 1m x 1m, resulting in 10000 elements.

Owing to the moderately poor performance of the IFD and IFV models, the size of the grid was reduced to half its original size and the standard errors were calculated again. The result is shown in Figure 4.6. The standard errors were reduced to 0.032 (IFD) and 0.024 (IFV) under the finer grid structure. However, these findings indicate that a detailed investigation of grid spacing is required to improve the models' performances.

Similar findings were discovered when solving the head equation (Figure 4.7). The drawdown estimation by the FE model was slightly more accurate than the IFD and IFV models associated with a coarse grid arrangement (1m x 1m), in comparison with the analytical solutions. The standard errors were 0.058 for the FE model and 0.059 for both the IFD and IFV models. The standard errors of the IFD and IFV models were reduced to 0.052 when using a finer mesh setting of 0.8m x 0.8m (15625 elements) (Figure 4.8).

To summarise, the FE approach initially appeared to be the most preferable option to solve the problem, requiring the smallest number of elements to give the best solutions among all the investigated models. However, the commercial 'toolbox' method used would not readily permit the casting of the problem in three spatial dimensions, which would mean that investigations involving SCWs of differing lengths could not be explored. Furthermore, 'toolbox' techniques of this kind lack transparency and generality (for use by other researchers) and flexibility (essential when it comes to superimposing the well models).

Nevertheless, these comparisons prove that IFD and IFV models could be adapted with an efficiency and accuracy approaching that of the FE approach if careful selections of the grid

arrangements were made. According to the accuracy of solutions, the IFV method performed slightly better than the IFD and hence was chosen to be the discretisation scheme for the model. A further advantage in the use of a finite volume scheme is that continuity (between elements) is assured, whereas finite difference discretisation can lead to small errors – though these errors are unlikely to be significant in the very low rates of change inherent in the present problem.

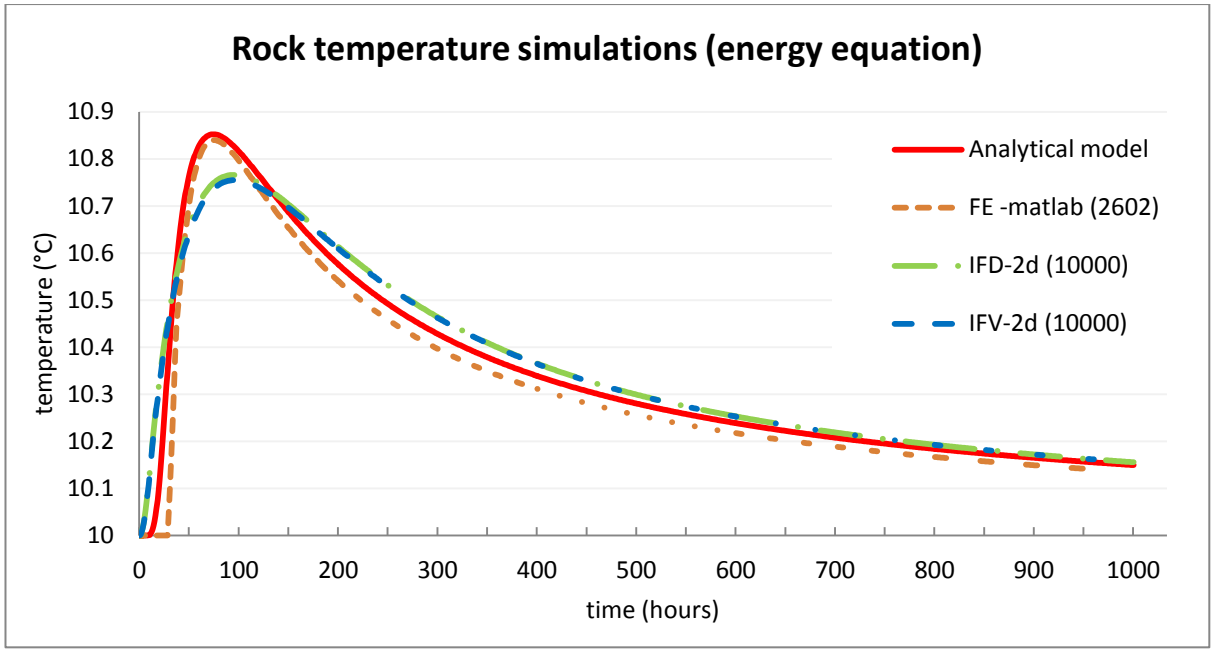

Figure 4.5 Rock temperature simulations by FE, IFD and IFV models

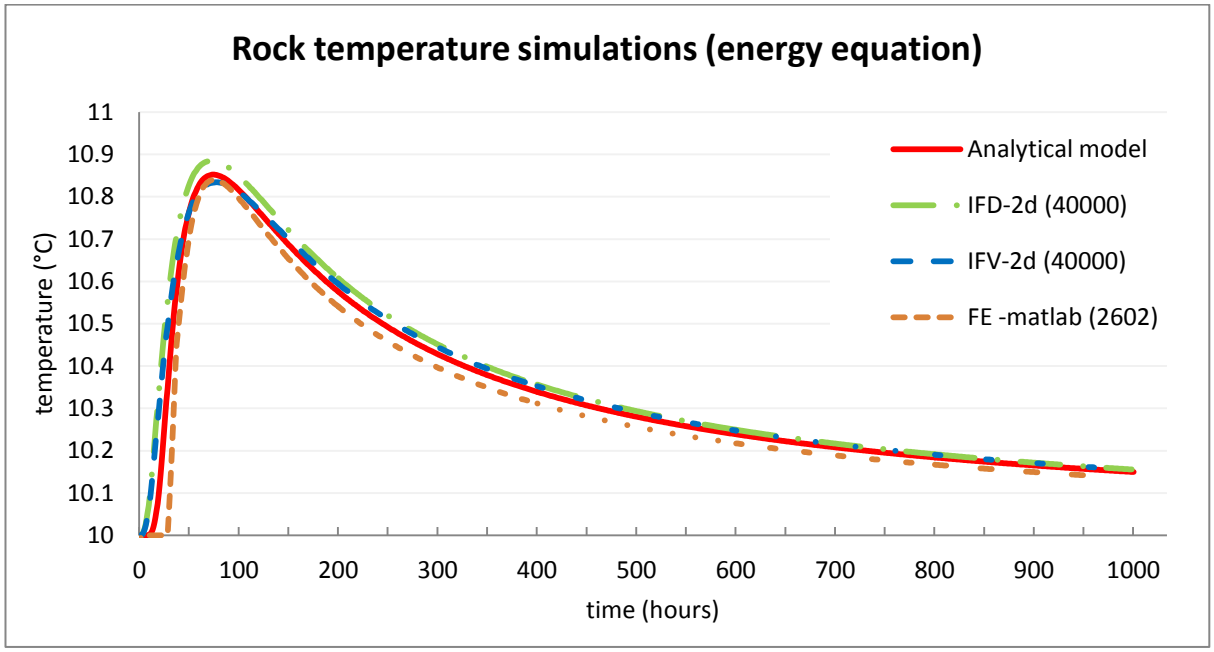

Figure 4.6 Rock temperature simulations by FE, IFD (refined) and IFV (refined) models.

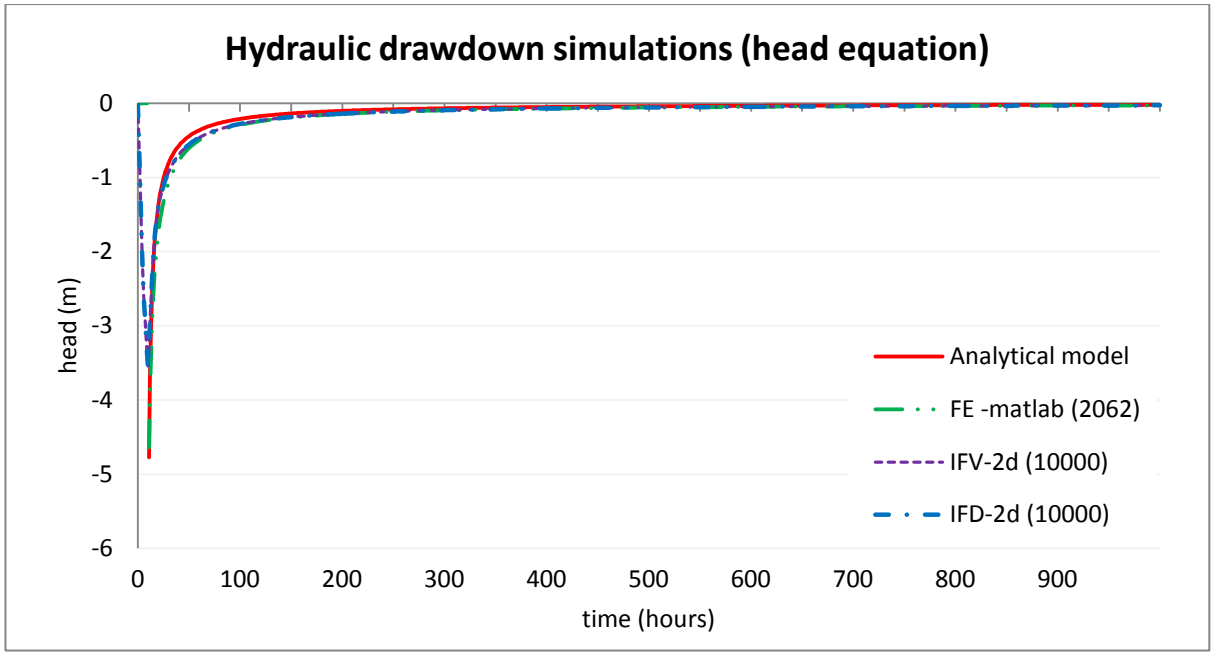

Figure 4.7 Hydraulic drawdown and recovery simulations by FE, IFD and IFV models

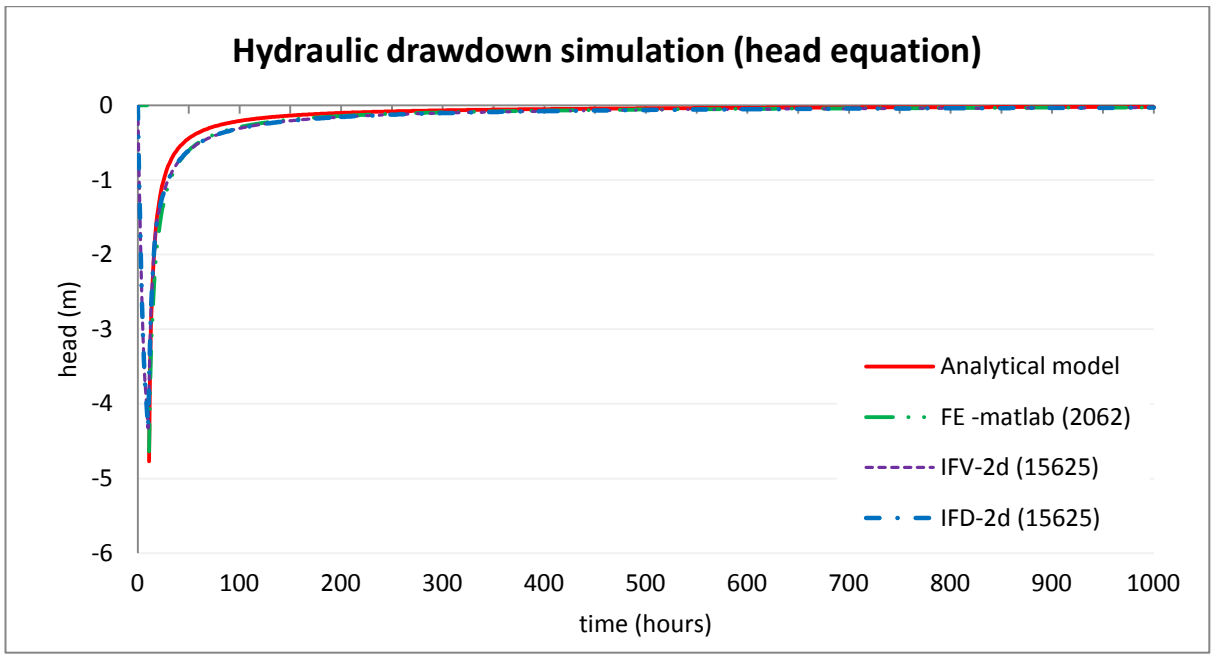

Figure 4.8 Hydraulic drawdown and recovery simulations by FE, IFD and IFV (grid refined) models

4.2.5 Grid dependence study

The computational 'efficiency' of a numerical model depends on the accuracy requirements of the approximations and times of implementation, both of which are sensitive to the structure of the grid mesh and choice of time increments.

The results from the previous section (particularly the accuracy improvement by refining the grid size) perhaps suggest that a detailed analysis of the grid meshing arrangement is necessary. In addition, the field model developed in this work is assembled by two different PDEs: the relatively fast acting head equations and the relatively slow acting energy equations. Various time increments may therefore possibly be applied to different equations to take advantage of improvements in computation speeds.

The best way to explore these issues is by a grid dependency study in which the most suitable grid and time increment strategies can be confirmed by observing the relative convergence and computation cost characteristics of the approximated solutions from the numerical model, under various choices of grid and time step arrangements.

4.2.6 Methodology of grid dependency study

The relative precision of the SCW model under various grid mesh schemes and time increments was investigated. The influences of the iterative tolerances on the solution accuracy and the computation consumption were also examined.

A continuous line source (a heat flux or pumping rate) was located in the middle of a cubic domain (48m x 48m x 48m) to represent disturbances. The temperatures and hydraulic head responses at 1.2m from the disturbance (source) were measured and compared with an exact solution (Barry, *et al.*, 2000). The chosen distance had to be divisible by the grid mesh scheme for a direct comparison.

The selected mesh schemes for this study were 1.2m, 0.6m, 0.4m and 0.3m. Any mesh size smaller than 0.2m was not considered as it might be potentially smaller than the size of the well and suction pipe. The mesh arrangement can be found in figure 4.9.

Each set of equations was computed using different time increments. A preliminary test was performed prior to the detailed investigation to evaluate the suitable range of time increments for the study.

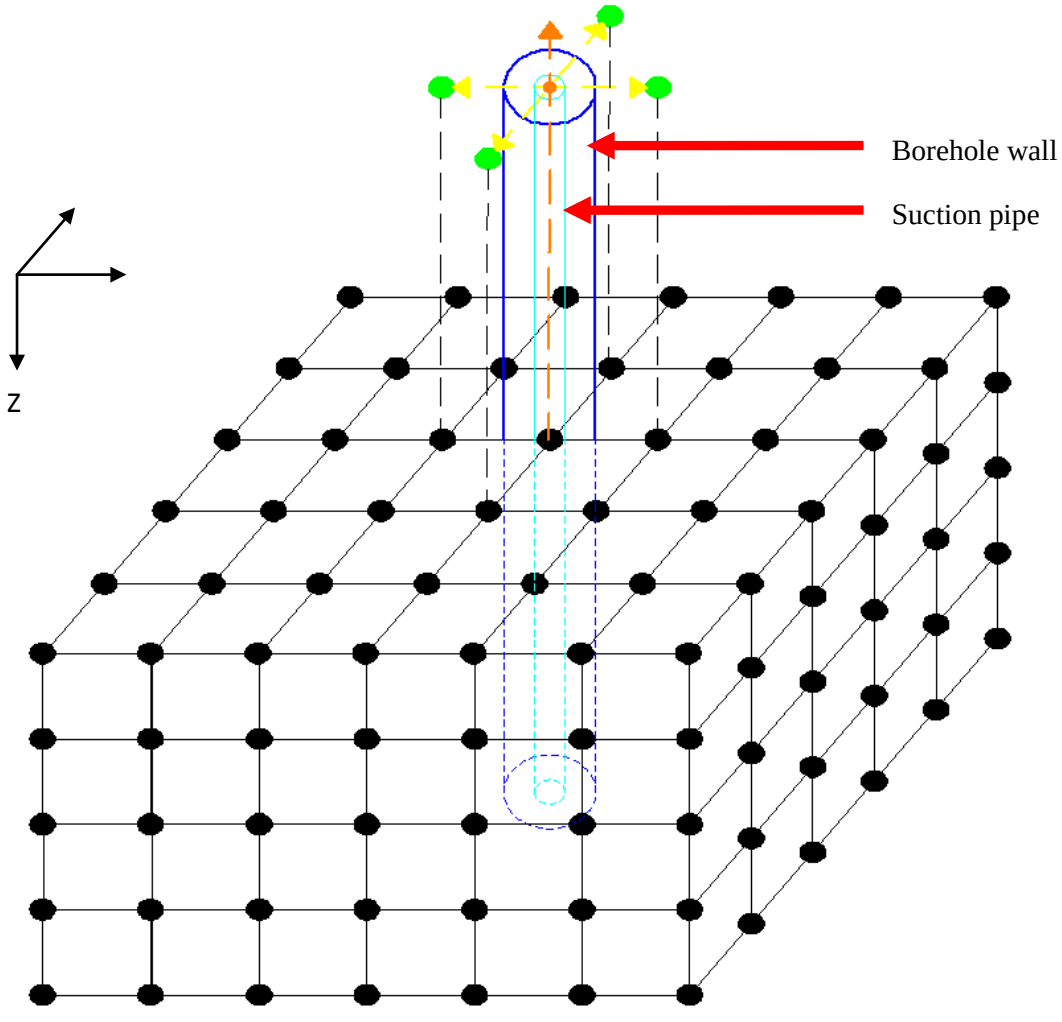

Figure 4.9 The mesh arrangement of the SCW model.

4.2.7 Preliminary grid sensitivity test and results

Alternative spatial grid mesh sizes were first evaluated for the field equations by imposing a fixed time increment of 3600s and then performing step-response simulations with reference to the analytical solution of Barry, *et al*. (2000). The thermal response and hydraulic drawdown response were alternatively extracted.

The numerical solutions from the energy equation in almost all the mesh schemes were very close to the exact solutions from the analytical model, with absolute errors less than 0.1°C in all cases with the exception of 0.3m, as shown in Figures 4.10 and 4.11. The best result for the energy equations was with a grid mesh size of 0.6m. Wider time increments were then explored (with the potential for benefits in computation speeds). The time steps applied to the energy equation were 3600s, 14400s, 21600s, 43200s and 86400s.

Larger amounts of errors were found when applying the same spatial grid mesh sizes to the hydraulic drawdown estimations (Figures 4.12 and 4.13). A range of shorter time increments for this case were therefore explored (60s, 600s, 1200s, 1800s and 3600s).

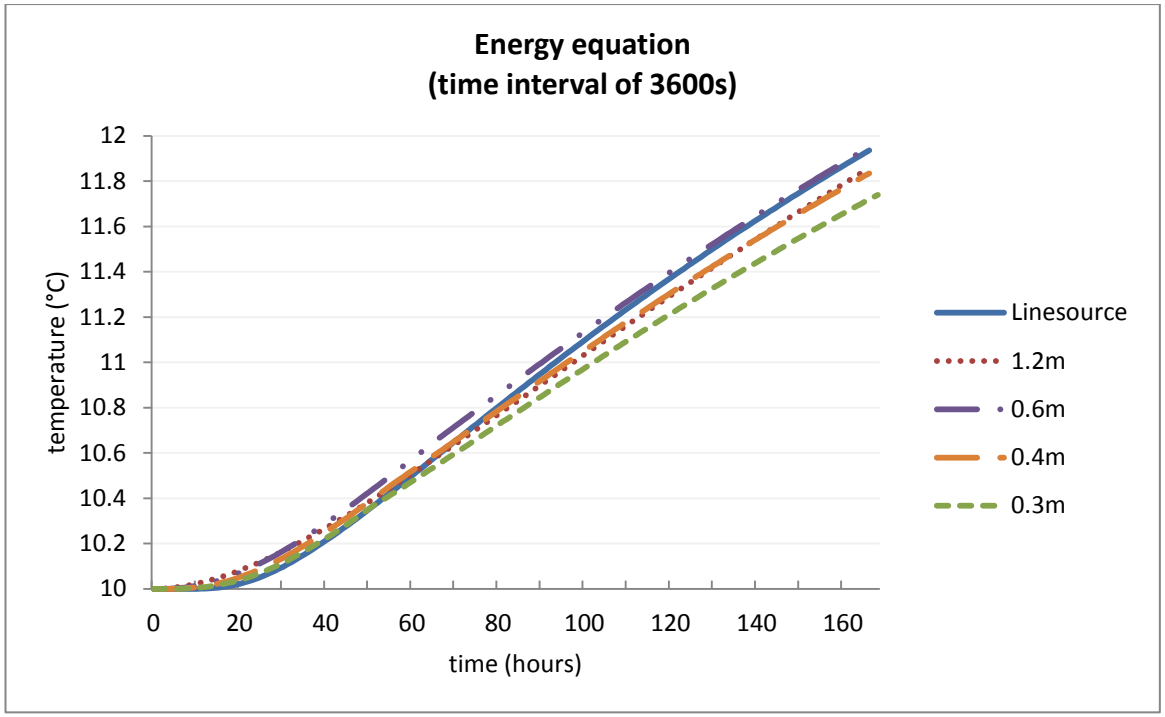

Figure 4.10 Preliminary grid sensitivity test on the energy equation

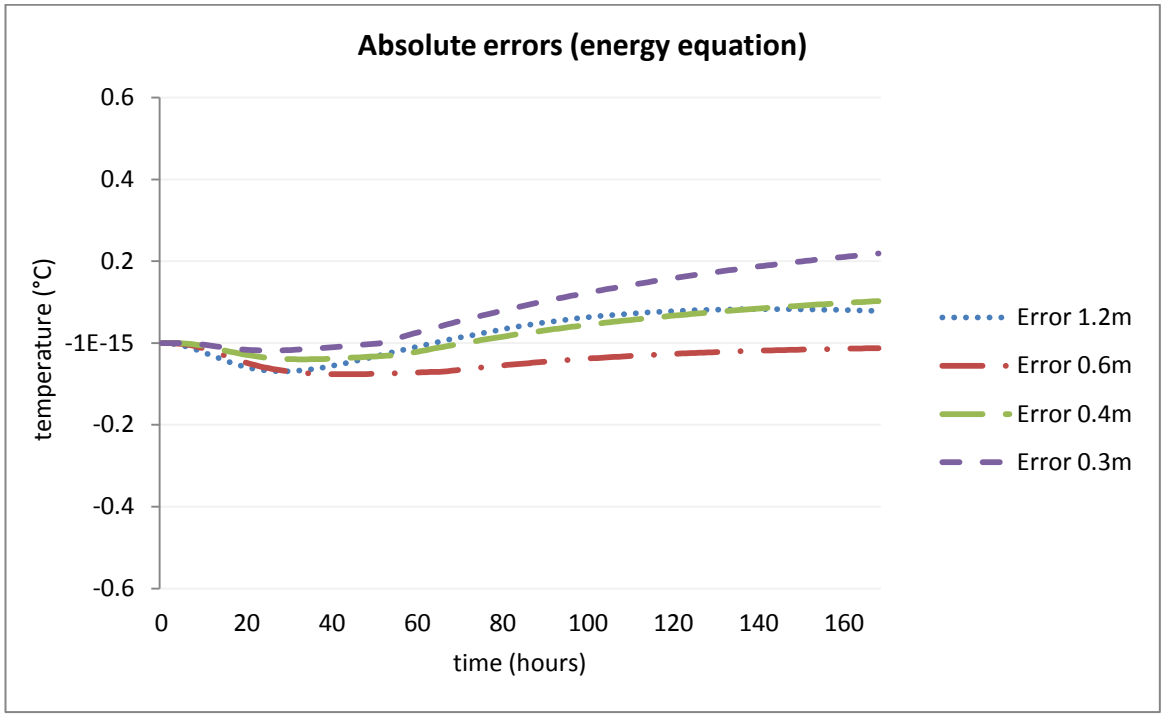

Figure 4.11 Absolute errors on the preliminary grid sensitivity test on the energy equation

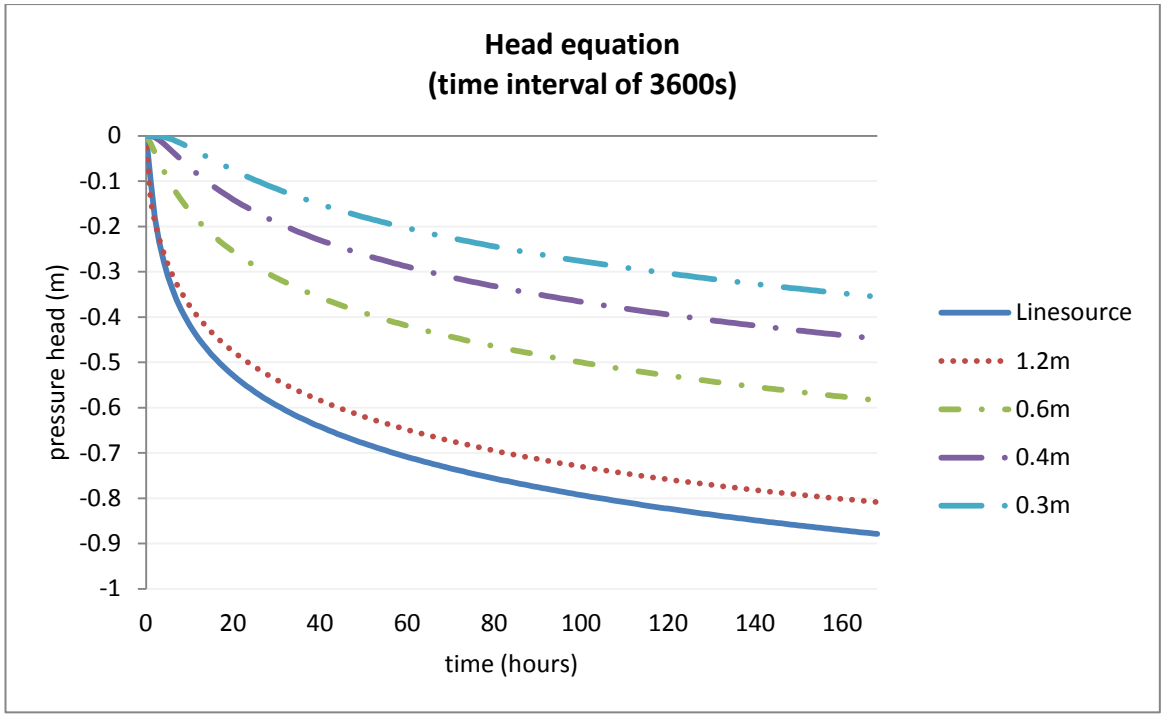

Figure 4.12 Preliminary grid sensitivity test on the head equation

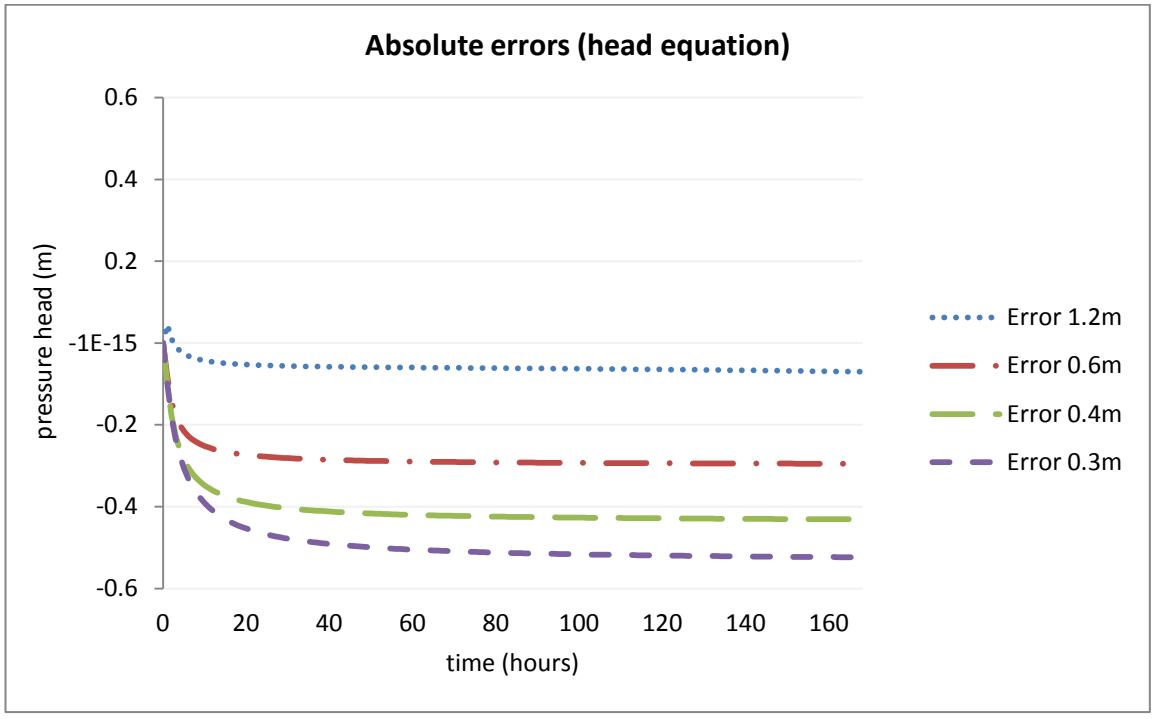

Figure 4.13 Absolute errors on the preliminary grid sensitivity test on the head equation

4.2.8 Grid dependency study on energy equation

The relative performance of the field model in solving the energy equation with different time increments (3600s, 14400s, 21600s, 43200s and 86400s), alternative spatial grid mesh sizes (1.2m, 0.6m, 0.4m and 0.3m) and two alternative iterative tolerances (0.05 and 0.01) was investigated. A continuous line source of heat flux stepped in at t = 0s was placed in the centre of the domain to excite a temperature profile in the field. The temperature responses near to the source (at 1.2m) were extracted and compared with the analytical solution.

Figure 4.14 indicates the time increment under an initial tolerance setting of 0.05 and a grid mesh size of 0.6m is 43200 seconds (12 hours), if the maximum acceptable absolute error of the numerical solution is 0.1°C in comparison with the exact solution. Refining the tolerance from 0.05 to 0.01 offered a certain amount of improvement in terms of accuracy, particularly on those models constructed with relatively small mesh sizes (such as 0.4m and 0.3m), achieving an average reduction of about 63% (0.4m) and 74% (0.3m) across the whole range of time increments (Figure 4.15). However, reducing the tolerance value increased the computation cost by at least 20% for all combinations (Figure 4.18).

Figures 4.16 and 4.17 show that the mesh scheme of 0.6m yielded the smallest values of root mean square errors for both tolerance settings, in comparison with other grid mesh sizes (1.2m, 0.4m and 0.3m) for the same time increment settings.

Therefore, taking into account both the computation cost as well as the relative accuracy, a time increment of 12 hours (43200s), an iterative tolerance of 0.05 and a mesh size of 0.6m were selected to compute the energy governing equations. Figure 4.19 demonstrates that the chosen values measured at the 168th hour agree reasonably well with the exact solutions at four different locations from the heat source.

The related model parameters of the hydraulic head equation are now considered separately

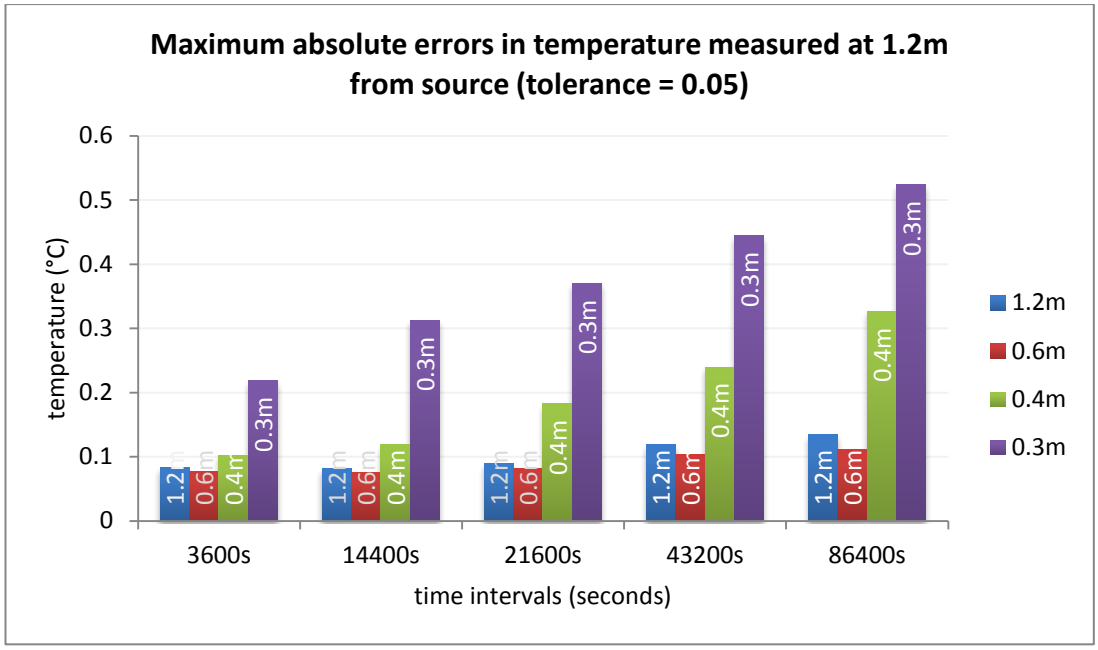

Figure 4.14 Maximum absolute errors of solving the energy equation with various grid sizes and time increments (tolerance=0.05)

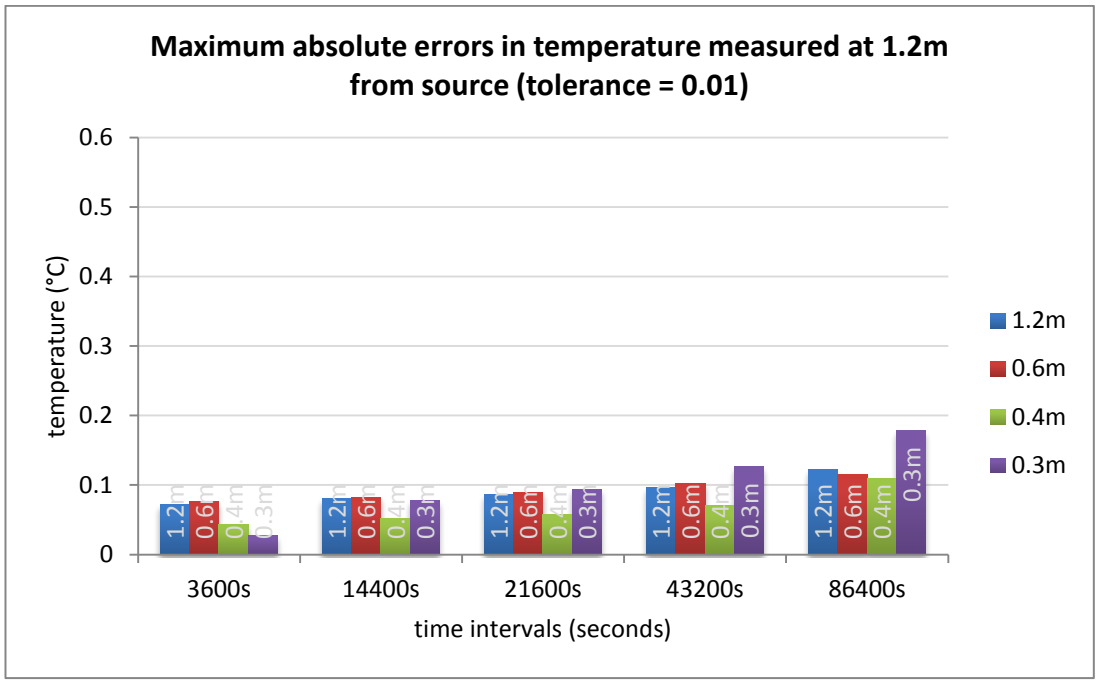

Figure 4.15 Maximum absolute errors of solving the energy equation with various grid sizes and time increments (tolerance = 0.01)

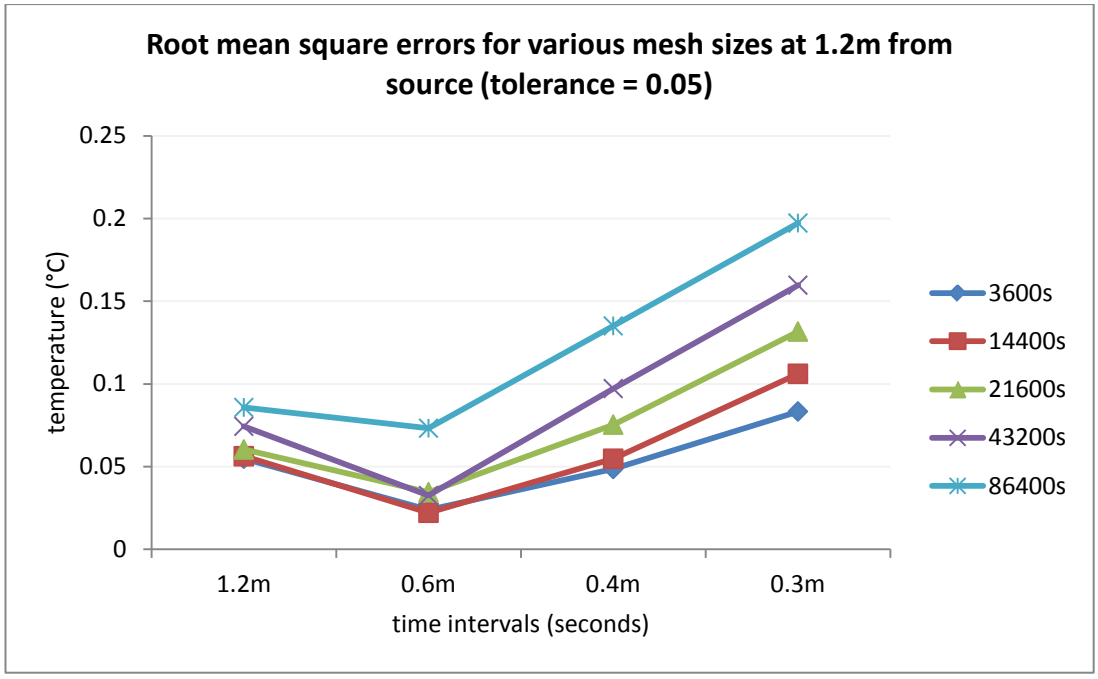

Figure 4.16 Root mean square errors of solving the energy equation with various grid sizes and time increments (tolerance = 0.05)

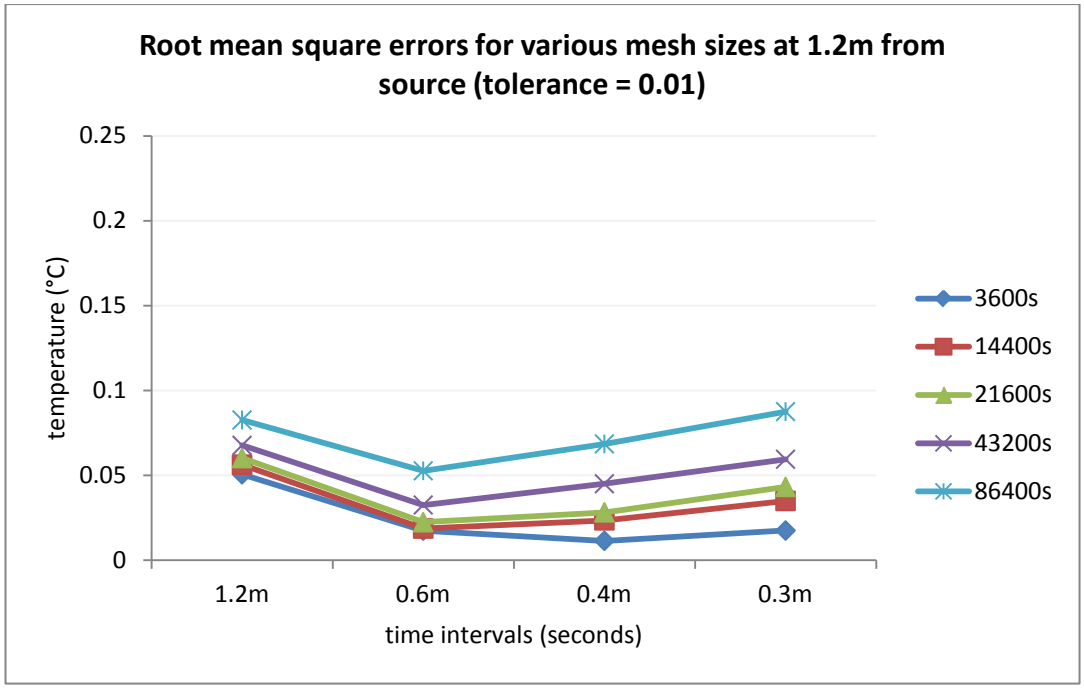

Figure 4.17 Root mean square errors of solving the energy equation with various grid sizes and time increments (tolerance = 0.01)

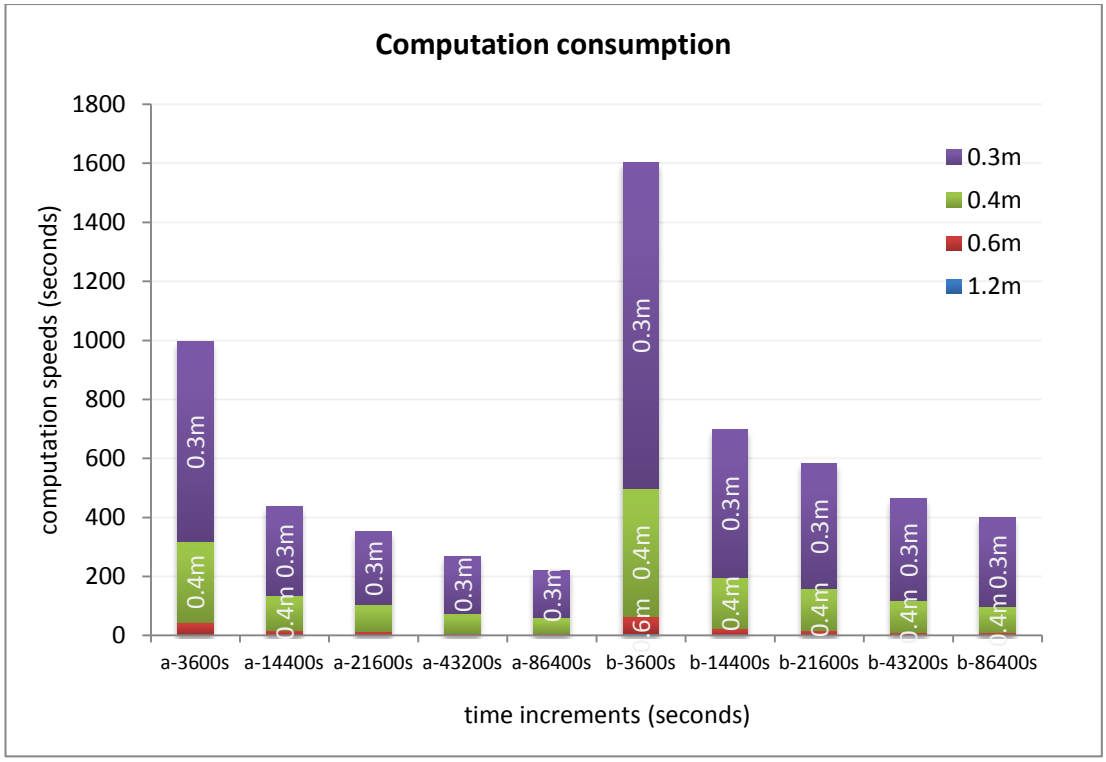

Figure 4.18 Computation consumption of solving the energy equation under two different tolerance settings: a) tolerance = 0.05, b) tolerance = 0.01

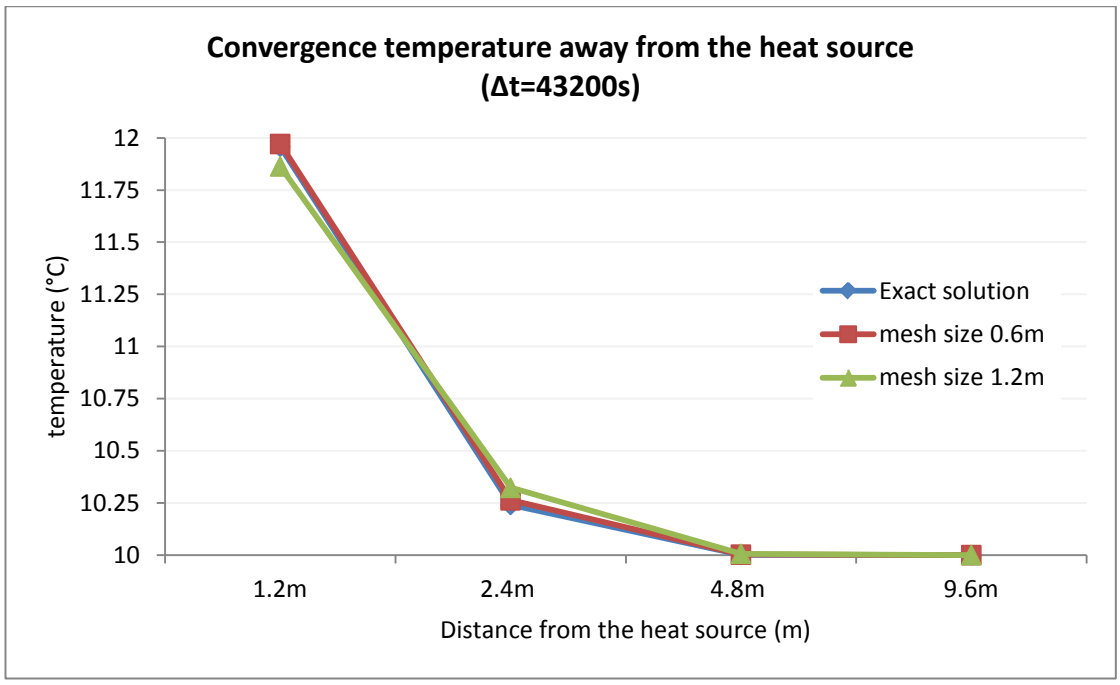

Figure 4.19 Accuracy of the model under the chosen strategy of time steps (43200s), grid arrangement (0.6m) and tolerance (0.05)

4.2.9 Grid dependency study on head equation

The efficiency of solving the head equation under a variety of numerical model configurations was investigated, in which five different time increments (60s, 600s, 1200s, 1800s and 3600s) and four grid mesh sizes (1.2m, 0.6m, 0.4m and 0.3m) were compared.

A line flow source was located in the middle of the field to represent pumped flow. The hydraulic response near to the source was calculated by the discretised head equation and compared with the analytical solution generated using Barry, *et al.*'s (2000) method.

The maximum relative absolute errors associated with the above parameters are shown in Figures 4.20 and 4.21. It is clear that the time step of 10 minutes (600 seconds), mesh size of 0.6m and tolerance setting of 0.1 provided the lowest absolute errors of 0.02m among all the cases.

Figures 4.22 and 4.23, which show the root mean square errors at two different tolerance values, also confirm this. Therefore, the largest possible time increment suitable for solving the head equation should be 600 seconds. The mesh scheme of 0.6m was finally confirmed to be used as it provided acceptable performance for solving both equations.

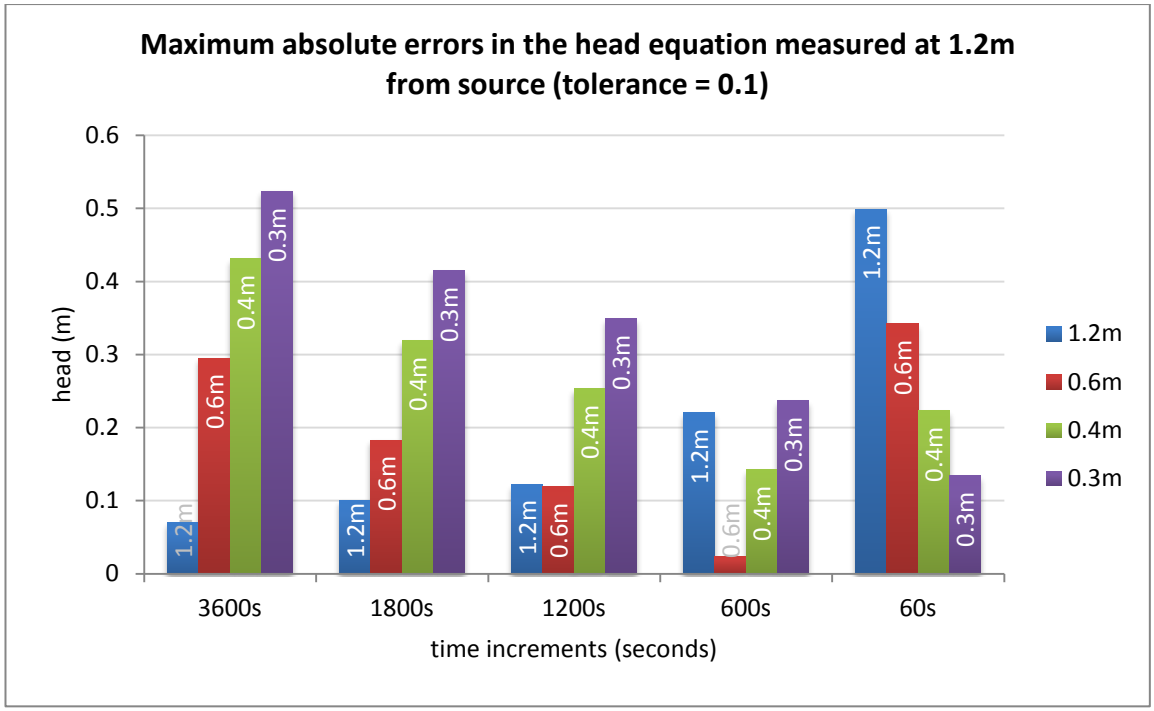

Figure 4.20 Maximum absolute errors of solving head equation with various grid sizes and time increments (tolerance = 0.1)

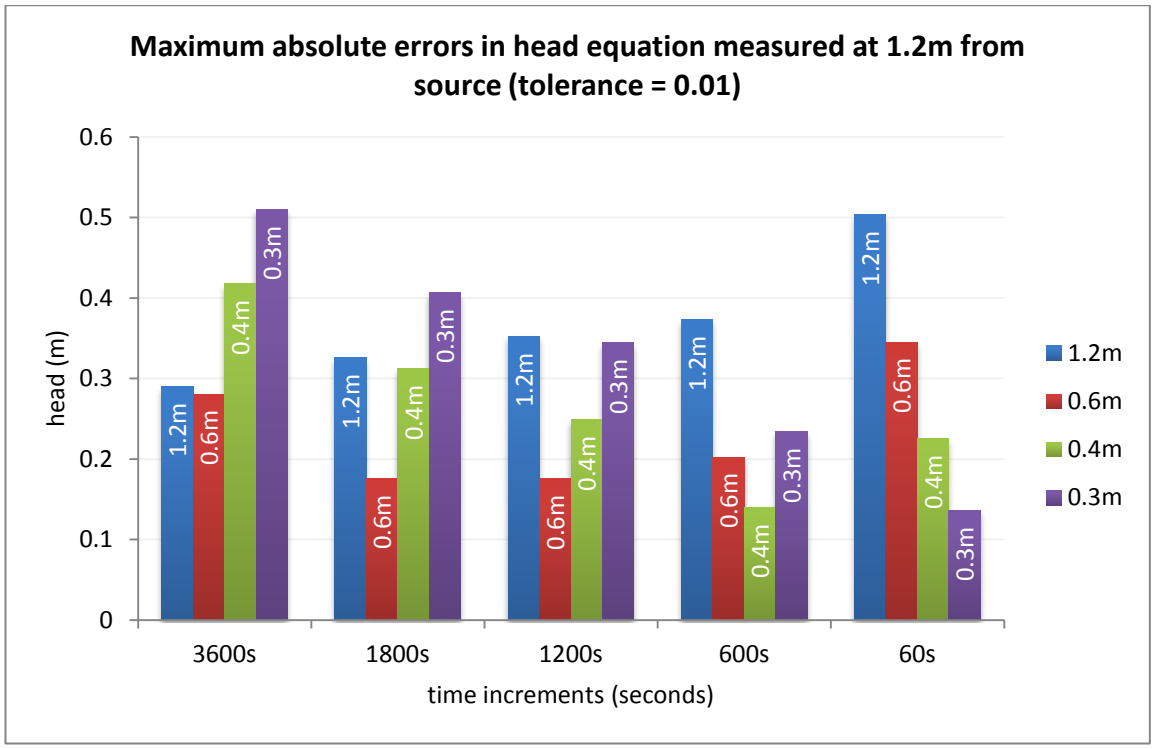

Figure 4.21 Maximum absolute errors of solving head equation with various grid sizes and time increments (tolerance = 0.01)

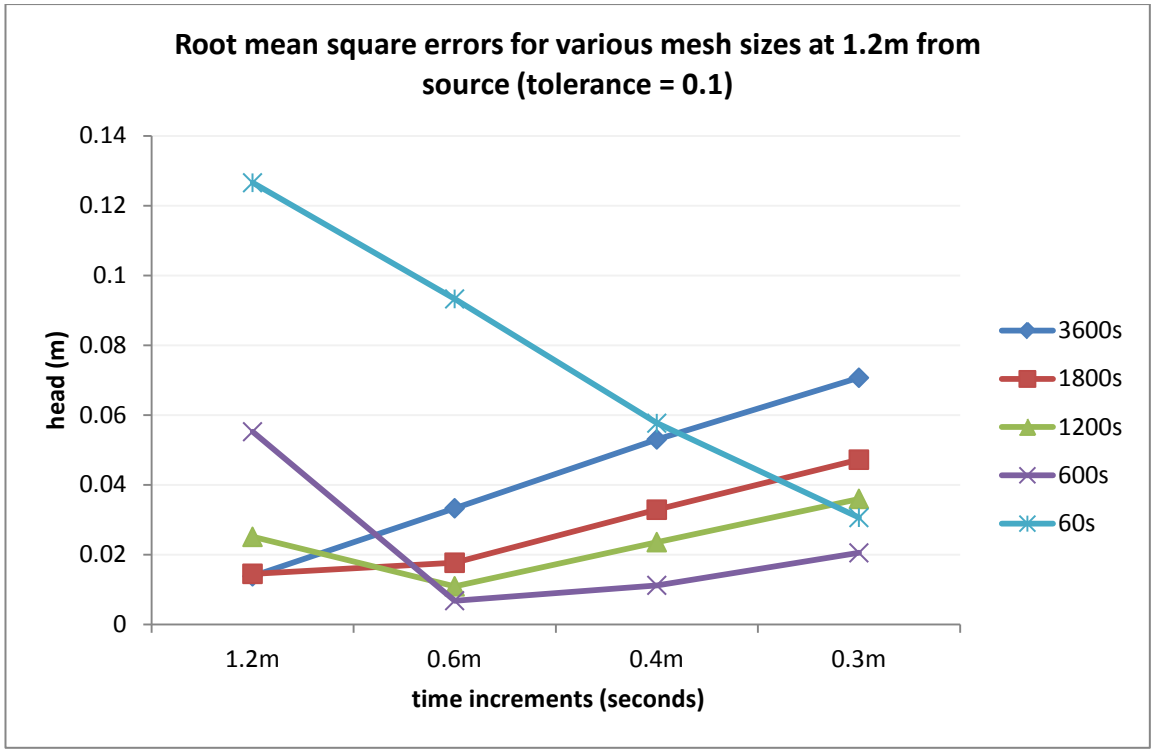

Figure 4.22 Standard errors of solving head equation with various grid sizes and time increments (tolerance = 0.1)

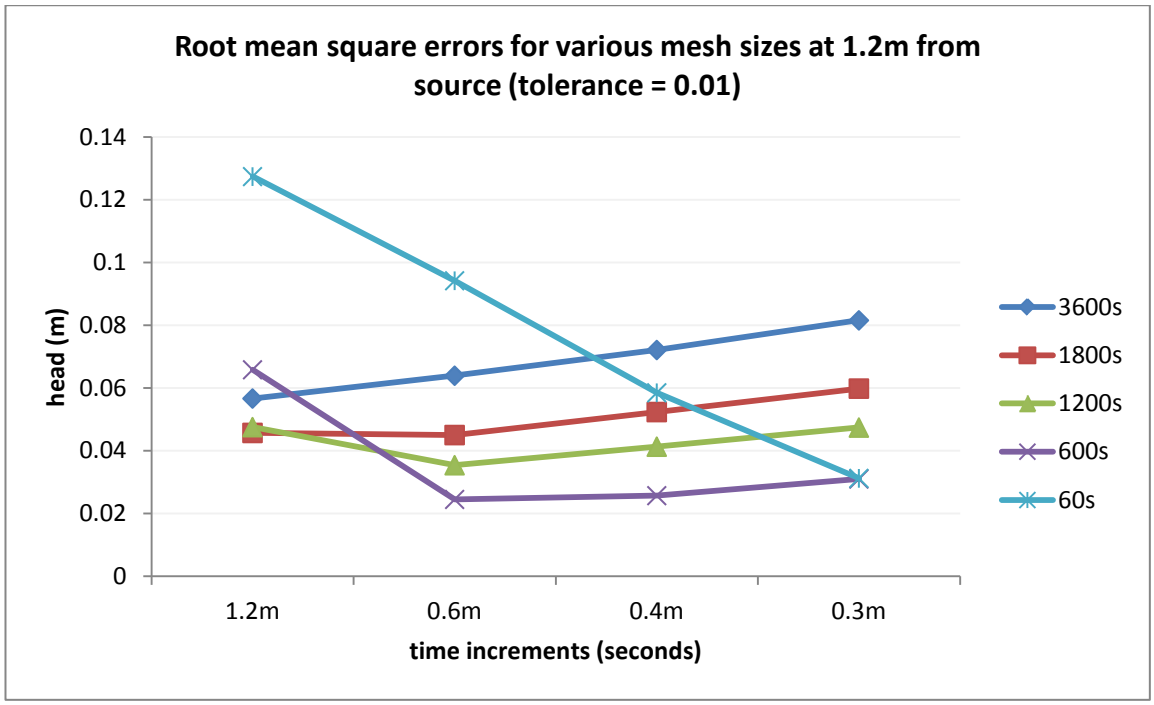

Figure 4.23 Standard errors of solving head equation with various grid sizes and time increments (tolerance = 0.01)

4.3 Well model development

4.3.1 Concept of the well model

In this work, SCW construction is taken to consist of a well borehole in which an internal suction 'sleeve' pipe is located. The suction pipe extends the full extent of the well and it opens at the bottom. A submersible pump is placed into the suction pipe at a location below the well static water level (the extent below the static water level will be very low and determined by the drawdown, which will be zero during balanced flow and quite small during bleed operation). A bottom-entry submersible pump thus draws well water up through the suction pipe from its open end at the bottom of the well. Return well water is discharged at the top of the well. There will be an annulus formed between the outside of the suction pipe and the well wall. The width of the annulus will be one half of the difference between the well's diameter and the suction pipe's outside diameter. Figure 4.25 illustrates the concept.

An energy balance for the water in the annulus will be:

Equation 4.4

$$C_{\mathrm{A}}\frac{\partial T_{\mathrm{A}}}{\partial t} - c_{\mathrm{pw}}\frac{\partial m_{\mathrm{A}}T_{\mathrm{A}}}{\partial z} - Q_{\mathrm{A}} - Q_{\mathrm{S}} = 0$$

where:

C_{A} = annulus thermal capacity ($JK^{-1}m^{-1}$)

m_{A} = water mass flow rate in the annulus (kgs^{-1})

T_{A} = annulus water temperature (°C)

c_{pw} = specific heat capacity of water ($Jkg^{-1}K^{-1}$)

Q_{A} = heat transfer (annulus to rock, $\mathrm{Wm^{-1}}$)

$= AU_{\mathrm{A}}(T_{\mathrm{f}} - T_{\mathrm{A}}) + c_{\mathrm{pw}}\, m_{\mathrm{bleed}}\, T_{\mathrm{f}}$

Q_{S} = heat transfer (annulus to suction pipe, $\mathrm{Wm^{-1}}$)

$= AU_{\mathrm{sp}}(T_{\mathrm{s}} - T_{\mathrm{A}})$

where:

m_{bleed} = bleed water flow rate (m_{w}) at each dz level due to the pressure difference between the standing column well and rock ($\mathrm{kg\ s^{-1}}$)

$= \frac{\sum m_{\mathrm{w}}}{\partial z}$

AU = heat transfer rate ($\mathrm{WK^{-1}}$). The subscript A and sp represent the annulus wall (A) and the suction pipe (sp) wall

T_{f} = the field temperature (from the field model) where the SCW is located (°C)

m_{bleed} = the bleed rate ($\mathrm{kg\ s^{-1}}$)

$= \frac{\sum m_{\mathrm{w}}}{\partial z}$

An energy balance in the suction pipe can be expressed as:

Equation 4.5

$$C_{\mathrm{sp}} \frac{\partial T_{\mathrm{s}}}{\partial t} - m_{\mathrm{sp}} c_{\mathrm{pw}} \frac{\partial T_{\mathrm{s}}}{\partial z} + Q_{\mathrm{s}} = 0$$

where:

m_{sp} = total pumped water flow rate (kgs^{-1})

C_{sp} = heat capacity of the suction pipe water ($JK^{-1}m^{-1}$)

T_s = suction pipe water temperature (°C)

The well equations describe zones of much lower thermal capacity than the parent field equations. Therefore, they need to be solved at a much lower time increment. The spatial increment along the *z* plane for the well equations was chosen to be the same as that of the field model equations (0.6m). Trial and error suggested a suitable time increment for the well equation of 60s and that an explicit discretisation scheme could be applied with little consequence on computation cost, due to a relatively low number of calculations for the well equations. Therefore, the well equations were solved using an explicit ('forward-marching') scheme with an integration interval of 60s. At each time accumulation of 600s, a call was made to the field model equations with the current well wall heat transfer rate and bleed flow rate passed directly into the field equation source terms. In turn, the field model equations were solved using a fully implicit Gauss-Seidel scheme. Figure 4.24 shows the resulting model structure.

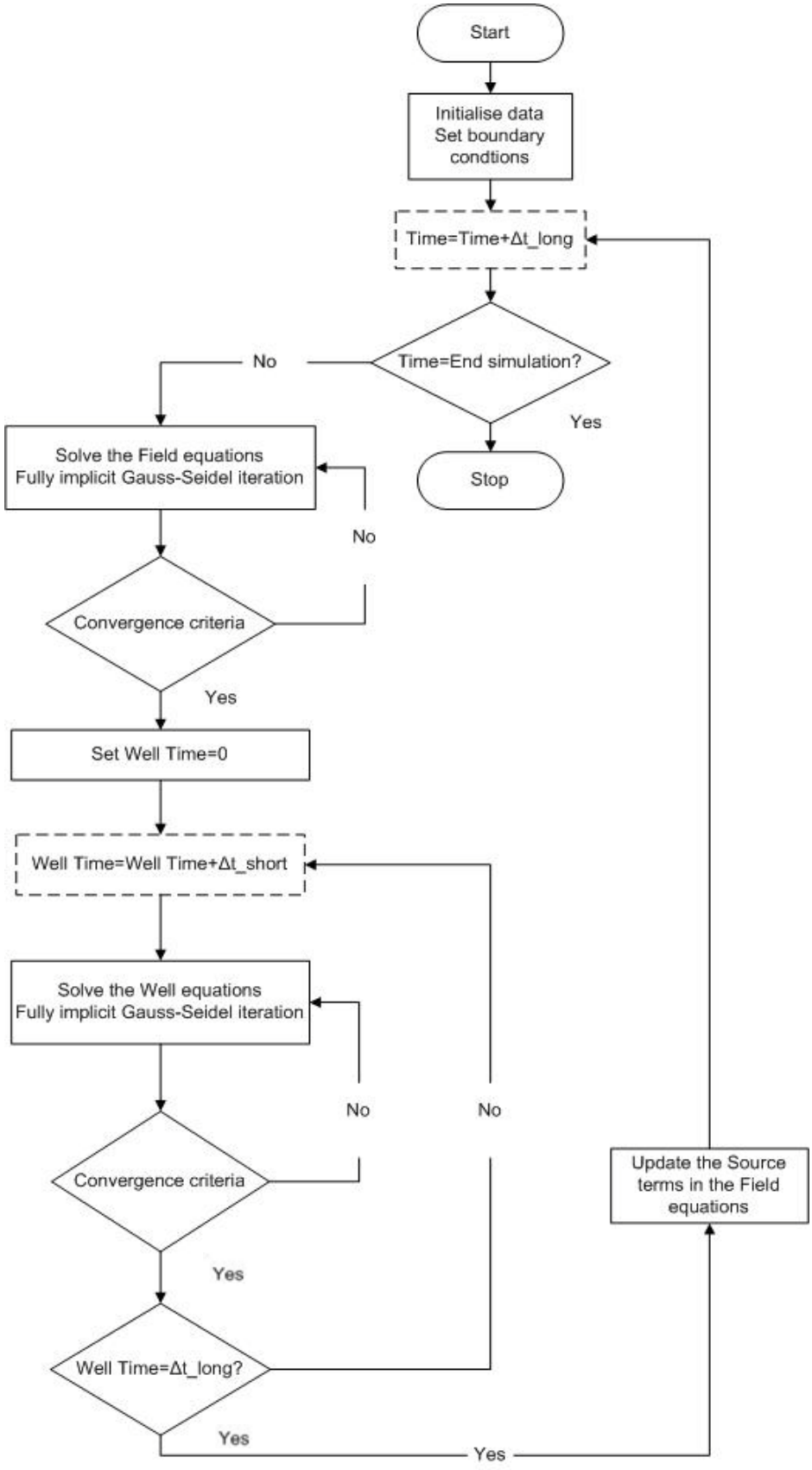

Figure 4.24 Flow chart of the computer algorithm of the SCW model

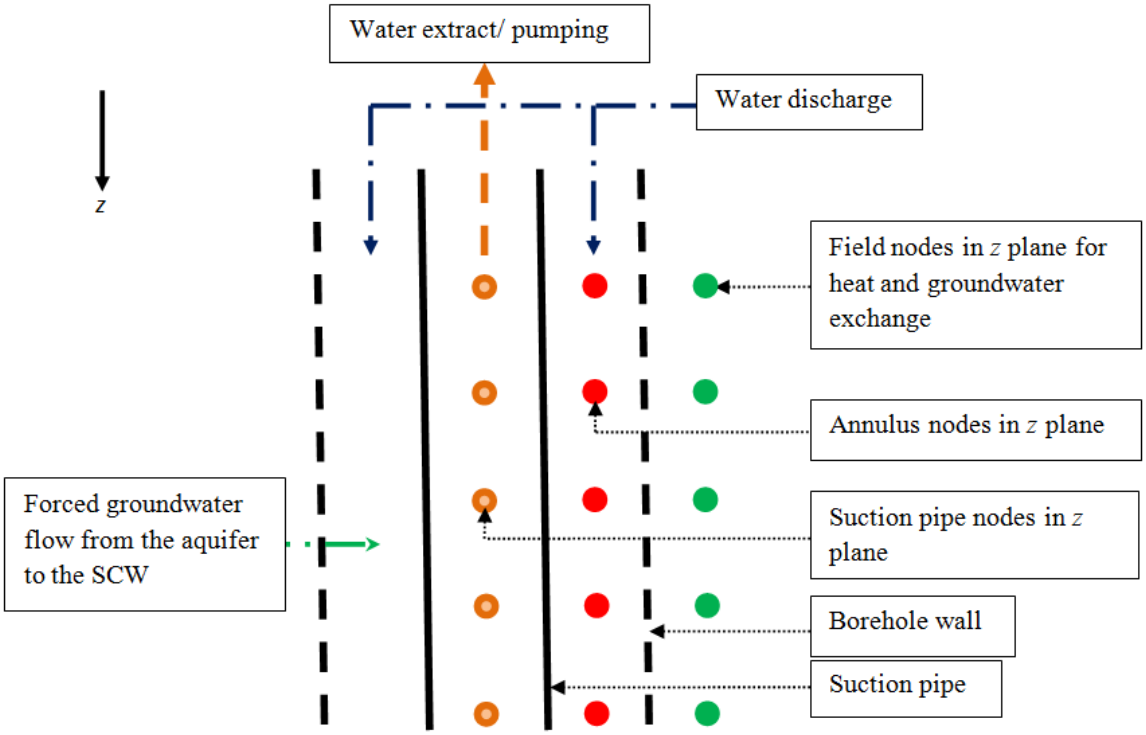

Figure 4.25 Cross section of the well model (the borehole and pipe wall resistance are omitted in this figure)

4.3.2 Convection heat transfer in the well

The ratio of convective to conductive heat transfer in the borehole is expressed by the Nusselt number (Nu), which was determined from the flow characteristics (the Reynolds number - Re) and the properties of the water (the Prandtl number - Pr). The relationships between Nu, Re and Pr can be found in figure 4.26. The convective coefficient can be derived from the Nusselt number and reflected in the borehole and suction pipe surface resistances to account for the heat transfer by both mechanisms. Gnielinski's simplified correlations were used in this work for convection across the inner annulus and suction pipe surfaces (Holman, 1997).

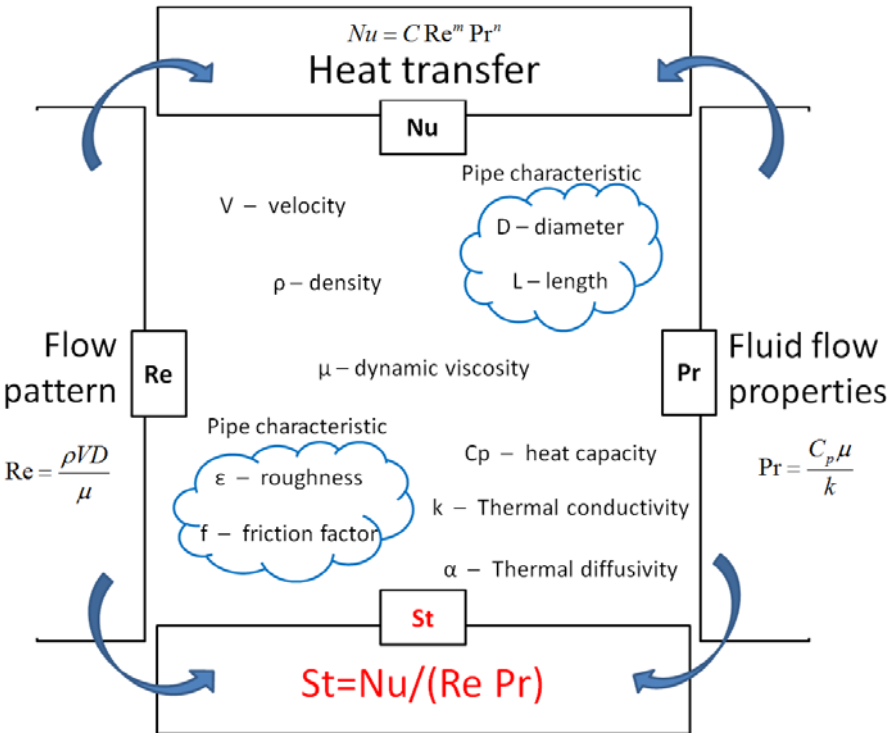

Figure 4.26 Relationships between Nu (Nusselt Number), Re (Reynolds number), Pr (Prandtl Number)

The borehole surface is normally rougher than the surface of the suction pipe, depending on the local geologic formation and also the drilling process. In some cases, a well screen may be applied and the roughness of a generic screen is about 3mm to 10mm. In general, the heat transfer rate of the well can be improved by increasing the surface roughness. In addition, enlarging the size of the well increases the heat transfer area; hence increasing the heat transfer rate too. However, in a semi-open-loop system such as a SCW, there is a penalty on pumping cost by increasing the well size.

All these physical aspects of SCWs (including the shape, surface and size of the well boreholes) increase the challenge of estimating heat transfer performance, since conventional correlations for circular smooth tubes/pipes are inapplicable. A detailed analysis of this aspect is therefore warranted and this follows in the next section.

4.3.3 Development of a convection heat transfer correlation for SCWs

Experiments have proven that internal water flow heat transfer characteristics in a narrow annulus are different from those in a circular tube (Dirker & Meyer, 2002; Lu & Wang, 2008). Lu and Wang (2008) indicated that the transition from laminar flow to turbulent flow appeared earlier in a narrow annulus than in circular tubes in the range of Reynolds numbers from 800 to 1200. Dirker and Meyer (2002) expressed a relationship between the annular diameter ratios and heat transfer performance, and also indicated that the conventional correlation for turbulent flow in circular smooth tubes (Dittus-Boelter) underestimates the Nusselt number, particularly in large annular diameter ratios. These sources suggest that most of the conventional empirical correlations (Sieder & Tate, 1936; Petukhov, 1970; Gnielinski, 1976; Dittus & Boelter, 1985) based on circular tubes may not be suitable to use directly to assess the heat transfer performance in SCW systems. Therefore, a detailed analysis is conducted in this section to evaluate suitable surface heat transfer coefficients for

rough well walls forming the outer surfaces of narrow annuli within SCWs. Computational fluid dynamics (CFD) simulations are used for this purpose.

The aim of the CFD simulations is to analyse the heat transfer mechanism in these annuli, particularly for SCW design under various roughness and fluid flow conditions.

A commercial CFD software (Phoenics) (Spalding, 1974) was adopted for this task. A simple annulus channel was built within the Phoenics environment; the predicted inlet and outlet water temperatures under a range of well wall screening (surface) roughness (3mm to 10mm), flow velocities (0.25ms^{-1}, 0.75ms^{-1}, 1.25ms^{-1} and 1.75ms^{-1}) and annulus diameters (hydraulic diameters of 0.05m, 0.1m and 0.15m) were used in the analysis. In practice, well screening might not be needed where the formation is firm and consolidated. The initial diameters of the borehole and outer suction pipe were 0.15m and 0.1m, respectively, giving an annulus equivalent hydraulic diameter of 0.05m. The suction pipe diameter was maintained at 0.1m, whilst alternative well borehole diameters of 0.2m and 0.25m were also considered. Due to the relatively low range of water temperatures likely to be experienced in a wide range of SCW operations, it was possible to keep the Prandtl number constant at 10.5 for this analysis. The results from the CFD simulations were translated into Nusselt numbers and compared with Lu & Wang's (2008) correlations (Equations 4.6 and 4.7).

Equation 4.6

$Nu = 0.0059Re^{0.99}Pr^{0.4}$ correlation (1)

with an application range of *Re > 1200* and *4.7 < Pr < 6.6*

Equation 4.7

$Nu = 0.00222Re^{1.09}Pr^{0.4}$ correlation (2)

with an application range of *Re > 3000*

4.3.4 CFD modelling results

The results are divided into three groups according to the annulus hydraulic diameter (D_h). These are:

- Group 1: D_h = 0.05m
- Group 2: D_h = 0.1m
- Group 3: D_h = 0.15m.

Due to the shape of the annulus (non circular tube), hydraulic diameter is used:

Equation 4.8

$$D_h = 2\,(r_{scw} - r_{sp})$$

where:

r_{scw} = radius of the well (m)

r_{sp} = radius of the suction pipe (m)

i. Group 1

At a velocity of 0.25ms^{-1} (Figure 4.28), the CFD simulation results achieved very good agreement with both of Lu & Wang's correlations (particularly with correlation (2) for narrow channels), with maximum percentage errors of 2.4%. The differences between correlations (1) and (2) were not significant in a low Reynolds number flow situation. In this case (D_h = 0.05m and V = 0.25ms^{-1}), the Reynolds number varied from 8833 to 10000 depending on the roughness value. When increasing the velocity, the approximations from the CFD simulations were considerably lower than the estimations from both correlations,

but the results were closer to correlation (1) than (2), with maximum percentage errors from correlation (1) of 16.2%, 18.6% and 19.4% for the velocities 0.75ms^{-1}, 1.25ms^{-1} and 1.75ms^{-1}, correspondingly.

In general, the Nusselt number increased as the surface roughness increased. In this simulation, the surface roughness increased by 0.002m at every step and the initial roughness was 0.003m. The CFD results indicate that a significant improvement in the heat transfer rate (i.e. the Nusselt number) due to higher roughness values would be achievable for the first three increments of roughness (from 0.003m to 0.009m), as shown in Figure 4.27. Under turbulent flow condition, the benefit of increasing the surface roughness is very significant throughout the entire velocity range (0.25ms^{-1} – 1.75ms^{-1}) in this case. However, this influence reduced dramatically after the roughness reached 0.009m. In addition, the Nusselt number also increased as the velocity increased, but the rate of increase reduced after a certain velocity was reached. In this case, the optimal velocity was 1.25ms^{-1}. In Figure 4.27 it can be seen that surface roughness was not included in Lu & Wang's (2008) correlation as an input variable and hence the impact on the roughness associated with different levels of velocity was not significant.

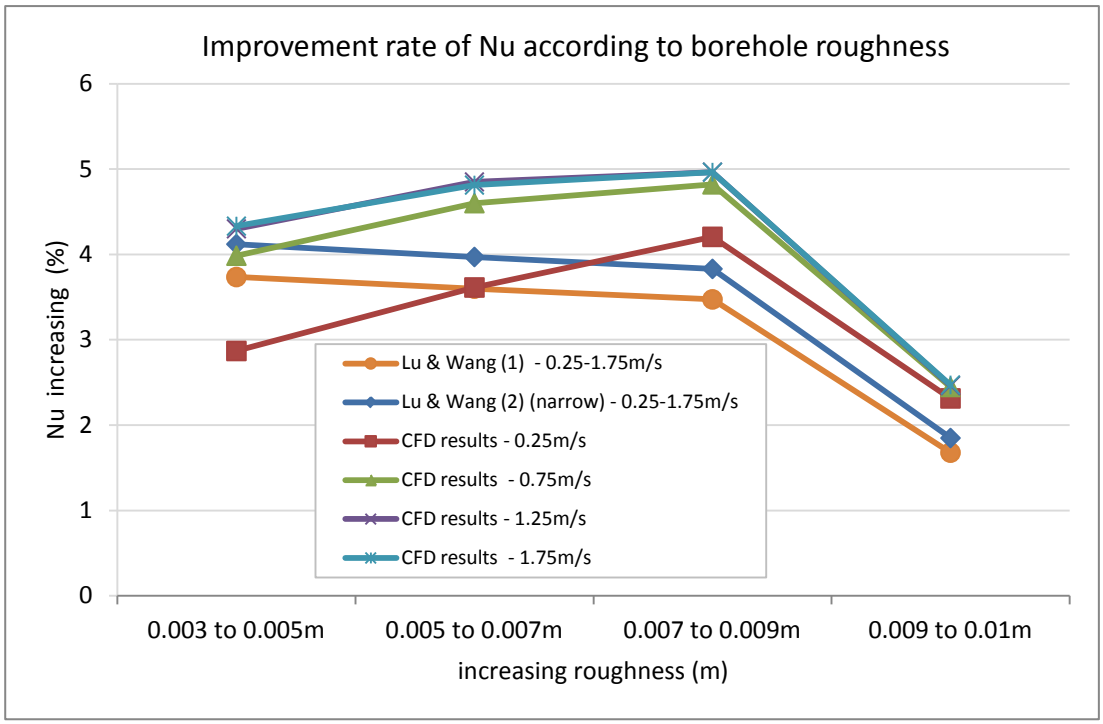

Figure 4.27 Improvement rate of the heat transfer performance (i.e. Nu) according to roughness on the borehole wall (based on the results in Group 1)

ii. Group 2

In group 2, the best agreement between the CFD simulation results and Lu & Wang's (2008) estimations occurred at the lowest velocity of 0.25ms^{-1}, as was the case with the results in Group 1, with maximum errors of 5.1% and 4.9% for correlations (1) and (2), respectively. This was because the Re range covered at this velocity (0.25ms^{-1}) in this group was closer to the Re values used in Lu & Wang's (2008) experiment (from 10000 to 30000). In the case of D_h = 0.1m and V = 0.25ms^{-1}, the Re varied from 17166 to 18333 across the whole range of roughness values (0.003m to 0.1m). The results at other velocities were found to lie between correlations (1) and (2). Interestingly, the approximations from the CFD simulations at lower roughness values were closer to the prediction from correlation (1); however, they approached correlation (2) as the roughness value increased. It is obvious that the heat transfer improvement rate associated with roughness is more pronounced with the CFD

simulations than with Lu & Wang's (2008) correlations, as represented by slightly steeper slopes in Figures 4.33, 4.34 and 4.35.

iii. Group 3

The CFD model in this group contained the largest annulus space, with a hydraulic diameter of 0.15m. The disagreement between the CFD results and Lu & Wang's (2008) estimation was large, with a maximum disagreement of 46% occurring at the lowest velocity option ($0.25ms^{-1}$). This is to be expected as the range of the Re and the annulus size in this group were completely out of the range applicable to Lu & Wang's (2008) experiment.

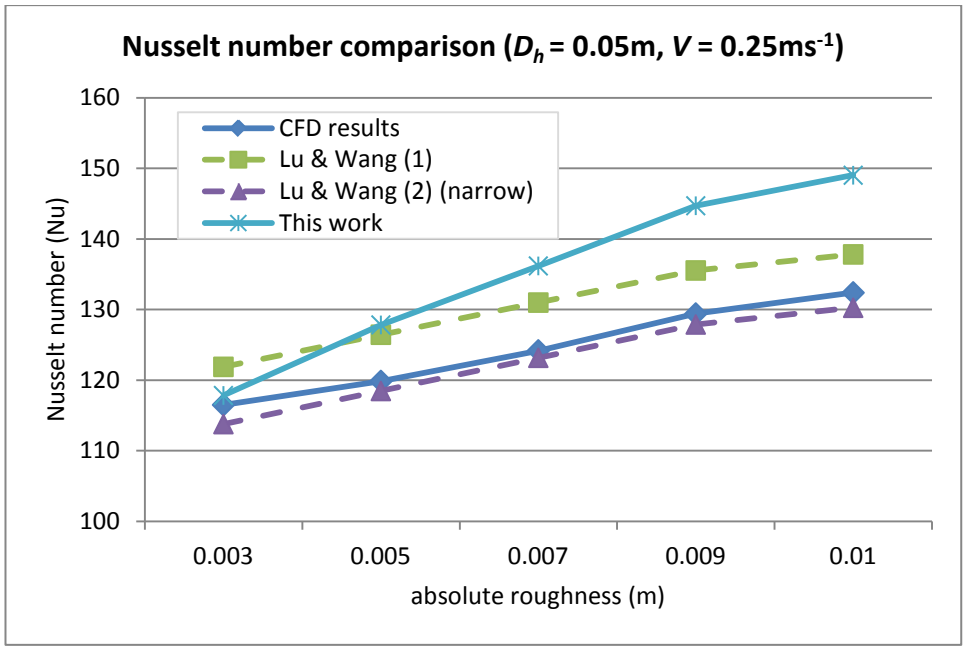

Figure 4.28 Group 1 results – hydraulic diameter = 0.05m, velocity = $0.25ms^{-1}$

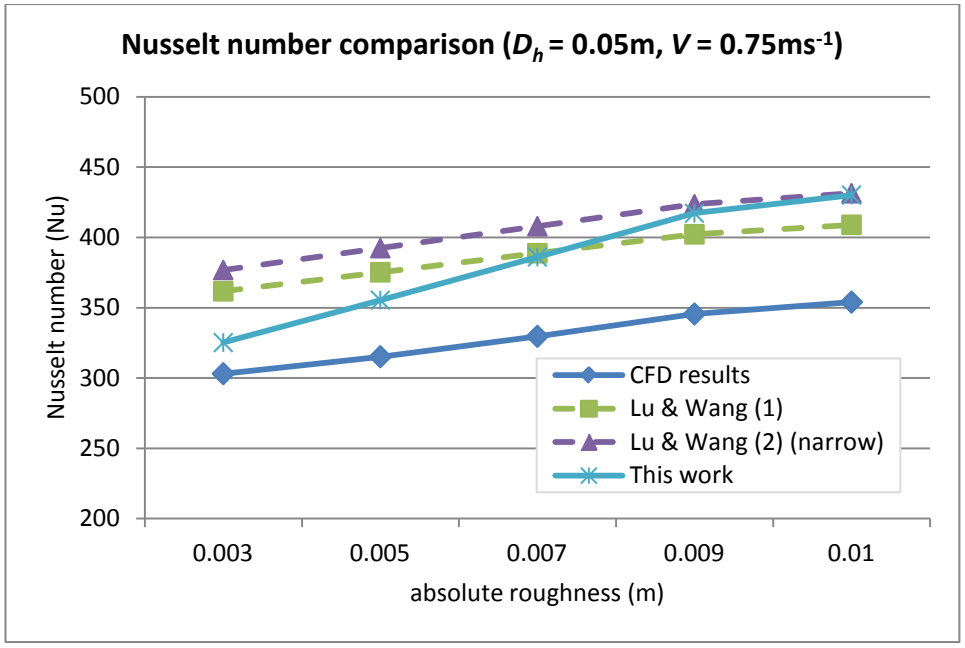

Figure 4.29 Group 1 results – hydraulic diameter = 0.05m, velocity = 0.75ms^{-1}

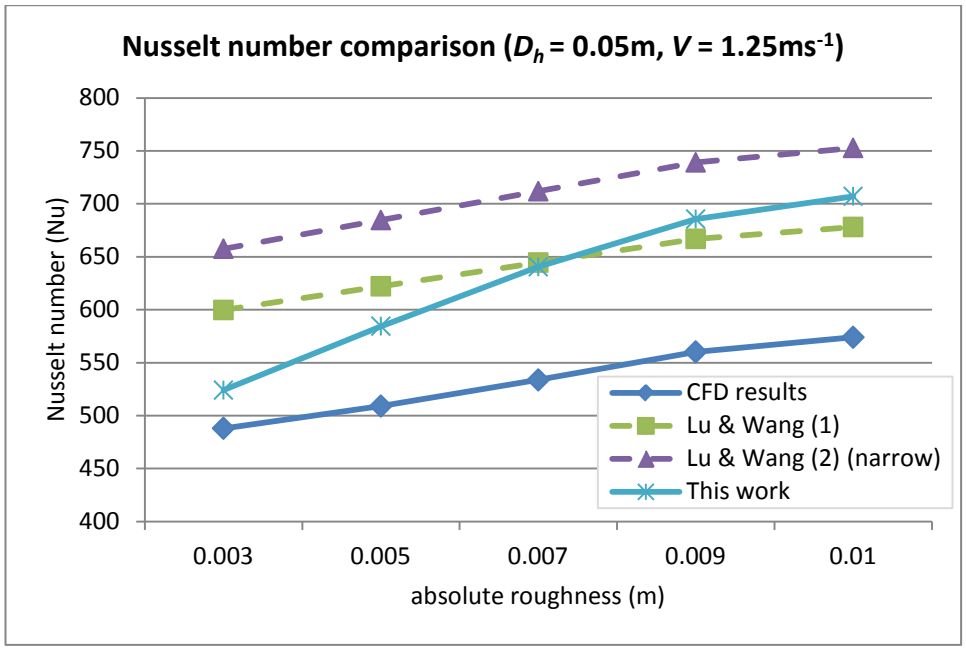

Figure 4.30 Group 1 results – hydraulic diameter = 0.05m, velocity = 1.25ms^{-1}

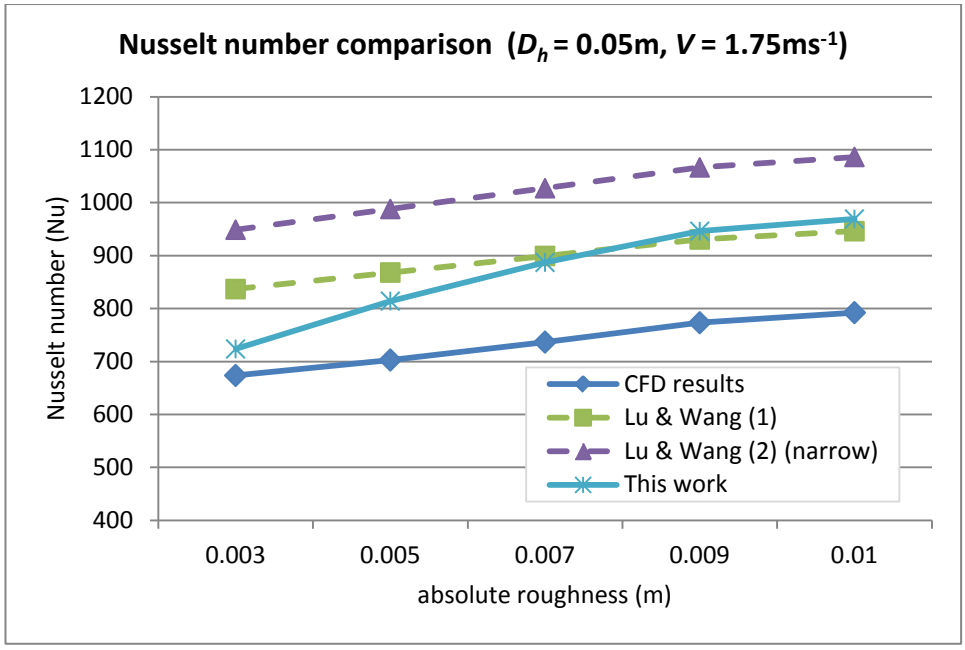

Figure 4.31 Group 1 results – hydraulic diameter = 0.05m, velocity = 1.75ms^{-1}

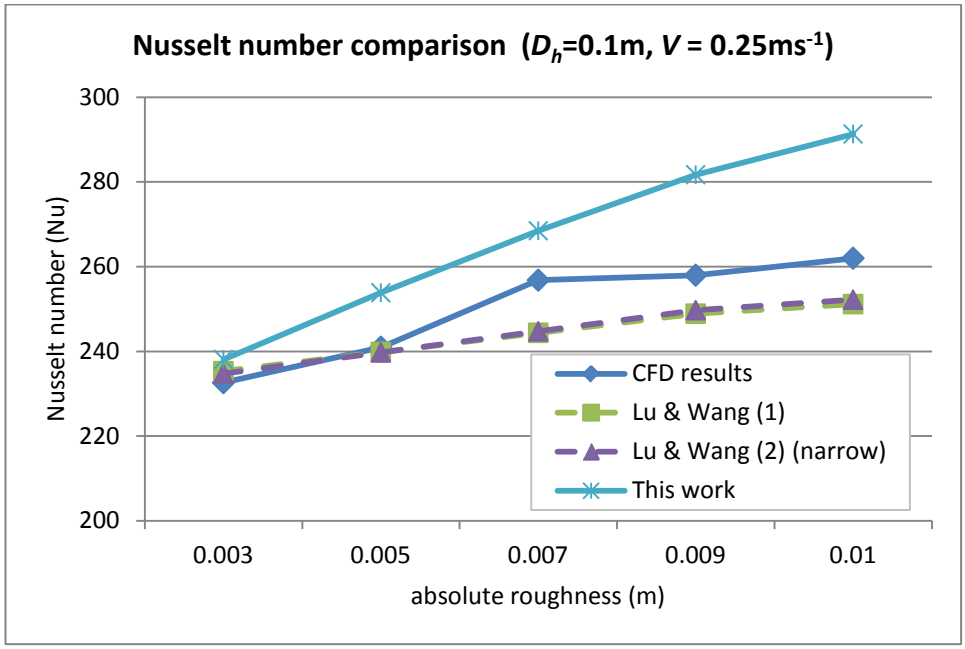

Figure 4.32 Group 2 results – hydraulic diameter = 0.1m, velocity = 0.25ms^{-1}

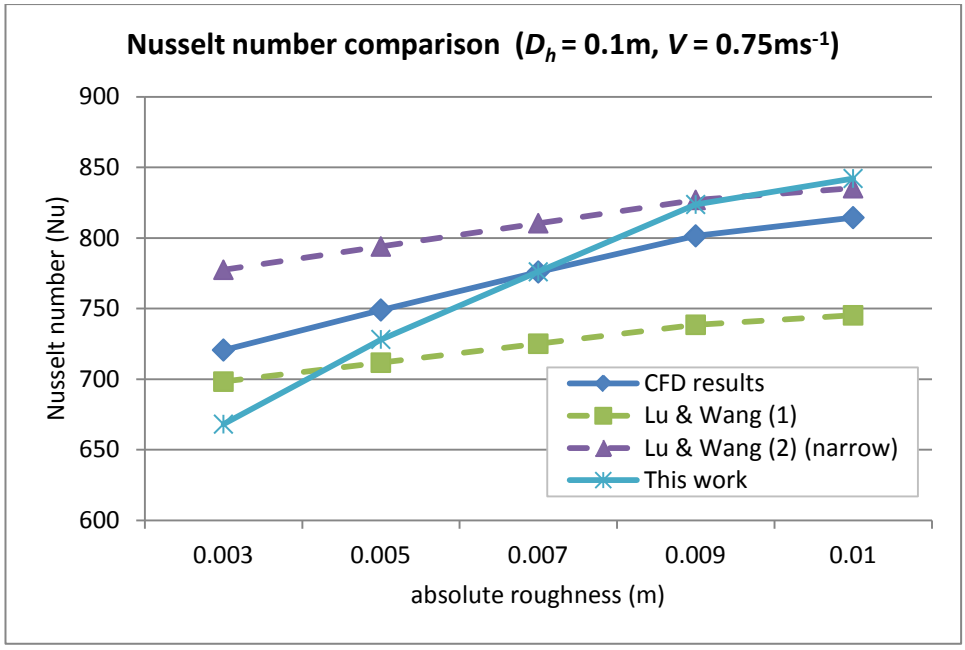

Figure 4.33 Group 2 results – hydraulic diameter = 0.1m, velocity = 0.75ms^{-1}

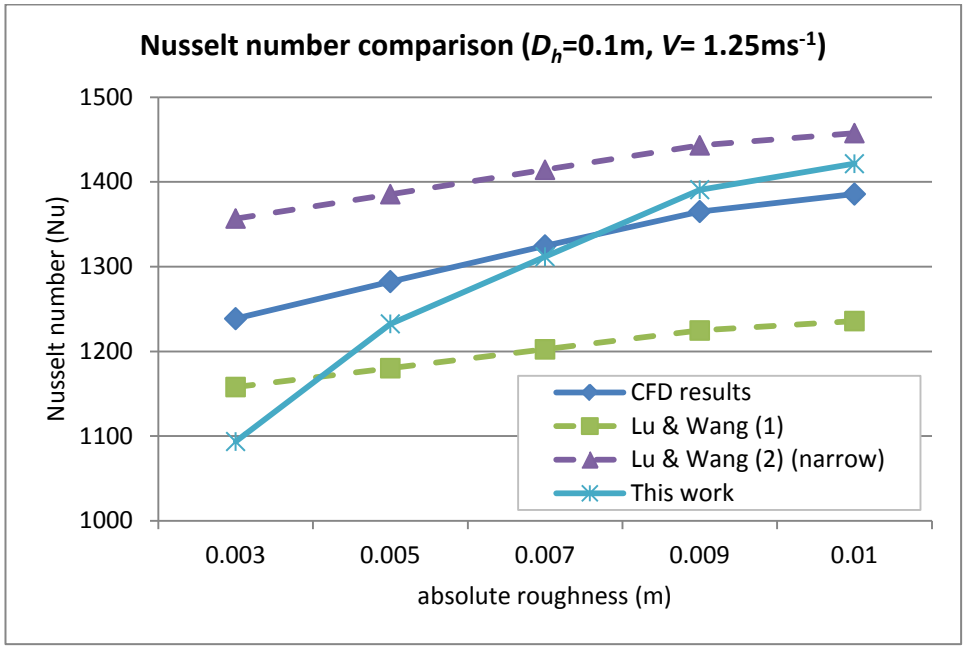

Figure 4.34 Group 2 results – hydraulic diameter = 0.1m, velocity = 1.25ms^{-1}

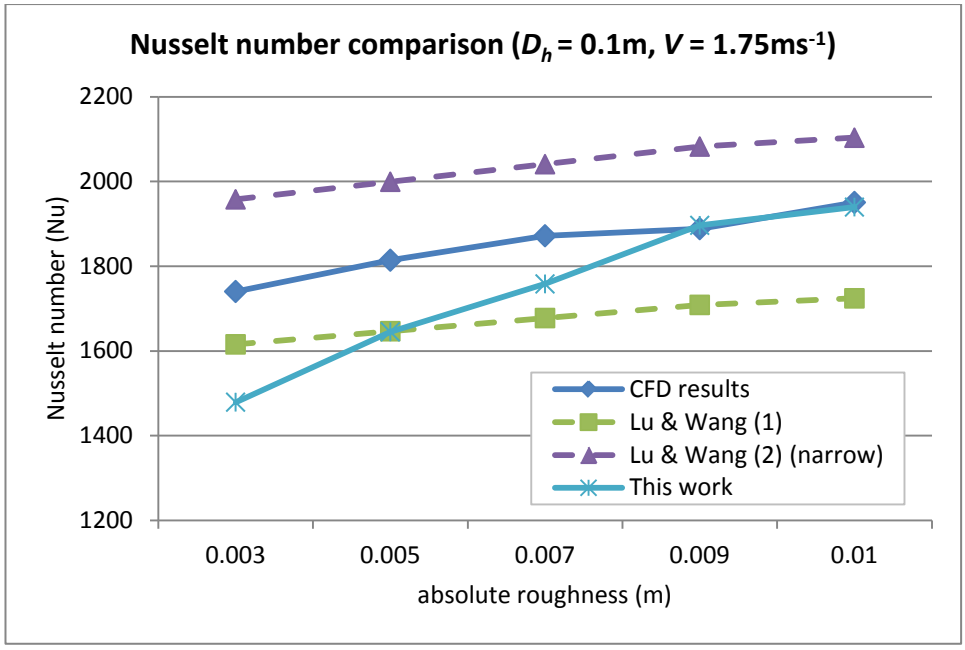

Figure 4.35 Group 2 results – hydraulic diameter = 0.1m, velocity = 1.75ms^{-1}

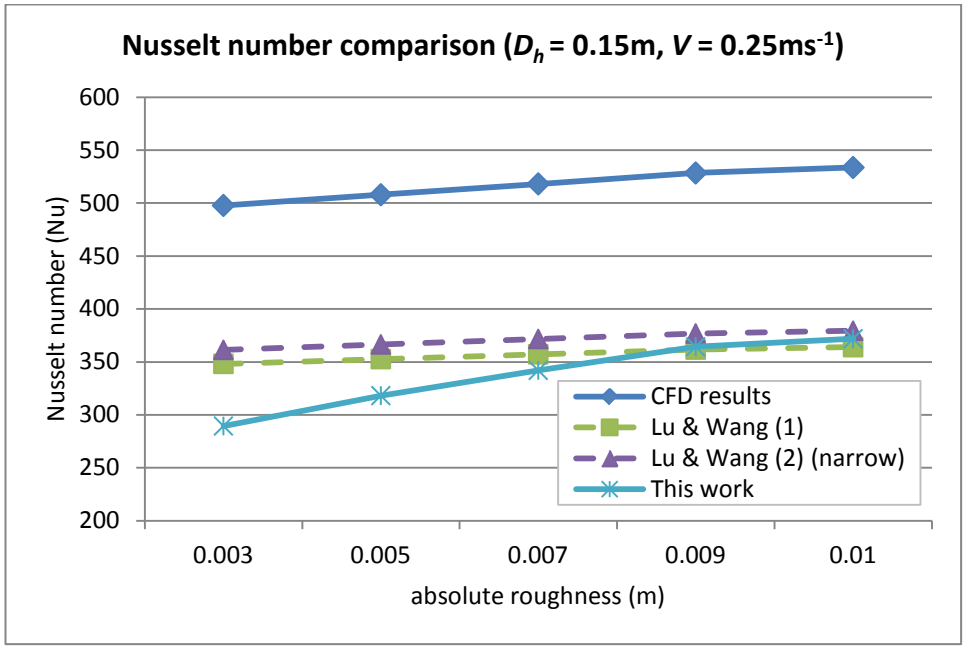

Figure 4.36 Group 3 results – hydraulic diameter = 0.15m, velocity = 0.25ms^{-1}

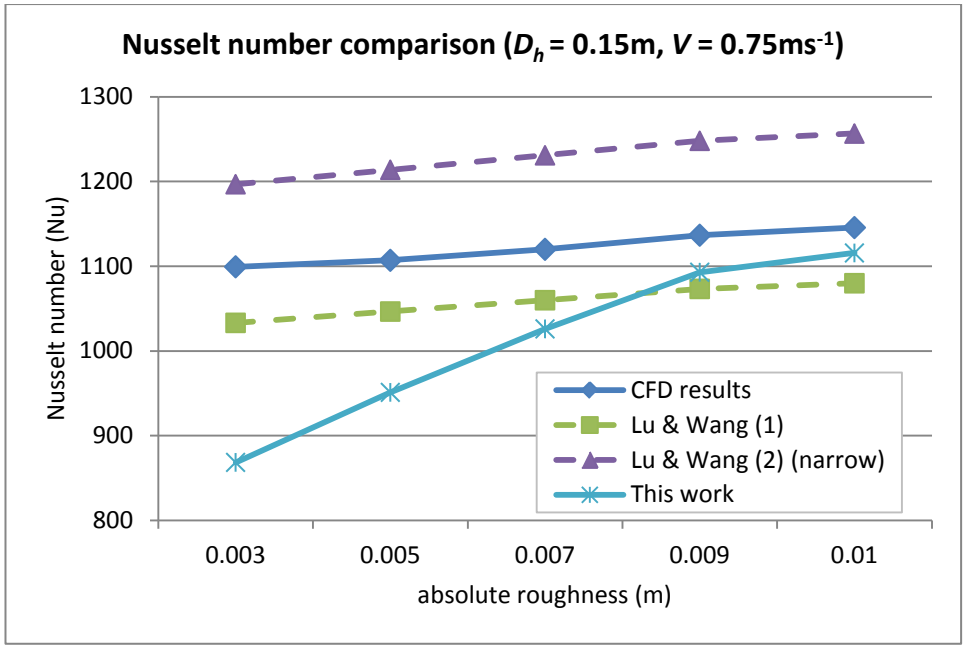

Figure 4.37 Group 3 results – hydraulic diameter = 0.15m, velocity = 0.75ms^{-1}

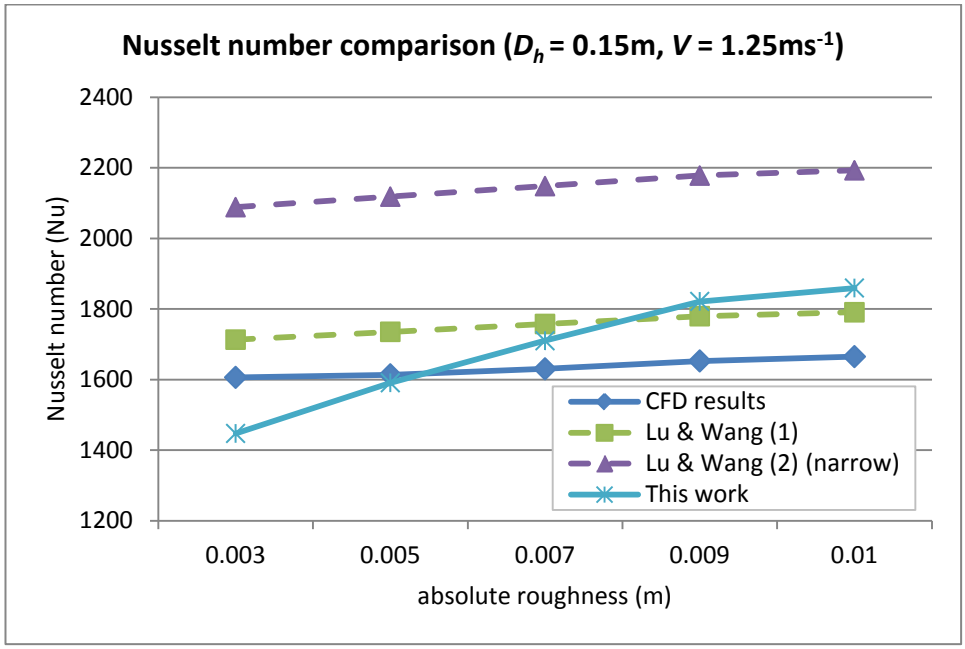

Figure 4.38 Group 3 results – hydraulic diameter = 0.15m, velocity = 1.25ms^{-1}

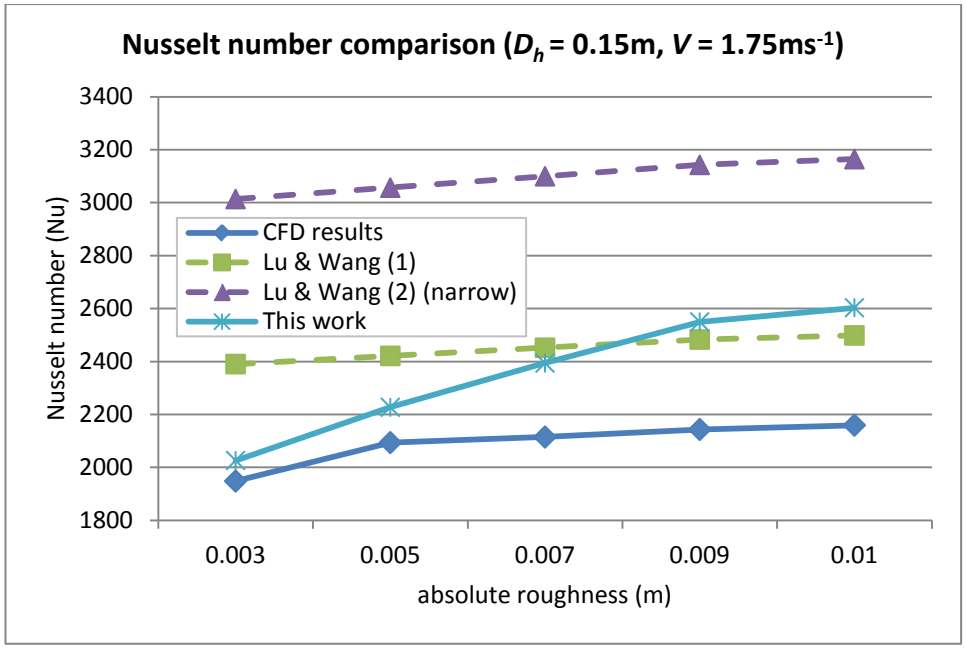

Figure 4.39 Group 3 results – hydraulic diameter = 0.15m, velocity = 1.75ms^{-1}

Petukhov's (1970) correlation for smooth tubes was adopted as a basis to form a new correlation (Equation 4.9) covering the range of roughness values, Reynolds numbers and annulus sizes applicable to standing column well design. The data from the CFD simulations was utilised to modify the constants in his correlation as follows:

Convection heat transfer correlation for SCW:

Equation 4.9

$$Nu = \frac{10.5\left(\frac{f}{8}\right)\mathrm{Re_D}}{0.26 + 47.88\left(\frac{f}{8}\right)^{\frac{1}{2}}}$$

The correlation was verified with Lu & Wang's correlation (2008) for a wide range of Reynolds numbers, as shown in Figures 4.40 and 4.41.

The correlation agreed well with Lu & Wang's correlation (1) for a wide range of Re. The highest percentage error was only 6.7%, occurring at the smallest value of Re, but the percentage error reduced significantly at higher values of Re to as low as 0.7%.

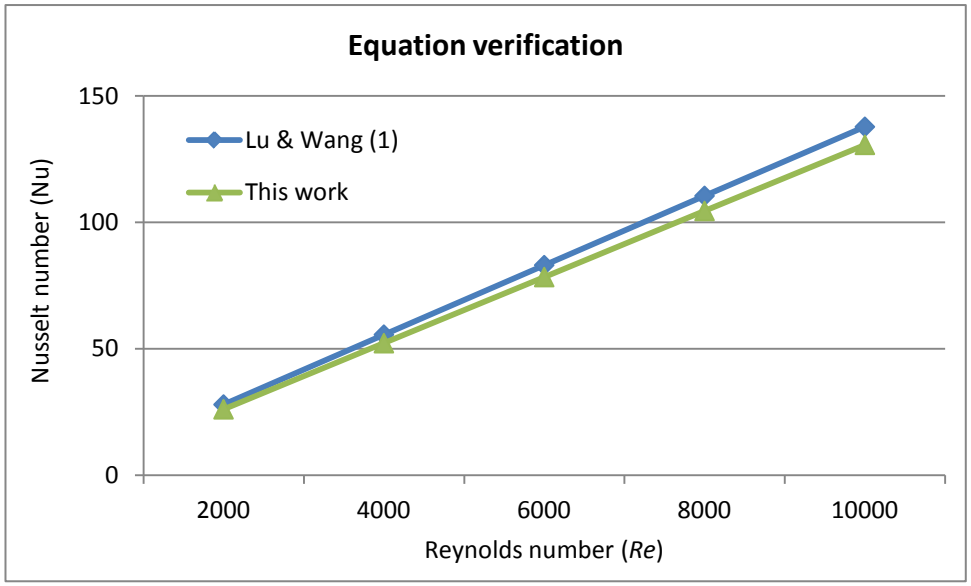

Figure 4.40 Equation verification results, *Re* from 2000 to 10000

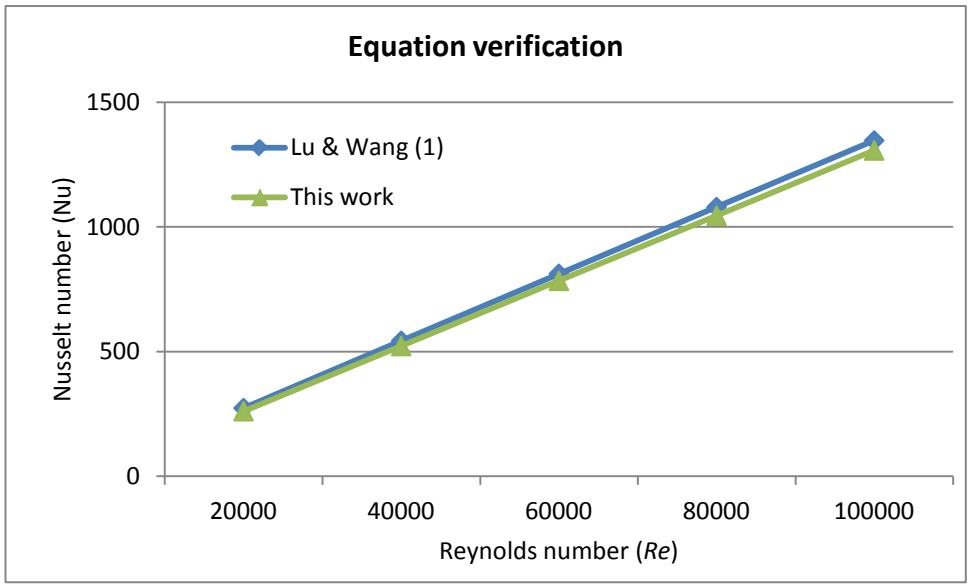

Figure 4.41 Equation verification results, *Re* from 20000 to 100000

5. Model validations

Three alternative model verification tests were carried out using experimental data obtained from a variety of field tests. The first test made use of results from a short-time thermal response test in order to evaluate the energy prediction behaviour of the model. The second used data from a short-time pumping test in order to evaluate head predictions; the third test made use of longer term field data from a single SCW installation in order to evaluate the complete model behaviour. The performance of the model was determined by comparing the numerical predictions with the experimental measurements.

5.1 Model verification with thermal response test data

A thermal response test (TRT) was carried out in June 2007 on a test borehole heat exchanger at a site in the centre of Gateshead, Tyne & Wear. The geology consisted of Coal Measures comprising mudstone, sandstone and coal seams.

A heat source of 3kW was applied to a 52m deep U-tube collector for 68.8 hours to interpret the effective ground thermal conductivity and borehole thermal resistance based on the line 'sink' assumption, as represented in Equation 5.1. The thermal parameters evaluated from this method are only valid for values of time where $4at/r_b^2 > 20$ (Ingersoll *et al.*, 1950) (i.e. $t > 5\ r_b^2/a$; t > 300 minutes in this case).

Line sink equation:

Equation 5.1

$$\Delta T = \frac{Q}{4\pi k_{\mathrm{eff}} H}\ln(t) + \frac{Q}{4\pi k_{\mathrm{eff}} H}\left[\ln\left(\frac{4a}{r_b^2}\right) - \gamma\right] + \frac{Q}{H}R_{\mathrm{b}}$$

where:

H = borehole collector depth (m)

= 52m

k_{eff} = ground thermal conductivity ($Wm^{-1}K^{-1}$)

a = ground thermal diffusivity ($m^2 s^{-1}$)

= λ/S_c

S_c = specific heat capacity of subsurface ($JK^{-1}m^{-3}$)

Q = heat power input (W)

r_{b} = borehole radius

= 82.5mm

γ = Euler's constant

= 0.5772

R_{b} = borehole thermal resistance (kmW^{-1})

t = time (s)

The results from the thermal response test are as follows and these values were used in the model:

Thermal conductivity = 4.16 $Wm^{-1}K^{-1}$

Borehole thermal resistances = 0.127 mKW^{-1}

The inlet water temperatures measured from the TRT were employed as an input to the model, in order to predict the outlet water temperature from the U-tube. The actual outlet water measurements were used to compare with the predicted outlet water temperature from the model.

The TRT data was measured from a closed-loop system. The well model that is part of the SCW model is not applicable to a closed-loop U-tube heat exchanger; thus, an adjustment to the well model was needed to suit the closed-loop case. A simple heat transfer expression was adopted according to the temperature gradient and the borehole resistance between the ground and the closed-loop U-tube was adopted. The ground temperature at each grid slice in the *z* plane was calculated by the field model and used by the adjusted well model to work out the heat transfer rate using the U-tube resistance from the original commercial TRT report. For a simple closed-loop system, this method would be accurate enough to yield good results at times greater than the threshold mentioned previously (i.e. 5h). The borehole resistance provided by the original commercial TRT report was.$0.127 mKW^{-1}$.

The results of the outlet water temperature predicted by the model and the measured outlet water temperature are shown in Figure 5.1. The largest absolute error is -0.96K (i.e. a percentage error of 6.3%) observed early in the transient, but the error declined towards zero (a percentage error of 0.02%) at the end of the test (Figure 5.2). The early disagreement is due to the limitations inherent in the method used to extract the model parameters from the TRT data.

The small later errors verify that the SCW model is able to reliably predict the thermal response of the ground at least over the short term, although it is acknowledged that further work is needed to verify the model's performance over much longer time periods of relevance to building energy transfers. In addition, the results show that the values of the input parameters (rock conductivity, borehole resistance, etc.) can have a great impact on the accuracy of the model; hence, employing appropriate experiments to acquire accurate

parameters is crucial for successful model construction and model simulation success. Deng's (2004) parameters confirmed that hydraulic conductivity and thermal conductivity are two of the most sensitive parameters in this type of model.

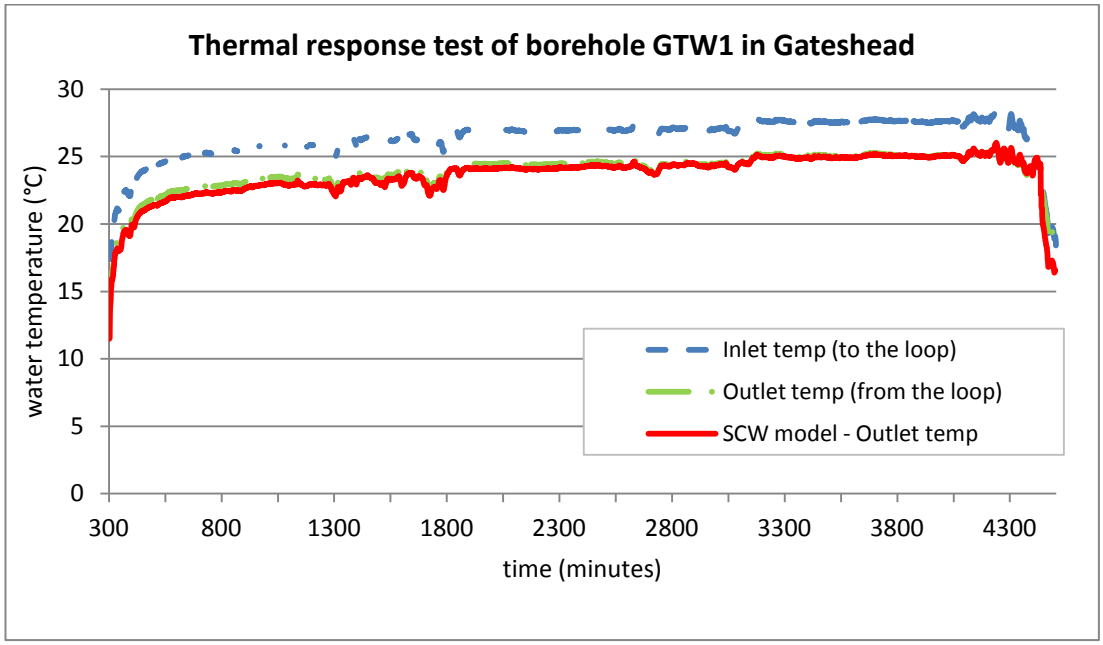

Figure 5.1 TRT results of Borehole GTW1 in Gateshead and SCW model results

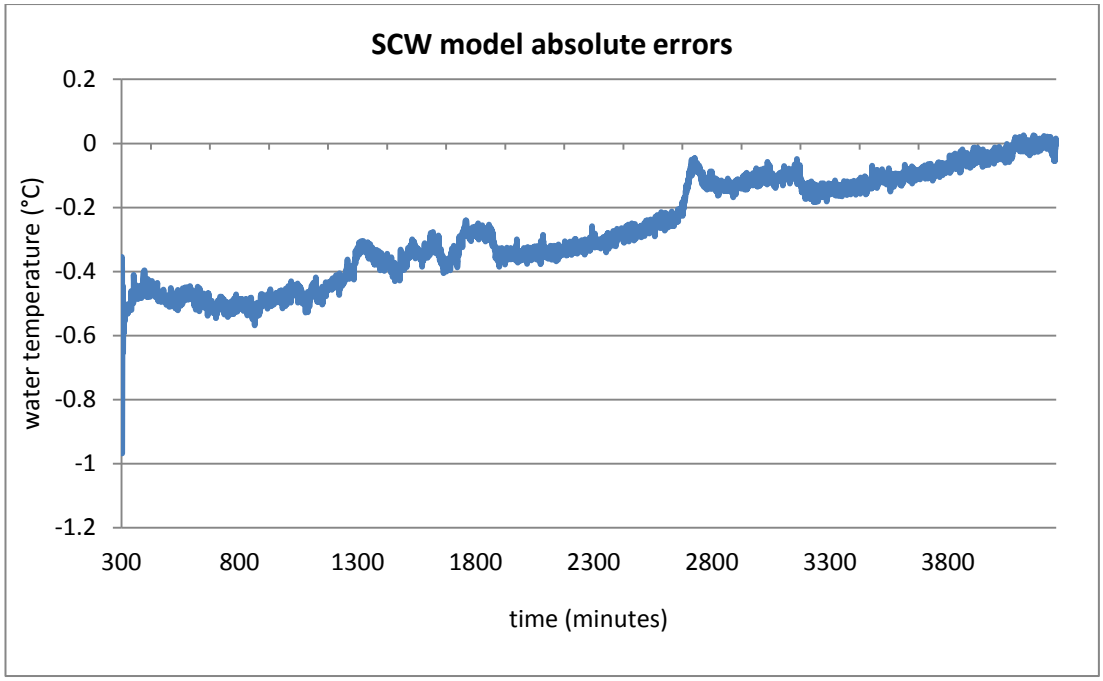

Figure 5.2 Absolute errors of SCW model when compared with TRT

5.2 Model verification with pumping test data

Results from a pumping test carried out in December 2006 on a site near Belfast city centre were used to verify the head prediction capability of the model. The site geology consisted mainly of red sandstone and was water-bearing. A 200mm diameter water well was constructed to a depth of 108m and pumped at a constant rate of 3 ls^{-1} for a period of just under three days. The aquifer hydraulic conductivity was obtained (by a commercial contractor) using both the Theis and Cooper and Jacob methods (see, for example, Freeze and Cherry, 1979), both of which gave very similar results. The hydraulic conductivity was thus found to be 6.04 x $10^{-7}ms^{-1}$.

A comparison of measured and predicted hydraulic drawdown based on this pumping test is shown in Figure 5.3. A maximum percentage error of 7.2% occurred at the initial stage of the drawdown test, decreasing to 0.7% later in the test and averaging 2.0% for the complete test. Thus, the model yielded a good prediction based on a short-term test, although further work is again needed to evaluate performance over the longer term.

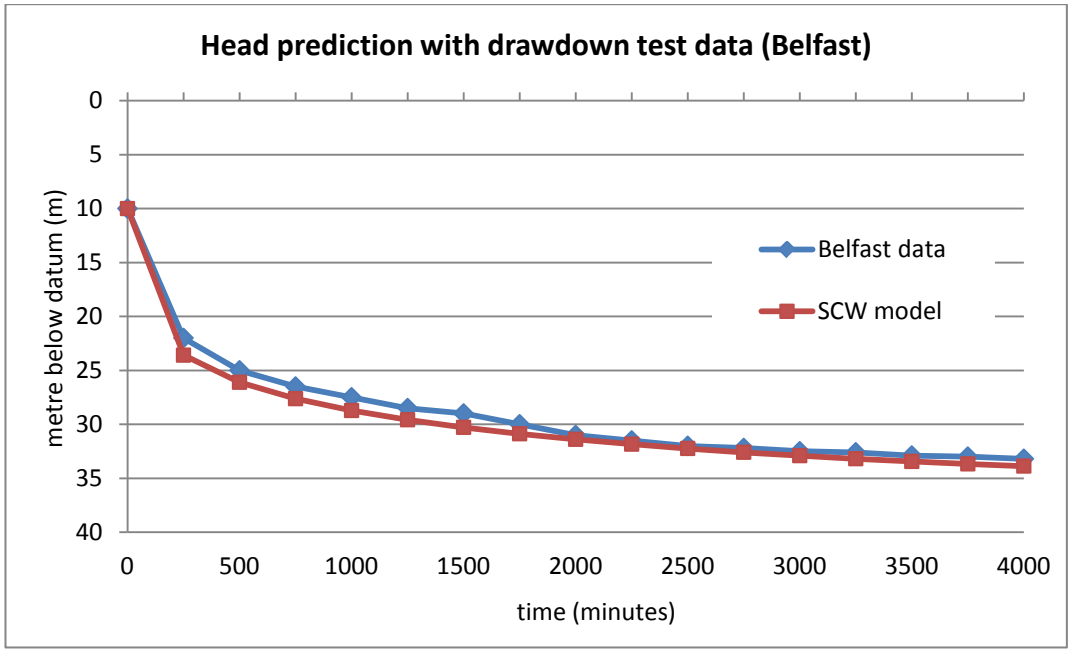

Figure 5.3 Model comparison with drawdown test data from Belfast

5.3 Model verification using operational data from a SCW installation

The space heating and cooling in Haverhill library in Massachusetts is provided by a SCW installation (Deng, 2004). Two wells were initially installed in 1994 but only one well was active before June 1996. Two additional wells were added after 1996 due to the expansion of the library. Each of the boreholes was 457m deep and the diameter was 0.1524m. Only one of the wells was active at the time of monitoring.

As there was no drawdown test data available, geological information provided by the U.S. Geological Survey was used. This indicated that Ordovician and Cambrian sedimentary rocks are found in the Haverhill region and hence the following properties were applied:

K = hydraulic conductivity (ms^{-1}) = 1.00×10^{-5}

K can thus be defined as the rate of water flow through porous rock per unit gradient in head.

n = porosity = 0.025

S = specific storage (m^{-1}) = 1.00×10^{-5}

k_{eff} = thermal conductivity ($Wm^{-1}K^{-1}$) = 3.9

ρ = density (kgm^{-3}) = 2200

c_p = specific heat capacity ($Jkg^{-1}K^{-1}$) = 1000

The measured inlet and outlet water temperatures were the key variables for this validation. The hourly Haverhill inlet water temperatures data (figure 5.4) were applied to the model as an input to the annulus space and the outlet water temperatures from the suction pipe were

predicted by the model (with the SCW 'child model' fully included) and compared with the measured outlet water temperatures. The initial conditions before the experiment were not known and hence inaccurate predictions to a certain extent at the initial period might be expected from the model. Deng (2004) compared her model results with the Haverhill experiment data but included a set of self-generated initial conditions to obtain better agreement with the data. The results of the measured and predicted outlet water temperatures during a 2400 hour period, together with the corresponding absolute errors between the two, are plotted in Figures 5.5 and 5.6.

A good fit between the predicted and observed outlet water temperatures is demonstrated in Figure 5.5. The largest absolute error of 0.78°C was observed immediately after the simulation started (at the 2nd hour): this is attributed to the unknown initial ground conditions on the site. The magnitude of errors improved later in the simulation and the overall root mean square error was 0.268K. This reasonably low error result reveals a good level of accuracy in the model. In addition, about 95% of the predicted values from the SCW model were within ±0.4°C throughout the entire verification test period (Figure 5.6). Note that there are some missing data segments from the Haverhill experiment data set between 300 and 400h, 1200 and 1300h, and 2200 and 2300h.

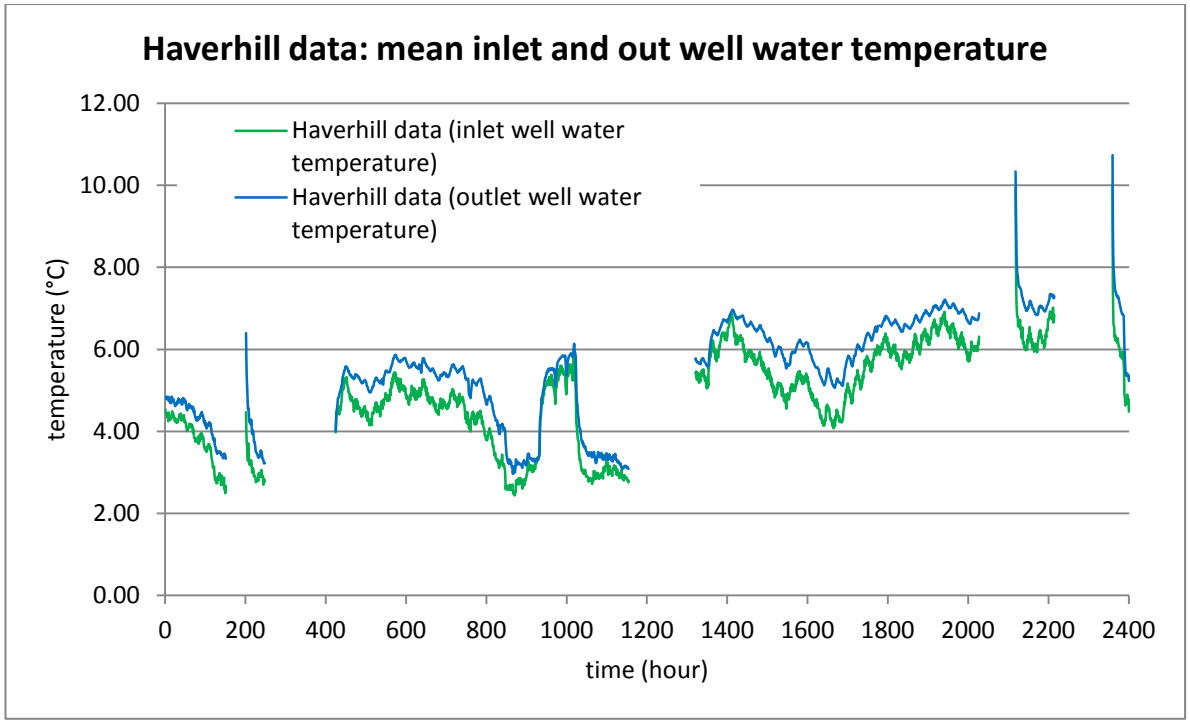

Figure 5.4 Haverhill data: Mean inlet and outlet well water temperature

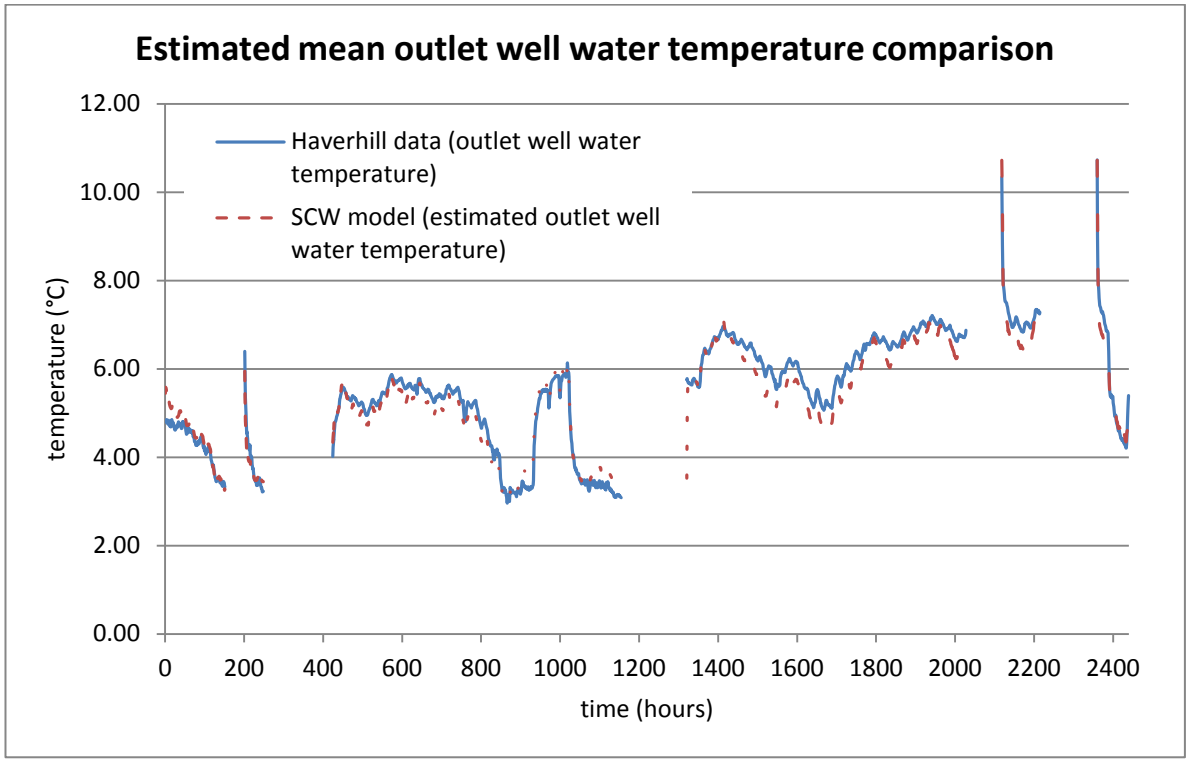

Figure 5.5 Model comparison with Haverhill SCW data

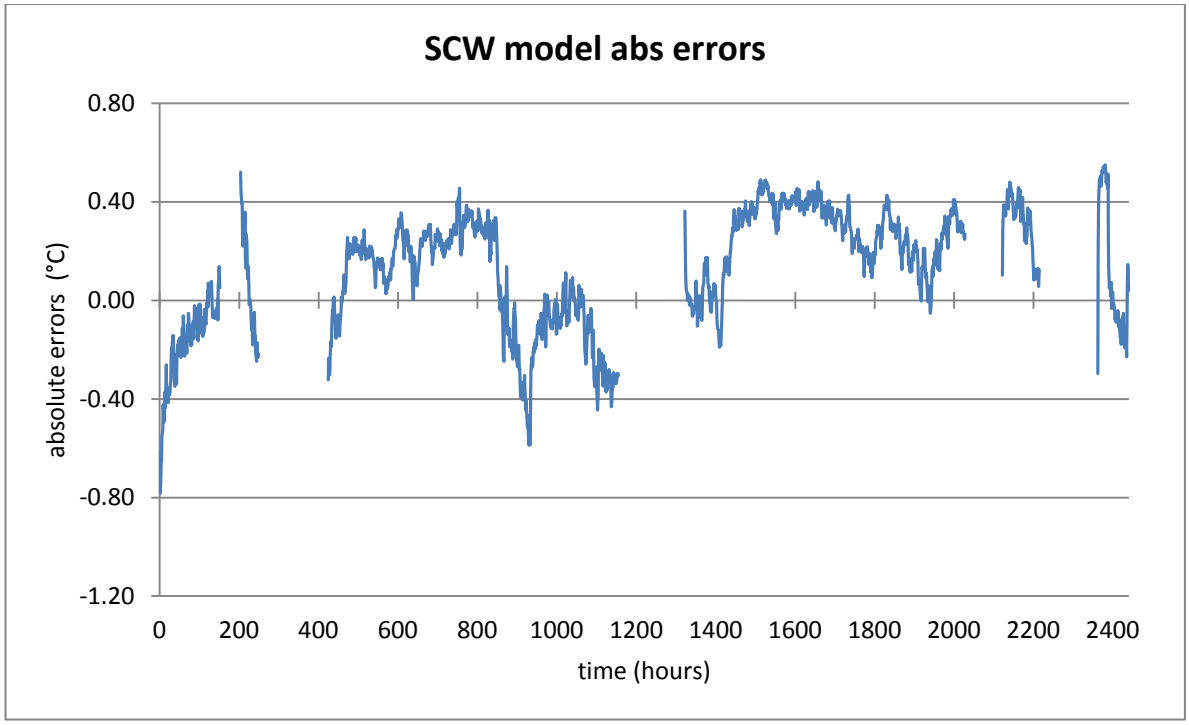

Figure 5.6 Absolute errors of SCW model and Haverhill data

6. Evaluative study

6.1 Methodology of the evaluation study

The model has been applied to two case studies for evaluative purposes. A well cluster of 4 × 100m deep SCWs with a 10m grid spacing at the centre of a 50m × 50m × 120m (deep) domain were investigated and applied to these case studies.

Case 1 = heating only

Case 2 = heating and direct cooling

Case 1 compares the performance of a variety of SCW cluster options compared with a conventional vertical borehole heat exchange array for an example building. Details of the example building and the conventional array design can be found in Underwood and Spitler (2007). Additionally, a sensitivity test case (case 2) is carried out in order to identify the SCW cluster performance associated with variations in typical earth property conditions in the UK. The earth properties described in Younger and Milne's work (1997) related to the Penrith and St Bees aquifers in Cumbria, UK, representing an example of commonly found hydogeological properties to be found in UK conditions and likely to be helpful to SCW applications.

[The findings from these two test cases were published at the Building Simulation 09 conference in Glasgow (Ng, Underwood & Walker, 2009) and the paper was included in Appendix D)]

A further investigation based on the results in Case 2 was carried out in order to evaluate the performance comparison between the SCW cluster and an equivalent conventional vertical closed-loop array system. Additionally, a property sensitivity test was done in order to

identify the impact of rock properties on SCW performance, based on rock formations typically found in the UK.

Case 2A = system performance comparison: SCW vs. closed-loop array

Case 2B = property sensitivity test

[The findings from these two additional cases were published in ASHRAE HVAC&R Journal in 2011 (Ng, Underwood & Walker, 2011)]

From the grid dependency study, a grid mesh size of 0.6m was selected as a compromise between accuracy and computation cost. However, a slightly smaller (and better) spacing of 0.5m was actually used as the chosen domain size and well spacing would then be convenient whole number multiples of this. All PDEs were solved as initial value problems and thus all temperature nodes were set at 10^{o}C, whereas all initial heads were set at zero since the model was derived to predict the head distribution due to pumping only (i.e. local groundwater flow effects were not considered). Details of the rock properties and SCW parameters can be found in Tables 6.1 and 6.2.

Table 6.1 Thermal properties

Thermal conductivity of rock k **(Wm^{-1}K^{-1})**	**Hydraulic conductivity of rock** K **(ms^{-1})**	**Volumetric specific heat capacity of rock** c_{ps} **(Jm^{-3}K^{-1})**	**Porosity** n
3.9	0.00001	1.86x10^{6}	0.275

Table 6.2 Standing column well setting

SCW diameter (m)	**Total borehole length (m)**	**Pumping rate (Ls^{-1})**	**Bleed rate (%)**
0.2	400	1	10

6.1.1 Case 1 - heating only

The first case consisted of applying a heating load and well mass flow rate using values within the range of those observed for a survey of 35 standing column well installations carried out by Orio, *et al*. (2005) in North America. This would enable results to be compared with the range of observed capacities of the surveyed wells. The surveyed wells consisted of a mix of residential and commercial installations (heating mainly in residential applications with some commercial applications of cooling) with a mean specific rate of heat transfer of $275Wm^{-1}$ and a mean overall well mass flow rate of $1.4kgs^{-1}$. Two simulations were carried out: one with bleed (set at 10% of nominal well flow rate) and one without bleed. In the former case, a simple bleed control strategy was adopted in which bleed was applied at all times when there is a demand for heat. It is stressed that this exercise was merely an attempt to *verify* the results of the model with the results summarised by Orio, *et al*. (2005), rather than an attempt at a full and precise comparison (which would not be possible in any case due to the incompleteness of the data presented in Orio, *et al*.'s (2005) survey). Figure 6.1 shows the simulated heating delivered by the cluster of four wells (and, superimposed, are the bounds of heat transfer rates reported by Orio, *et al*. (2005) for the 35 installations in North America). Figure 6.2 shows the simulated mean monthly temperatures over one year of well cluster operation, with and without bleed operation. The mean rock temperatures 1m away from the four wells are also plotted in Figure 6.2.

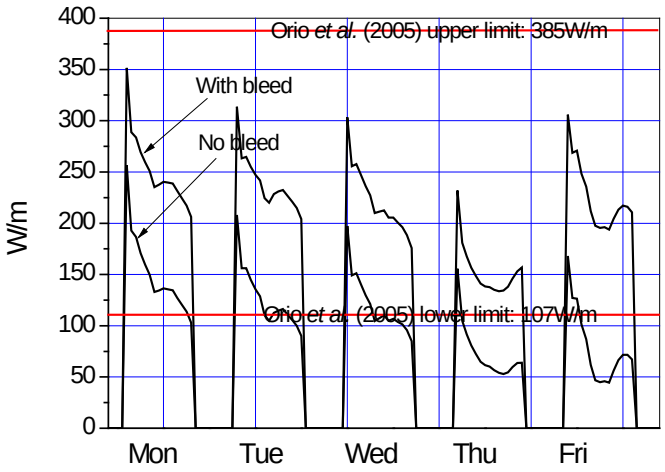

Figure 6.1 Simulated heating delivered by a cluster of 4 x 100m deep SCWs operating at capacities within the range of that reported by Orio, *et al.* (2005)

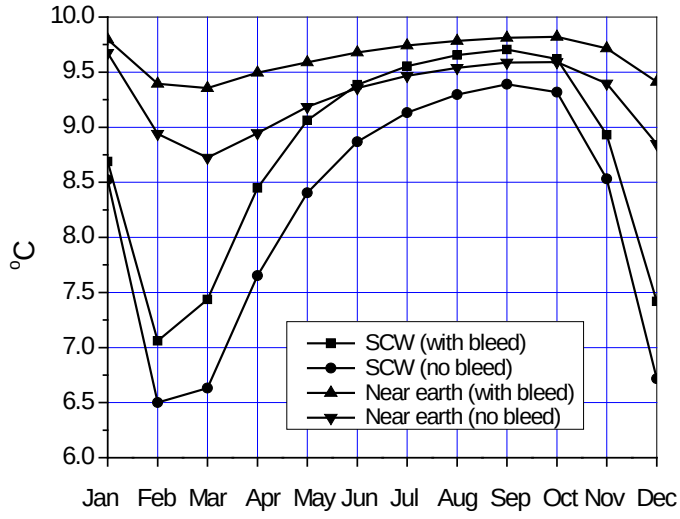

Figure 6.2 Mean well water temperatures and local rock temperatures for the cluster of four wells ('near rock' represents the rock temperature 1m from the well centre and half way through the well depth)

The simulated isotherms and isobars around the well cluster were found to be uniform, as might be expected for the identical well specifications occupying a uniform grid pattern. As an illustration, Figure 6.3 shows isobars on the x-y plane at half well depth (50m) after one year.

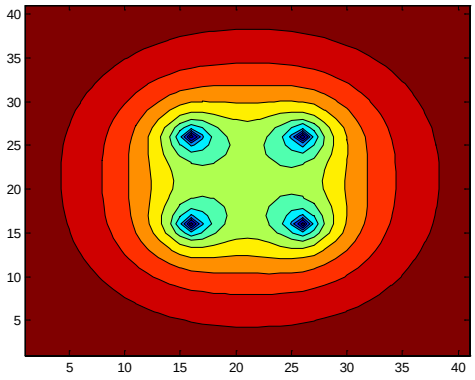

Figure 6.3 Simulated x-y isobars at half well depth for a cluster of four identical SCWs

Sample differential values (reference pressure = 0Nm^{-2}):

Well centre = -751Nm^{-2}

Domain centre = -362Nm^{-2}

Between wells = -353Nm^{-2}

12, 20 = -31Nm^{-2}

6, 20 = -13Nm^{-2}

1, 20 = -4Nm^{-2}

6.1.2 Case 2 - heating and direct cooling

The second test case consisted of a heating and direct cooling application using data given by Underwood and Spitler (2007). A design analysis of vertical closed-loop borehole heat exchangers was carried out for a range of air conditioning system alternatives. It is thus possible to compare the response of the closed-loop array performance with that of a standing column well cluster in the present exercise.

The peak requirements of this application were 44kW (heating: heat sourced from the geothermal array) and 55kW (direct cooling: heat rejected to the geothermal array). The corresponding annual energy rates were 18900kWh (heat sourced) and 41400kWh (heat rejected). Thus, the application is cooling-dominant. Again, the same cluster of four well was applied, as used in the previous case, and the simulated energy demands were applied to the well clusters, first with a conditional bleed rate of 10% of nominal well flow rate (bleed applied at all times when a load exists) and then without any bleed. The results of the annual mean water loop temperatures and near rock temperatures are given in Figure 6.4.

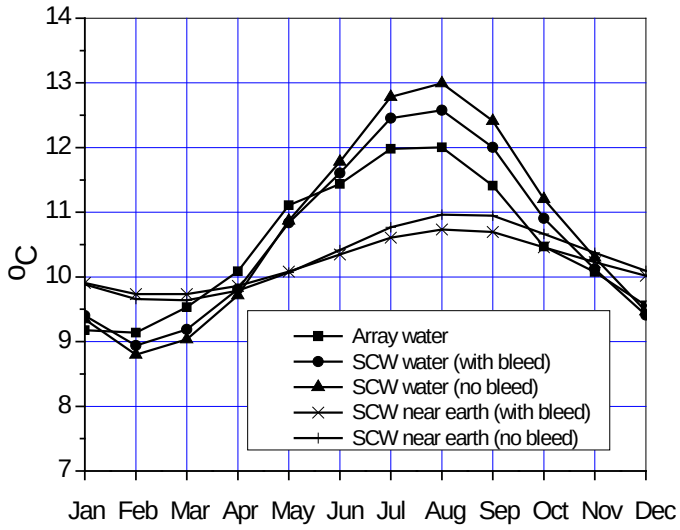

Figure 6.4 Comparison of annual monthly mean water temperatures derived from a 2800m borehole field for closed loop array (50×56m) and a 400m cluster of four SCWs ('near rock' represents the rock condition at 1m from well centre)

6.1.3 Case 2A - system performance comparison, SCW vs. closed-loop array system

The purpose of this further investigation is to determine the number of wells required for the SCW cluster system to deliver the same amount of heating and cooling to the building as the closed-loop array system of the previous case. The rock properties and the model parameters were the same as in Case 2. Figure 6.5 shows the mean water temperature from the closed-loop array system and the SCW cluster system with four wells, six wells and eight wells (all of 100m depth).

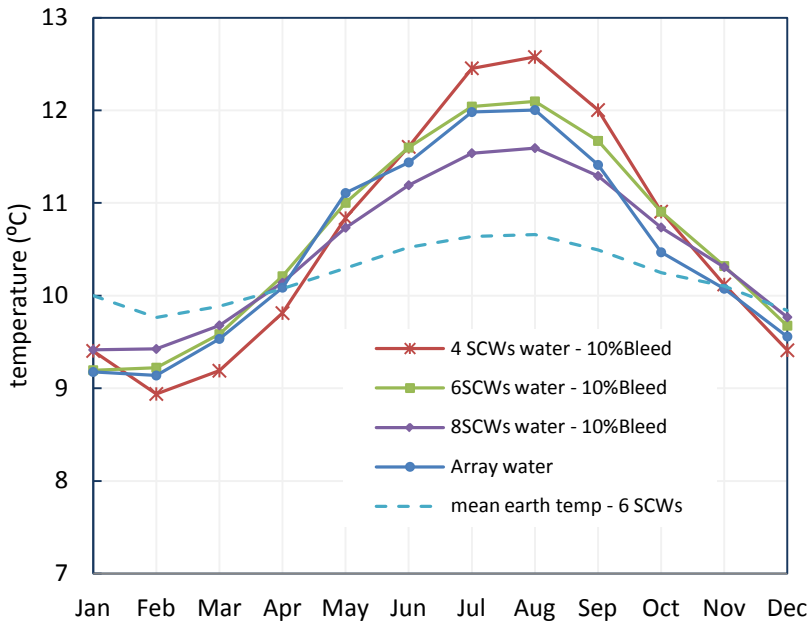

Figure 6.5 Comparison of annual monthly mean water temperatures derived from a 2800m borehole field closed loop array, 400m (four well) SCW cluster system, 600m (six well) SCW cluster system and 800m (eight well) SCW cluster system

6.1.4 Case 2B - rock properties sensitivity test

For the sensitivity case, extreme values of rock thermal conductivity, specific heat capacity, hydraulic conductivity and storativity observed for a typical UK site were alternatively applied. Use was made of a range of rock properties observed in Cumbria (Younger & Milne, 1997). The property values are presented in Table 6.3. For convenience in the interpretation of results, the high conductivity property case was labelled ‘good’ and the low conductivity case ‘bad’. The same loads and array application data from Cases 2 and 3 were also used in this case, although only the six well case was considered. The results are illustrated in Figure 6.6.

Table 6.3 Rock properties adopted in the sensitivity test (Younger & Milne, 1997)

	Thermal conductivity of rock k **(Wm^{-1}K^{-1})**	**Hydraulic conductivity of rock** K **(ms^{-1})**	**Volumetric specific heat capacity of rock** c_{ps} **(Jm^{-3}K^{-1})**	**Storativity** S
Good scenario	4.3	1.16 x 10^{-4}	5.00 x 10^{6}	0.045
Base case	3.9	0.00001	1.86 x 10^{6}	0.0014
Bad scenario	2.5	3.47 x 10^{-6}	1.00 x 10^{6}	1.40 x 10^{-9}

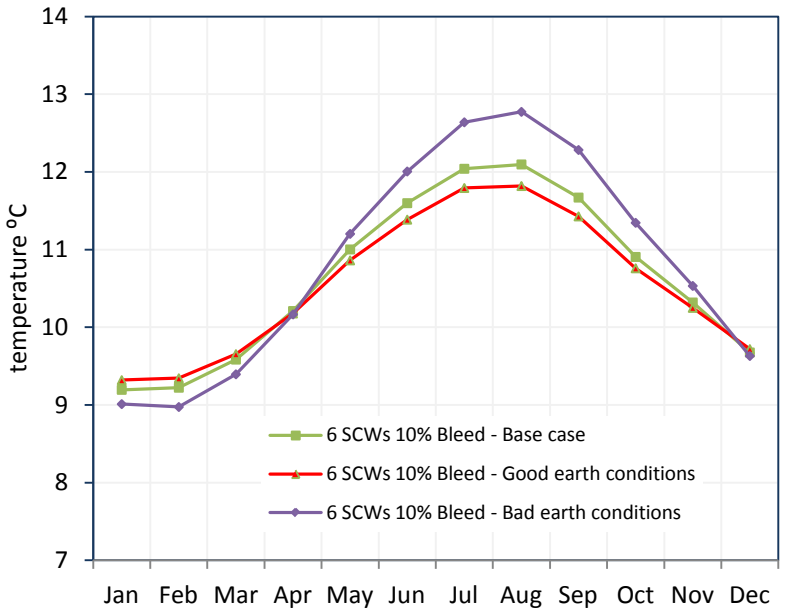

Figure 6.6 Comparison of annual monthly mean water temperatures derived from the 600m SCW cluster system under different rock properties

6.1.5 Discussion of the evaluative test results

For the heating only case (Case 1), the four well cluster simulation resulted in per-metre well heat transfer rates that were between the limits observed in existing standing column well installations (Figure 6.1); a significant increase in heat transfer is noted when groundwater bleed is used. The initial rock temperature at the start of the simulation was 10^{o}C and, precisely one year later, had declined to 9.3^{o}C and 8.6^{o}C for the bleed and no bleed cases, respectively. This implies a gradual but significant decline in rock temperature for the heating only case over several years of operation, resulting in a corresponding decline in the heat pump coefficient of performance and, of greater seriousness, in capacity through the danger of freezing. A larger cohort (or greater depth) of standing column wells would, of course, reduce this decline. Further work is needed to investigate long-term performance.

For the heating and cooling case, an exemplar four well cluster competes well with a traditional closed-loop borehole heat exchanger array in that, for a similar performance in annual monthly mean water temperatures, just 400m of standing column wells are needed as opposed to 2800m of a closed-loop array. Figure 6.4 shows that the mean water temperatures of the well cluster with and without bleed and the mean water temperatures of the closed-loop are consistently within 1K of one another over an annual simulation period. Furthermore, the mean temperatures imply satisfactory operation in winter with (essentially, in the case of SCWs) freshwater and that the summer temperatures are sufficient to enable direct cooling using direct ('static') building air conditioning methods, such as chilled ceilings or chilled beams.

Although the four well cluster competed reasonably well with the conventional array, further simulations (Case 2A) demonstrate that increasing the well capacity to six wells would give an annual performance almost identical to that of the conventional array. It is also evident from this case that increasing the SCW array sizes to 8 x 100m would bring little additional performance benefit. Underwood and Spitler (2007) found that this combination can deliver

carbon emission savings due to heating and cooling energy used by the plant of greater than 60%, based on conventional closed-loop technology, when direct cooling is used in summer (i.e. the heat pump is inactive and cooling is achieved by circulating fluid directly to the array). The major issue here is that the 6 x 100m deep SCW cluster involves significantly less groundwork than would be needed with the 50 × 56m deep borehole heat exchangers depicted in the closed-loop solution specified by Underwood and Spitler (2007). In this case, the mean rock temperature change after one year was found to be negligible. In terms of capital cost, the conventional closed loop system is still the most favourable option in UK at present, typically costing £35 – £40 per m of borehole depth, while well costs (including PVC well screens and submersible pumps) typically cost £70 - £150 pounds per m in the UK. This would suggest little difference in installation costs between the two technologies due to the reduced sizes need for a SCW installation.

In considering the sensitivity to the rock properties, Figure 6.6 illustrates that the mean water temperature in the cooling-dominant application during the cooling and heating seasons might vary by up to 1K between the 'good' and 'bad' rock cases. Again, it is important to note that the water temperature provided by a SCW system in both cases is sufficiently low in summer for direct cooling and thus can offer large savings in carbon emissions. The temperature conditions are also high enough in winter to avoid freezing. However, the impact of rock properties is sufficiently significant to necessitate the need to evaluate conditions on a site-by-site basis.

In this evaluative study, the model has been verified using a variety of existing measured data revealing good model behaviour over the short time horizon. There is a need to do further work on the long term response of multiple SCWs and, to this end, a test site consisting of two adjacent SCWs is currently being planned on the Northumbria University campus with a view to a more extensive and long-term validation test of the model. Further work is needed to measure the response of SCW clusters over extended time horizons (at

least 2-3 years) and the sensitivity of the well spacing in order to give further confidence in the model behaviour and, thus, develop it as a potential design tool.

7. Application and design study

In this study, the model has been applied onto 3 common types of commercial buildings and 3 common rock types occurred in UK for the purpose of investigating the long-term responses of SCW applications in the UK.

The objectives of this section are:

- To examine the sensitivity of several SCW design parameters.
- To investigate the long-term response of SCW system performance to a range of typical commercial building load profiles and UK rock properties.
- To estimate CO_2 emissions due to heating and air conditioning using SCWs and compare these with conventional heating and air conditioning systems.

7.1. Methodology of the application

A commercial building thermal performance simulation program "Integrated Environment Solution" (IES) (McLean, 1994) was used to generate heating and cooling demand profiles of the three typical and contrasting UK buildings for this application. The National Calculation Method (NCM) (DCLG, 2010), which is adopted by Building Regulation UK part L (BRUKL) to produce energy performance certificates (EPC) and other planning compliance requirements, was applied to each building within the IES environment to facilitate the generation of representative heating and cooling demands. Default weather data provided by the IES weather database was adopted for the simulations. The resulting heating and cooling demands were expressed as hourly time series values over one complete year and were used to form the base data from which a variety of SCW design studies were conducted. In all, 42 design variants were identified to be explored in detail and these are given in Tables 7.4 to 7.10 for the three selected buildings.

7.2. Details of the parameter

The three buildings selected were: an office building in Newcastle exhibiting moderate winter heating demands and high summer cooling, an apartment building in Liverpool comprising high rental flats exhibiting winter heating and moderate summer cooling and a school building in Glasgow exhibiting moderate winter heating and no cooling requirement. Thumbnail details of the buildings are given in Figure 7.1.

Regarding the construction, it is assumed that all 3 buildings were built from a standard brick wall construction in which complying the limited thermal transmittance (u-value) requirement from building regulation part L in 2002 (DCLG, 2001)

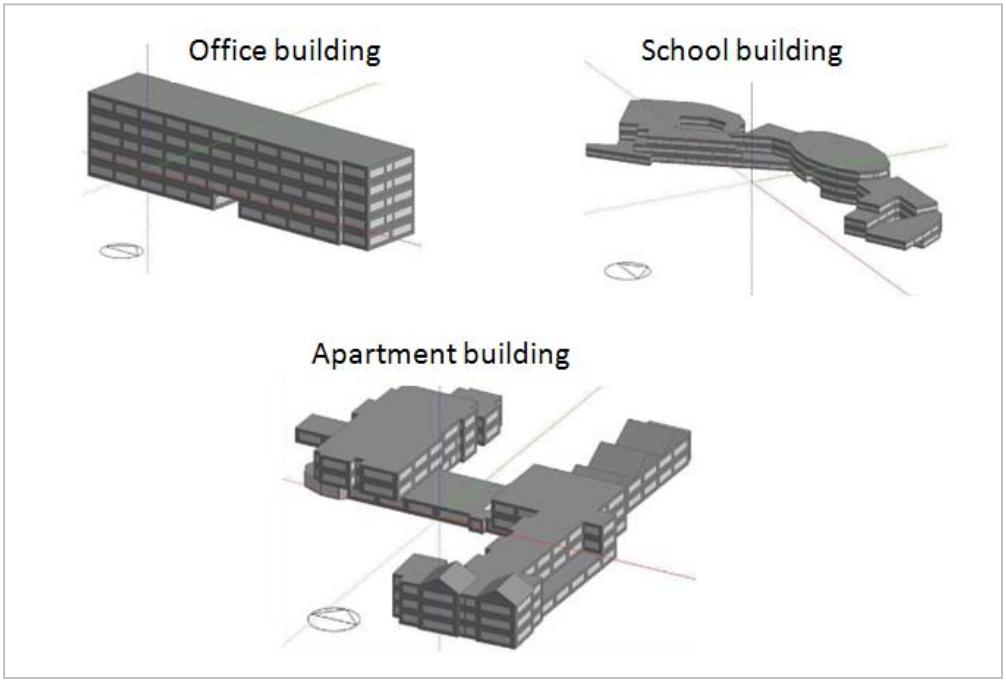

Figure 7.1 Thumbnail details of the buildings

With the intention of minimising the computation time for the SCW arrays, the simulated building loads were scaled down to less than 50kW (peak) for all buildings. The rescaled loads are plotted in Figures 7.2 to 7.4.

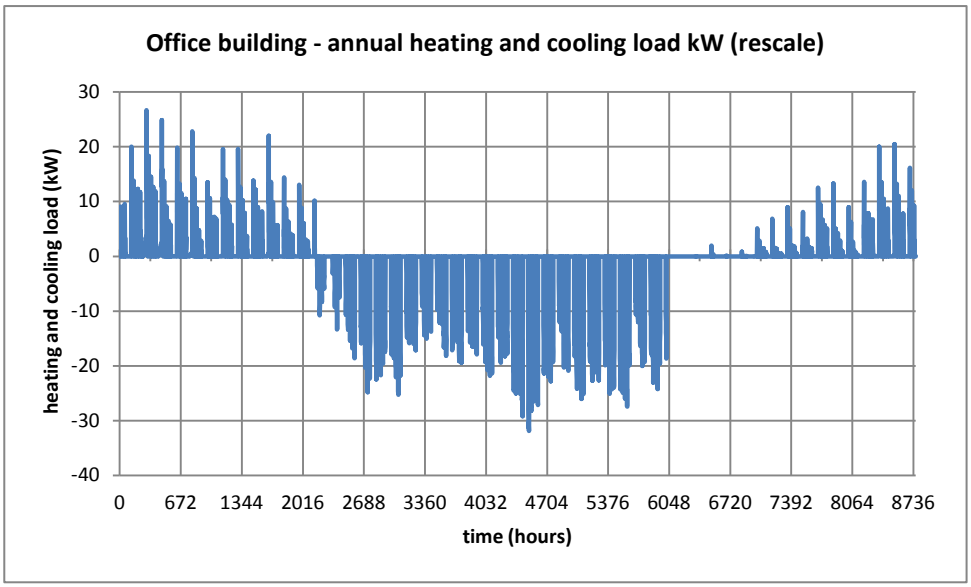

Figure 7.2 Annual heating and cooling loads for the office building

For the office building, the total cooling demand is 19378kWh with a peak load of 31.8kW; the total heating demand is 2550kWh with a peak load of 26.7kW. This is a cooling-dominant case.

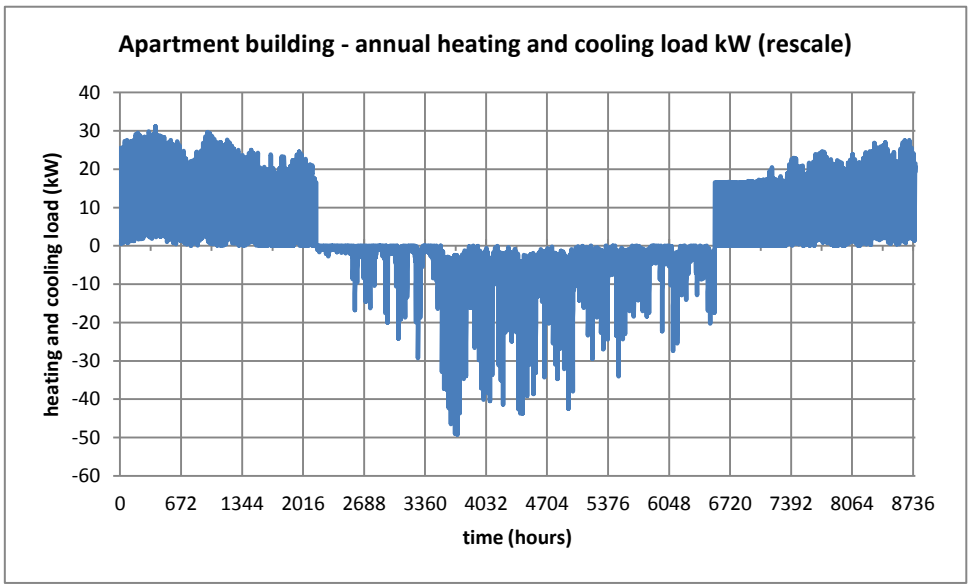

Figure 7.3 Annual heating and cooling loads for the apartment building

For the apartment building, the total cooling demand is 19360kWh with a peak load of 49.3kW; the total heating demand is 49784kWh with a peak load of 31.2kW. This is a heating-dominant case.

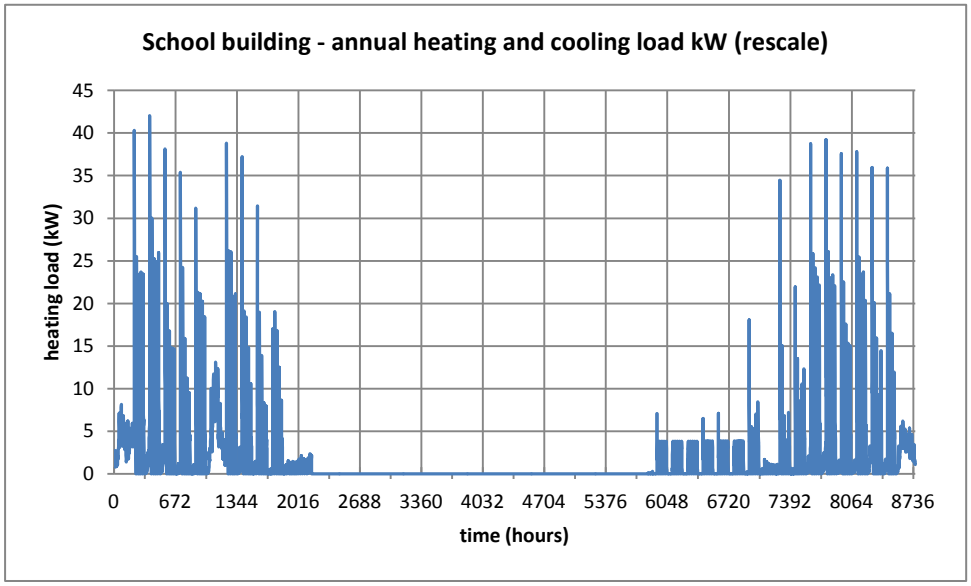

Figure 7.4 Annual heating loads for the school building

For the school building, the total heating demand is 11330kWh with a peak load of 42.0kW. There is no cooling to be met by air conditioning and thus this represents a heating-only case.

The heating demand of each building was assumed to be met by a geothermal source heat pump. Regarding the heat pump configuration, an indirect configuration is used. The SCWs do not connect to the GSHP unit directly but through a plate heat exchanger, as shown in Figure 7.5. For the purposes of the study, the assumed design flow and return water temperature of the LTHW (low temperature hot water) system and cooling system have been defined as 35°C and 30°C (heating) and 7°C and 12°C (cooling). It is assumed the heating

and cooling demands are always met by the system and the flow water temperatures remain constant all the time. The nominal *CoP* of the chosen water to heat pump for this task varies from 2.5 to 6 in cooling mode and from 3.5 to 7.6 in heat pump mode, according to the required output. A relatively low flow and return water temperature was chosen for the heating system in order to demonstrate the potential of this technology with a high (but feasible) *CoP*. The flow and return temperatures chosen would commonly apply when using a heat pump with an under-floor heating system which is a frequent choice of heating when using heat pumps.

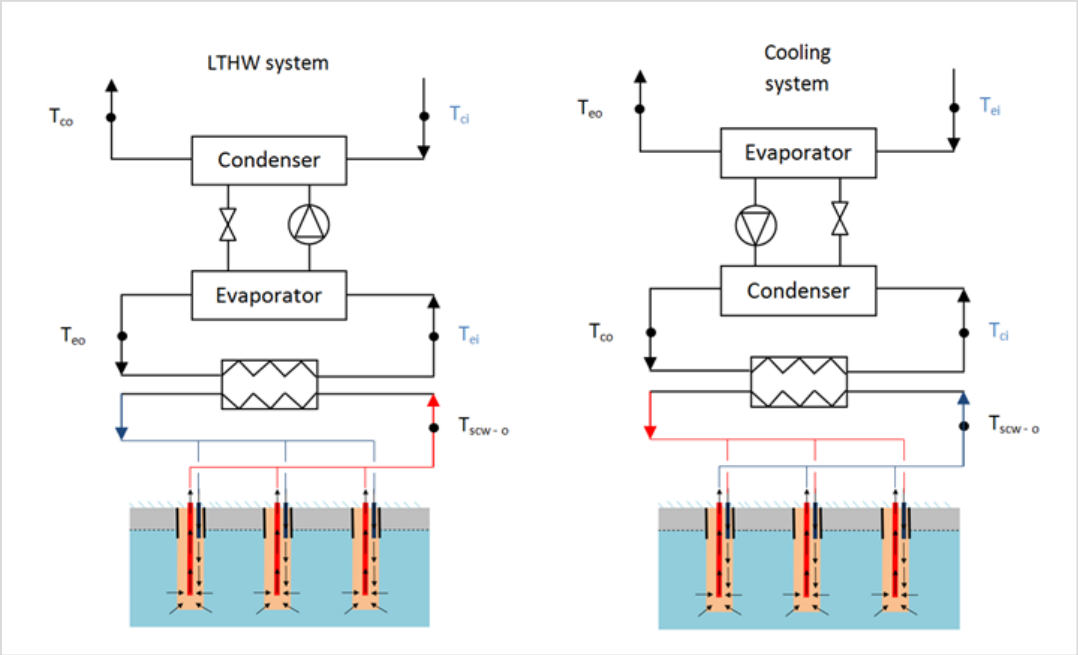

Figure 7.5 Indirect configuration of the SCW system

Three common UK lithostratigraphical formations (or rock types) were chosen for this application: London Clay, Magnesian Limestone and Old Red Sandstone.

London Clay is a marine geological formation that formed during the Palaeogene period. This formation mainly appears in the London Basin. The thermal conductivities on sediments like clay are usually very low due to the fine-grained structure.

Magnesian Limestone is formed of carbonate minerals found in Durham, Tyne and Wear and also stretching from Nottinghamshire northwards into Yorkshire. With a medium grained size, Magnesian Limestone offers a higher thermal conductivity than London Clay.

Old Red Sandstone is a non-marine sediment that is rich in iron oxide and hence appears red. It was formed in the Devonian period and is found in South Devon, North Cornwall, the Anglo-Welsh lowland areas and also the southern Scotland. This type of rock tends to have a relatively high thermal conductivity value due to the high content level of quartz.

Further details of the range of thermal conductivities in typical UK formations can be found in Rollin (1987) and Underwood (2011).

The thermal properties of these three soil types are included in Tables 7.1 to 7.3.

Table 7.1 Thermal properties of London Clay

		Source of the data
Thermal conductivity	2.45 $Wm^{-1}K^{-1}$	(Downing, Gray & survey, 1986)
Porosity	34.7 – 39.2% (36.95% is used)	(Graham, 2008)
Transmissivity	72.2m^2 per day	(Graham, 2008)
Hydraulic conductivity	4.45×10^{-5} ms^{-1}	(Banks, 2008) (Graham, 2008)
Compressibility	10^{-6} - 10^{-8} (for clay) 10^{-7} is used	(Freeze and Cherry, 1979)
Temperature gradient	31°C km^{-1}	(Burley, Edmunds & Gale, 1984)
Surface temperature	10.3°C (British national grid ref: NZ36)	(Burley, Edmunds & Gale, 1984)

Table 7.2 Thermal properties of Magnesian Limestone

		Source of the data
Thermal conductivity	3.32 $Wm^{-1}K^{-1}$	(Downing, Gray & survey, 1986)
Porosity	15%	(Graham, 2008)
Transmissivity	229m^2 per day	(Graham, 2008)
Hydraulic conductivity	10^{-6} – 10^{-9} ms^{-1} 1.6 x 10^{-8} - 6.3 x 10^{-9} ms^{-1} (1.6 x 10^{-8} is used)	(Banks, 2008) (Graham, 2008)
Compressibility	10^{-8} - 10^{-10} (for gravel and join rock) 10^{-8} is used	(Freeze and Cherry, 1979)
Temperature gradient	27°C km^{-1}	(Burley, Edmunds & Gale, 1984)
Surface temperature	9.3°C (British national grid ref: NZ36)	(Burley, Edmunds & Gale, 1984)

Table 7.3 Thermal properties of Old Red Sandstone

		Source of the data
Thermal conductivity	3.51 $Wm^{-1}K^{-1}$	(Downing, Gray & survey, 1986)
Porosity	5% - 30% 16% - 20% (18% is used)	(Banks, 2008) (Graham, 2008)
Transmissivity	10.7m^2 per day	(Graham, 2008)
Hydraulic conductivity	10^{-9} – 10^{-4} ms^{-1} 1.5x10^{-7} - 1.2x10^{-6} ms^{-1} (6.75x10^{-7} is used)	(Banks, 2008) (Graham, 2008)
Compressibility	10^{-8} - 10^{-10} (for gravel and join rock) 10^{-9} is used	(Freeze and Cherry, 1979)
Temperature gradient	16.8°C km^{-1}	(Burley, Edmunds & Gale, 1984)
Surface temperature	10.7°C (British national grid ref: SO50)	(Burley, Edmunds & Gale, 1984)

With regards to the SCW design parameters, four groups of variants are considered:

- Group 1 – variable bleed flow
- Group 2 – variable well borehole diameter
- Group 3 – well spacing (multiple well options only)
- Group 4 – undisturbed geothermal gradient

In order to explore the potential of SCW clusters (multiple wells – a key contribution of this work), the impact of the above are investigated under two sets of well arrangements: a) a single well arrangement and b) multiple well arrangements. Thus, all results from each group defined above are divided into two further groups: Group A and Group B.

The total length of the SCWs in each case is determined by the heating and cooling demands of the selected buildings, which form the depths of the SCW for each building. They are 120m for the school building, 360m for the office building and 480m for the apartment building under the single well arrangement (Group A). These lengths are estimated based on the minimum heat transfer rate per unit of borehole length observed from Orio's survey (Orio *et al.*, 2005) which was $100 Wm^{-1}$. In order to facilitate the direct comparison between the two well arrangements, the total lengths of the ground loops are kept exactly the same in both well arrangements. Therefore, a cluster design of two SCWs is adopted for the school building (i.e. 60m per well), three SCWs for the office building (120m per well) and only four SCWs for the apartment building (120m per well) under the multiple well arrangement in Group B. The influence of bleed flow is analysed through two options, which are 10% (of the nominal pumped flow) applied constantly and zero bleed flow. The results are included in Groups 1A and 1B. The impact of borehole diameters is analysed by considering three alternative well borehole diameters of 0.15m, 0.2m and 0.25m, forming Groups 2A and 2B. For the multiple well arrangements, the impacts of well spacing of 2m, 5m and 8m are investigated, forming Groups 3A and 3B.

To enable direct comparisons for the three different rock types, the undisturbed rock formation temperature was initially assumed to be 10°C for all soil types. However, it was considered that the rate of increase in temperature per unit depth in the earth (i.e. local geothermal gradients) might in some sites form a very influential parameter; thus one more application group (Group 4) was defined to reveal the actual SCW performance according to the local geothermal gradient observed in areas where these rocks occurred at the surface. The geothermal gradient information used in this test came from a geothermal data catalogue based in the UK (Burley, Edmunds & Gale, 1984).

Full details of each application group are given in Tables 7.4 to 7.10.

Table 7.4 Details of application test Group 1A – bleeding with single well arrangement

Group 1A bleeding – single well (base case)*	**Lithostrati-graphical formations**	**Number of wells**	**Total flow rate (Ls^{-1})**	**Flow rate per well (Ls^{-1})**	**Bleed flow (%)**	**Well depth (m)**	**Diameter of well (mm)**	**Well spacing (m)**	**Geothermal gradient ($°C\ km^{-1}$)**
1*	London Clay	1	2 - school 1.5 - office 2.4 - apartment	n/a	0	120 - school 360 - office 480 - apartment	200	5	N/A 10°C constant
2*	Magnesian Limestone	1	2 - school 1.5 - office 2.4 - apartment	n/a	0	120 - school 360 - office 480 - apartment	200	5	N/A 10°C constant
3*	Old Red Sandstone	1	2 - school 1.5 - office 2.4 - apartment	n/a	0	120 - school 360 - office 480 - apartment	200	5	N/A 10°C constant
4	London Clay	1	2 - school 1.5 - office 2.4 - apartment	n/a	10	120 - school 360 - office 480 - apartment	200	5	N/A 10°C constant
5	Magnesian Limestone	1	2 - school 1.5 - office 2.4 - apartment	n/a	10	120 - school 360 - office 480 - apartment	200	5	N/A 10°C constant
6	Old Red Sandstone	1	2 - school 1.5 - office 2.4 - apartment	n/a	10	120 - school 360 - office 480 - apartment	200	5	N/A 10°C constant

Table 7.5 Details of application test Group 1B – bleeding with multiple well arrangement

Group 1B bleeding – multiple wells	**Lithostrati-graphical formations**	**Number of wells**	**Total flow rate** (Ls^{-1})	**Flow rate per well** (Ls^{-1})	**Bleed flow** (%)	**Well depth** (m)	**Diameter of well** (mm)	**Well spacing** (m)	**Geothermal gradient** $(°C\ km^{-1})$
7	London Clay	2 - school	2 - school	1 - school	0	60 - school	200	5	N/A
		3 - office	1.5 - office	0.5 - office		120 - office			10°C constant
		4 - apartment	2.4 - apartment	0.6 - apartment		120 - apartment			
8	Magnesian Limestone	2 - school	2 - school	1 - school	0	60 - school	200	5	N/A
		3 - office	1.5 - office	0.5 - office		120 - office			10°C constant
		4 - apartment	2.4 - apartment	0.6 - apartment		120 - apartment			
9	Old Red Sandstone	2 - school	2 - school	1 - school	0	60 - school	200	5	N/A
		3 - office	1.5 - office	0.5 - office		120 - office			10°C constant
		4 - apartment	2.4 - apartment	0.6 - apartment		120 - apartment			
10	London Clay	2 - school	2 - school	1 - school	**10**	60 - school	200	5	N/A
		3 - office	1.5 - office	0.5 - office		120 - office			10°C constant
		4 - apartment	2.4 - apartment	0.6 - apartment		120 - apartment			
11	Magnesian Limestone	2 - school	2 - school	1 - school	**10**	60 - school	200	5	N/A
		3 - office	1.5 - office	0.5 - office		120 - office			10°C constant
		4 - apartment	2.4 - apartment	0.6 - apartment		120 - apartment			
12	Old Red Sandstone	2 - school	2 - school	1 - school	**10**	60 - school	200	5	N/A
		3 - office	1.5 - office	0.5 - office		120 - office			10°C constant
		4 - apartment	2.4 - apartment	0.6 - apartment		120 - apartment			

Table 7.6 Details of application test Group 2A – well diameter with single well arrangement

Group 2A well diameter – single well	**Lithostrati-graphical formations**	**Number of wells**	**Total flow rate** **(Ls^{-1})**	**Flow rate per well** **(Ls^{-1})**	**Bleed flow** **(%)**	**Well depth** **(m)**	**Diameter of well** **(mm)**	**Well spacing** **(m)**	**Geothermal gradient** **(°C km^{-1})**
13	London Clay	1	2 - school 1.5 - office 2.4 - apartment	n/a	0	120 - school 360 - office 480 - apartment	**150**	5	N/A 10°C constant
14	Magnesian Limestone	1	2 - school 1.5 - office 2.4 - apartment	n/a	0	120 - school 360 - office 480 - apartment	**150**	5	N/A 10°C constant
15	Old Red Sandstone	1	2 - school 1.5 - office 2.4 - apartment	n/a	0	120 - school 360 - office 480 - apartment	**150**	5	N/A 10°C constant
1	London Clay	1	2 - school 1.5 - office 2.4 - apartment	n/a	0	120 - school 360 - office 480 - apartment	200	5	N/A 10°C constant
2	Magnesian Limestone	1	2 - school 1.5 - office 2.4 - apartment	n/a	0	120 - school 360 - office 480 - apartment	200	5	N/A 10°C constant
3	Old Red Sandstone	1	2 - school 1.5 - office 2.4 - apartment	n/a	0	120 - school 360 - office 480 - apartment	200	5	N/A 10°C constant
16	London Clay	1	2 - school 1.5 - office 2.4 - apartment	n/a	0	120 - school 360 - office 480 - apartment	250	5	N/A 10°C constant
17	Magnesian Limestone	1	2 - school 1.5 - office 2.4 - apartment	n/a	0	120 - school 360 - office 480 - apartment	250	5	N/A 10°C constant
18	Old Red Sandstone	1	2 - school 1.5 - office 2.4 - apartment	n/a	0	120 - school 360 - office 480 - apartment	250	5	N/A 10°C constant

Table 7.7 Details of application test Group 2B – well diameter with multiple well arrangements

Group 2B well diameter - multiple wells	**Lithostrati-graphical formations**	**Number of wells**	**Total flow rate** (Ls^{-1})	**Flow rate per well** (Ls^{-1})	**Bleed flow** (%)	**Well depth** (m)	**Diameter of well** (mm)	**Well spacing** (m)	**Geothermal gradient** ($°C\ km^{-1}$)
19	London Clay	2 - school 3 - office 4 - apartment	2 - school 1.5 - office 2.4 - apartment	1 - school 0.5 - office 0.6 - apartment	0	60 - school 120 - office 120 - apartment	**150**	5	N/A 10°C constant
20	Magnesian Limestone	2 - school 3 - office 4 - apartment	2 - school 1.5 - office 2.4 - apartment	1 - school 0.5 - office 0.6 - apartment	0	60 - school 120 - office 120 - apartment	**150**	5	N/A 10°C constant
21	Old Red Sandstone	2 - school 3 - office 4 - apartment	2 - school 1.5 - office 2.4 - apartment	1 - school 0.5 - office 0.6 - apartment	0	60 - school 120 - office 120 - apartment	**150**	5	N/A 10°C constant
7*	London Clay	2 - school 3 - office 4 - apartment	2 - school 1.5 - office 2.4 - apartment	1 - school 0.5 - office 0.6 - apartment	0	60 - school 120 - office 120 - apartment	**200**	5	N/A 10°C constant
8*	Magnesian Limestone	2 - school 3 - office 4 - apartment	2 - school 1.5 - office 2.4 - apartment	1 - school 0.5 - office 0.6 - apartment	0	60 - school 120 - office 120 - apartment	**200**	5	N/A 10°C constant
9*	Old Red Sandstone	2 - school 3 - office 4 - apartment	2 - school 1.5 - office 2.4 - apartment	1 - school 0.5 - office 0.6 - apartment	0	60 - school 120 - office 120 - apartment	**200**	5	N/A 10°C constant
22	London Clay	2 - school 3 - office 4 - apartment	2 - school 1.5 - office 2.4 - apartment	1 - school 0.5 - office 0.6 - apartment	0	60 - school 120 - office 120 - apartment	**250**	5	N/A 10°C constant
23	Magnesian Limestone	2 - school 3 - office 4 - apartment	2 - school 1.5 - office 2.4 - apartment	1 - school 0.5 - office 0.6 - apartment	0	60 - school 120 - office 120 - apartment	**250**	5	N/A 10°C constant
24	Old Red Sandstone	2 - school 3 - office 4 - apartment	2 - school 1.5 - office 2.4 - apartment	1 - school 0.5 - office 0.6 - apartment	0	60 - school 120 - office 120 - apartment	**250**	5	N/A 10°C constant

Table 7.8 Details of application test Group 3B – well spacing with multiple well arrangement

Group 3B well spacing – multiple wells	**Lithostrati-graphical formations**	**Number of wells**	**Total flow rate** (Ls^{-1})	**Flow rate per well** (Ls^{-1})	**Bleed flow** (%)	**Well depth** (m)	**Diameter of well** (mm)	**Well spacing** (m)	**Geothermal gradient** ($°C\ km^{-1}$)
31	London Clay	2 - school 3 - office 4 - apartment	2 - school 1.5 - office 2.4 - apartment	1 - school 0.5 - office 0.6 - apartment	0	60 - school 120 - office 120 - apartment	200	**2**	N/A 10°C constant
32	Magnesian Limestone	2 - school 3 - office 4 - apartment	2 - school 1.5 - office 2.4 - apartment	1 - school 0.5 - office 0.6 - apartment	0	60 - school 120 - office 120 - apartment	200	**2**	N/A 10°C constant
33	Old Red Sandstone	2 - school 3 - office 4 - apartment	2 - school 1.5 - office 2.4 - apartment	1 - school 0.5 - office 0.6 - apartment	0	60 - school 120 - office 120 - apartment	200	**2**	N/A 10°C constant
7	London Clay	2 - school 3 - office 4 - apartment	2 - school 1.5 - office 2.4 - apartment	1 - school 0.5 - office 0.6 - apartment	0	60 - school 120 - office 120 - apartment	200	**5**	N/A 10°C constant
8	Magnesian Limestone	2 - school 3 - office 4 - apartment	2 - school 1.5 - office 2.4 - apartment	1 - school 0.5 - office 0.6 - apartment	0	60 - school 120 - office 120 - apartment	200	**5**	N/A 10°C constant
9	Old Red Sandstone	2 - school 3 - office 4 - apartment	2 - school 1.5 - office 2.4 - apartment	1 - school 0.5 - office 0.6 - apartment	0	60 - school 120 - office 120 - apartment	200	**5**	N/A 10°C constant
34	London Clay	2 - school 3 - office 4 - apartment	2 - school 1.5 - office 2.4 - apartment	1 - school 0.5 - office 0.6 - apartment	0	60 - school 120 - office 120 - apartment	200	**8**	N/A 10°C constant
35	Magnesian Limestone	2 - school 3 - office 4 - apartment	2 - school 1.5 - office 2.4 - apartment	1 - school 0.5 - office 0.6 - apartment	0	60 - school 120 - office 120 - apartment	200	**8**	N/A 10°C constant
36	Old Red Sandstone	2 - school 3 - office 4 - apartment	2 - school 1.5 - office 2.4 - apartment	1 - school 0.5 - office 0.6 - apartment	0	60 - school 120 - office 120 - apartment	200	**8**	N/A 10°C constant

Table 7.9 Details of application test Group 4A – thermal gradient with single well arrangement

Group 4A thermal gradient check – single well	**Lithostrati-graphical formations**	**Number of wells**	**Total flow rate** (Ls^{-1})	**Flow rate per well** (Ls^{-1})	**Bleed flow** (%)	**Well depth** (m)	**Diameter of well** (mm)	**Well spacing** (m)	**Geothermal gradient** (°C km^{-1})
37	London Clay	1	2 - school 1.5 - office 2.4 - apartment	n/a	0	120 - school 360 - office 480 - apartment	200	5	**31.0**
38	Magnesian Limestone	1	2 - school 1.5 - office 2.4 - apartment	n/a	0	120 - school 360 - office 480 - apartment	200	5	**27.0**
39	Old Red Sandstone	1	2 - school 1.5 - office 2.4 - apartment	n/a	0	120 - school 360 - office 480 - apartment	200	5	**16.8**
1	London Clay	1	2 - school 1.5 - office 2.4 - apartment	n/a	0	120 - school 360 - office 480 – apartment	200	5	N/A 10°C constant
2	Magnesian Limestone	1	2 - school 1.5 - office 2.4 - apartment	n/a	0	120 – school 360 - office 480 – apartment	200	5	N/A 10°C constant
3	Old Red Sandstone	1	2 - school 1.5 - office 2.4 - apartment	n/a	0	120 – school 360 - office 480 – apartment	200	5	N/A 10°C constant

Table 7.10 Details of application test Group 4B – geothermal gradient with multiple well arrangements

Group 4B thermal gradient check – multiple wells	**Lithostrati-graphical formations**	**Number of wells**	**Total flow rate** **(Ls^{-1})**	**Flow rate per well** **(Ls^{-1})**	**Bleed flow** **(%)**	**Well depth** **(m)**	**Diameter of well** **(mm)**	**Well spacing** **(m)**	**Geothermal gradient** **(°C km^{-1})**
40	London Clay	2 - school	2 - school	1 - school	0	60 - school	200	5	**31.0**
		3 - office	1.5 - office	0.5 - office		120 - office			
		4 - apartment	2.4 - apartment	0.6 - apartment		120 - apartment			
41	Magnesian Limestone	2 - school	2 - school	1 - school	0	60 - school	200	5	**27.0**
		3 - office	1.5 - office	0.5 - office		120 - office			
		4 - apartment	2.4 - apartment	0.6 - apartment		120 - apartment			
42	Old Red	2 - school	2 - school	1 - school	0	60 - school	200	5	**16.8**
	Sandstone	3 - office	1.5 - office	0.5 - office		120 - office			
		4 - apartment	2.4 - apartment	0.6 - apartment		120 - apartment			
7	London Clay	2 - school	2 - school	1 - school	0	60 - school	200	**5**	N/A
		3 - office	1.5 - office	0.5 - office		120 - office			10°C constant
		4 - apartment	2.4 - apartment	0.6 - apartment		120 - apartment			
8	Magnesian Limestone	2 - school	2 - school	1 - school	0	60 - school	200	**5**	N/A
		3 - office	1.5 - office	0.5 - office		120 - office			10°C constant
		4 - apartment	2.4 - apartment	0.6 - apartment		120 - apartment			
9	Old Red	2 - school	2 - school	1 - school	0	60 - school	200	**5**	N/A
	Sandstone	3 - office	1.5 - office	0.5 - office		120 - office			10°C constant
		4 - apartment	2.4 - apartment	0.6 - apartment		120 - apartment			

7.3. Description of the model output

To consider the performance of SCW operation with all of the variants described in the previous section requires a long-term perspective because the thermal capacity of rock formations is very large, thus changes in geothermal variables (particularly formation temperature) tend to occur gradually over long periods of time. This is a particularly important consideration when analysing changes in rock temperatures over time when variable heating and cooling loads are imposed. It is therefore necessary to consider time horizons of greater than one annual cycle. As a compromise for acceptable computation times, a five-year time horizon is used here. From this, it should be possible to identify the general direction of long-term change in the formation temperature. It has been assumed that the simulated building loads (Figures 7.2, 7.3 and 7.4) will concatenate to form five years of repeating annual sequences. Two variables are extracted and presented from each simulation:

1. The outlet well water temperature from the suction pipe (in each SCW or SCW array). It is useful to justify the heat transfer performance from the ground loop (SCW) under various design parameters and hence the overall system performance.
2. The mean rock formation temperature. This is the average temperature surrounding a well in four different directions at 0.6m (the grid size used in the model) below the water level. It is useful to determine the impact of the surrounding environment due to the operation of the GHCS.

These variables are outputted on an hourly basis from the SCW model (Appendix C); however, only the annual maximum and minimum values of these variables are presented here with the aim of simplifying the presentation of results over the five-year simulation period.

The annual maximum and minimum water temperatures represent the annual range of the source (heating)/sink (cooling) temperature to the GHCS during the annual operational

cycle, which defines the extreme operation boundary of the system each year. A lower maximum well water temperature is beneficial to system performance during summer. Likewise, a higher minimum well water temperature is beneficial during the heat pump mode in winter.

On the other hand, the annual maximum and minimum mean rock formation temperatures signify the impact of the heat rejection or abstraction from the GHCS to the surrounding rock environment. The initial formation temperature of 10°C is applied to all cases in Groups 1, 2 and 3. A range of geothermal gradients (expressed as a variable initial formation temperature along the vertical (z) plane) is applied to the cases in Group 4 to reveal the impact of significant variations in initial undisturbed formation temperatures (as has been noted, for example, by Banks, *et al*.(2009)).

In the results that follow (and, in general) the best results are those configurations that lead to the highest well water discharge (and, hence, mean formation) temperatures in winter and the lowest well water discharge (and, hence, mean formation) temperatures in summer.

7.4. Application test results – Groups 1A and 1B – influence of bleed flow in three different rock types

The impact of bleed flow on three selected soil types (London Clay, Magnesian Limestone and Old Red Sandstone) with two options (10% constant bleed or no bleed) was investigated. The results for Group 1A were based on a single well arrangement, while multiple well arrangements were adopted for Group 1B.

7.4.1. Group 1A and Group 1B - results for the office building

With regards to the impact of bleed, it is clear that the well water temperature in summer (cooling mode) decreased by at least 0.1K in London Clay, 0.8K in Magnesian Limestone and 0.7K in Old Red Sandstone when groundwater was bled into the system under the single well arrangement (Group 1A - Figure 7.6). Likewise, at least 0.6K well water temperature reduction was found in all three soil types under the influence of bleed with the multiple well arrangement (Group 1B - Figure 7.7) throughout a five-year period. Nevertheless, the bleed action did not have a significant impact on the well water temperature during the heat pump mode in winter. An increase of approximately 0.1K in well water temperature was found in Group 1A (office building) with reference to the same soil choices after the first winter year, but this improvement gradually diminished after five years' operation in all three soils. Similarly, no improvement was found on the well water in Group 1B during the winter by bleeding.

According to the choice of soil type, the results from Group 1A (the office building) clearly show that the two cases with London Clay were the worst cases in both summer and winter seasons. It returned the highest well water temperature in the summer and the lowest well water temperature in the winter over the entire operation period among all cases in this group. Likewise, it was also the worst soil type under the multiple well arrangement in

Group 1B (the office building) during summer, but this was not the case in winter. It appeared that the well water temperature under the multiple well arrangement (Group 1B) increased much faster than the same case (with the same soil type and bleed option) under the single well arrangement (Group 1A). Furthermore, a significant mean rock formation temperature rise occurred in all Group 1B cases (under the multiple well arrangement), as shown in Figure 7.9, particularly for the cases with no bleed or in London Clay during the winter. This is expected as it is a cooling-dominant building. This explains why the well water temperature of the two London Clay cases increased very quickly over time in Group 1B and eventually provided a relatively high temperature of well water after several years' operation. The other cases (with Magnesian Limestone or Old Red Sandstone) provided similar water temperatures in both groups, with reference to the same bleed options.

By comparing the water temperature of the relevant cases between Groups 1A and 1B, it is clear that the multiple well arrangement was able to offer a relatively wider well water temperature range over time; therefore a higher heat transfer rate was achieved under this arrangement.

Regarding the rock formation temperatures, Figures 7.8 and 7.9 clearly indicate an increase in mean temperature in both groups' results over the five year period. This was due to the relatively large cooling demands in this building (a heating to cooling demand ratio of 7:1). It can be seen that the maximum and minimum mean formation temperatures in both groups also increased rapidly between the 1st year and 2nd year, but the rate of increase gradually declined towards the end of the 5th year (Figure 7.8) for all cases in Group 1A (office building), especially for the Magnesian Limestone and Old Red Sandstone cases. On the other hand, a slowly but noticeable rise in mean rock formation temperature was found in most of the cases in Group 1B (office building) under the multiple well arrangement.

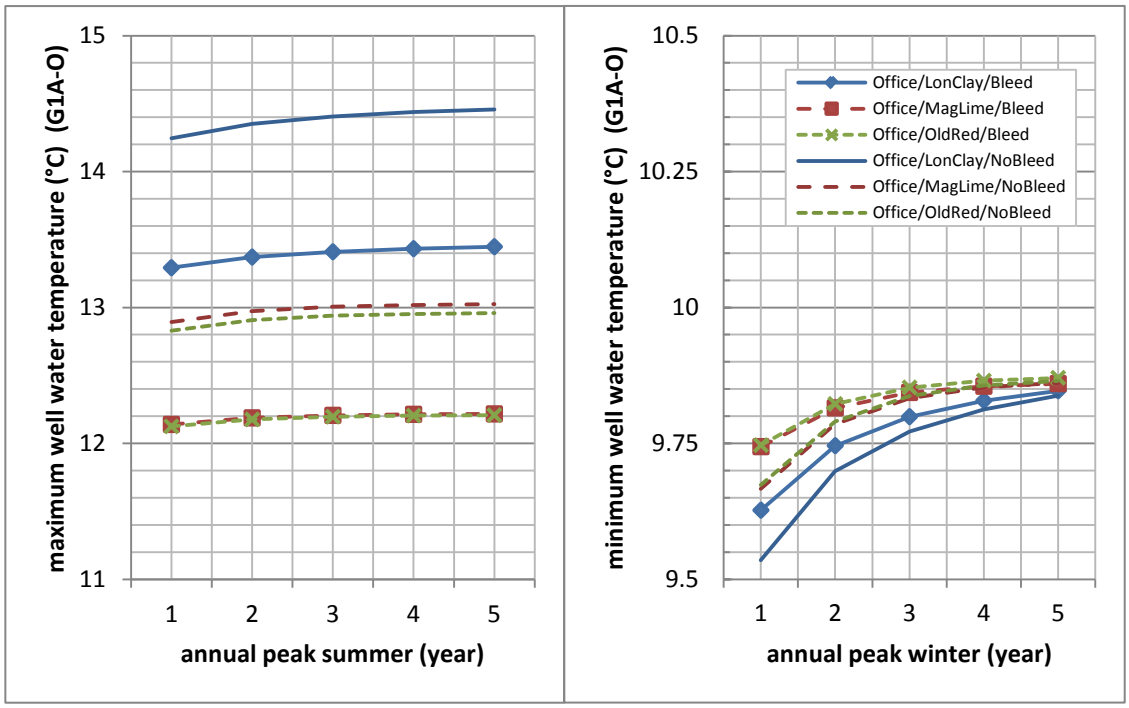

Figure 7.6 Results of Group 1A (office) – well outlet water temperature under the single well arrangement

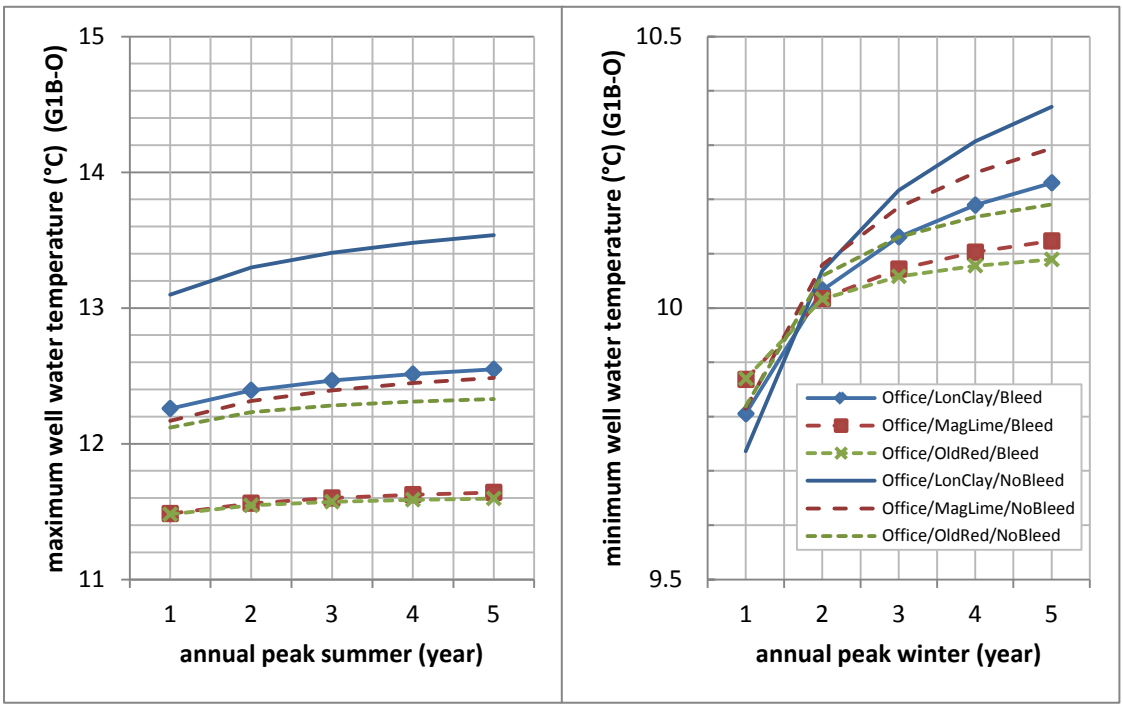

Figure 7.7 Results of Group 1B (office) – well outlet water temperature under the multiple well arrangement

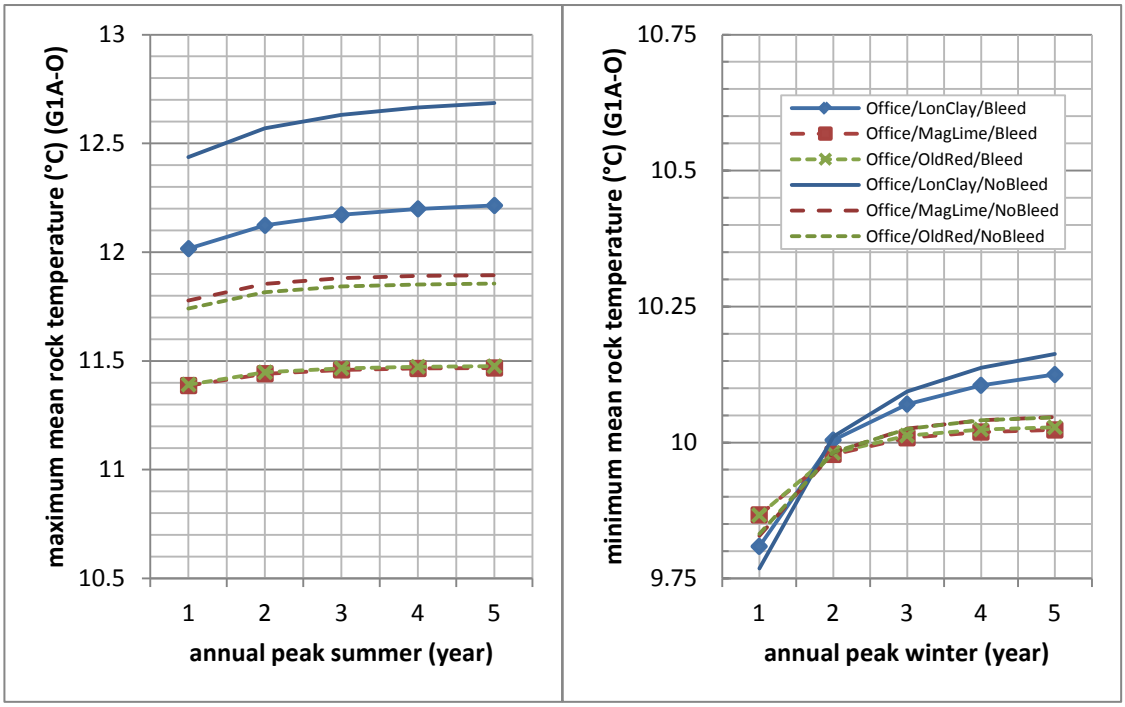

Figure 7.8 Results of Group 1A (office) – mean rock formation temperature under the single well arrangement

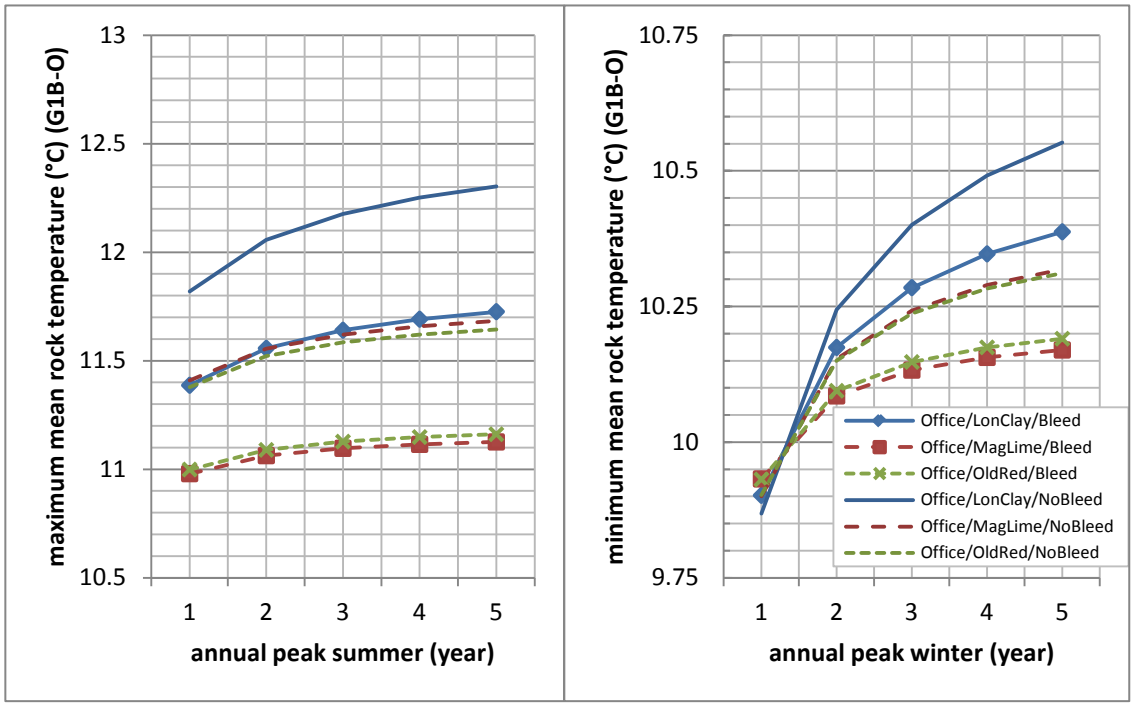

Figure 7.9 Results of Group 1B (office) – mean rock formation temperature under the multiple well arrangement

7.4.2. Group 1A and Group 1B - results for the apartment building

Reflecting on the results from the office building, similar findings were found for the apartment building with regards to the performance with various rock formations. The London Clay was still the least favourable formation in both heating and cooling seasons under the single well arrangement (Figure 7.10), but it was a different scenario under the multiple well arrangement in Group 1B (Figure 6.11). Regardless of the soil type, the three non-bleeding cases provided the highest well water temperature during summer; however, they also gave the highest well water temperature during the winter too after just two years of operation. Correspondingly, a significant mean formation temperature rise is evident in Figure 7.13. Again, the other cases with Magnesian Limestone and Old Red Sandstone provided very similar temperature curves in Figures 7.10 and 7.11 with reference to the same bleed choices.

With bleed applied, the well water temperature in summer was reduced by at least 2.2K in Group 1A and almost 2K in Group 1B for all formation types compared with their non-bleed counterparts over the entire operation period during the summer. In winter, the well water temperature increased by a minimum of 0.3K for all formation types under the influence of bleed in the 1st year (winter) in Group 1A, but this temperature difference reduced gradually over time due to the relatively fast rock formation temperature rise in non-bleed cases. The temperature rise in non-bleed cases was even more severe under multiple well arrangements.

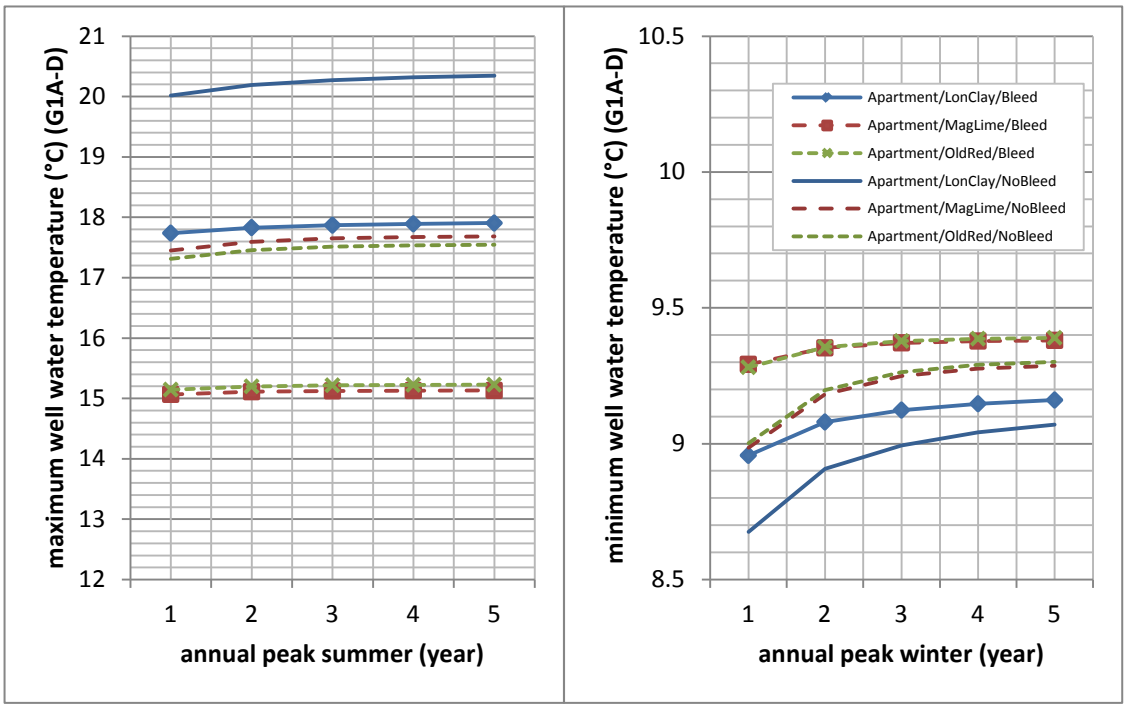

Figure 7.10 Results of Group 1A (apartment) – well outlet water temperature under the single well arrangement

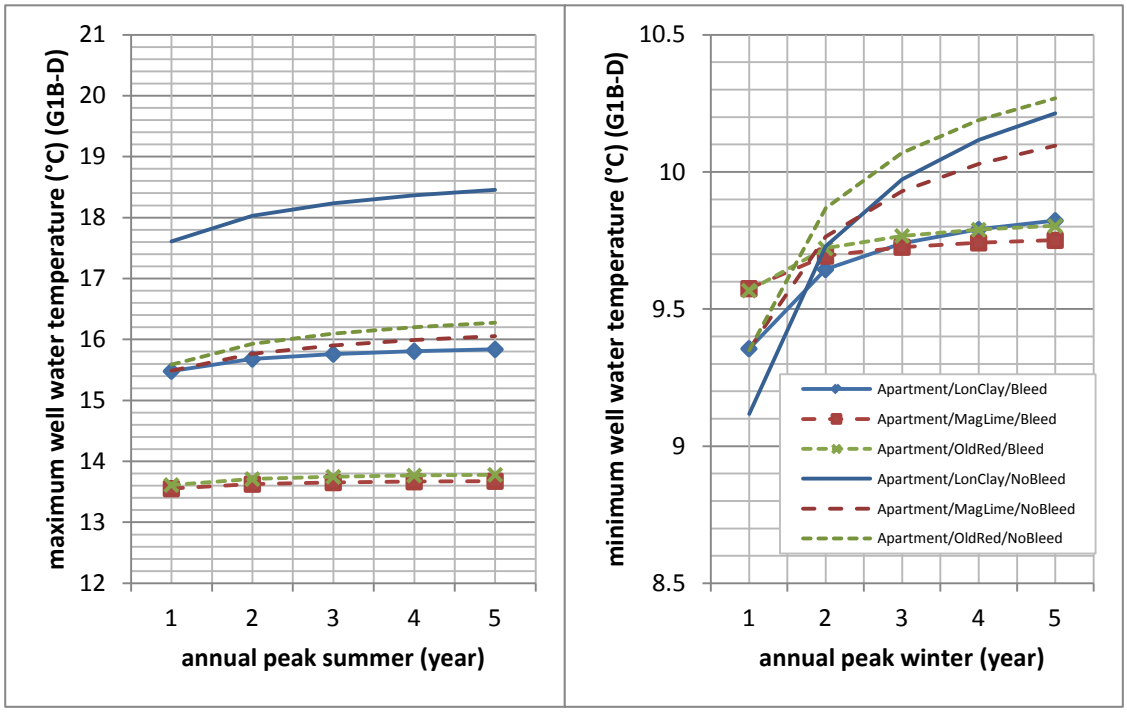

Figure 7.11 Results of Group 1B (apartment) – well outlet water temperature under the multiple well arrangement

By comparing the results of Group 1A and Group 1B for the apartment building, it is clear that higher heat transfer performance is likely to be achieved under the multiple well arrangement (Group 1B) in contrast to relevant cases under the single well arrangement (Group 1A). Multiple wells deliver relatively higher well water temperature in winter and relatively lower well water temperature in summer. A similar pattern (though a little less pronounced) is evident for the office building. A clear conclusion of this is that heat pump performance would be better under a multiple well cluster than it would with a single well of equivalent overall length. This is due to the larger conduction front (i.e. effective radius of conduction) involved in the multiple well cluster arrangement than is the case with a single well.

It is important to note that the heating demands of this building are higher than the cooling demands, with a heating to cooling demand ratio of 2.5:1. However, the mean rock formation temperature in both sets of results showed a slowly increasing trend over the five years.

One of the possible reasons for this is the poor seasonal performance (*CoP*) of the chosen heat pump for this particular application. As the heating/cooling demands fluctuate frequently in the apartment building, it always falls below the operation range of the chosen heat pump, resulting in relatively poor *CoP*. The average *CoP* for this application are 1.66 (heat pump mode) and 1.07 (cooling mode), which are far below the design *CoP* value between 3 – 5 based on the heat pump rated output.

Given that the annual heating and cooling demands of this building are 49784kWh (heating) and 19360.1kWh (cooling), it is possible to calculate the heat balance across the seasons by following Equation 6.1. At equilibrium, the annual cooling demands have to be 10184kWh to balance out the actual heating demand of 49784kWh; however, this balanced cooling demand value is slightly lower than the actual annual cooling requirement. Perhaps this explains why the mean formation temperature increases over time in this heating-dominant

building. However, this is an unusual case which is considered as a bad design. For comparison purpose, only one heat pump unit is chosen for each building to match the peak load. In practice, a number of smaller heat pump modules should be used in order to achieve a better part loads performance.

Equation 7.1

$$\sum H = \frac{COP_{\text{Heating}}(COP_{\text{Cooling}} + 1)}{COP_{\text{Cooling}}(COP_{\text{Heating}} - 1)} \sum C$$

where:

$\sum C$ = cooling demand from the building (kW)

$\sum H$ = heaing demand from the building (kW)

In cooling mode:

CoP_{cooling} = cooling effect / (heat rejected to the ground - cooling effect)

In heating mode:

CoP_{heating} = heating effect / (heating effect - heat extracted from the ground)

Equation 7.1 is derived from the following expression of *CoP* in cooling mode and heating mode. It is assumed that the heat rejected to the ground is same as the heat extracted from the ground at equilibrium.

The mean formation temperature grew slowly over time in Group 1A, especially during summer: the mean rock formation temperature for five out of six cases in this group grew by less than 1.5K over five years. A slightly more significant rise in mean rock formation temperature was found for most of the non-bleed cases in Group 1B, regardless of the rock formation choice.

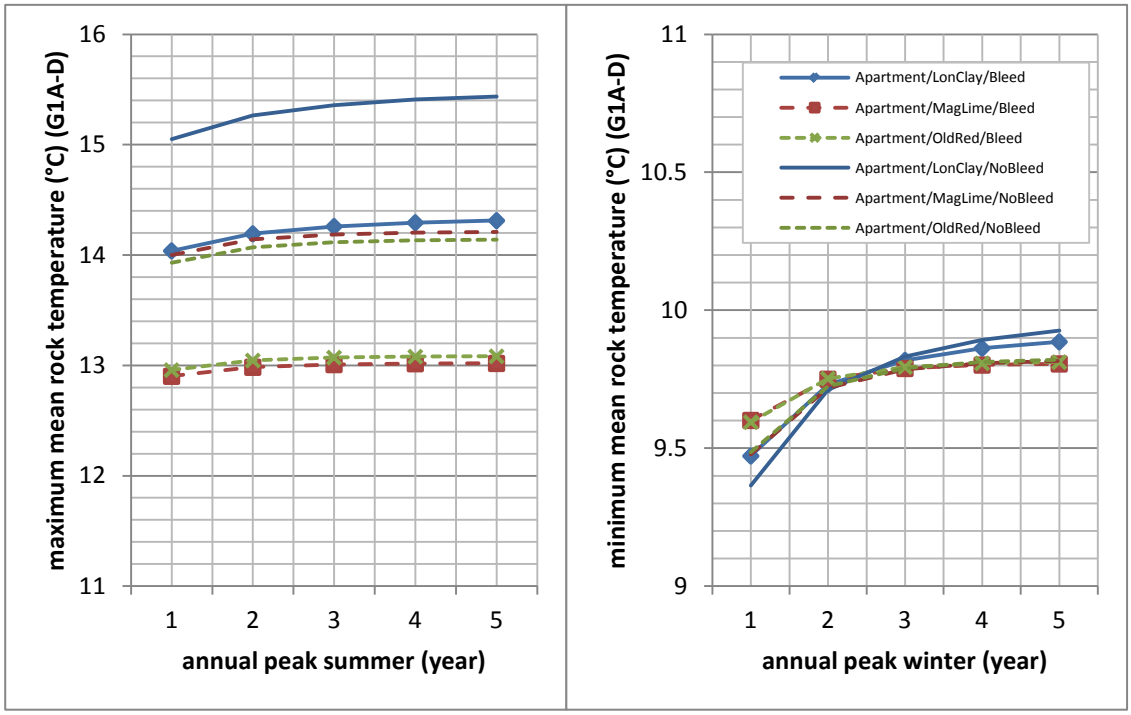

Figure 7.12 Results of Group 1A (apartment) – mean rock formation temperature under the single well arrangement

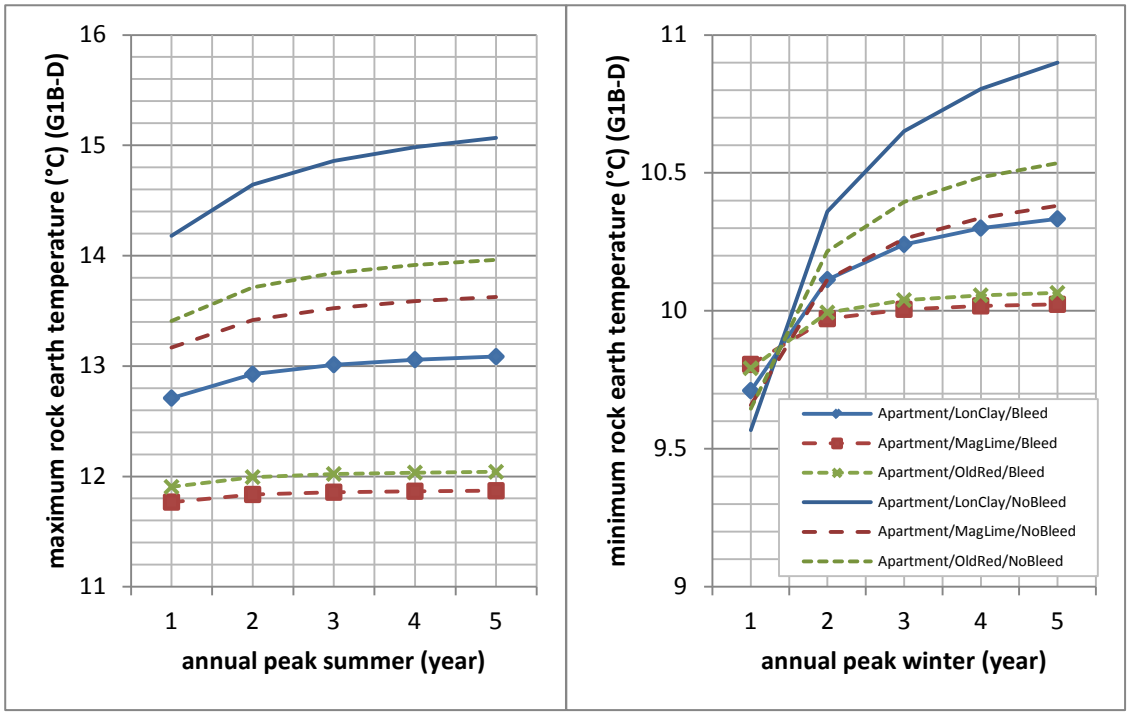

Figure 7.13 Results of Group 1B (apartment) – mean rock formation temperature under multiple well arrangement

7.4.3. Group 1A and Group 1B - results for the school building

This building does not have any cooling loads. Thus, only the minimum well water temperature during the winter season was of concern in the following analysis.

The London Clay performed least well out of the three formation choices for both the bleed flow case and the non-bleed case, returning the lowest well water temperature during the winter. The results are summarised in Figures 7.14 and 7.15.

Regarding the bleed flow option, it appears that all three formation types were capable of delivering a significantly higher water temperature than the non-bleed cases for both well arrangements over the entire operation period, unlike the situations observed in the office

and apartment buildings during the winter time, for which the improvement in winter temperatures was more modest.

Comparing the water temperature results of Group 1A and Group 1B, it clearly shows that a slightly higher water temperature was achieved under the multiple well arrangements with reference to the relevant cases of single well arrangement.

With regards to the mean formation temperature, a very small reduction (less than 0.15K over five years) was observed for both bleed options. However, it was very clear that the mean formation temperature of the non-bleed cases reduced significantly faster than those with bleed.

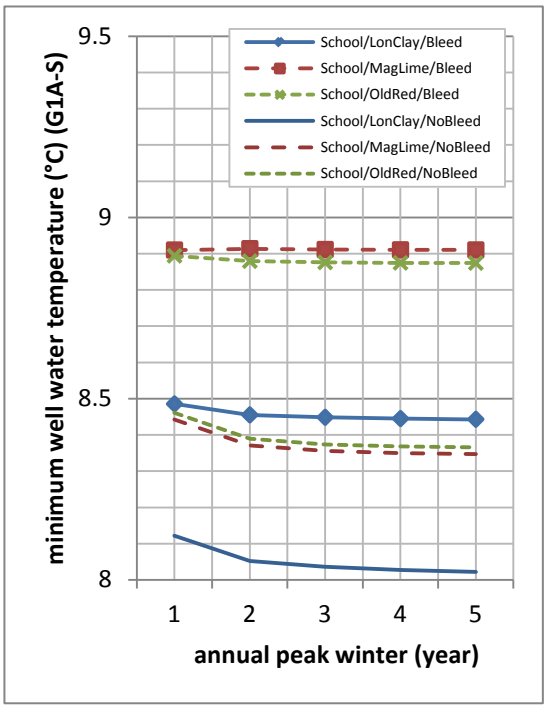

Figure 7.14 Results of Group 1A (school) – well outlet water temperature under single well arrangement

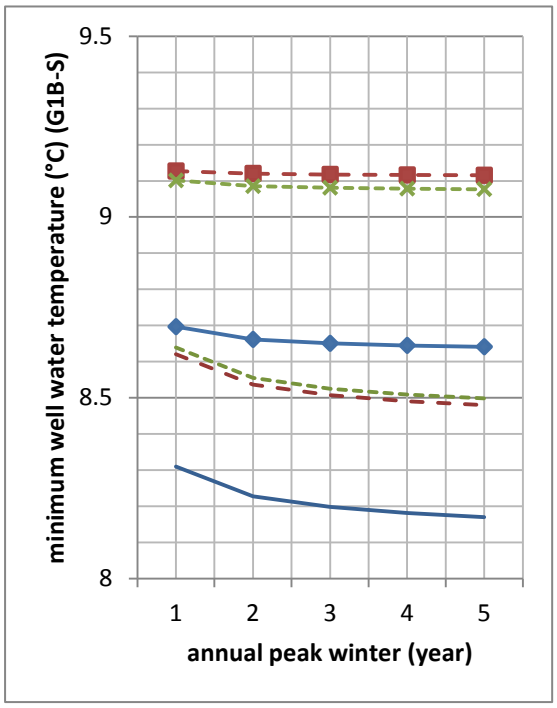

Figure 7.15 Results of Group 1B (school) – well outlet water temperature under multiple well arrangement

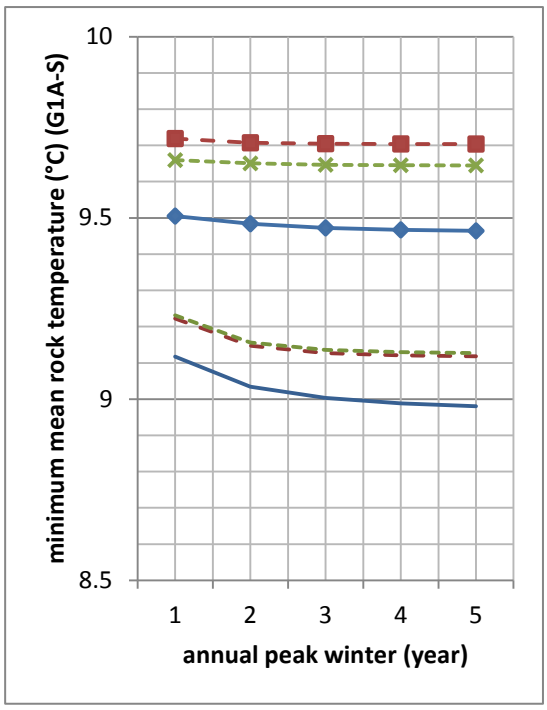

Figure 7.16 Results of Group 1A (school) – mean rock formation temperature under singe well arrangement

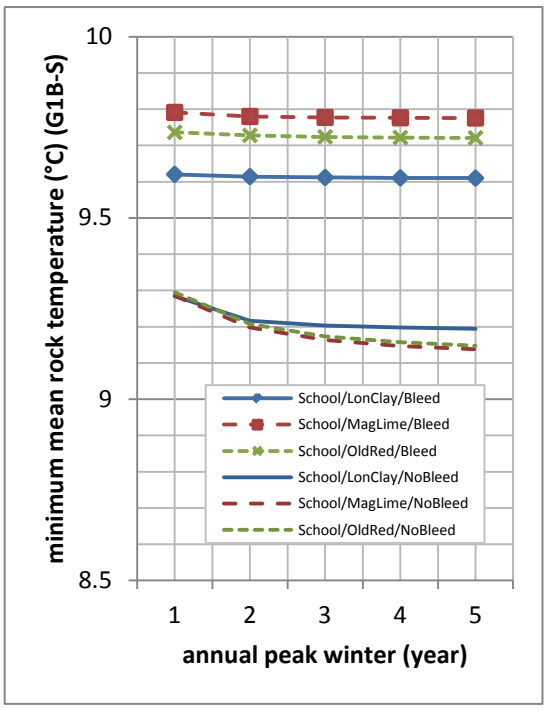

Figure 7.17 Results of Group 1B (school) – mean rock formation temperature under multiple well arrangement

7.4.4. Conclusion of the results of Groups 1A and 1B

The results for all three buildings indicate that the outlet well water temperature from the ground loop (SCW) was influenced by the choice of rock formation type. The Magnesian Limestone and Old Red Sandstone were better choices than London Clay. This was due to their higher thermal conductivity values. In addition, the results indicate that the variation of the mean rock temperature in London Clay was slightly higher than in the other two rock types under the same heating and cooling demands.

The results show that bleed action reduces swings in temperature, leading to a more stable environment for heat transfer. The results from the office and apartment buildings reveal the benefit of bleed during the summer in terms of reducing the well water temperature in summer, and the results from a heated-only building (i.e. the school building) also confirm the satisfactory operation against well water freezing in typical UK winter conditions. Thus, bleed should always be considered in order to enhance system performance by providing higher and lower water temperatures to the GHCS during winter and summer operation, correspondingly. There are, of course, numerous bleed control possibilities that merit detailed analysis and this forms a basis for future work.

With regards to the well arrangement, the results show that multiple wells is capable of offering slightly higher heat transfer performance than the equivalent single well for all three buildings, based on the same rock type. This is considered to be due to the larger conduction front generating by the multiple well cluster arrangement than is the case with the equivalent single well arrangement. This finding is very useful to promote the use of multiple wells arrangements as it can offer considerable savings on the geotechnical drilling cost.

In addition, the increasing mean rock formation temperature observed in the heating dominate building cases (i.e. the apartment building) revealed a negative impact attributed to the insufficient part load performance of the heat pump plant. In practice, a number of

smaller heat pump modules would have been used for this case to improve the part load performance instead of one huge plant.

7.5. Application test results – Group 2A and 2B – influence of borehole diameter

The sensitivity of the well water temperature to well borehole diameter was investigated. Three different borehole diameters (0.15m, 0.2m and 0.25m) were studied.

7.5.1. Group 2A and Group 2B results for the office building

Figures 7.18 and 7.19 show that the well water temperature improved (i.e. increased in winter; reduced in summer) as the well borehole diameter was increased for both well arrangements. In a single well arrangement, increasing the borehole diameter from 0.15m to 0.2m reduced the summer well water temperature by at least 26% and also increased the winter well water temperature by at least 6% for each formation type. Further improvement was possible by increasing the borehole diameter up to 0.25m; the summer well water temperature was reduced by a further 11% (minimum) and the winter well water temperature was increased by a further 1.6% (minimum). Similar improvements were noted with the multiple well case.

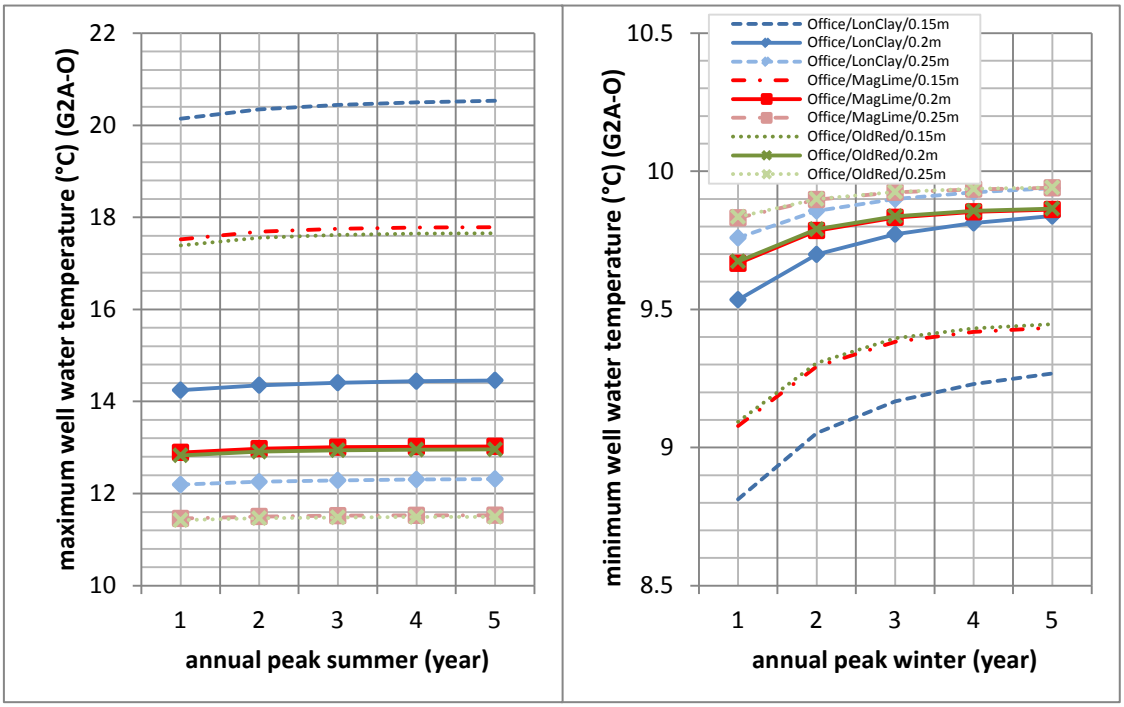

Figure 7.18 Results of Group 2A (office) – well outlet water temperature under single well arrangement

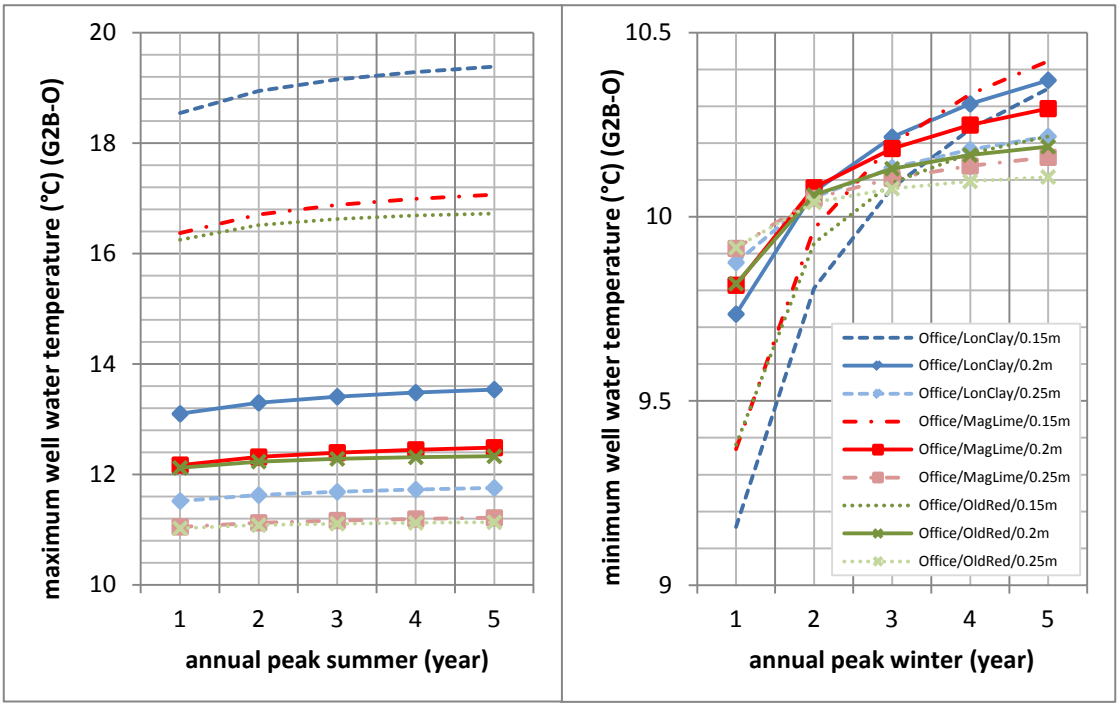

Figure 7.19 Results of Group 2B (office) – well outlet water temperature under multiple well arrangement

Figures 7.20 and 7.21 show a relatively rapid mean rock temperature rise with the smallest well borehole diameter (0.15m) regardless of the choice of rock type, particularly during winter. The minimum mean rock temperature (in winter) of these three small diameter cases under both well arrangements also increased by more than 4% during five years of operation, while only an average 2% rise was found in the other six cases with larger diameter sizes over the same period of time.

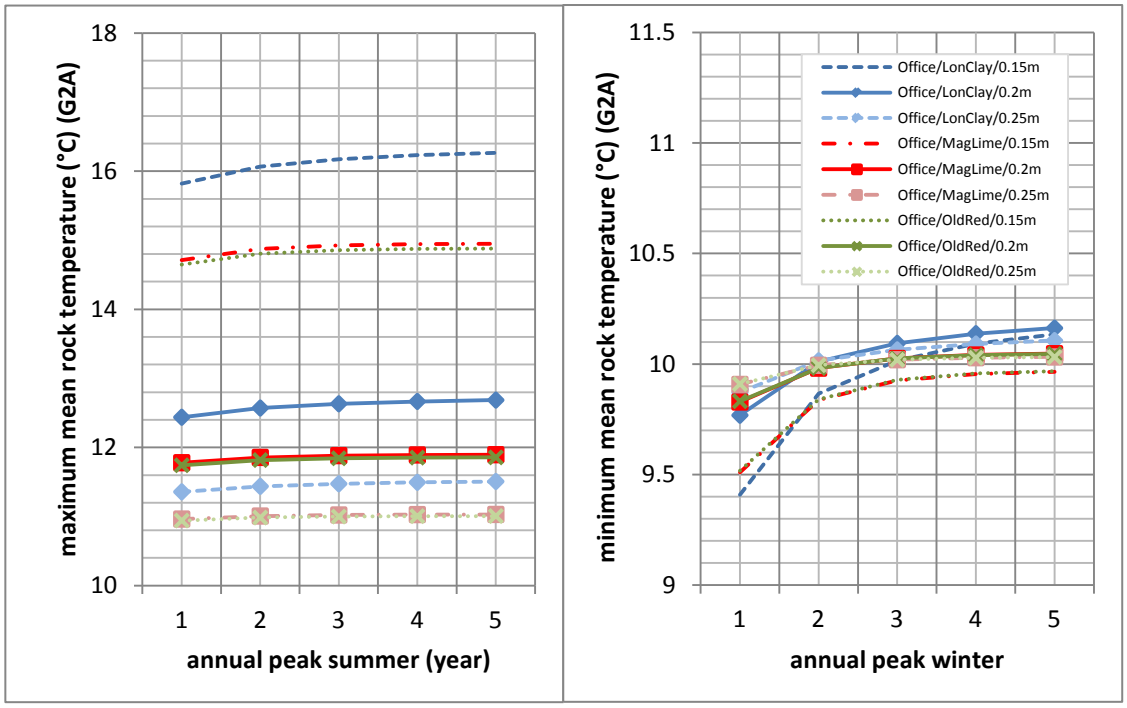

Figure 7.20 Results of Group 2A (office) – mean rock formation temperature under single well arrangement

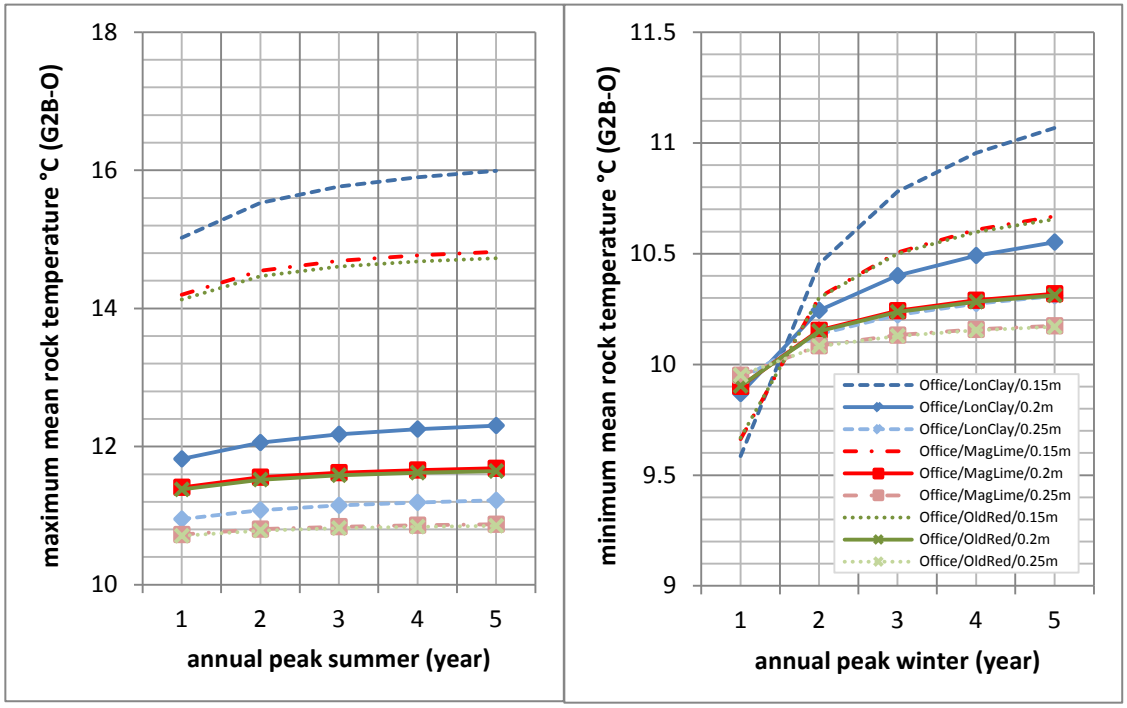

Figure 7.21 Results of group 2B (office) – mean rock formation temperature under multiple well arrangement

7.5.2. Group 2A and Group 2B - results for the apartment building

Given the results from office buildings, it seems that a larger borehole could offer better performance, but this did not completely agree with data from the apartment building. Increasing the borehole diameter from 0.15m to 0.2m suggests higher improvement than was obtained with the office building by reducing the summer well water temperature by over 50% and increasing the winter well water temperature by a minimum of 17% for all options (Figures 7.22 and 7.23). However, increasing the diameter beyond 0.2m resulted in declining heat transfer rates, lowering the well water temperature in winter and increasing it in summer.

One of the possible reasons might lie in the relative changes in the well surface heat transfer coefficient. Therefore, the impact on the (well surface) Nusselt number (Nu) due to the change of the borehole diameter (and hence the flow velocity and Reynolds number (Re) in

the annulus) in this building case was investigated. Gnielinski's expression (1976) (Equation 7.2 and 7.3) for turbulent flow condition in smooth tube was adopted to estimate the Nu. Only the London Clay cases were examined in this context.

Equation 7.2

$$Nu = 0.0219\ (Re^{0.8} - 100)Pr^{0.4}$$

for $0.5 < Pr < 1.5$; $10^4 < Re < 5 \times 10^6$

Equation 7.3

$$Nu = 0.012\ (Re^{0.87} - 280)Pr^{0.4}$$

for $1.5 < Pr < 500$; $3000 < Re < 10^6$

The results (figure 7.24) clearly showed that a relatively large reduction in Nu was found in the apartment building across all three borehole diameter measurements but it was not the case in the office building. The reduction in Nu in the office building case slowed down significantly after the first 50mm increment in borehole diameter (from 150mm to 200mm). The strong Nu reduction (in the apartment building) obviously offset the benefit of increasing the heat transfer area (i.e. borehole size) and hence explains why the largest borehole size of 250mm did not offer any further improvement in the heat transfer performance in this building.

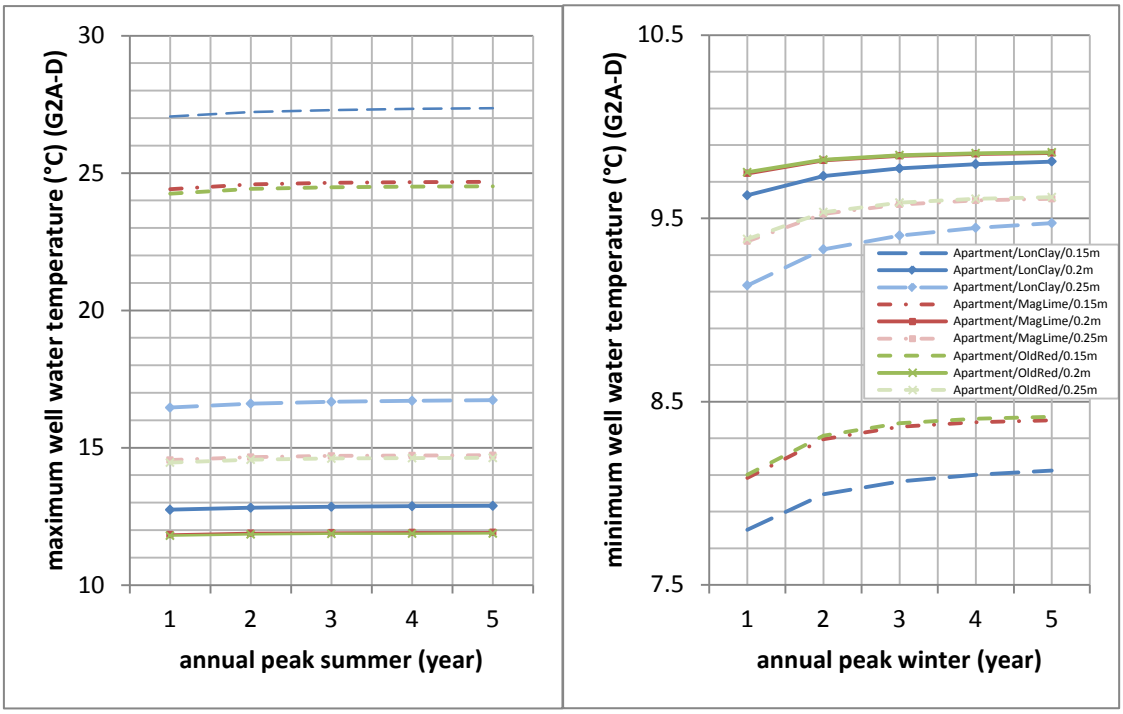

Figure 7.22 Results of Group 2A (apartment) – well outlet water under single well arrangement

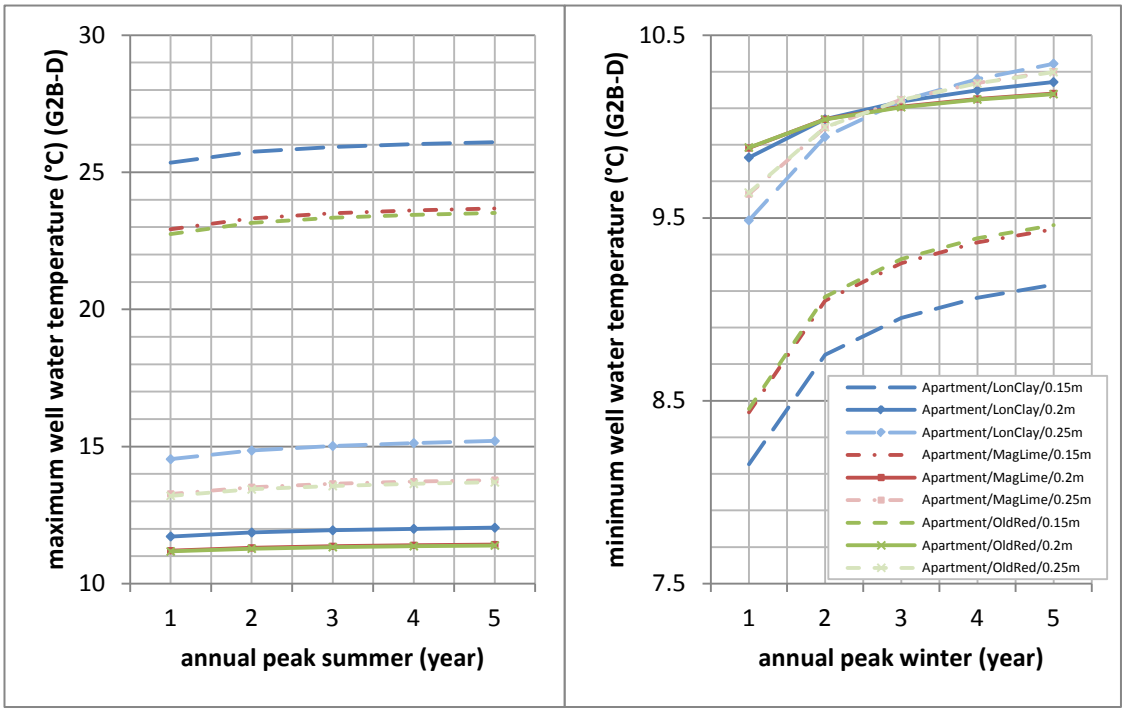

Figure 7.23 Results of Group 2B (apartment) – well outlet water under multiple well arrangement

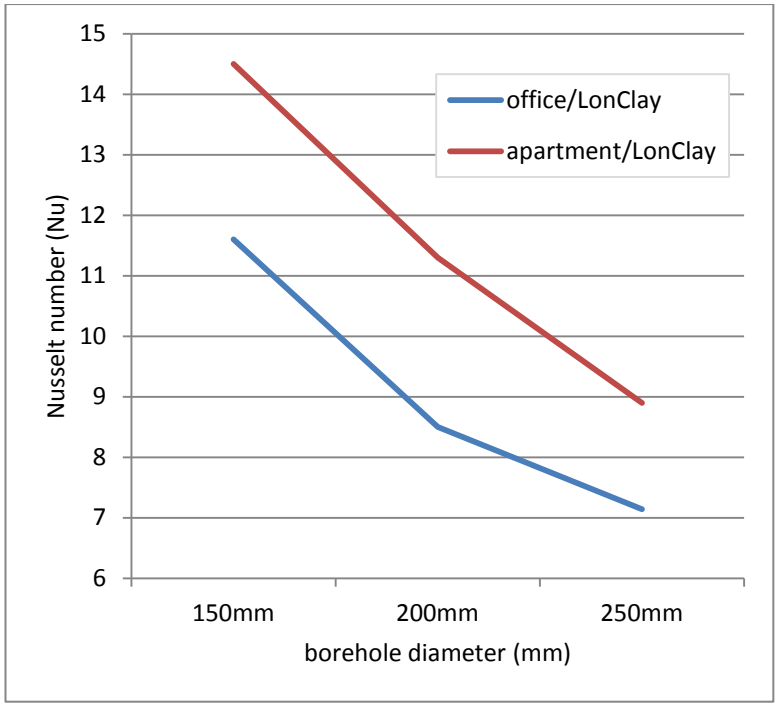

Figure 7.24 Nusselt number of one selected case in Group 2A for the office and apartment building

The mean rock formation temperature remained fairly steady for all but the smallest borehole diameter of 0.15m (Figures 7.25 and 7.26). In the worst scenario, the minimum mean rock temperature in Group 2B (London Clay with a borehole diameter of 0.15m) increased by more than 17% over five years of operation. In addition, a relatively significant mean rock temperature rise was also found based with the London Clay.

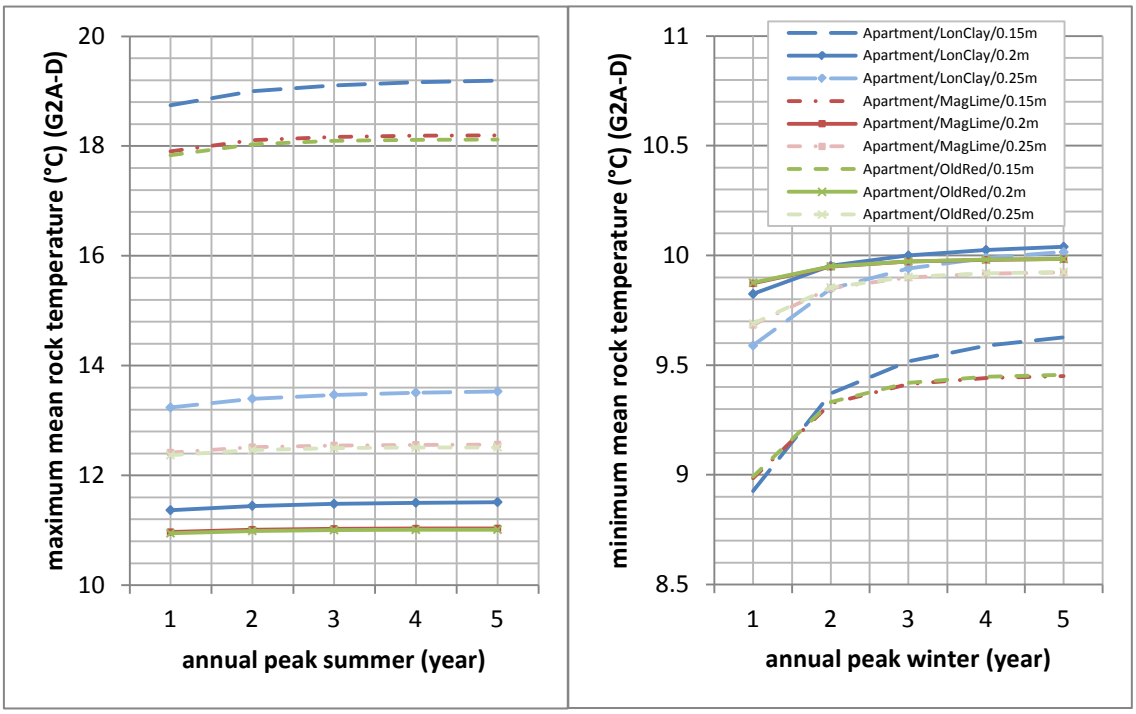

Figure 7.25 Results of Group 2A (apartment) – mean rock formation temperature under single well arrangement

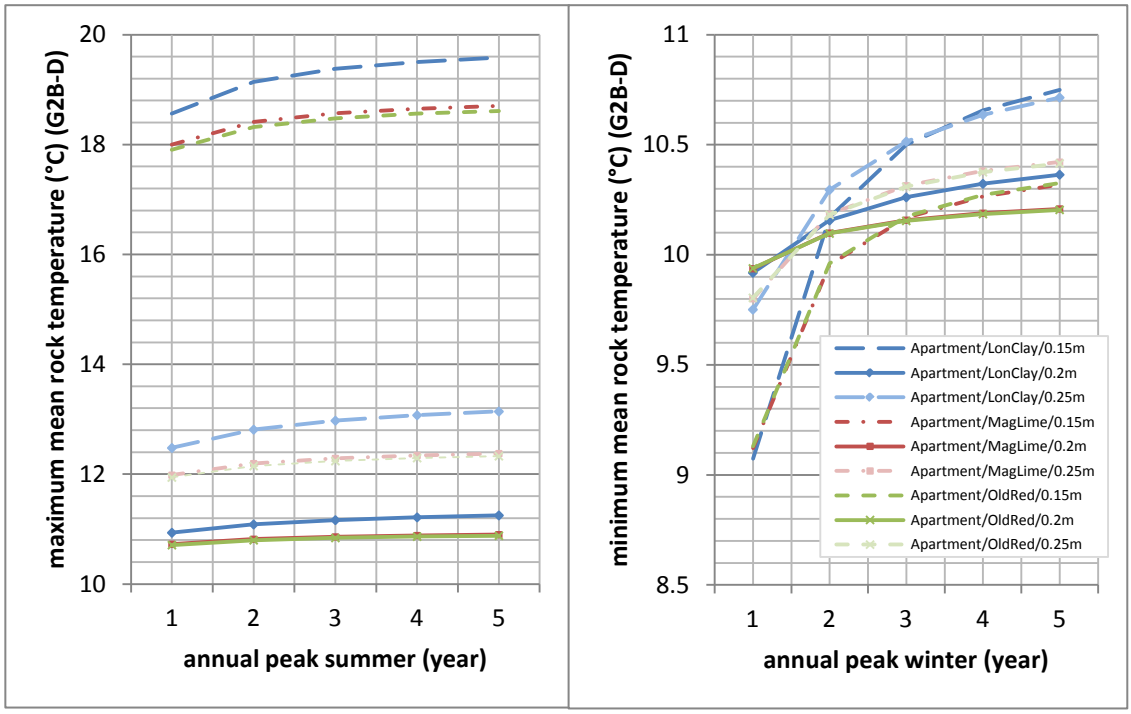

Figure 7.26 Results of Group 2B (apartment) – mean rock formation temperature under multiple well arrangement

7.5.3. Group 2A and Group 2B - results for the school building

In this heating-only application, it appears that the borehole with the smallest diameter (0.15m) provided the lowest winter well water temperature, while the largest diameter size of 0.25m offered the highest value among all cases and under both well arrangements, as shown in 7.27 and 7.28.

The results also indicate that the winter well water temperature increased by at least 8.5% for each rock formation after increasing the borehole diameter from 0.15m to 0.2m. A further increase of 5.8% (minimum) in winter well water temperature was achieved by increasing the well diameter from 0.2m to 0.25m.

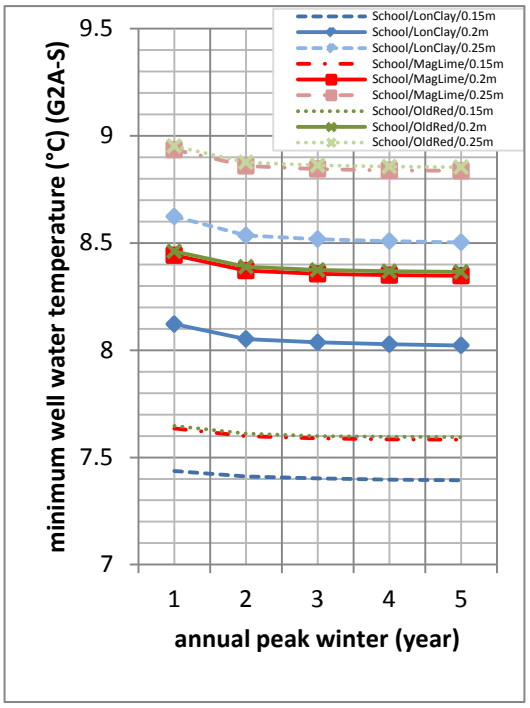

Figure 7.27 Results of Group 2A (school) – well outlet water temperature under single well arrangement

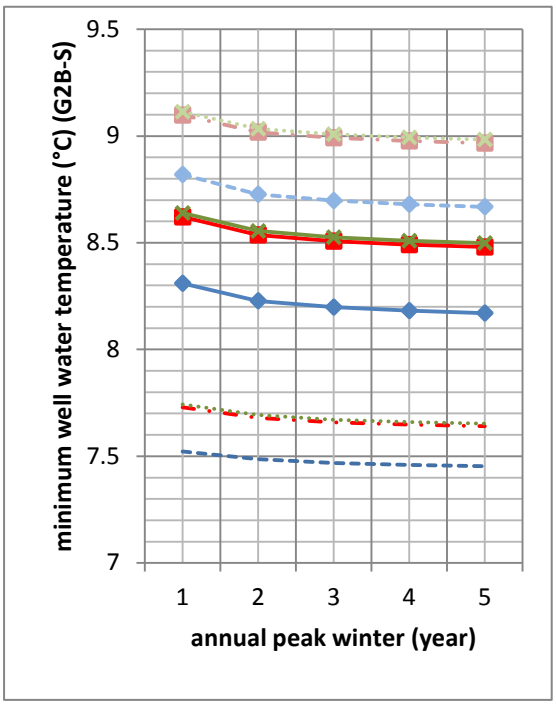

Figure 7.28 Results of Group 2B (school) – well outlet water temperature under multiple well arrangement

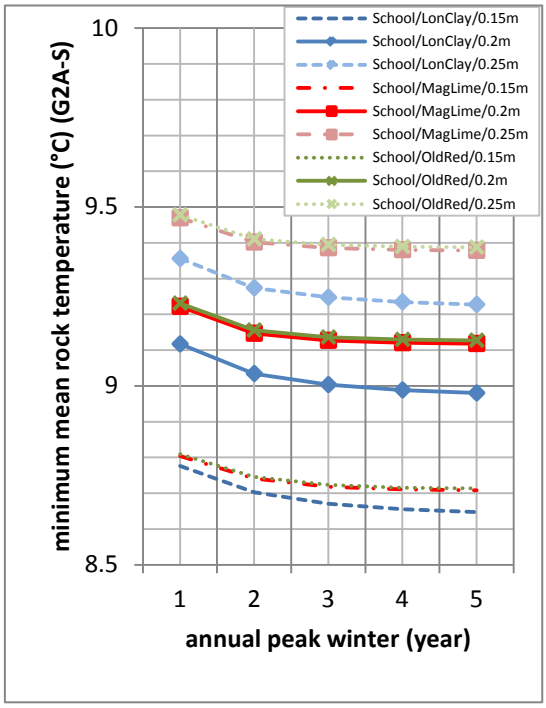

Figure 7.29 Results of Group 2A (school) – mean rock formation temperature under single well arrangement

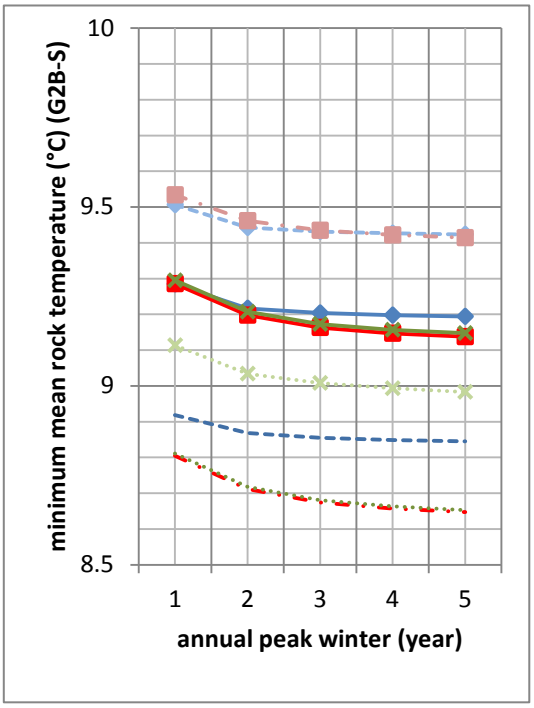

Figure 7.30 Results of Group 2B (school) – mean rock formation temperature under multiple well arrangement

A small fall in mean rock formation temperature over the five-year period is evident across all well borehole diameters (Figures 7.29 and 7.30).

7.5.4. Conclusion of the results in Groups 2A and 2B

The benefit of using a larger well borehole diameter to maximise the winter well water temperature and minimise the summer well water temperature is revealed from the results in this group, which were due to the increasing heat transfer area as the well borehole diameter increased.

However, a reduction in performance occurred for the apartment building when the well borehole diameter was increased beyond 0.2m. This was probably due to the relative changes in the well surface heat transfer coefficient. The significant drop in Nu counteracted the increase in heat transfer area (i.e. borehole size) in this application.

The results also show that a relatively small borehole had a bigger impact on the surrounding formation temperature than a larger borehole. The reason for this is reduced heat transfer from the smaller borehole/rock surface area caused a higher mean well water temperature (i.e. the average water temperature between the inlet and outlet from the well) in summer and a lower mean well water temperature in winter in order to meet the required load.

7.6. Application test results – Groups 3A and 3B - influence of borehole to borehole spacing

The impact of well spacing was analysed by varying the well spacing from 2m to 8m with 3m increments, based on the multiple well arrangements.

7.6.1. Group 3 - results for the office building

Figure 7.31 shows a deterioration in performance with the narrowest spacing of 2m (compared with the original spacing of 5m), as it returned the highest summer well water temperature for all the variants considered. However, the impact of increasing the spacing from 5m to 8m was very limited.

Interestingly, the narrower spacing (of 2m) offered a small benefit during the winter based on London Clay due to the significant rate of mean formation temperature rise (due to summer heat rejection).

On average, the minimum and maximum mean formation temperatures (Figure 7.32) based on these London Clay cases increased about 7.1% and 3.8% over 5 years' operation, respectively, which were significantly higher than the other six cases with an average rise of 4.3% and 2.2% in minimum and maximum mean rock formation temperatures over the same period of time.

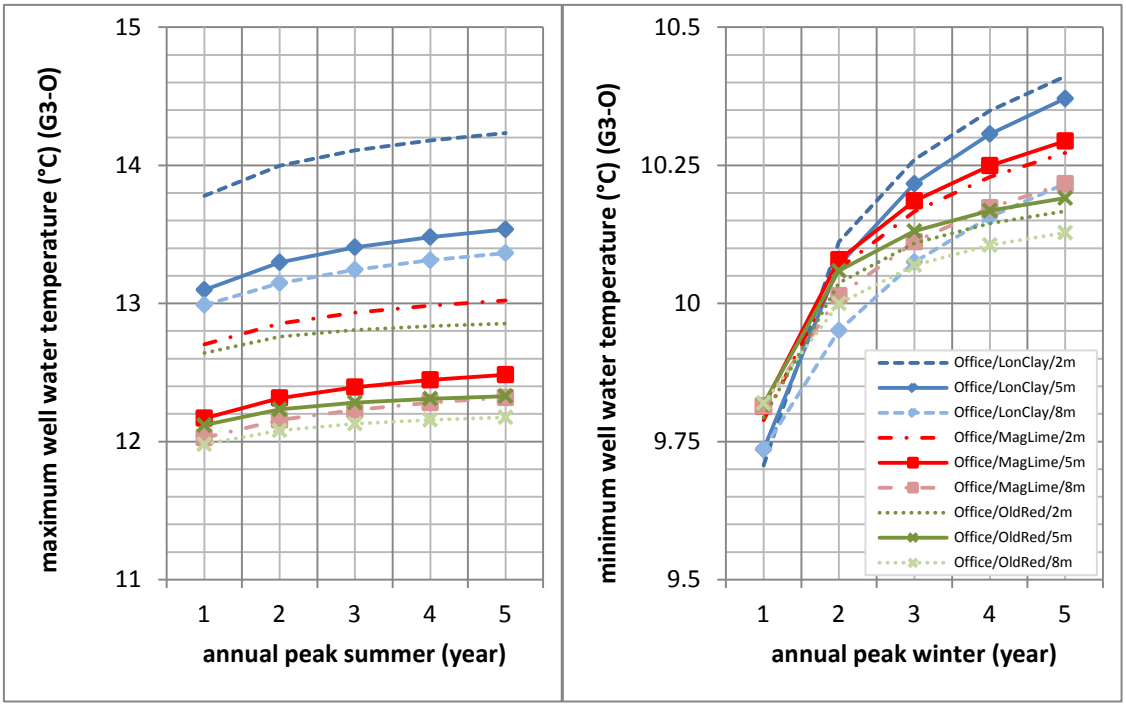

Figure 7.31 Results of Group 3 (office) – well outlet water under multiple well arrangements

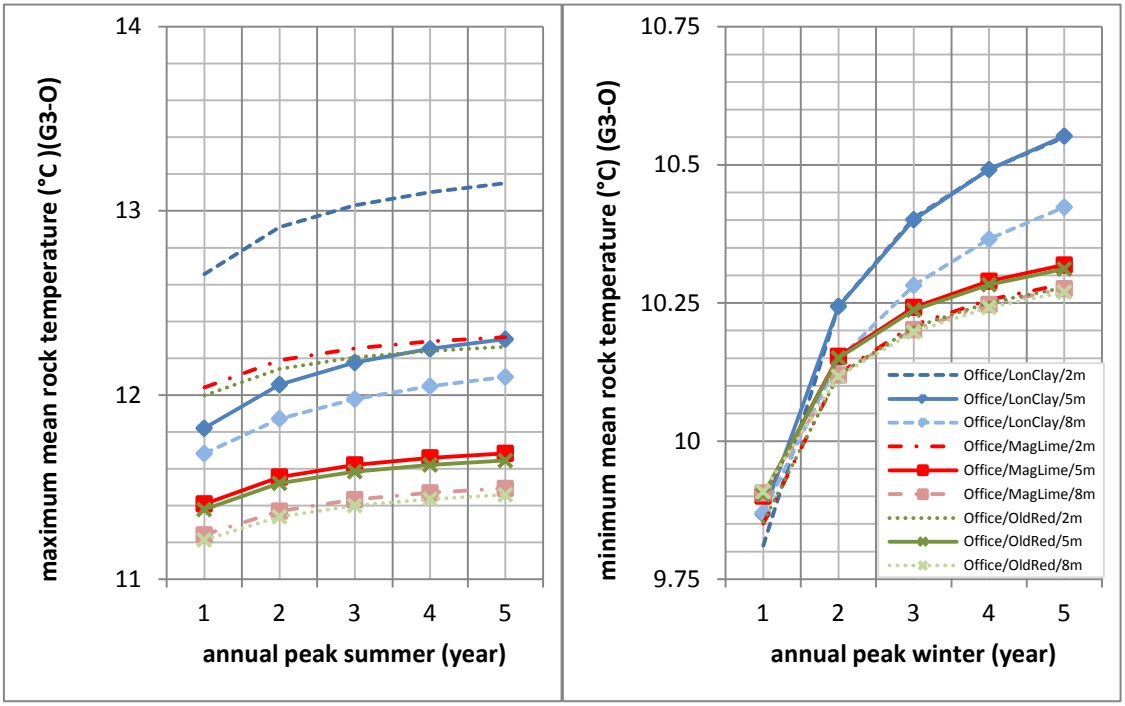

Figure 7.32 Results of Group 3 (office) – mean rock formation temperature under multiple well arrangements

7.6.2. Group 3 - results for the apartment building

Figure 7.33 indicates that the smallest spacing of 2m performed relatively poorly in comparison with the other cases involving wider spacing of 5m and 8m. A relatively high summer well water temperature and a low winter well water temperature are evident.

Increasing the well spacing from 2m to 5m lowered the summer well water temperature by at least 1.5K and increased the winter well water temperature by 0.1K over all variants. However, further increasing the well spacing beyond 5m did not offer any significant improvement, as before.

Figure 7.34 shows a significant mean formation temperature rise in the three London Clay cases, in which increases of 11% in the minimum mean rock formation temperature and 4% in the maximum mean rock formation temperature were found after 5 years' operation. This was slightly higher than the average mean rock formation temperature rise of the other six cases, which had extreme values of 8% and 3.5%, respectively.

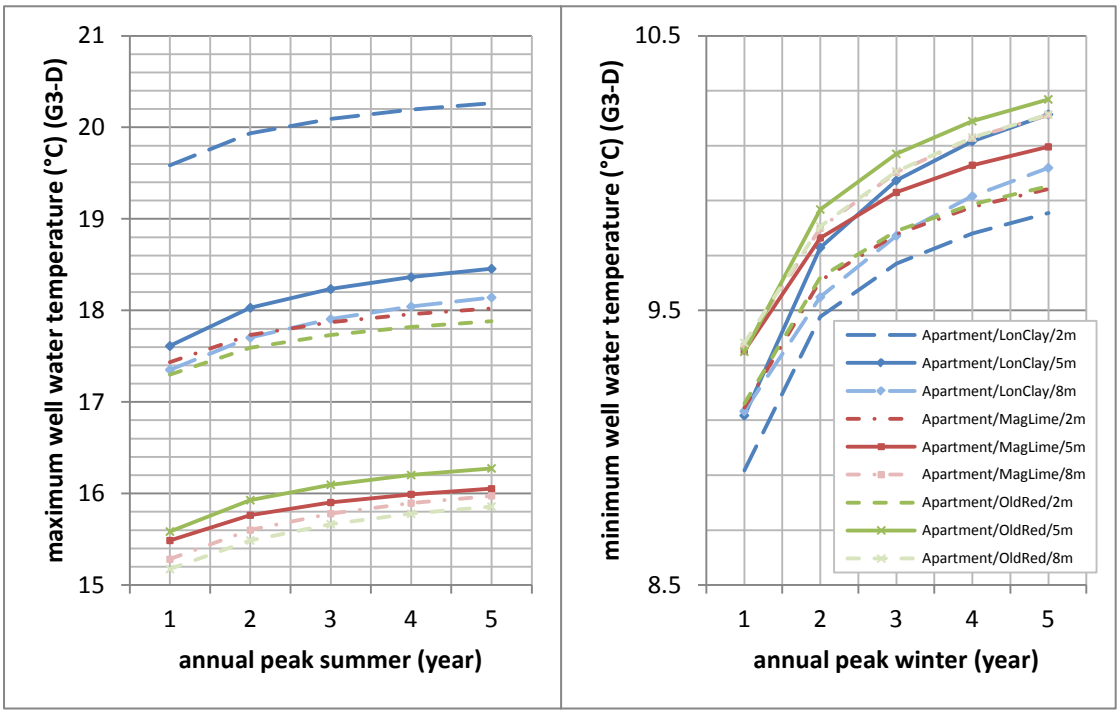

Figure 7.33 Results of Group 3 (apartment) – well outlet water under multiple well arrangements

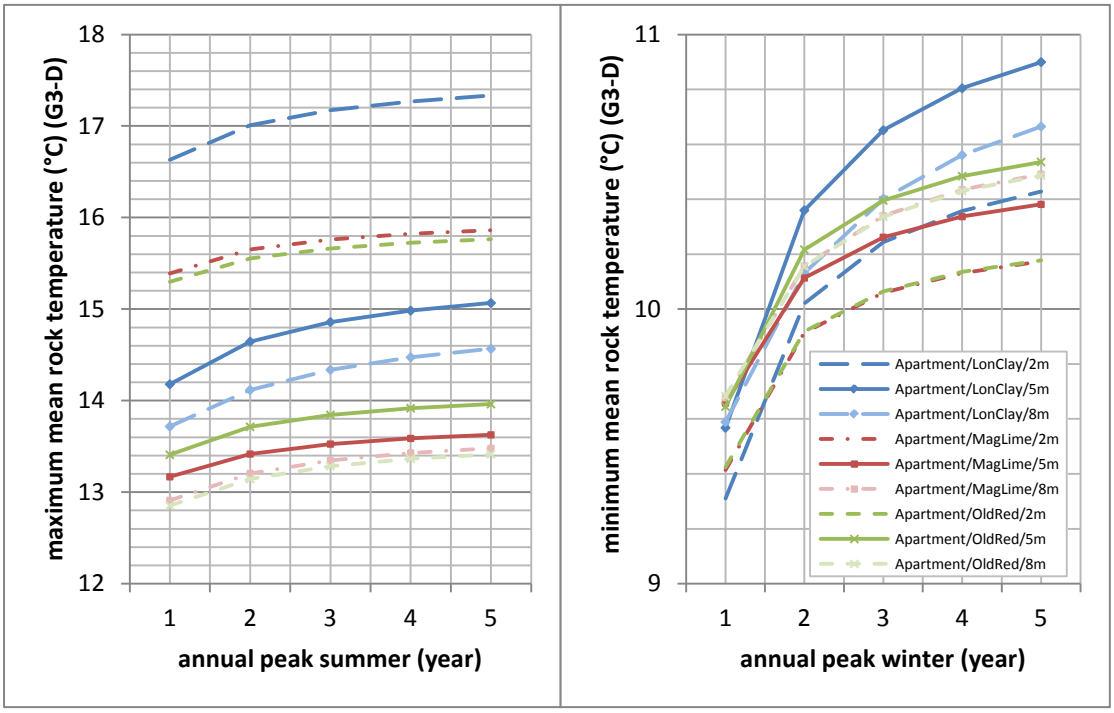

Figure 7.34 Results of Group 3 (apartment) – mean rock formation temperature under multiple well arrangements

7.6.3. Group 3 - results for the school building

Figure 7.35 shows that a well borehole spacing of 2m or 8m with reference to the same soil type provided very similar winter well water temperatures. The spacing of 5m was the best option for this building as it provided the highest winter well water temperatures within each soil group.

According to the mean rock formation temperature (Figure 7.36), it is clear that the most significant mean formation temperature drop was between the 1st year and the 2nd year, and then it gradually slowed down until the end of the 5th year.

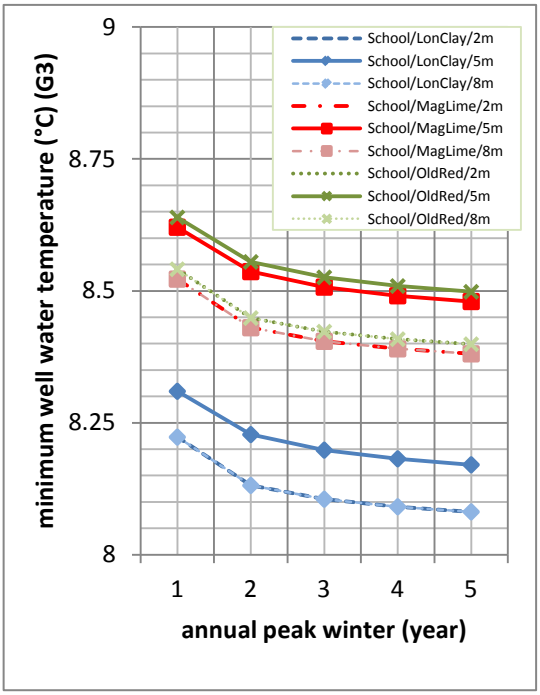

Figure 7.35 Results of Group 3 (school) – well outlet water temperature

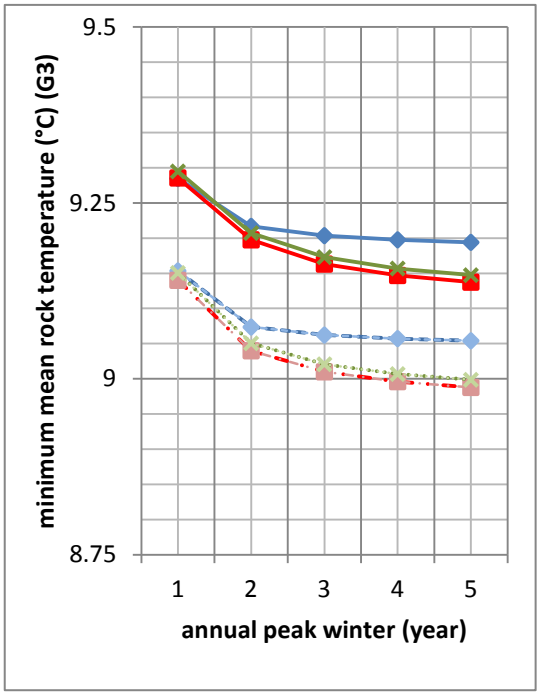

Figure 7.36 Results of Group 3 (school) – mean rock temperature

7.6.4. Conclusion of the results in Group 3

The results from the office and apartment buildings (both of which have cooling as well as heating) indicated that larger borehole spacing enabled a small improvement in the heat transfer performance for all three rock formation types, as narrow spacing might lead to strong interference between the boreholes and hence weaken the performance. The existence of interference between wells has been confirmed from the results in Group 1.

Interestingly, the results from the office building indicate that under certain circumstances, a very small benefit might be achieved by adopting a relatively small borehole to borehole distance. As the narrow borehole spacing accelerated the mean rock formation temperature rise in this large cooling application, the warmer surrounding formation environment offered higher water temperature in winter but also in summer (i.e. this rapid mean formation temperature rise offered no benefits to summer operation and may, in time, inhibit summer cooling performance). This situation did not occur in the apartment building as it has a more balanced heating and cooling demand compared with the office building (with a heating to cooling ratio of 2.5:1, while it was 1:7 for the office building).

For the school building, it was found that spacing of 5m was the best option and the wider spacing of 8m did not offer any benefit. It is important to note that there was no cooling load in this building but the water was constantly recirculated in the well.

7.7. Application test results – Groups 4A and 4B - influence of geothermal gradient

The purpose of application Group 4 was to reveal the actual outlet well water temperature returning to the GHCS under a natural geothermal gradient occurring in the selected formation types and a constant formation temperature of 10°C, based on the three base cases set out in Group 1A.

7.7.1. Group 4A and Group 4B - results for the office building

Under the influence of the natural geothermal gradient, the SCW model reveals that the outlet water temperature varied from 18.7°C (minimum) to 23.6°C (maximum) in London Clay, from 17.4°C (minimum) to 20.8°C (maximum) in Magnesian Limestone and from 15.5°C (minimum) to 18.8°C (maximum) in Old Red Sandstone over five years in Group 4A (single well arrangement). These results are significantly higher than the three base cases under a constant undisturbed formation temperature setting of 10°C, which gave a minimum temperature of 9.5°C and a maximum temperature of 14.4°C across all cases (Figure 7.37). The reason is simply because a constant formation temperature of 10°C were applied to the 3 base cases while a geothermal gradient in relation to the formation types were applied to the 3 test cases here.

In Group 1B (multiple well arrangement) (Figure 7.38), the Magnesian Limestone and Old Red Sandstone provided very similar outlet water temperatures. The well water temperature varied from 9.8°C (minimum) to 12.4°C (maximum) for both rock types under the constant initial temperature setting, while it varied from 12.1°C (minimum) to 14.7°C (maximum) when the variable undisturbed temperature was applied. In London Clay, a minimum well water temperature of 9.7°C and a maximum temperature of 13.5°C were found under a

constant temperature setting, while it varied from 13.3°C (minimum) to 16.9°C (maximum) under the influence of an initial gradient.

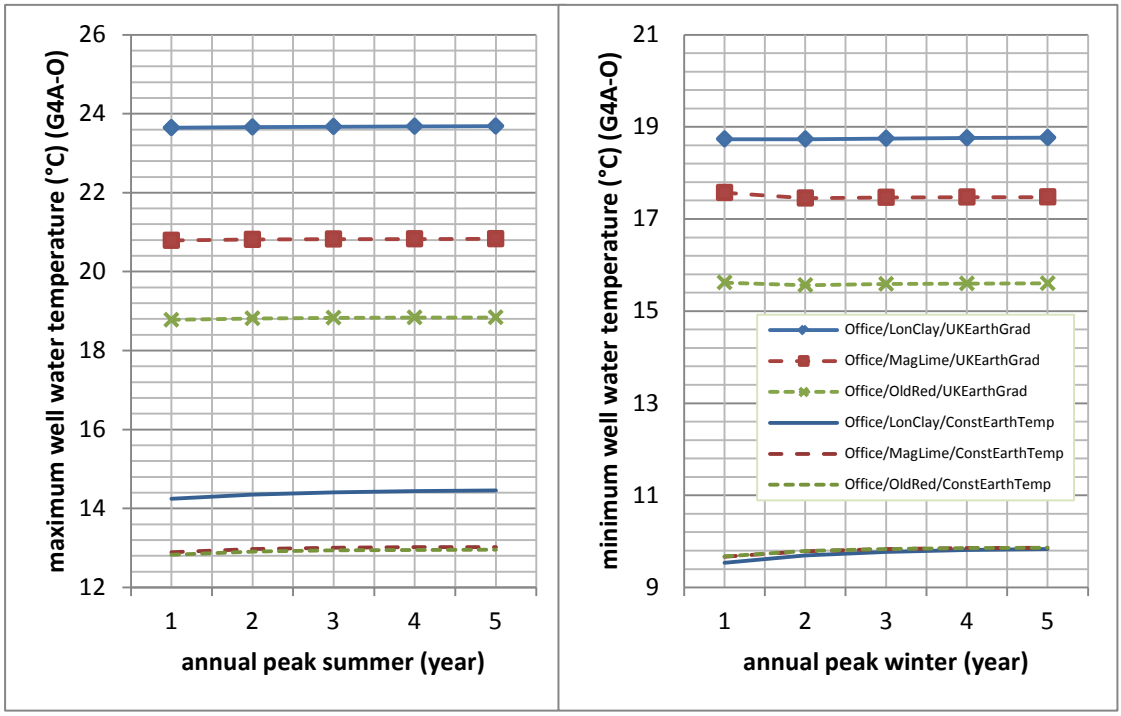

Figure 7.37 Results of Group 4A (office) – well outlet water temperature under the single well arrangement

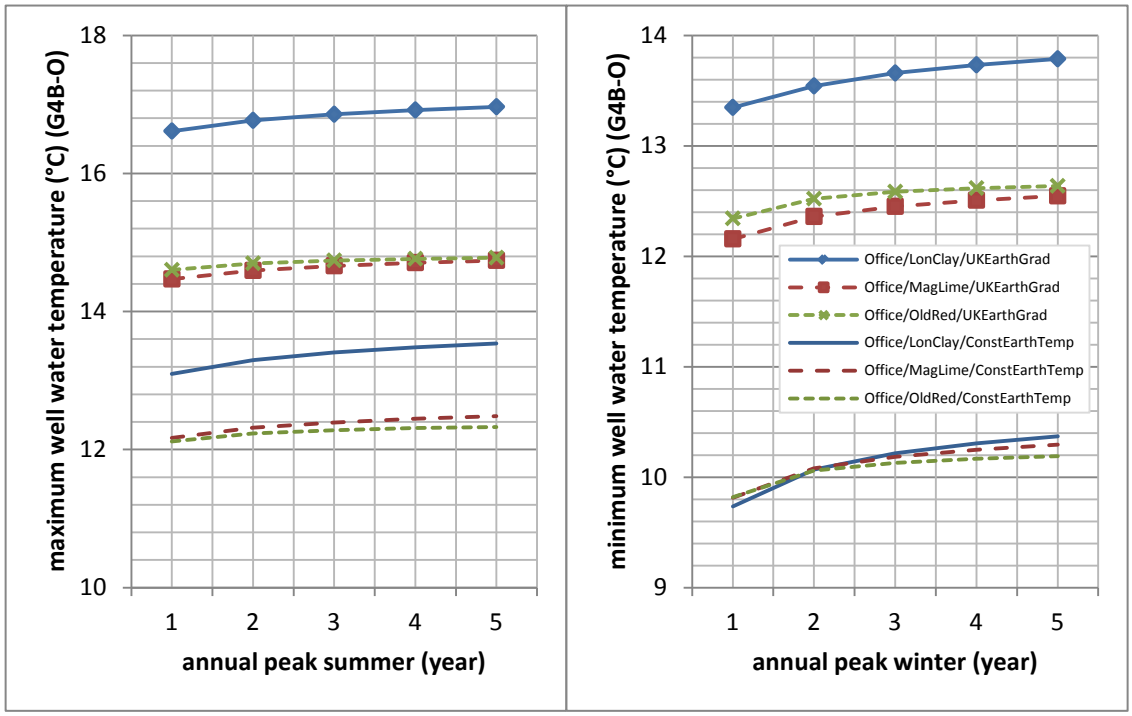

Figure 7.38 Results of Group 4B (office) – well outlet water temperature under the multiple well arrangement

7.7.2. Group 4A and Group 4B - results for the apartment building

Under the influence of the geothermal gradient, the outlet water temperature varied from 16.5°C (minimum) to 28.7°C (maximum) in London Clay, from 16.6°C (minimum) to 25.7°C (maximum) in Magnesian Limestone and from 14.6°C (minimum) to 23.3°C (maximum) in Old Red Sandstone over five years in Group 4A (Figure 7.39). The outlet water temperature under a constant initial formation temperature setting was significantly lower, with a minimum of 9.6°C and a maximum of 12.8°C across all variants. These conditions (particularly in London Clay) would be excellent for heating but the performance advantage for cooling at these levels begins to diminish.

With a multiple well arrangement (Figure 7.40), the water temperature varied from 9.5°C (minimum) to 13.7°C (maximum) in both Magnesian Limestone and Old Red Sandstone under a constant initial formation temperature setting over the five years, while it varied from 11.2°C (minimum) to 18.1°C (maximum) with the geothermal gradient applied. In London Clay, a minimum water temperature of 9.3°C and a maximum temperature of 15.8°C were found under a constant initial temperature setting, while it varied from 11.8°C (minimum) to 20.9°C (maximum) under the influence of a geothermal gradient.

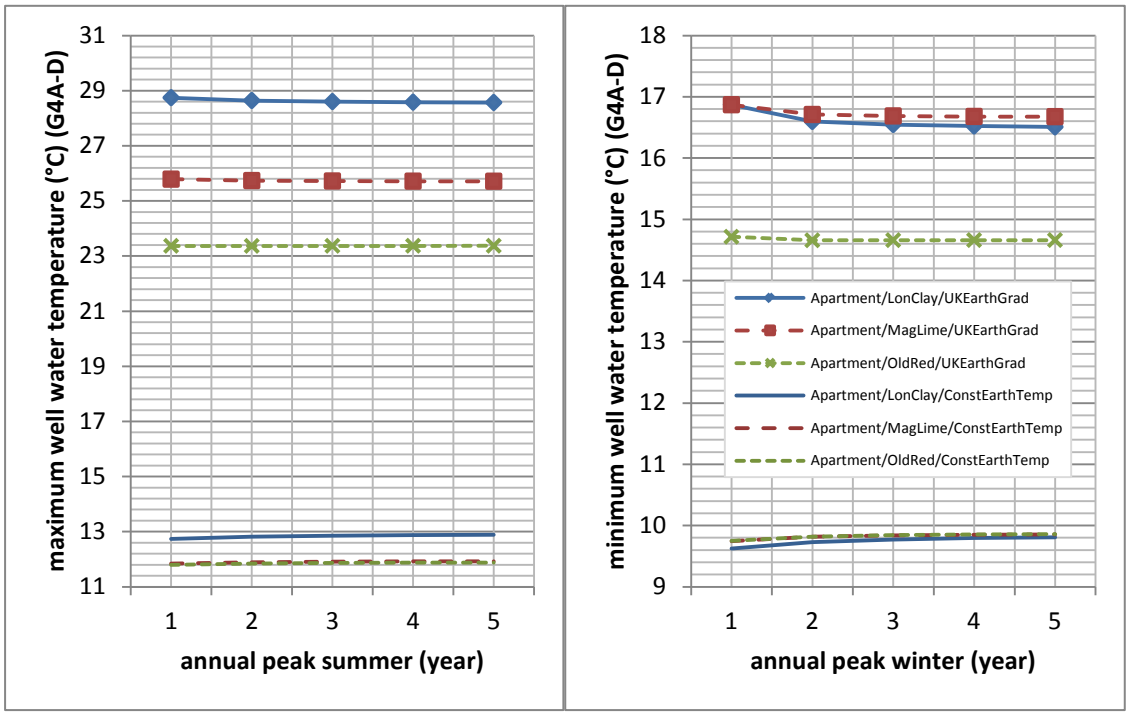

Figure 7.39 Results of Group 4A (apartment) – well outlet water temperature under the single well arrangement

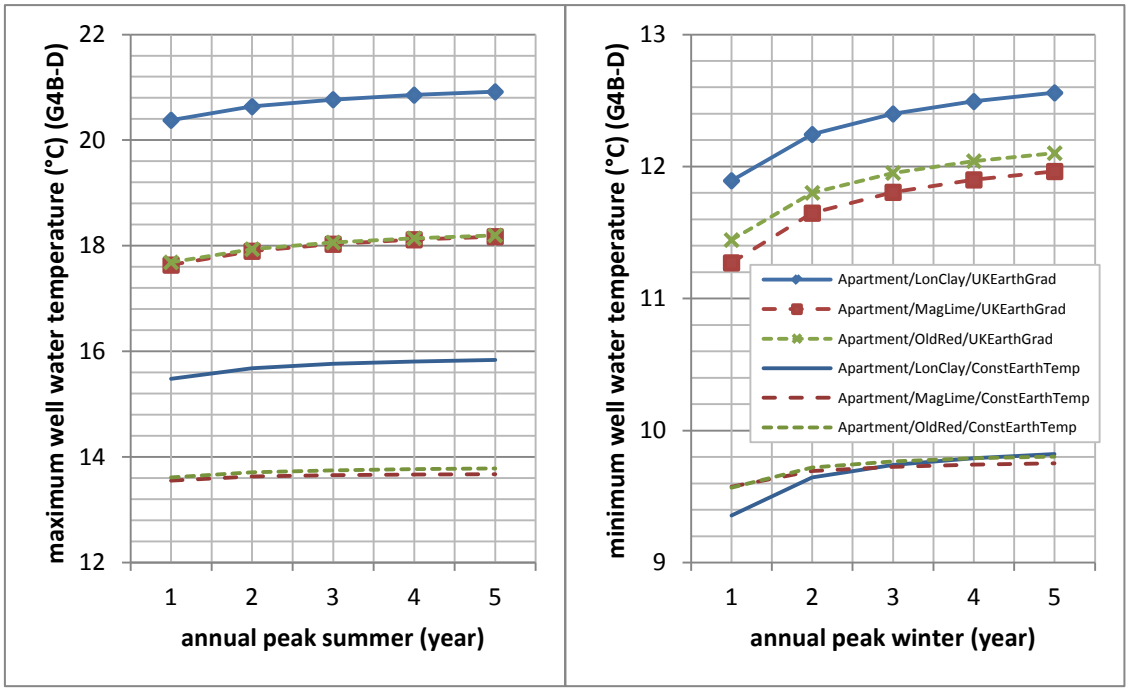

Figure 7.40 Results of Group 4B (apartment) – well outlet water temperature under the multiple well arrangement

7.7.3. Group 4A and Group 4B - results for the school building

In Group 1A (school building), the well water temperature varied from 9.3°C (minimum) to 9.6°C (maximum) over five years for all three formation types under the influence of a geothermal gradient (Figure 7.41). This compares with the variation of 8°C (minimum) to 8.4°C (maximum) evident across all variants when a constant initial formation temperature was applied.

In Group 1B (school building) (Figure 7.42), the outlet water temperature varied from 8.9°C (minimum) to 9.5°C (maximum) over five years for all three formation types when a geothermal gradient was applied, while it varied from 8.2°C to 8.6°C under a constant initial formation temperature.

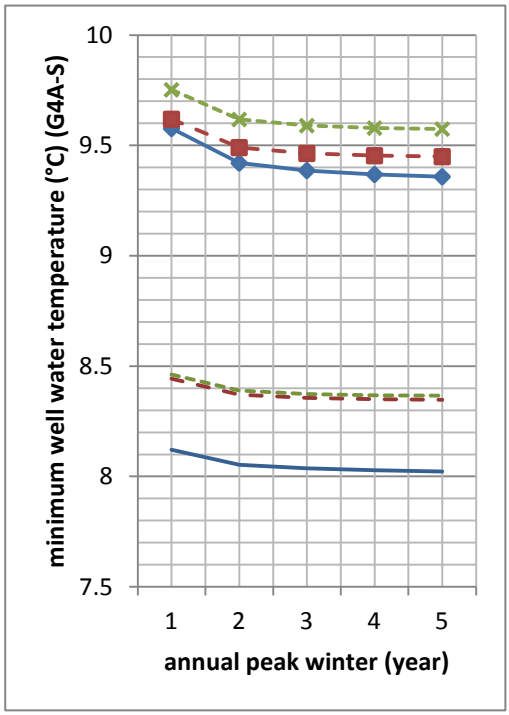

Figure 7.41 Results of Group 4A (school) – well outlet water temperature under single well arrangement

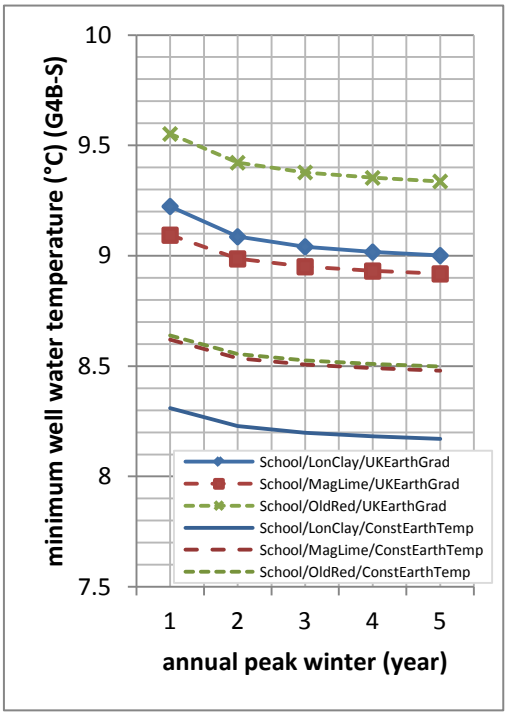

Figure 7.42 Results of Group 4B (school) – well outlet water temperature under multiple well arrangement

7.7.4. Conclusion of the results in Groups 4A and 4B

In the heating-only application (the school), it was clear that the well water temperature difference between the single well and multiple well arrangements was relatively small in comparison with the other two applications with the existence of the geothermal gradient.

In general, the results from this group confirm that the existence of an initial undisturbed geothermal gradient is influential, especially for a single well arrangement with a relatively deep well construction. The geothermal gradient information of the rock formation should always be applied to the model where the information is available in order to have an accurate output from the model.

8. Carbon dioxide emission comparison

With the intention to demonstrate the benefit of investing in and using a SCW, the carbon dioxide emission from a geothermal system using a SCW design (referring to the base cases 4, 5 and 6 in Table 7.4) is estimated and compared with a conventional heating and cooling system

The most commonly used heating and cooling system for commercial buildings in the UK consists of a gas-fired condensing boiler and an (electric) air-cooled chiller. These conventional system choices are used as a base case system alternative.

8.1. Methodology

The simulated heating and cooling demands from the three selected buildings in chapter 7 were employed to determine the energy used by various plants and hence their associate CO_2 emission (Equation 8.1). It is important to note that only the energy required for generating the heating and cooling source (i.e. hot and chilled water) was considered for comparsion. The energy used by the auxiliary plant (i.e. the heating circulation pump) was ignored since these auxiliary loads would, in any case, also apply to other system configurations in equal measure.

Equation 8.1

$$\mathrm{CO_2\ emissions\ (kg)} = \mathrm{annual\ energy\ consumption\ (kWh)} \times \mathrm{CO_2\ conversionfactor\ (kg\,kWh^{-1})}$$

The CO_2 conversion factors were obtained from CIBSE guide F (2004):

0.43kg kWh^{-1}(electricity) and 0.19kg kWh^{-1} (natural gas) were used for this calculation.

8.1.1. Energy consumption by the conventional system (condensing boiler and air-cooled chiller)

The energy consumption is usually derived from the efficiency of a system. A typical condensing boiler efficiency of 95% was used in this calculation to estimate the energy consumption according to the heating demands of the building. However, the coefficient of performance (*CoP*) of the air-cooled chiller varies according to the external air temperature (Equations 8.2 and 8.3). Therefore, the *CoP* was calculated by using a regression (curve-fitting) technique (Equation 8.4), in which the cooling capacity and compressor rated power of the air-cooled chiller were calculated as a function of external air temperature and evaporator inlet fluid temperature. Data suitable for curve-fitting is usually available in the technical product catalogue of the equipment provided by the manufacturer.

Equation 8.2

$$\text{Annually boiler energy consumption (kWh)} = \frac{\text{annual heating load from the building (kWh)}}{\text{efficiency of the boiler}}$$

The following curve-fitted equation is used for the chiller, based on suggestions by Underwood and Yik (2004).

Equation 8.3

$$Q_{com} = 1 + x2 \times T_{ei} + x3 \times {T_{ei}}^2 + x4 \times T_{ao} + x5 \times {T_{ao}}^2 + x6 \times T_{ei} \times T_{ao}$$

where:

$Q_{\text{com}} = \text{estimated instant compressor rated power (kW)}$

$T_{\text{ei}} = \text{evaporator inlet fluid temperature (°C)}$

T_{ao} = external air temperature (°C)

x1 to x6 = coefficients calculated from the manufacturer's data

$(x1 = 6.338;\ x2 = 0.123;\ x3 = -7.9 \times 10^{-5};\ x4 = 0.082;\ x5 = 0.002;\ x6 = 4 \times 10^{-4})$ for compressor load estimation – air cooled chiller

$(x1 = 35.682;\ x2 = 1.420;\ x3 = 0.007;\ x4 = -0.277;\ x5 = -5 \times 10^{-4};\ x6 = -0.012)$ for evaporator load estimation – air cooled chiller

$(x1 = 3.545;\ x2 = 0.053;\ x3 = -2.4 \times 10^{-4};\ x4 = 0.022;\ x5 = 0.002;\ x6 = 4 \times 10^{-4})$ for compressor load estimation – GHCS

$(x1 = 22.817;\ x2 = 1.034;\ x3 = 0.012;\ x4 = -0.021;\ x5 = -0.003;\ x6 = -0.009)$ for evaporator load estimation – GHCS

Equation 8.4

$$CoP = \frac{\text{the rated chiller cooling capacity}}{\text{the rated compressor power}} = \frac{Q_{eva}}{Q_{com}}$$

It was assumed that the cooling demand is always met by the chiller. Thus, the actual power consumption by the chiller can be calculated in relation to the instantaneous cooling demand from the building as follows (Equation 8.5):

Equation 8.5

$$\text{Hourly energy consumption (kW)} = \frac{\text{hourly cooling loads from the building (kW)}}{CoP}$$

8.1.2. Energy consumption by the GHCS with SCW design

There were two major components that consume electricity in a GHCS: the compressor and the submersible water pump (Figure 6.48). In fact, there is also a small pump on the

intermediate circuit between the condenser and the plate heat exchanger, but it was ignored in this calculation due to its relatively small electricity consumption. The auxiliary plant energy consumption (e.g. heating system circulating pump) was also ignored in this calculation.

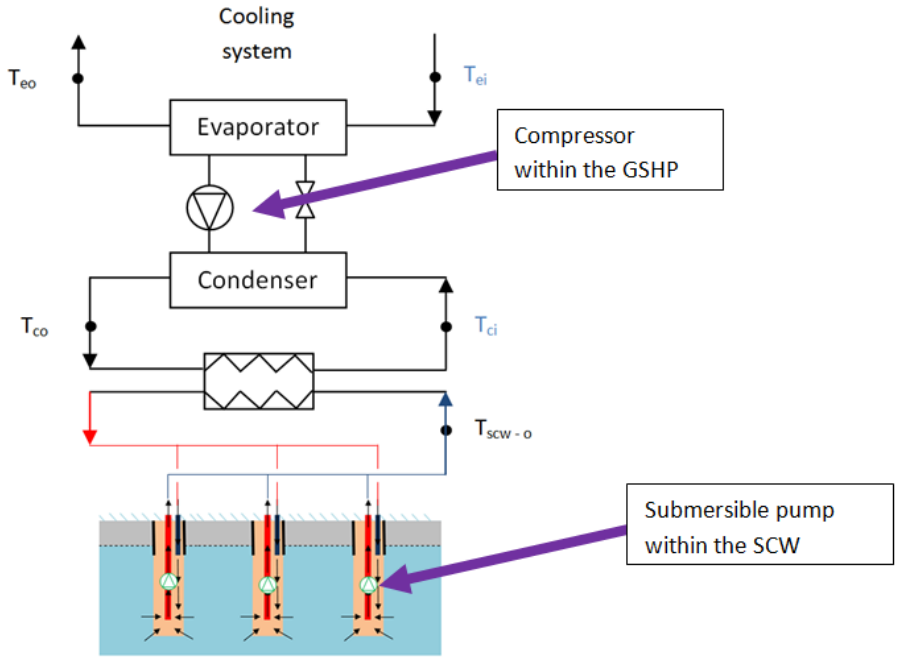

Figure 8.1 SCW configuration (cooling mode)

i. Pump power

With regards to the submersible pump, the efficiency of the pump, the handled water flow rate and the pressure developed across the system are required to estimate the power consumed by the pump according to Equation 8.6.

Equation 8.6

$$\text{Pump power} = \left(\frac{q \times P}{\eta}\right) \times h$$

where:

$\eta =$ the efficiency of the pump amd motor

$P =$ the total pressure developed across the system (kPa)

$q =$ the volume flow rate ($m^3 s^{-1}$)

$h =$ the operating hours of the pump (hours)

A typical submersible pump efficiency of 80% was adopted for this calculation and assumed to remain constant throughout the entire operation, as a constant volume flow rate was adopted between the SCW and the heat exchanger.

The duty of the submersible pump must be able to overcome the pressure developed across the underground loop (SCW), the pipe work above the ground and the heat exchanger.

The pressure drop across the SCW including the lifting head was determined by the SCW model, according to the pressure developed on the surface of the annulus and the suction pipe. Sonnad and Goudar's (2008) explicit Colebrook White Equation (Equation 8.7) was used for the estimation of the Darcy friction factor across these surfaces, and then the well-known Darcy-Weisbach formula (Equation 8.8) was used to calculate the pressure head loss in metres.

The explicit Colebrook White Equation by Sonnad and Goudar (2008):

Equation 8.7

$$\frac{1}{\sqrt{f}} = a\left[\ln\left(\frac{d}{q}\right) + \delta_{CFA}\right]$$

where:

f = Darcy friction factor

$= \frac{2}{\ln(10)}$

d $= \left(\frac{\ln(10)}{5.02}\right) Re$ where: Re = Reynolds number

q $= s^{\left(\frac{s}{s+1}\right)}$

s $= bd + \ln(d)$;

b $= \frac{\varepsilon/D_h}{3.7}$ where: D_h = Hydraulic diameter of the pipe (m) and

ε = roughness of the pipe (m)

δ_{CFA} $= \delta_{LA}\left(1 + \frac{Z/2}{(g+1)^2+(z/3)(2g-1)}\right)$

δ_{LA} $= \left(\frac{g}{g+1}\right) z$

z $= \ln\left(\frac{q}{g}\right)$;

g $= bd + \ln\left(\frac{d}{q}\right)$;

The Darcy-Weisbach formula:

Equation 8.8

$$h_f = f \frac{L}{D_h} \frac{V^2}{2g}$$

where:

f = Darcy friction factor

D_h = pipe diameter (hydraulic diameter) (m)

L = pipe length (according to grid size of the model) (m)

V = flow velocity (ms^{-1})

g = gravitational acceleration (ms^{-2})

It was assumed that the pressure drop across the heat exchanger connected to the GHCS was 50kPa. A 10m pipe run (flow and return) was required to connect the heat exchanger with the SCW. A pipe loss of $200Pam^{-1}$ was assumed along this 10m pipe run, in which 50% fitting loss was added as well (Figure 6.50).

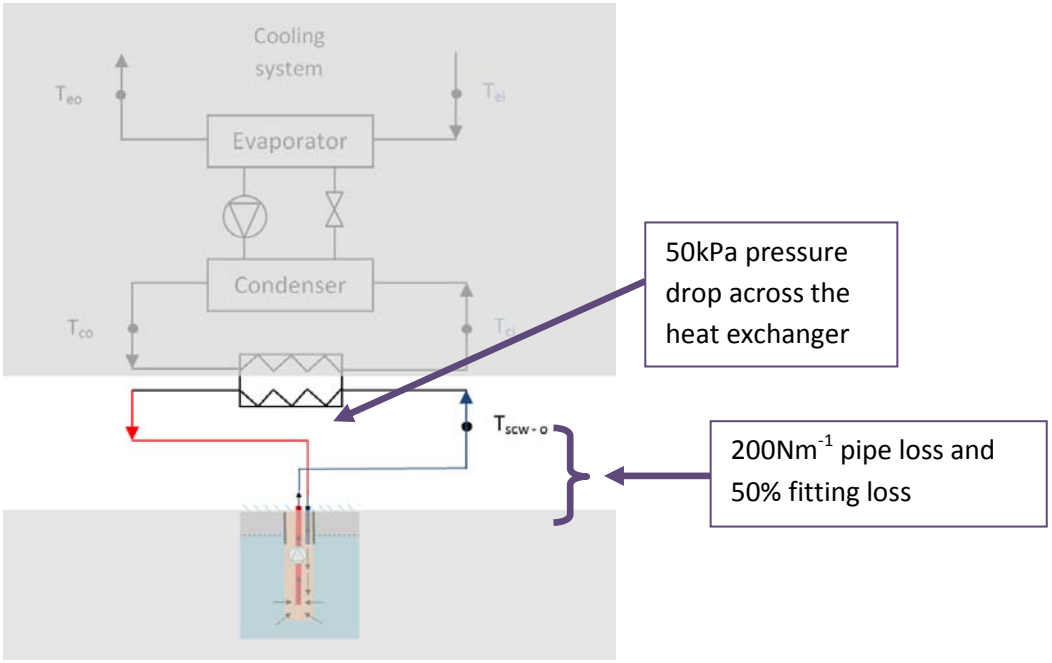

Figure 8.2 Illustration of the pipe work above the ground and the heat exchanger

ii. Compressor power

In contrast to an air-cooled chiller, the *CoP* of a vertical geothermal system (GHCS) does not fluctuate with the weather (external air temperature) but varies with the source temperature, including the outlet water temperature from the SCW and the condenser or evaporator inlet fluid temperature (to the GHCS), depending on operation mode (i.e. heating or cooling). The regression (curve-fitting) technique was used again to determine the GHCS rated compressor power associated with the variation of the source (winter) or sink (summer) temperatures.

It was assumed that the maximum temperature drop across the condenser or evaporator was 5K. The design hot water flow temperature (T_{co}) was 35°C during the heating mode and the chilled water flow temperature (T_{eo}) was 7°C during the cooling mode; they were maintained at constant values at all times.

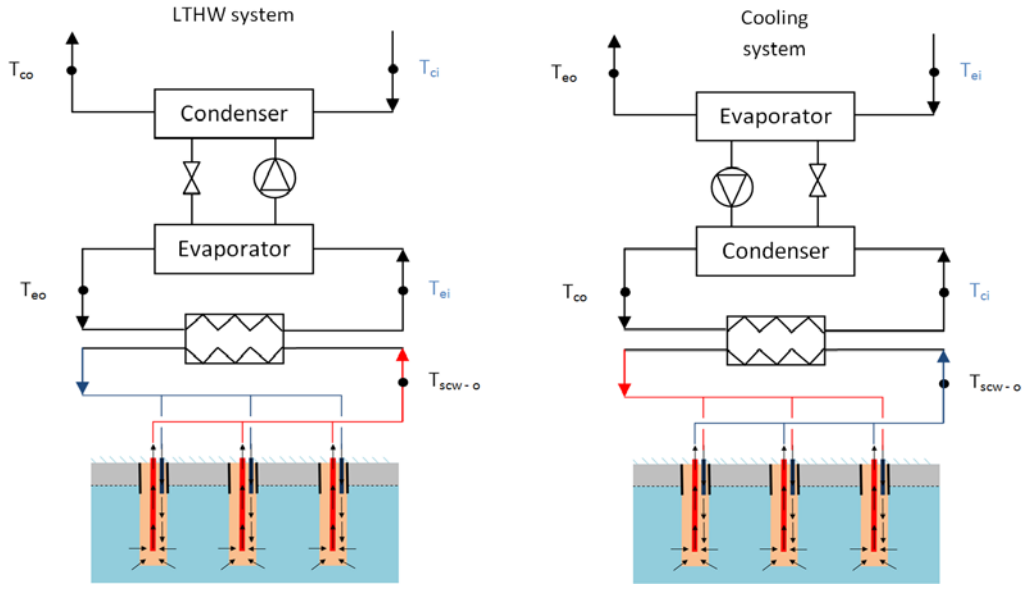

Figure 8.3 Heating (left) and cooling (right) configuration with the SCW system

The mass flow rate of the water circulating through the LTHW system and cooling system was estimated in accordance with the peak (design) heating and cooling demands from the building, correspondingly.

Once the mass flow rate was fixed, the hourly return water temperature (T_{ci} and T_{ei}) can be determined in relation to the hourly heating or cooling demands as follows:

Equation 8.9

$$Q_{LTHW} = m\, C_p\, (T_{co} - T_{ci})$$

where:

Q_{LTHW} = hourly heating demands from the building (kW)

m = mass flow rate of the LTHW loop (ms^{-1})

C_p = specific heat capacity ($kJ\ kg^{-1}K^{-1}$)

T_{co}, T_{ci} = outlet, inlet fluid temperature to the condenser (°C)

Equation 8.10

$$Q_{cooling} = m\ C_p\ (T_{ei} - T_{eo})$$

where:

$Q_{cooling}$ = hourly cooling demands from the building (kW)

m = mass flow rate of the LTHW loop (ms^{-1})

C_p = specific heat capacity ($kJ\ kg^{-1}K^{-1}$)

T_{ei}, T_{eo} = inlet, outlet fluid temperature to the condenser (°C)

The outlet water temperature from the SCW ($T_{scw\text{-}o}$) was provided by the SCW model and the outlet water temperatures from the evaporator and condenser were fixed at their respective design (thus controlled) values. Therefore, the theoretical maximum heat transfer rate through the plate heat exchanger could be determined by Equation 8.11.

Equation 8.11

$$Q_{heat\ ex\_max} = m\ C_p\ (T_{scw\ -\ o} - T_{eo}) = Q_{eva} \text{ (winter) or } Q_{con} \text{ (summer)}$$

where:

T_{scw-o} = the outlet water temperature from the SCW (°C)

It was assumed the efficiency of the plate heat exchanger was 85% and hence the actual heat transfer rate could be predicted from Equation 8.12. Modern brazed plate heat exchangers are capable of achieving pinch temperatures of 1K and better. For example, a well discharging water at 11°C cooled to 5°C whilst receiving secondary source water from the heat pump at 4°C raised to 10°C will have an effectiveness of (10 – 4) / (11 – 4) = 6 / 7 = 0.857 (i.e. 85.7%).

Equation 8.12

$$Q_{\text{heat ex\_actual}} = \varepsilon\, Q_{\text{heat ex\_max}}$$

where:

ε = efficiency of the plate heat exchanger

The inlet water temperature back to the ground loop (T_{scw-i}) could be determined by Equation 8.13.

Equation 8.13

$$Q_{\text{heat ex\_actual}} = m\, C_p\, (T_{scw-o} - T_{scw-i})$$

The outlet water temperature from the evaporator or condenser can be calculated from Equations 8.14 and 8.15.

Equation 8.14

$Q_{\text{heat ex\_actual}} = m\, C_p\, (T_{\text{ei}} - T_{\text{eo}})$ during heating mode in winter

Equation 8.15

$Q_{\text{heat ex\_actual}} = m\, C_p\, (T_{\text{co}} - T_{\text{ci}})$ during cooling mode in summer

With the details of the inlet/outlet water temperatures throughout the entire system, Equations 8.16 and 8.17 can be used to determine the hourly compressor power input and the heating or cooling capacity output of the GHCS. This information allows the hourly *CoP* to be calculated and hence the actual hourly compressor power consumption associated with the instantaneous heating and cooling demands from the building can be estimated as well.

Equation 8.16

$$CoP = \frac{\text{the rated condenser or evaporator output (kW)}}{\text{the rated compressor power consumption (kW)}}$$

Equation 8.17

$$\text{Actual compressor consumption (kW)} = \frac{\text{hourly heating or cooling demand (kW)}}{CoP}$$

8.2. Discussion of results

The results of the energy consumption and carbon emissions due to the SCW-GHCS system (referring to the base cases 4, 5 and 6 in Table 7.4) and, alternatively, the conventional system (with gas fired boiler and air-cooled chiller) are given in Tables 8.1, 8.2 and 8.3 for all three buildings. It is clear from these results that the geothermal systems produced significant lower CO_2 emissions than the conventional system alternative.

Evidently, the different rock formation types did not have significant differences in terms of CO_2 emissions.

The highest CO_2 emission reduction was found in the apartment building (Table 8.1) with an annual reduction of 46% when compared with the conventional system. Similarly, an annual 26% saving in carbon emissions was evident in the office building (Table 8.2) and somewhat smaller (17%) reduction for the school building (Table 8.3) in comparison with conventional systems.

Table 8.1 Annual CO_2 emissions and power consumption of the office building

	Annual power consumption (kWh)	**Annual CO_2 emissions (kg CO_2)**
GHCS – Office / Clay	**Total: 4495.1**	**Total: 1932.9**
	Heating: 1001.5 Cooling: 3493.6	Heating: 430.6 Cooling: 1502.3
GHCS – Office / Limestone	**Total: 4433.8**	**Total: 1906.5**
	Heating: 1000.7 Cooling: 3433.1	Heating: 430.3 Cooling: 1476.2
GHCS – Office / Red Sandstone	**Total: 4432.5**	**Total: 1906.0**
	Heating: 1000.7 Cooling: 3431.9	Heating: 430.3 Cooling: 1475.7
Boiler + air-cooled chiller	**Total: 7494.6**	**Total: 2578.6**
	Heating: 2683.7 Cooling: 4810.9	Heating: 509.9 Cooling: 2068.7

Table 8.2 Annual CO_2 emissions and power consumption of the apartment building

	Annual power consumption (kWh)	**Annual CO_2 emission (kg CO_2)**
GHCS – Apartment / Clay	**Total: 15458.0**	**Total: 6647.0**
	Heating: 11027.3 Cooling: 4430.7	Heating: 4741.8 Cooling: 1905.2
GHCS – Apartment / Limestone	**Total: 15215.9**	**Total: 6542.9**
	Heating: 10988.4 Cooling: 4227.5	Heating: 4725.1 Cooling: 1817.8
GHCS – Apartment / Red Sandstone	**Total: 15203.1**	**Total: 6537.3**
	Heating: 10985.8 Cooling: 4217.3	Heating: 4723.9 Cooling: 1813.4
Boiler + air-cooled chiller	**Total: 57483.7**	**Total: 12140.8**
	Heating: 52404.8 Cooling: 5078.9	Heating: 52404.8 Cooling: 5078.9

Table 8.3 Annual CO_2 emissions and power consumption of the school building

	Annual power consumption (kWh)	**Annual CO_2 emission (kg CO_2)**
GHCS – School / Clay	Total (heating): 2721.6	Total (heating): 1170.3
GHCS – School / Limestone	Total (heating): 2708.4	Total (heating): 1165
GHCS – School / Red Sandstone	Total (heating):2709.1	Total (heating):1165.0
Boiler	Total (heating):7383.8	Total (heating):1402.7

The use of a GHCS is much more effective when required to deliver heating in winter and cooling in summer (as opposed to merely delivering heating in winter with no cooling provision). Thus, a building with slightly larger heating loads than cooling loads would

benefit most from a GHCS, such as the apartment building in this case, which is a heating-dominant application with a heating to cooling demand ratio of 2.5:1. The office building is mainly a cooling application with a heating to cooling demand ratio of 1:7, hence a relatively smaller carbon saving was to be expected since the cooling model *CoP* tends to decline with time as the formation temperature increases. For the heating-only building (the school building), although a substantial saving in the power consumption was achieved, the carbon saving by the GHCS was lower. Note that, though not explored here, when direct cooling is used instead of refrigeration in summer, the carbon savings due to GHCS rise sharply as reported by Underwood and Spitler (2007). The well water temperatures reported in the present work for a number of the design variants considered are well within the range for feasible direct cooling and this is a matter for further work.

9. Conclusions

This research has described the development of a model for simulating clusters of SCWs for use in geothermal heating and cooling systems.

A partially decoupled model, allowing the well and field equations to be solved individually with different time intervals, was developed to offer a faster and more flexible simulation. The resulting well model (child) and field model (parent) were 'connected' through the latter's source terms. The resulting model provides flexibility to adopt different types of geothermal systems easily whilst retaining the parent code structure.

The model has been verified using several data sources reported in the literature in order to examine its accuracy. Good agreement with short-time thermal and hydraulic response data was obtained. In addition, the precision of the whole model (the parent and the child model) was verified against a set of real SCW operation data for a single well with good agreement.

A number of evaluative tests have been applied to the model to reveal the benefits of adopting the SCW system. It can offer a higher rate of heat transfer, typically up to 250 Wm^{-1}, especially when groundwater is bled into the well system. For the test case involving both heating and cooling, SCW clusters offer the potential for very substantial reductions in geotechnical drilling compared with conventional closed-loop vertical borehole heat exchanger arrays. This offers significant opportunities for geothermal heating and cooling systems in regions with high water tables, such as are frequently found in the United Kingdom. However, the conventional closed loop system is still the most favourable option in UK at present in terms of capital cost.

A range of application studies was conducted on three contrasting buildings (an office building, an apartment building and a school). These results confirm that bleed operation is very influential to the performance of SCWs, offering up to 2.2K improvement (reduction) in the outlet well water temperature in summer and a similar improvement (increase) in well

water temperature in winter. Bleed operation is able to extend the 'reach' of geothermal systems by drawing in warmer (winter) and cooler (summer) groundwater from the far-field. The results from a heating-only application (the school example) also confirm that satisfactory operation against well water freezing can be expected in typical UK winter conditions.

The results also confirm that larger well borehole diameters offer improved heat transfer performance under certain circumstances. Therefore, computer simulation is very useful to determine the optimal borehole size in order to maximise heat transfer performance.

Analysis of borehole to borehole spacing seems to suggest that, in most cases, a 5m grid pattern is appropriate: reductions below this value resulted in a decrease in performance. On the other hand, increases in spacing beyond 5m resulted in relatively little improvement. This consideration is important in applications where land is at a premium.

As far as rock formation is concerned, analyses were carried out for London Clay, Old Red Sandstone and Magnesian Limestone. The results show that SCW installations in London Clay performed least well, whereas Magnesian Limestone and Old Red Sandstone appeared to have similar performance characteristics (both of which were favourable) throughout most of the test cases; they seemed to be appropriate formation types to work with for this type of application.

The findings also confirm the advantage of adopting multiple well arrangements (SCW clusters) over the use of single wells: even though the total heat transfer area was exactly the same under both arrangements, reduced well water temperatures in summer and increased temperatures in winter compared with single well (of equivalent sizes) performances were obtained. Therefore, a potential reduction in the geotechnical complexity could also be achieved as the required borehole depth reduces substantially under the multiple well arrangements.

The results gathered from the three different buildings reveal that the balance between heating and cooling demands (such as in the apartment building) appeared to have a significant impact on the mean formation temperature change rather than the large cooling application (i.e. office), which is of benefit to maintaining steady system performance over a long period of time. The results also suggest that the impact of the rock formation was very dominant in the first few years but it declined towards the end of the five-year analysis period used in this work. Computer simulation is vital to reveal the variation of the formation conditions in order to determine the system performance over long time periods.

The CO_2 emissions have been estimated for the three different building types using SCW-GHCS and, for comparison, conventional systems consisting of a gas-fired condensing boiler and a conventional air-cooled chiller. The results demonstrate that an annual carbon emission reduction of up to 46% can be achieved by using a geothermal system with SCWs instead of a condensing boiler and an air-cooled chiller. This result was applicable to the apartment building with a heating-to-cooling demand ratio of 2.5:1. For the office building (with a ratio of 7:1), the saving was 26% and for the school (heating only; no cooling) the saving was 17%. Thus, the most favourable applications for SCW-GHCS technology are buildings requiring winter heating and summer cooling and the balance between the two is crucial in relation to the carbon savings achievable.

To conclude, the benefits of using SCW systems have been revealed in this research and a three-dimensional dynamic thermofluid model has been developed to deal with SCW cluster design and analysis. The model has been demonstrated for use in the long-term performance evaluation of multiple SCW systems.

The recommendations for future research are as follows:

- Investigate the extent to which the model can cope with combinations of different types of vertical group- loop designs (such as conventional closed-loop and open-loop systems) to form hybrid systems.
- Extent the model complexity to deal with a more complex earth properties (such as heterogeneous formation) and structures.
- Explore ranges of SCW design parameters within which direct cooling may be feasible.
- Explore the economic issues associated with SCW design, including the capital cost and payback calculation.
- Adopt a matrix structure (a tridiagonal matrix algorithm - TDMA) to solve the partial differential equations in order to further improve the computational efficiency of the model.
- Fully validate the model with existing SCW cluster installations to verify the accuracy of the model over a long time period.
- Explore simplified model structures (‘tuned’ by the detailed model reported here) for use by design practitioners.

References

Addison, R. & Floyd, J. D. (2007) *British Geological Survey 1:625000 Scale Bedrock Geology UK South (South of National Grid Line 540km N)*, HarperCollins Publishers Ltd.

ASHRAE (2007). HVAC applications. Atlanta, GA, American Society of Heating, Refrigerating and Air-Conditioning Engineers, Inc., Atlanta, GA.

ASHRAE (2009). Fundamentals, American Society of Heating, Refrigerating and Air-Conditioning Engineers, Inc., Atlanta, GA.

Banks, D. (2008) *An introduction to thermogeology: ground source heating and cooling*. Wiley-Blackwell.

Banks, D., Gandy, C., Younger, P., Withers, J. & Underwood, C. (2009) 'Anthropogenic thermogeological'anomaly'in Gateshead, Tyne and Wear, UK', *Quarterly Journal of Engineering Geology & Hydrogeology,* 42 (3), p. 307.

Barry, D. A., Parlange, J. Y. & Li, L. (2000) 'Approximation for the exponential integral (Theis well function)', *Journal of Hydrology,* 227 (1-4), pp. 287-291.

Bear, J. (1972) *Dynamics of fluids in porous media*. Dover, Mineola, NY.

Bear, J. & Verruijt, A. (1987) *Modeling groundwater flow and pollution: with computer programs for sample cases*. Dordrecht: D. Reidel Publishing Company.

Bose, J., Smith, M. & Spitler, J. (2002) *Advances in ground source heat pump systems-an international overview: Proceedings of the Seventh International Energy Agency Heat Pump Conference*. Beijing.

Botte, G. G., Ritter, J. A. & White, R. E. (2000) 'Comparison of finite difference and control volume methods for solving differential equations', *Computers and Chemical Engineering,* 24, pp. 2633-2654.

Burley, A. J., Edmunds, W. M. & Gale, I. N. (1984) *Catalogue of geothermal data for the land area of the United Kingdom* 2edn. Keyworth: British Geological Survey, Investigation of the geothermal potential of the UK.

Cane, R. & Forgas, D. (1991) 'Modeling of ground source heat pump performance', *Ashrae Transactions,* 97 (1), pp. 909-925.

Carslaw, H. S. & Jaeger, J. C. (1959) *Conduction of heat in solids*. 2 edn. Oxford University Press, Ely House, London W.I.

Chen, N. H. (1979) 'An explicit equation for friction factor in pipe', *Industrial & Engineering Chemistry Fundamentals,* 18 (3), pp. 296-297.

Chiasson, A. D., Rees, S. J. & Spitler, J. D. (2000) 'A preliminary assessment of the effects of groundwater flow on closed-loop ground-source heat pump systems', *ASHRAE TRANSACTIONS 2000,* 106 (1), pp. 380-393.

Churchill, S. W. & Chu, H. S. (1975) 'Correction equations for laminar and turbulent free convection from a vertical plate', *International Journal of Heat and Mass Transfer,* 18, pp. 1326-1329.

Churchill, S. W. & Usagi, R. (1972) 'A general expression for the correlation of rates of transfer and other phenomena', 18 (6), pp. 1121-1128.

CIBSE (2004) *Energy Efficiency in Buildings CIBSE Guide F*. 2 edn. London: Chartered Institution of Building Services Engineers.

CIBSE (2005) 'Ventilating, air conditioning and refrigeration CIBSE guide B', *Chartered Institution of Building Services Engineers London*.

Colburn, A. (1933) 'A method of correlating forced convection heat transfer data and a comparison with fluid friction', *Transactions of the American Institute of Chemical Engineers,* 29, pp. 174-210.

Colebrook, C. F. & White, C. M. (1937) 'Experiments with fluid friction in roughened pipes', *Proceedings of the Royal Society of London. Series A, Mathematical and Physical Sciences,* 161 (906), pp. 367-381.

DCLG. (2010) *National calculation methodology (NCM) modelling guide (for buildings other than dwellings in England and Wales)* London: Department for communities and local government

Deerman, J. D. & Kavanaugh, S. P. (1991) 'Simulation of vertical U-tube ground-coupled heat pump systems using the cylindrical heat source solution', *ASHRAE Transactions 1991,* 97 (1), pp. 287-295.

Deng, Z. (2004) *Modeling of standing column wells in ground source heat pump systems.* PhD Thesis. Oklahoma State University.

Deng, Z., Rees, S. J. & Spitler, J. D. (2005) 'A model for annual simulation of standing column well ground heat exchangers', *HVAC&R Research,* 11 (4), pp. 637-656.

Deng, Z., Spitler, J. D. & Rees, S. J. (2006) 'Performance analysis of standing column well ground heat exchanger systems', *ASHRAE Transactions 2006,* 112 (2), pp. 633-643.

Dirker, J. & Meyer, J. (2002) 'Heat transfer coefficients in concentric annuli', *Journal of Heat Transfer,* 124, p. 1200.

Dittus, F. & Boelter, L. (1985) 'Heat transfer in automobile radiators of the tubular type', *International Communications in Heat and Mass Transfer,* 12 (1), pp. 3-22.

Downing, R. A., Gray, D. & survey, G.-B. G. (1986) *Geothermal energy: The potential in the United Kingdom*. HMSO.

DTI (2007) *Meeting the energy challenge: a White Paper on energy Department of Trade and Industry* The Stationery Office (TSO).

Edmonds, E. A. & Woodland, A. W. (1977) *British Geological Survey Quaternary Map of The United Kingdom (South)*, Director General of the Ordnance Survey, Southamptom, Institue of Geological Sciences.

Florides, G. & Kalogirou, S. (2007) 'Ground heat exchangers--A review of systems, models and applications', *Renewable Energy,* 32 (15), pp. 2461-2478.

Freeze, R. A. & Cherry, J. A. (1979) *Groundwater*. Englewood Cliffs: Prentice Hall, Inc.

Gnielinski, V. (1976) 'New equations for heat and mass transfer in turbulent pipe and channel flow', *Int. Chem. Eng,* 16 (2), pp. 359–368.

Goudar, C. T. & Sonnad, J. R. (2008) 'Comparison of the iterative approximations of the Colebrook-White equation', *Hydrocarbon Processing,* 87 (8), p. 79.

Graham, R. (2008) *The use of pulverised fuel ash and furnace bottom ash - generic risk assessment for the waste protocols project.* Banbury: RPS Planning and Development Ltd.

Hall, W. B. (1962) 'Heat transfer in channels having rough and smooth surfaces', *Journal of Mechanical Engineering Science,* 4 (3).

Holman, J. P. (1997) *Heat transfer*. McGraw-Hill, New York.

Illangasekare, T. & Morel-Seytoux, H. (1986) 'A discrete kernel simulation model for conjunctive management of a stream-aquifer system', *Journal of hydrology(Amsterdam),* 85 (3-4), pp. 319-338.

Ingersoll, L., Adler, F., Plass, H. & Ingersoll, A. (1950) 'Theory of earth heat exchangers for the heat pump', *ASHVE Trans,* 56, pp. 167-188.

Ingersoll, L. & Plass, H. (1948) 'Theory of the ground pipe heat source for the heat pump', *Heating, Piping & Air Conditioning,* 20 (7), pp. 119-122.

Ingersoll, L. R. (1954) *Heat conduction: with engineering, geological, and other applications*. Madison: University of Wisconsin Press.

Kavanaugh, S. P. & Rafferty, K. (1997) *Ground source heat pumps: Design of geothermal systems for commerical and institutional buildings*. American Society of Heating, Refrigeration and Air-conditioning Engineers, Inc., Altanta.

Little, J. & Moler, C. (1984) *Matlab* (R2010a) [Computer Program].

Lu, G. & Wang, J. (2008) 'Experimental investigation on heat transfer characteristics of water in a narrow annulus', *Applied Thermal Engineering,* 28, pp. 8-13.

Lund, J. (2010) 'Direct Utilization of Geothermal Energy', *Energies,* 3 (8), pp. 1443-1471.

Lund, J. W., Freeston, D. H. & Boyd, T. L. (2005) 'Direct application of geothermal energy: 2005 Worldwide review', *Geothermics,* 34 (6), pp. 691-727.

Lund, J. W., Sanner, B., Rybach, L., Curtis, R. & Hellström, G. (2004) 'Geothermal (Ground-source) heat pumps a world overview', *Geo-heat Centre Quarterly Bulletin,* 25 (3).

Maddock, T. (1972) 'Algebraic technological functional from a siumlation model ', *Water Resources Research,* 8 (1).

McLean, D. (1994) *Intergrated Environmental Solutions* (6.0.4) [Computer Program]. Glasgow, UK.

Morel-Seytoux, H. (1975) 'A simple case of conjunctive surface-ground-water management', *Ground Water,* 13 (6), pp. 505-515.

Morel-Seytoux, H. J. & Daly, C. J. (1975) 'A discrete kernel generator for stream-aquifer studies', *Water Resources Research,* 11 (2), pp. 253-260.

Ng, B., Underwood, C. & Walker, S. (2009) 'Numerical modelling of multiple standing column wells for heating and cooling buildings', *Building Simulation 2009 Eleventh International IBPSA Conference*. Glasgow Scotland, pp. 49-55.

Ng, B., Underwood, C. & Walker, S. (2011) 'Standing Column Wells - Modelling the potential for applications in geothermal heating and cooling', *HVAC&R Research,* 17 (6), pp. 1089-1100.

Norris, R. H. (1971) 'Some simple approximate heat transfer correlations for turbulent flow in ducts with rough faces', *ASME Augmentation of Convective Heat and Mas Transfer*, pp. 16-26.

Oliver, J. & Braud, H. (1981) 'Thermal exchange to earth with concentric well pipes', *Transactions of ASAE,* 24 (4), pp. 906-910.

Orio, C. D., Chiasson, A., Johnson, C. N., Deng, Z., Rees, S. J. & Spitler, J. D. (2005) 'A survey of standing column well installations in North America', *ASHRAE Transactions 2005,* 111 (2), pp. 109-121.

Orio, C. D., Johnson, C. N. & Poor, K. D. (2006) 'Geothermal standing column wells: Ten years in a New England school', *ASHRAE Transactions 2006,* 112 (2), pp. 57-64.

Patankar, S. V. (1980) 'Numerical heat transfer and fluid flow, Series in Computational Methods in Mechanics and Thermal Sciences', *McGraw Hill*.

Petukhov, B. (1970) 'Heat transfer and friction in turbulent pipe flow with variable physical properties', *Advances in heat transfer,* 6, pp. 503-565.

Rafferty, K. (1997) 'An Information Survival Kit for the Prospective Geothermal Heat Pump Owner', *Geo-heat Centre Quarterly Bulletin,* 18 (2).

Rawlings, R. (1999) *Ground source heat pumps: a technology review*. Berks, UK: Building Services Research and Information Association (BSRIA).

Rees, S. J., Spitler, J. D., Deng, Z., Orio, C. D. & Johnson, C. N. (2004) 'A study of geothermal heat pump and standing column well performance', *ASHRAE Transactions 2004,* 110 (1), pp. 3-13.

Remson, I., Hornberger, G. M. & Molz, F. J. (1971) *Numerical methods in subsurface hydrology, with an introduction to the finite element method*. New York: John Wiley & Sons, Inc.

Romero, G., Urchueguía, J. F., Witte, H., Cambien, W. & Magraner, T. (2005) *Comparative study between a Geothermal Heat Pump System and an Air-to-Water Heat Pump System for heating and cooling in typical conditions of the European Mediterranean Coast.: Proceedings World Geothermal Congress 2005*. 24-29 April 2005. Antalya, Turkey.

Rushton, K. R. & Redshaw, S. C. (1979) 'Seepage and groundwater flow: numerical analysis by analog and digital methods', in: John Wiley & Sons, Incorporated, pp. 162-168.

Sanner, B. (2001) 'Some history of shallow geothermal energy use', *International summer school on direct application of geothermal energy: Institute of Applied Geosciences, Justus-Liebig-University*.

Sanner, B., Karytsas, C., Mendrinos, D. & Rybach, L. (2003) 'Current status of ground source heat pumps and underground thermal energy storage in Europe', *Geothermics,* 32 (4-6), pp. 579-588.

Sieder, E. & Tate, G. (1936) 'Heat transfer and pressure drop of liquids in tubes', *Industrial & Engineering Chemistry,* 28 (12), pp. 1429-1435.

Smith, G. D. (1985) 'Numerical solution of partial differential equations: finite difference methods', in: Oxford University Press, pp. 11-29.

Spalding, B. (1974) *Phoenics* (2009) [Computer Program].

Spitler, J. (2005) 'Ground-source heat pump system research—past, present and future', *HVAC&R Research,* 11 (2), pp. 165-167.

Spitler, J. D., Liu, X., Rees, S. J. & Yavuzturk, C. (2005) 'Simulation and optimization of ground source heat pump systems', *8th International Energy Agency Heat Pump Conference*. May 30-June 2. Las Vegas.

Theis, C. (1935) 'The relation between the lowering of the piezometric surface and the rate and duration of discharge of a well using groundwater storage: American Geophysical Union Transactions, v. 16', *reprinted as US Geological Survey Ground-Water Note,* 5 (1952), pp. 519-524.

Todd, D. K. (1980) *Groundwater hydrology*. 2 edn. John Wiley & Sons, New York.

Tseng, P. H. & Lee, T. C. (1998) 'Numerical evaluation of exponential integral: Theis well function approximation', *Journal of Hydrology,* 205 (1-2), pp. 38-51.

Underwood, C. P. & Spitler, J. D. (2007) 'Analysis of vertical ground loop heat exchangers aplied to buildings in the UK', *Building Services Engineering Research and Technology,* 28 (2), pp. 133-160.

Underwood, C. P. & Yik, F. W. H. (2004) *Modelling methods for energy in buildings*. Wiley Online Library.

Versteeg, H. K. & Malalasekera, W. (1995) *An introduction to computational fluid dynamics: the finite volume method*. Essex: Prentice Hall.

Wang, H. & Anderson, M. P. (1982) *Introduction to groundwater modeling*. California: Academic Press Inc.

Yavuzturk, C. (1999) *Modeling of vertical ground loop heat exchangers for ground sources heat pump systems.* PhD Thesis. Oklahoma State University.

Yavuzturk, C. & Chiasson, A. D. (2002) 'Performance analysis of U-tube, concentric tube, and standing column well ground heat exchangers using a system simulation approach', *ASHRAE Transactions: Symposia*, pp. 925-938.

Younger, P. L. & Milne, C. A. (1997) 'Hydrostratigraphy and hydrogeochemistry of the Vale of Eden, Cumbria, UK', *PROCEEDINGS-YORKSHIRE GEOLOGICAL SOCIETY,* 51, pp. 349-366.

Yuill, G. K. & Mikler, V. (1995) 'Analysis of the effect of induced groundwater flow on heat transfer from a vertical open-hole concentric-tube thermal well', *ASHRAE Transactions 1995,* 101 (1), pp. 173-185.

Appendix A - Discretisation of the field model equations (IFV)

1. Heat diffusion equation

$$\frac{S}{K}\frac{\partial h}{\partial t}-\frac{F}{K}=\left[\frac{\partial^2 h}{\partial x^2}+\frac{\partial^2 h}{\partial y^2}+\frac{\partial^2 h}{\partial z^2}\right]$$

$$\frac{S}{K}\left[\left(h_p-h_{\bar{p}}\right)\frac{\Delta x\Delta y\Delta z}{\Delta t}\right]-\frac{F}{K}=\frac{\partial^2 h}{\partial x^2}+\frac{\partial^2 h}{\partial y^2}+\frac{\partial^2 h}{\partial z^2}$$

$$\frac{S}{K}\left[\left(h_p-h_{\bar{p}}\right)\frac{\Delta x\Delta y\Delta z}{\Delta t}\right]-\frac{F}{K}=\left[\Delta y\Delta z\left(\frac{\partial h}{\partial x}\Big|_e-\frac{\partial h}{\partial x}\Big|_w\right)+\Delta x\Delta z\left(\frac{\partial h}{\partial y}\Big|_n-\frac{\partial h}{\partial y}\Big|_s\right)+\Delta x\Delta y\left(\frac{\partial h}{\partial z}\Big|_t-\frac{\partial h}{\partial z}\Big|_b\right)\right]$$

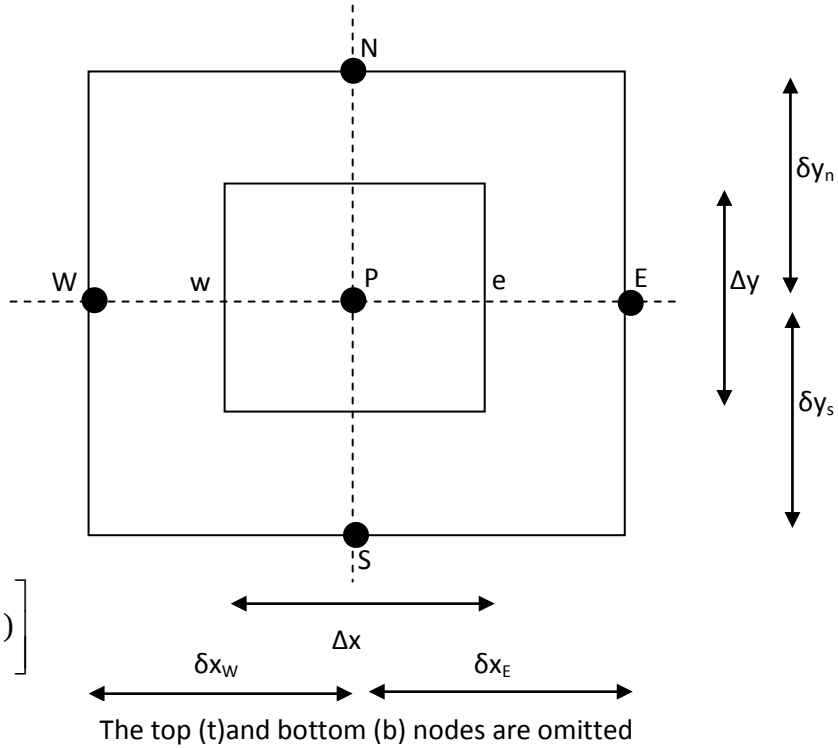

The top (t)and bottom (b) nodes are omitted

$$\frac{S}{K}\left[\left(h_p-h_{\bar{p}}\right)\frac{\Delta x\Delta y\Delta z}{\Delta t}\right]-\frac{F}{K}=\left[\frac{\Delta y\Delta z(h_E-h_P)}{\delta x_E}-\frac{\Delta y\Delta z(h_P-h_W)}{\delta x_W}+\frac{\Delta x\Delta z(h_N-h_P)}{\delta y_N}-\frac{\Delta x\Delta z(h_P-h_S)}{\delta y_S}+\frac{\Delta x\Delta y(h_T-h_P)}{\delta z_T}-\frac{\Delta x\Delta y(h_P-h_B)}{\delta z_B}\right]$$

$$\frac{S}{K}\left[\left(h_p - h_{\bar{p}}\right)\frac{\Delta x\Delta y\Delta z}{\Delta t}\right] - \frac{F}{K} =$$

$$\left[\frac{\Delta y\Delta z(h_E)}{\delta x_E} - \frac{\Delta y\Delta z(h_P)}{\delta x_E} - \frac{\Delta y\Delta z(h_P)}{\delta x_W} + \frac{\Delta y\Delta z(h_W)}{\delta x_W} + \frac{\Delta x\Delta z(h_N)}{\delta y_N} - \frac{\Delta x\Delta z(h_P)}{\delta y_N} - \frac{\Delta x\Delta z(h_P)}{\delta y_S} + \frac{\Delta x\Delta z(h_S)}{\delta y_S} + \frac{\Delta x\Delta y(h_T)}{\delta z_T} - \frac{\Delta x\Delta y(h_P)}{\delta z_T} - \frac{\Delta x\Delta y(h_P)}{\delta z_B} + \frac{\Delta x\Delta y(h_B)}{\delta z_B}\right]$$

$$\frac{S}{K}\left[\left(h_p - h_{\bar{p}}\right)\frac{\Delta x\Delta y\Delta z}{\Delta t}\right] =$$

$$h_p\left(-\frac{\Delta y\Delta z}{\delta x_E} - \frac{\Delta y\Delta z}{\delta x_W} - \frac{\Delta x\Delta z}{\delta y_N} - \frac{\Delta x\Delta z}{\delta y_S} - \frac{\Delta x\Delta y}{\delta z_T} - \frac{\Delta x\Delta y}{\delta z_B}\right) + \frac{\Delta y\Delta z}{\delta x_E}h_E + \frac{\Delta y\Delta z}{\delta x_W}h_W + \frac{\Delta x\Delta z}{\delta y_N}h_N + \frac{\Delta x\Delta z}{\delta y_S}h_S + \frac{\Delta x\Delta y}{\delta z_T}h_T + \frac{\Delta x\Delta y}{\delta z_B}h_B + \frac{F}{K}$$

$$h_p\frac{\Delta x\Delta y\Delta z}{\Delta t}\frac{S}{K} - h_{\bar{p}}\frac{\Delta x\Delta y\Delta z}{\Delta t}\frac{S}{K}$$

$$= h_p\left(-\frac{\Delta y\Delta z}{\delta x_E} - \frac{\Delta y\Delta z}{\delta x_W} - \frac{\Delta x\Delta z}{\delta y_N} - \frac{\Delta x\Delta z}{\delta y_S} - \frac{\Delta x\Delta y}{\delta z_T} - \frac{\Delta x\Delta y}{\delta z_B}\right) + \frac{\Delta y\Delta z}{\delta x_E}h_E + \frac{\Delta y\Delta z}{\delta x_W}h_W + \frac{\Delta x\Delta z}{\delta y_N}h_N + \frac{\Delta x\Delta z}{\delta y_S}h_S + \frac{\Delta x\Delta y}{\delta z_T}h_T + \frac{\Delta x\Delta y}{\delta z_B}h_B + \frac{F}{K}$$

$$h_p\frac{\Delta x\Delta y\Delta z}{\Delta t}\frac{S}{K} - h_{\bar{p}}\frac{\Delta x\Delta y\Delta z}{\Delta t}\frac{S}{K}$$

$$= -h_p\left(\frac{\Delta y\Delta z}{\delta x_E} + \frac{\Delta y\Delta z}{\delta x_W} + \frac{\Delta x\Delta z}{\delta y_N} + \frac{\Delta x\Delta z}{\delta y_S} + \frac{\Delta x\Delta y}{\delta z_T} + \frac{\Delta x\Delta y}{\delta z_B}\right) + \frac{\Delta y\Delta z}{\delta x_E}h_E + \frac{\Delta y\Delta z}{\delta x_W}h_W + \frac{\Delta x\Delta z}{\delta y_N}h_N + \frac{\Delta x\Delta z}{\delta y_S}h_S + \frac{\Delta x\Delta y}{\delta z_T}h_T + \frac{\Delta x\Delta y}{\delta z_B}h_B + \frac{F}{K} + h_{\bar{p}}\frac{\Delta x\Delta y\Delta z}{\Delta t}\frac{S}{K}$$

$$h_p \frac{\Delta x \Delta y \Delta z}{\Delta t}\frac{S}{K} + h_p\left(\frac{\Delta y \Delta z}{\delta x_E} + \frac{\Delta y \Delta z}{\delta x_W} + \frac{\Delta x \Delta z}{\delta y_N} + \frac{\Delta x \Delta z}{\delta y_S} + \frac{\Delta x \Delta y}{\delta z_T} + \frac{\Delta x \Delta y}{\delta z_B}\right)$$
$$= \frac{\Delta y \Delta z}{\delta x_E} h_E + \frac{\Delta y \Delta z}{\delta x_W} h_W + \frac{\Delta x \Delta z}{\delta y_N} h_N + \frac{\Delta x \Delta z}{\delta y_S} h_S + \frac{\Delta x \Delta y}{\delta z_T} h_T + \frac{\Delta x \Delta y}{\delta z_B} h_B + \frac{F}{K} + h_{\bar{p}} \frac{\Delta x \Delta y \Delta z}{\Delta t}\frac{S}{K}$$

$$h_p\left[\frac{\Delta x \Delta y \Delta z}{\Delta t}\frac{S}{K} + \left(\frac{\Delta y \Delta z}{\delta x_E} + \frac{\Delta y \Delta z}{\delta x_W} + \frac{\Delta x \Delta z}{\delta y_N} + \frac{\Delta x \Delta z}{\delta y_S} + \frac{\Delta x \Delta y}{\delta z_T} + \frac{\Delta x \Delta y}{\delta z_B}\right)\right]$$
$$= \frac{\Delta y \Delta z}{\delta x_E} h_E + \frac{\Delta y \Delta z}{\delta x_W} h_W + \frac{\Delta x \Delta z}{\delta y_N} h_N + \frac{\Delta x \Delta z}{\delta y_S} h_S + \frac{\Delta x \Delta y}{\delta z_T} h_T + \frac{\Delta x \Delta y}{\delta z_B} h_B + \frac{F}{K} + h_{\bar{p}} \frac{\Delta x \Delta y \Delta z}{\Delta t}\frac{S}{K}$$

$$h_p = \frac{\frac{\Delta y \Delta z}{\delta x_E} h_E + \frac{\Delta y \Delta z}{\delta x_W} h_W + \frac{\Delta x \Delta z}{\delta y_N} h_N + \frac{\Delta x \Delta z}{\delta y_S} h_S + \frac{\Delta x \Delta y}{\delta z_T} h_T + \frac{\Delta x \Delta y}{\delta z_B} h_B + \frac{F}{K} + h_{\bar{p}} \frac{\Delta x \Delta y \Delta z}{\Delta t}\frac{S}{K}}{\frac{\Delta x \Delta y \Delta z}{\Delta t}\frac{S}{K} + \left(\frac{\Delta y \Delta z}{\delta x_E} + \frac{\Delta y \Delta z}{\delta x_W} + \frac{\Delta x \Delta z}{\delta y_N} + \frac{\Delta x \Delta z}{\delta y_S} + \frac{\Delta x \Delta y}{\delta z_T} + \frac{\Delta x \Delta y}{\delta z_B}\right)}$$

2. Darcy flow equation

Velocity in each direction

$$\bar{U}_x = -K\frac{\partial h}{\partial x}$$

$$\bar{U}_y = -K\frac{\partial h}{\partial y}$$

$$\bar{U}_z = -K\frac{\partial h}{\partial z}$$

X direction:

$$nU_x = -K\left(\frac{(h_E + h_P)}{2} - \frac{(h_P + h_W)}{2}\right)\Delta y\Delta z$$

$$nU_x = -K\left(\frac{h_E + h_P - h_P - h_W}{2}\right)\Delta y\Delta z$$

$$nU_x = -K\left(\frac{h_E - h_W}{2}\right)\Delta y\Delta z$$

$$U_x = -\frac{h_E K\Delta y\Delta z}{2n} + \frac{h_W K\Delta y\Delta z}{2n}$$

Y Direction:

$$nU_y = -K\left(\frac{(h_N + h_P)}{2} - \frac{(h_P + h_S)}{2}\right)\Delta x\Delta z$$

$$nU_y = -K\left(\frac{h_N + h_P - h_P - h_S}{2}\right)\Delta x\Delta z$$

$$nU_y = -K\left(\frac{h_N - h_S}{2}\right)\Delta x\Delta z$$

$$U_y = -\frac{h_N K\Delta x\Delta z}{2n} + \frac{h_S K\Delta y\Delta z}{2n}$$

Z Direction:

$$nU_Z = -K\left(\frac{(h_T + h_P)}{2} - \frac{(h_P + h_B)}{2}\right)\Delta x\Delta y$$

$$nU_Z = -K\left(\frac{h_T + h_P - h_P - h_B}{2}\right)\Delta x\Delta y$$

$$nU_Z = -K\left(\frac{h_T - h_B}{2}\right)\Delta x\Delta y$$

$$U_Z = -\frac{h_T K\Delta x\Delta y}{2n} + \frac{h_B K\Delta x\Delta y}{2n}$$

3. Energy equation

$$\left[n\rho_L C_{pL} + (1-n)\rho_S C_{pS}\right]\frac{\partial T}{\partial t} - k_{eff}\nabla^2 T + \left[n\rho_L C_{pL}\right]\nabla uT = Sources$$

Solving the terms $\nabla^2 T$:

$$\nabla^2 T = \frac{\partial^2 T}{\partial x^2} + \frac{\partial^2 T}{\partial y^2} + \frac{\partial^2 T}{\partial z^2}$$

$$\nabla^2 T == \left[T_p \left(-\frac{\Delta y \Delta z}{\delta x_e} - \frac{\Delta y \Delta z}{\delta x_w} - \frac{\Delta x \Delta z}{\delta y_n} - \frac{\Delta x \Delta z}{\delta y_s} - \frac{\Delta x \Delta y}{\delta z_t} - \frac{\Delta x \Delta y}{\delta z_b} \right) + \frac{\Delta y \Delta z}{\delta x_e} T_E + \frac{\Delta y \Delta z}{\delta x_w} T_W + \frac{\Delta x \Delta z}{\delta y_n} T_N + \frac{\Delta x \Delta z}{\delta y_s} T_S + \frac{\Delta x \Delta y}{\delta z_t} T_T + \frac{\Delta x \Delta y}{\delta z_b} T_B \right]$$

Solving the terms ∇uT :

$$\nabla uT = \frac{\partial uT}{\partial x} + \frac{\partial uT}{\partial y} + \frac{\partial uT}{\partial z}$$

$$\nabla uT = u_x \left(\frac{(\Delta x \Delta z T_E + \Delta x \Delta z T_P)}{2} - \frac{(\Delta x \Delta z T_P + \Delta x \Delta z T_W)}{2} \right) + u_y \left(\frac{(\Delta x \Delta z T_N + \Delta x \Delta z T_P)}{2} - \frac{(\Delta x \Delta z T_P + \Delta x \Delta z T_S)}{2} \right) + u_z \left(\frac{(\Delta x \Delta z T_T + \Delta x \Delta z T_P)}{2} - \frac{(\Delta x \Delta z T_P + \Delta x \Delta z T_B)}{2} \right)$$

$$\nabla uT = u_x \left(\frac{(\Delta x \Delta z T_E - \Delta x \Delta z T_W)}{2} \right) + u_y \left(\frac{(\Delta x \Delta z T_N - \Delta x \Delta z T_S)}{2} \right) + u_z \left(\frac{(\Delta x \Delta z T_T - \Delta x \Delta z T_B)}{2} \right)$$

$$\nabla uT = \frac{T_E \Delta x \Delta z \cdot u_x}{2} - \frac{T_W \Delta x \Delta z \cdot u_x}{2} + \frac{T_N \Delta x \Delta z \cdot u_y}{2} - \frac{T_S \Delta x \Delta z \cdot u_y}{2} + \frac{\Delta x \Delta z \cdot u_z T_T}{2} - \frac{\Delta x \Delta z \cdot u_z T_B}{2}$$

Making three coefficients to simplify the following terms:

$$\left[n\rho_L C_{pL} + (1-n)\rho_S C_{pS}\right] = C$$

$$\frac{k_{eff}}{C} = C_1$$

$$\frac{\rho_L C_{pL}}{C} = C_2$$

Finally, solving the whole equation:

$$\left[n\rho_L C_{pL} + (1-n)\rho_S C_{pS}\right]\frac{\partial T}{\partial t} - k_{eff}\nabla^2 T + \left[n\rho_L C_{pL}\right]\nabla uT = Sources$$

$$\left[n\rho_L C_{pL} + (1-n)\rho_S C_{pS}\right]\frac{\partial T}{\partial t} = Sources + k_{eff}\nabla^2 T - \rho_L C_{pL}\, u\nabla T$$

$$\frac{\partial T}{\partial t} = \frac{Sources + k_{eff}\nabla^2 T - \rho_L C_{pL}\, u\nabla T}{\left[n\rho_L C_{pL} + (1-n)\rho_S C_{pS}\right]}$$

$$\frac{\partial T}{\partial t} = \frac{Sources}{\left[n\rho_L C_{pL} + (1-n)\rho_S C_{pS}\right]} + \frac{k_{eff}}{\left[n\rho_L C_{pL} + (1-n)\rho_S C_{pS}\right]}\nabla^2 T - \frac{\rho_L C_{pL}}{\left[n\rho_L C_{pL} + (1-n)\rho_S C_{pS}\right]}\nabla uT$$

Replacing certain terms into the coefficients C, C_1 and C_2:

$$\frac{\partial T}{\partial t} = \frac{Sources}{C} + C_1\,\nabla^2 T - C_2\,\nabla uT$$

$$\frac{\partial T}{\partial t} = \frac{Sources}{C} + C_1\left[T_p\left(-\frac{\Delta y\Delta z}{\delta x_E} - \frac{\Delta y\Delta z}{\delta x_W} - \frac{\Delta x\Delta z}{\delta y_N} - \frac{\Delta x\Delta z}{\delta y_S} - \frac{\Delta x\Delta y}{\delta z_T} - \frac{\Delta x\Delta y}{\delta z_B}\right) + \frac{\Delta y\Delta z}{\delta x_E}T_E + \frac{\Delta y\Delta z}{\delta x_W}T_W + \frac{\Delta x\Delta z}{\delta y_N}T_N + \frac{\Delta x\Delta z}{\delta y_S}T_S + \frac{\Delta x\Delta y}{\delta z_T}T_T + \frac{\Delta x\Delta y}{\delta z_B}T_B\right] \cdots$$

$$- C_2\left\{\frac{T_E\Delta x\Delta z\cdot u_x}{2} - \frac{T_W\Delta x\Delta z\cdot u_x}{2} + \frac{T_N\Delta x\Delta z\cdot u_y}{2} - \frac{T_S\Delta x\Delta z\cdot u_y}{2} + \frac{\Delta x\Delta z\cdot u_z T_T}{2} - \frac{\Delta x\Delta z\cdot u_z T_B}{2}\right\}$$

$$\frac{\partial T}{\partial t} = \frac{Sources}{C} + C_1 \left[T_p \left(-\frac{\Delta y \Delta z}{\delta x_E} - \frac{\Delta y \Delta z}{\delta x_W} - \frac{\Delta x \Delta z}{\delta y_N} - \frac{\Delta x \Delta z}{\delta y_S} - \frac{\Delta x \Delta y}{\delta z_T} - \frac{\Delta x \Delta y}{\delta z_B} \right) + \frac{\Delta y \Delta z}{\delta x_E} T_E + \frac{\Delta y \Delta z}{\delta x_W} T_W + \frac{\Delta x \Delta z}{\delta y_N} T_N + \frac{\Delta x \Delta z}{\delta y_S} T_S + \frac{\Delta x \Delta y}{\delta z_T} T_T + \frac{\Delta x \Delta y}{\delta z_B} T_B \right] \cdots$$

$$- \frac{C_2 T_E \Delta y \Delta z \cdot u_x}{2} + \frac{C_2 T_W \Delta y \Delta z \cdot u_x}{2} - \frac{C_2 T_N \Delta x \Delta z \cdot u_y}{2} + \frac{C_2 T_S \Delta x \Delta z \cdot u_y}{2} \cdots$$

$$- \frac{C_2 T_T \Delta x \Delta y \cdot u_z}{2} + \frac{C_2 T_B \Delta x \Delta y \cdot u_z}{2}$$

$$\frac{\partial T}{\partial t} = \frac{Sources}{C} + T_p \left(-\frac{C_1 \Delta y \Delta z}{\delta x_E} - \frac{C_1 \Delta y \Delta z}{\delta x_W} - \frac{C_1 \Delta x \Delta z}{\delta y_N} - \frac{C_1 \Delta x \Delta z}{\delta y_S} - \frac{C_1 \Delta x \Delta y}{\delta z_T} - \frac{C_1 \Delta x \Delta y}{\delta z_B} \right)$$

$$+ \frac{C_1 \Delta y \Delta z}{\delta x_E} T_E - \frac{C_2 T_E \Delta y \Delta z \cdot u_x}{2} + \frac{C_1 \Delta y \Delta z}{\delta x_W} T_W + \frac{C_2 T_W \Delta y \Delta z \cdot u_x}{2} + \frac{C_1 \Delta x \Delta z}{\delta y_N} T_N - \frac{C_2 T_N \Delta x \Delta z \cdot u_y}{2}$$

$$+ \frac{C_1 \Delta x \Delta z}{\delta y_S} T_S + \frac{C_2 T_S \Delta x \Delta z \cdot u_y}{2} + \frac{C_1 \Delta x \Delta y}{\delta z_T} T_T - \frac{C_2 T_T \Delta x \Delta y \cdot u_z}{2} + \frac{C_1 \Delta x \Delta y}{\delta z_B} T_B + \frac{C_2 T_B \Delta x \Delta y \cdot u_z}{2}$$

$$\frac{\Delta x\Delta y\Delta z}{\Delta t}T_P-\frac{\Delta x\Delta y\Delta z}{\Delta t}T_P^-=\frac{Sources}{C}+T_p\left(-\frac{C_1\Delta y\Delta z}{\delta x_E}-\frac{C_1\Delta y\Delta z}{\delta x_W}-\frac{C_1\Delta x\Delta z}{\delta y_N}-\frac{C_1\Delta x\Delta z}{\delta y_S}-\frac{C_1\Delta x\Delta y}{\delta z_T}-\frac{C_1\Delta x\Delta y}{\delta z_B}\right)$$
$$+T_E\left(\frac{C_1\Delta y\Delta z}{\delta x_E}-\frac{C_2\,\Delta y\Delta z\cdot u_x}{2}\right)+T_W\left(\frac{C_1\Delta y\Delta z}{\delta x_W}+\frac{C_2\,\Delta y\Delta z\cdot u_x}{2}\right)+T_N\left(\frac{C_1\Delta x\Delta z}{\delta y_N}-\frac{C_2\,\Delta x\Delta z\cdot u_y}{2}\right)$$
$$+T_S\left(\frac{C_1\Delta x\Delta z}{\delta y_S}+\frac{C_2\,\Delta x\Delta z\cdot u_y}{2}\right)+T_T\left(\frac{C_1\Delta x\Delta y}{\delta z_T}-\frac{C_2\,\Delta x\Delta y\cdot u_z}{2}\right)+T_B\left(\frac{C_1\Delta x\Delta y}{\delta z_B}+\frac{C_2\,\Delta x\Delta y\cdot u_z}{2}\right)$$

$$\frac{\Delta x\Delta y\Delta z}{\Delta t}T_P-T_p\left(-\frac{C_1\Delta y\Delta z}{\delta x_E}-\frac{C_1\Delta y\Delta z}{\delta x_W}-\frac{C_1\Delta x\Delta z}{\delta y_N}-\frac{C_1\Delta x\Delta z}{\delta y_S}-\frac{C_1\Delta x\Delta y}{\delta z_T}-\frac{C_1\Delta x\Delta y}{\delta z_B}\right)=\frac{Sources}{C}$$
$$+T_E\left(\frac{C_1\Delta y\Delta z}{\delta x_E}-\frac{C_2\,\Delta y\Delta z\cdot u_x}{2}\right)+T_W\left(\frac{C_1\Delta y\Delta z}{\delta x_W}+\frac{C_2\,\Delta y\Delta z\cdot u_x}{2}\right)+T_N\left(\frac{C_1\Delta x\Delta z}{\delta y_N}-\frac{C_2\,\Delta x\Delta z\cdot u_y}{2}\right)$$
$$+T_S\left(\frac{C_1\Delta x\Delta z}{\delta y_S}+\frac{C_2\,\Delta x\Delta z\cdot u_y}{2}\right)+T_T\left(\frac{C_1\Delta x\Delta y}{\delta z_T}-\frac{C_2\,\Delta x\Delta y\cdot u_z}{2}\right)+T_B\left(\frac{C_1\Delta x\Delta y}{\delta z_B}+\frac{C_2\,\Delta x\Delta y\cdot u_z}{2}\right)+\frac{\Delta x\Delta y\Delta z}{\Delta t}T_P^-$$

$$T_P\left(\frac{\Delta x\Delta y\Delta z}{\Delta t}+\frac{C_1\Delta y\Delta z}{\delta x_E}+\frac{C_1\Delta y\Delta z}{\delta x_W}+\frac{C_1\Delta x\Delta z}{\delta y_N}+\frac{C_1\Delta x\Delta z}{\delta y_S}+\frac{C_1\Delta x\Delta y}{\delta z_T}+\frac{C_1\Delta x\Delta y}{\delta z_B}\right)=\frac{Sources}{C}+\frac{\Delta x\Delta y\Delta z}{\Delta t}T_P^-$$
$$+T_E\left(\frac{C_1\Delta y\Delta z}{\delta x_E}-\frac{C_2\,\Delta y\Delta z\cdot u_x}{2}\right)+T_W\left(\frac{C_1\Delta y\Delta z}{\delta x_W}+\frac{C_2\,\Delta y\Delta z\cdot u_x}{2}\right)+T_N\left(\frac{C_1\Delta x\Delta z}{\delta y_N}-\frac{C_2\,\Delta x\Delta z\cdot u_y}{2}\right)$$
$$+T_S\left(\frac{C_1\Delta x\Delta z}{\delta y_S}+\frac{C_2\,\Delta x\Delta z\cdot u_y}{2}\right)+T_T\left(\frac{C_1\Delta x\Delta y}{\delta z_T}-\frac{C_2\,\Delta x\Delta y\cdot u_z}{2}\right)+T_B\left(\frac{C_1\Delta x\Delta y}{\delta z_B}+\frac{C_2\,\Delta x\Delta y\cdot u_z}{2}\right)$$

Appendix B - Discretisation of the well model equations

1. Energy balance for the water in the annulus

$$V_{annu}\rho_L C_{pL}\frac{dT_{(annu,z)}}{dt} + m_{annu}C_{pL}\frac{dT_{(annu,z)}}{dz} - Q_{annu} - Q_{sp} = 0$$

$$V_{annu}\rho_L C_{pL}\frac{\Delta x\Delta y\Delta z}{\Delta t}\left(T_{(annu,z)} - T_{(annu,z)}{}^{-}\right) + m_{annu}C_{pL}\left(T_{(annu,z)} - T_{(annu,z-1)}\right) - \left[AU_{annu}\left(T_{(x,y,z)} - T_{(annu,z)}\right) + m_{bleed}T_{(x,y,z)}\right] - \left[AU_{sp}\left(T_{sp(x,y,z)} - T_{(annu,z)}\right)\right] = 0$$

$$V_{annu}\rho_L C_{pL}\frac{\Delta x\Delta y\Delta z}{\Delta t}\left(T_{(annu,z)}\right) + m_{annu}C_{pL}\left(T_{(annu,z)}\right) + AU_{annu}T_{(annu,z)} + AU_{sp}T_{(annu,z)} = V_{annu}\rho_L C_{pL}\frac{\Delta x\Delta y\Delta z}{\Delta t}\left(T_{(annu,z)}{}^{-}\right) + m_{annu}C_{pL}\left(T_{(annu,z-1)}\right) + AU_{annu}T_{(x,y,z)} + m_{bleed}T_{(x,y,z)} + AU_{sp}T_{sp(x,y,z)}$$

$$T_{(annu,z)}\left[\quad V_{annu}\rho_L C_{pL}\frac{\Delta x\Delta y\Delta z}{\Delta t} + m_{(annu,z)}C_{pL} + AU_{annu} + AU_{sp}\quad\right] = V_{annu}\rho_L C_{pL}\frac{\Delta x\Delta y\Delta z}{\Delta t}\left(T_{(annu,z)}{}^{-}\right) + m_{(annu,z-1)}C_{pL}\left(T_{(annu,z-1)}\right) + AU_{annu}T_{(x,y,z)} + m_{(bleed,z)}T_{(x,y,z)} + AU_{sp}T_{sp(x,y,z)}$$

$$T_{(annu,z)} = \frac{V_{annu}\rho_L C_{pL}\frac{\Delta x\Delta y\Delta z}{\Delta t}\left(T_{(annu,z)}{}^{-}\right) + m_{(annu,z-1)}C_{pL}\left(T_{(annu,z-1)}\right) + AU_{annu}T_{(x,y,z)} + m_{(bleed,z)}T_{(x,y,z)} + AU_{sp}T_{sp(x,y,z)}}{\left[\quad V_{annu}\rho_L C_{pL}\frac{\Delta x\Delta y\Delta z}{\Delta t} + m_{(annu,z)}C_{pL} + AU_{annu} + AU_{sp}\quad\right]}$$

2. Energy balance for the water in the suction pipe

$$V_{sp}\rho_L C_{pL}\frac{dT_{sp(x,y,z)}}{dt} + (m_{ann} + m_{bleed})C_{pL}\frac{dT_{sp(x,y,z)}}{dz} + Q_{sp} = 0$$

$$V_{sp}\rho_L C_{pL}\frac{dT_{sp(x,y,z)}}{dt} + (m_{ann} + m_{bleed}) \cdot C_{pL} \cdot \left(T_{sp(x,y,z+1)} - T_{sp(x,y,z)}\right) + AU_{sp}\left(T_{(annu,z)} - T_{sp(x,y,z)}\right) = 0$$

$$V_{sp}\rho_L C_{pL}\frac{dT_{sp(x,y,z)}}{dt} + (m_{ann} + m_{bleed}) \cdot C_{pL} \cdot \left(T_{sp(x,y,z+1)} - T_{sp(x,y,z)}\right) + AU_{sp}\left(T_{(annu,z)} - T_{sp(x,y,z)}\right) = 0$$

$$V_{sp}\rho_L C_{pL}\frac{\Delta x\Delta y\Delta z}{\Delta t}\left(T_{sp(x,y,z)} - T_{sp(x,y,z)}{}^{-}\right) + (m_{ann} + m_{bleed}) \cdot C_{pL} \cdot \left(T_{sp(x,y,z+1)} - T_{sp(x,y,z)}\right) + AU_{sp}\left(T_{(annu,z)} - T_{sp(x,y,z)}\right) = 0$$

$$V_{sp}\rho_L C_{pL}\frac{\Delta x\Delta y\Delta z}{\Delta t}\left(T_{sp(x,y,z)} - T_{sp(x,y,z)}{}^{-}\right) + (m_{ann} + m_{bleed}) \cdot C_{pL} \cdot \left(T_{sp(x,y,z)} - T_{sp(x,y,z+1)}\right) + AU_{sp}\left(T_{(annu,z)} - T_{sp(x,y,z)}\right) = 0$$

$$V_{sp}\rho_L C_{pL}\frac{\Delta x\Delta y\Delta z}{\Delta t}\left(T_{sp(x,y,z)}\right) + (m_{ann} + m_{bleed}) \cdot C_{pL} \cdot \left(T_{sp(x,y,z)}\right) - AU_{sp}\left(T_{sp(x,y,z)}\right)$$
$$= V_{sp}\rho_L C_{pL}\frac{\Delta x\Delta y\Delta z}{\Delta t}\left(T_{sp(x,y,z)}{}^{-}\right) + (m_{ann} + m_{bleed}) \cdot C_{pL} \cdot \left(T_{sp(x,y,z+1)}\right) - AU_{sp}\left(T_{(annu,z)}\right)$$

$$T_{sp(x,y,z)}\left[\quad V_{sp}\rho_L C_{pL}\frac{\Delta x\Delta y\Delta z}{\Delta t}+(m_{ann}+m_{bleed})\cdot C_{pL}-AU_{sp}\quad\right]$$
$$=V_{sp}\rho_L C_{pL}\frac{\Delta x\Delta y\Delta z}{\Delta t}\left(T_{sp(x,y,z)}{}^{-}\right)+(m_{ann}+m_{bleed})\cdot C_{pL}\cdot\left(T_{sp(x,y,z+1)}\right)-AU_{sp}\left(T_{(annu,z)}\right)$$

$$T_{sp(x,y,z)}=\frac{V_{sp}\rho_L C_{pL}\frac{\Delta x\Delta y\Delta z}{\Delta t}\left(T_{sp(x,y,z)}{}^{-}\right)+(m_{ann}+m_{bleed})\cdot C_{pL}\cdot\left(T_{sp(x,y,z+1)}\right)-AU_{sp}\left(T_{(annu,z)}\right)}{\left[\quad V_{sp}\rho_L C_{pL}\frac{\Delta x\Delta y\Delta z}{\Delta t}+(m_{ann}+m_{bleed})\cdot C_{pL}-AU_{sp}\quad\right]}$$

Appendix C - Detailed monthly data plot of the application test results (Groups 1 to 4 in Chapter 6.2)

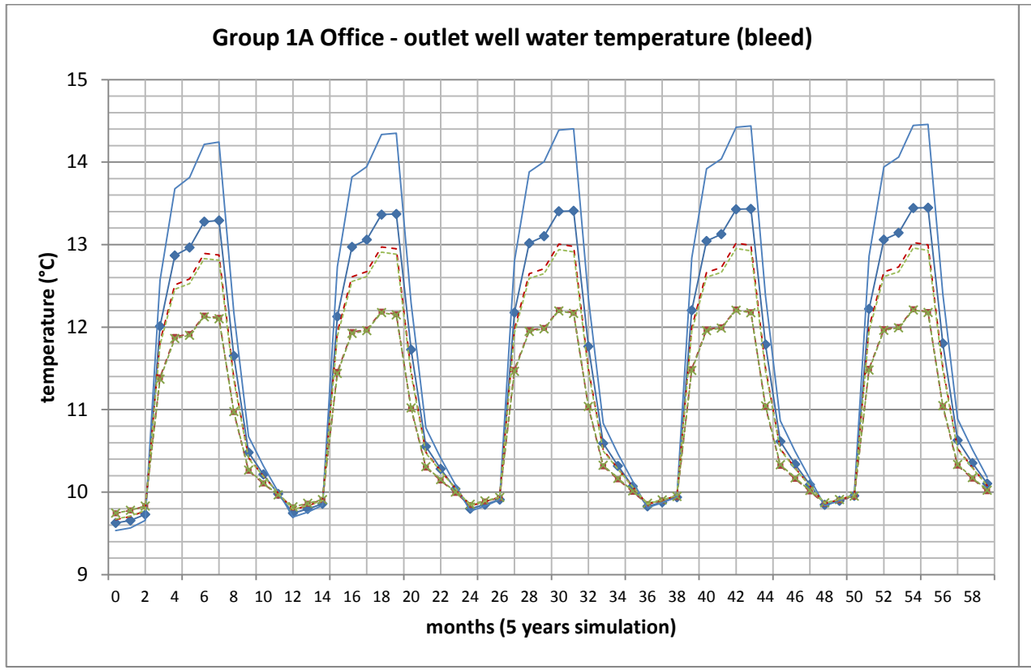
Group 1A Office - outlet well water temperature (bleed)
temperature (°C)
months (5 years simulation)

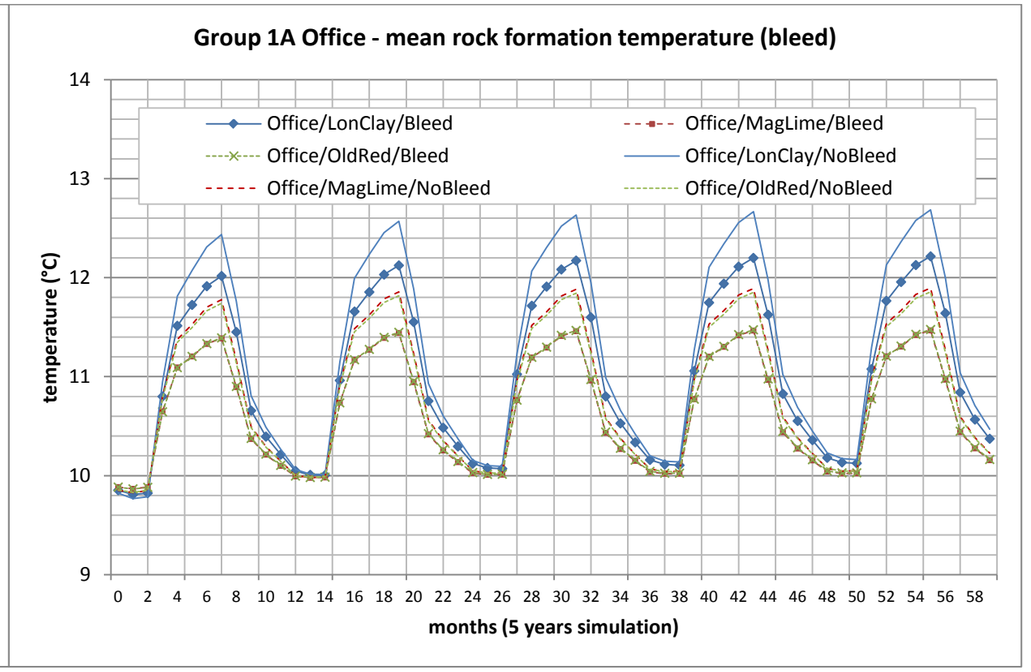
Group 1A Office - mean rock formation temperature (bleed)
Office/LonClay/Bleed
Office/MagLime/Bleed
Office/OldRed/Bleed
Office/LonClay/NoBleed
Office/MagLime/NoBleed
Office/OldRed/NoBleed
temperature (°C)
months (5 years simulation)

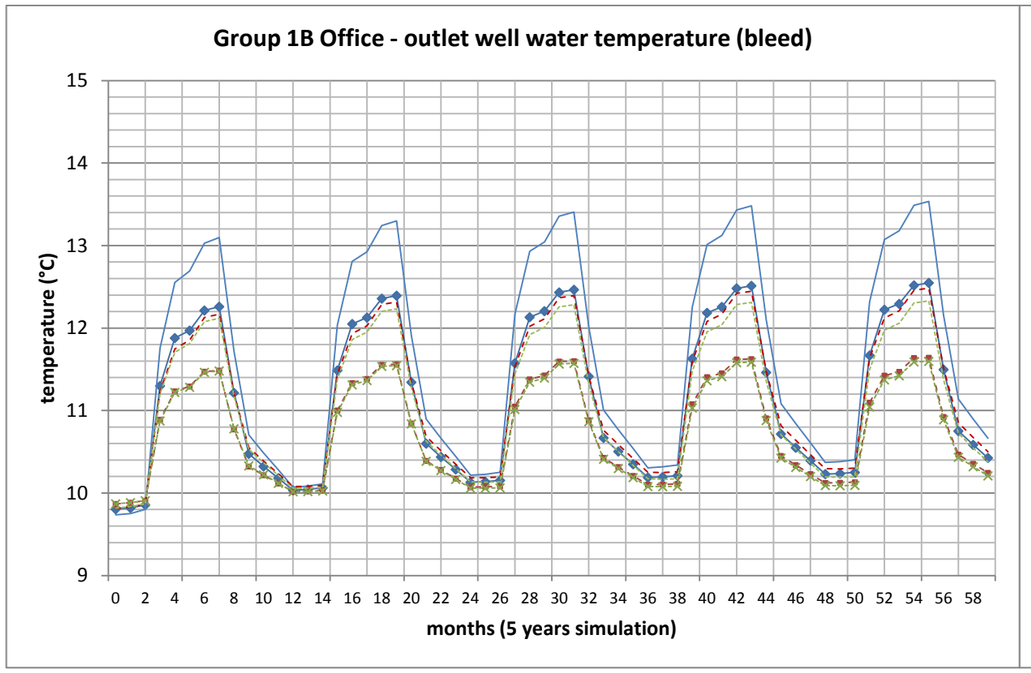
Group 1B Office - outlet well water temperature (bleed)
temperature (°C)
months (5 years simulation)

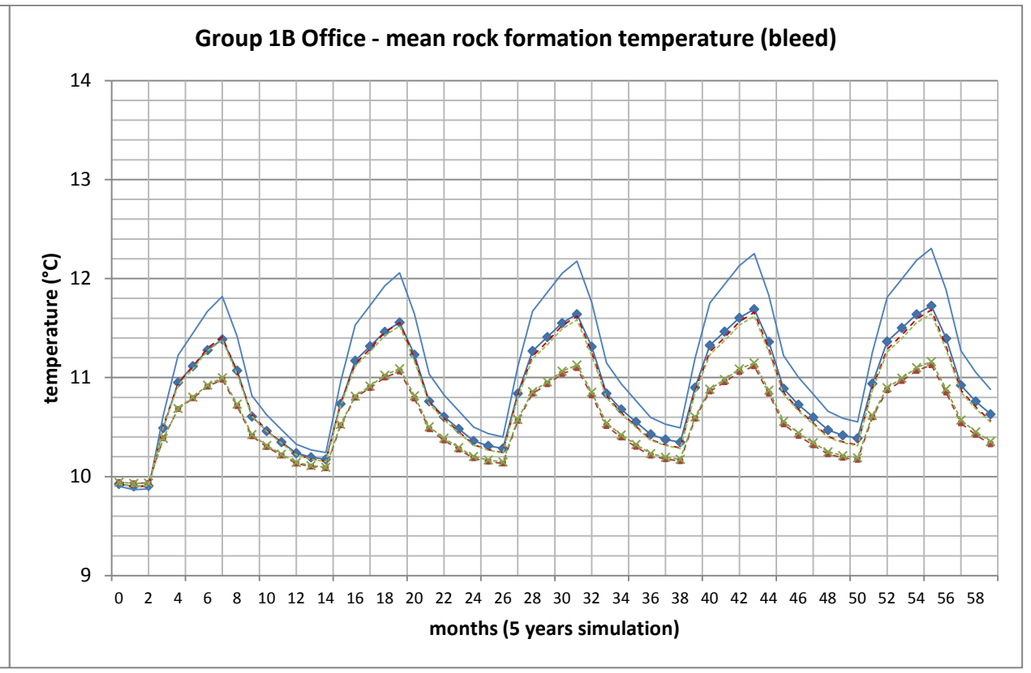
Group 1B Office - mean rock formation temperature (bleed)
temperature (°C)
months (5 years simulation)

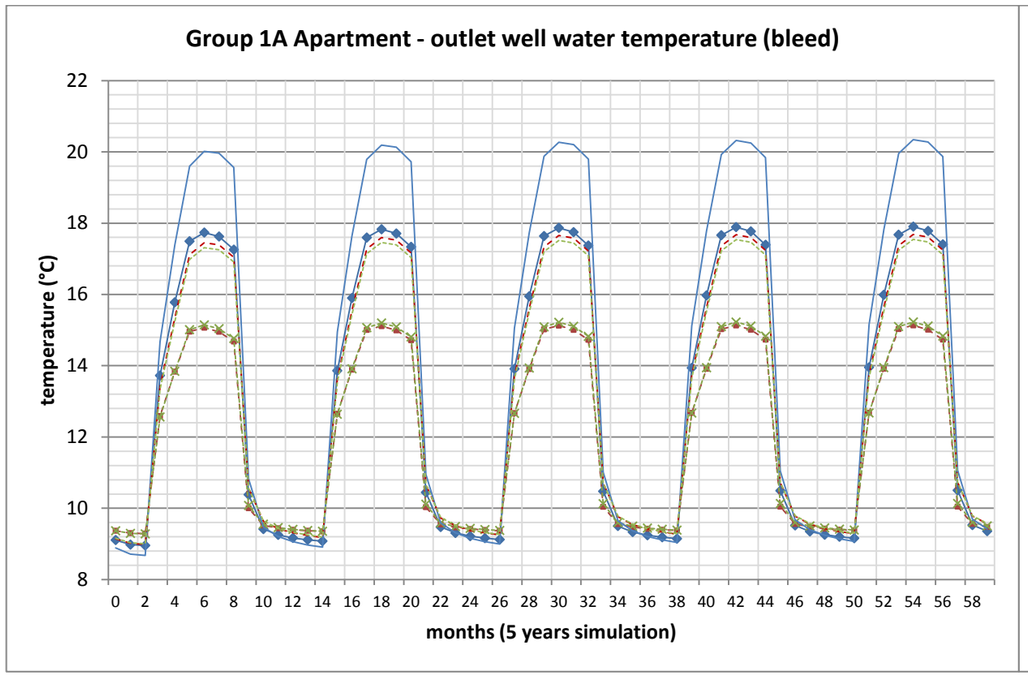
Group 1A Apartment - outlet well water temperature (bleed)
temperature (°C)
months (5 years simulation)

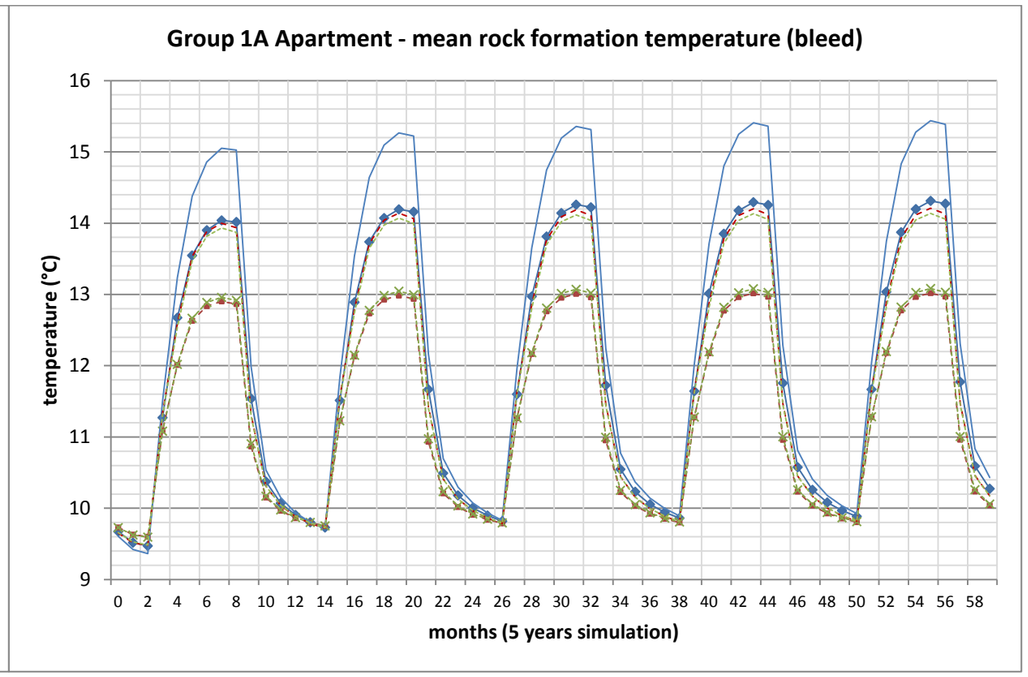
Group 1A Apartment - mean rock formation temperature (bleed)
temperature (°C)
months (5 years simulation)

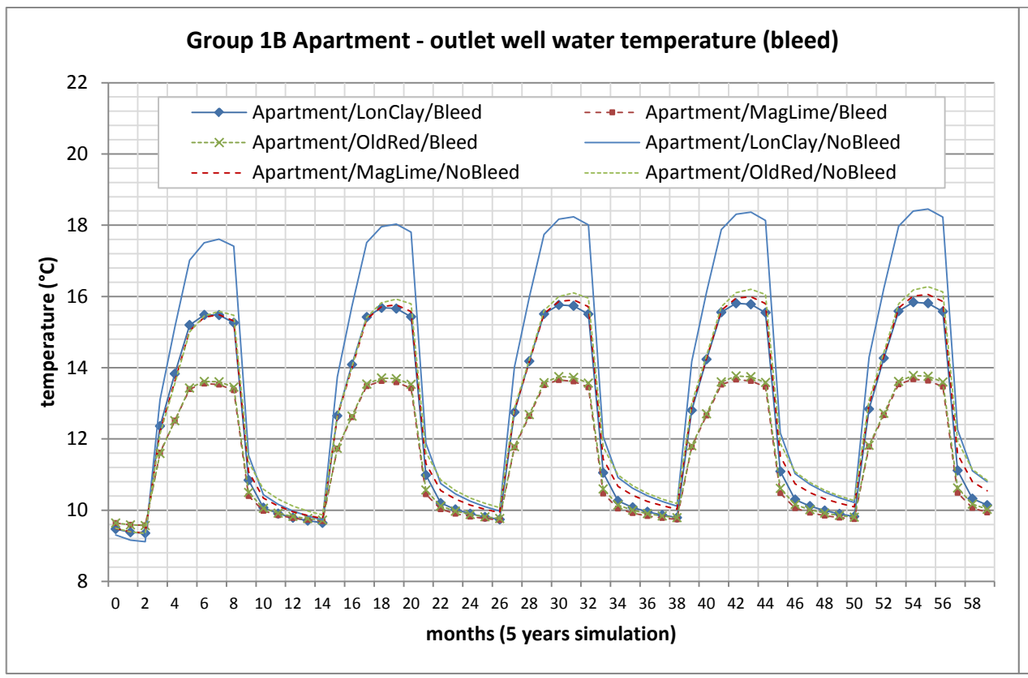
Group 1B Apartment - outlet well water temperature (bleed)
Apartment/LonClay/Bleed
Apartment/MagLime/Bleed
Apartment/OldRed/Bleed
Apartment/LonClay/NoBleed
Apartment/MagLime/NoBleed
Apartment/OldRed/NoBleed
temperature (°C)
months (5 years simulation)

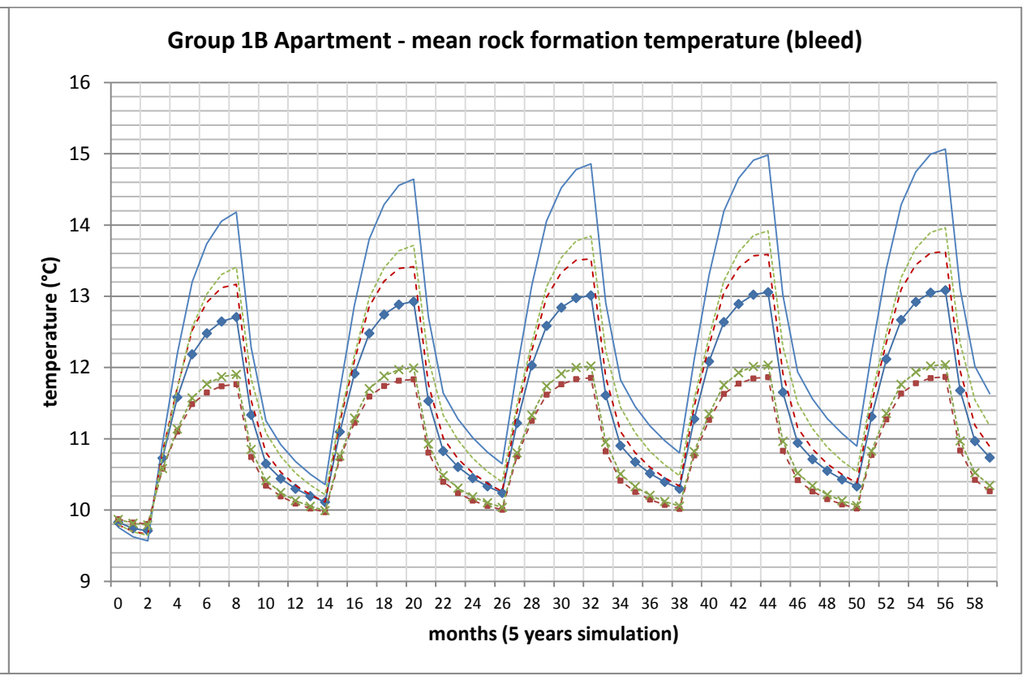
Group 1B Apartment - mean rock formation temperature (bleed)
temperature (°C)
months (5 years simulation)

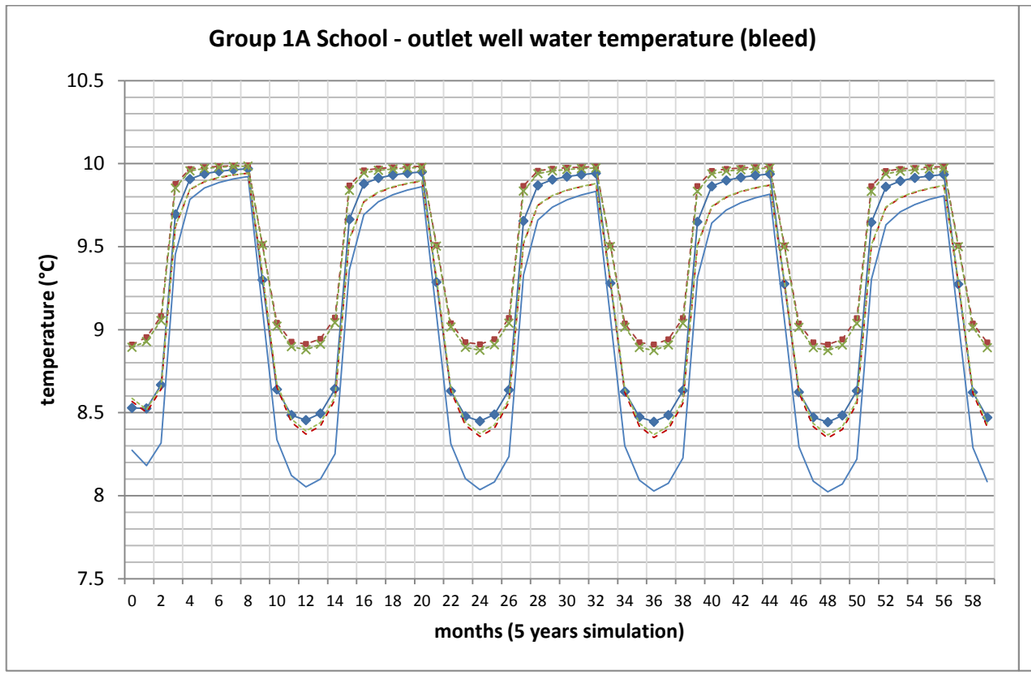
Group 1A School - outlet well water temperature (bleed)
temperature (°C)
10.5
10
9.5
9
8.5
8
7.5
0 2 4 6 8 10 12 14 16 18 20 22 24 26 28 30 32 34 36 38 40 42 44 46 48 50 52 54 56 58
months (5 years simulation)

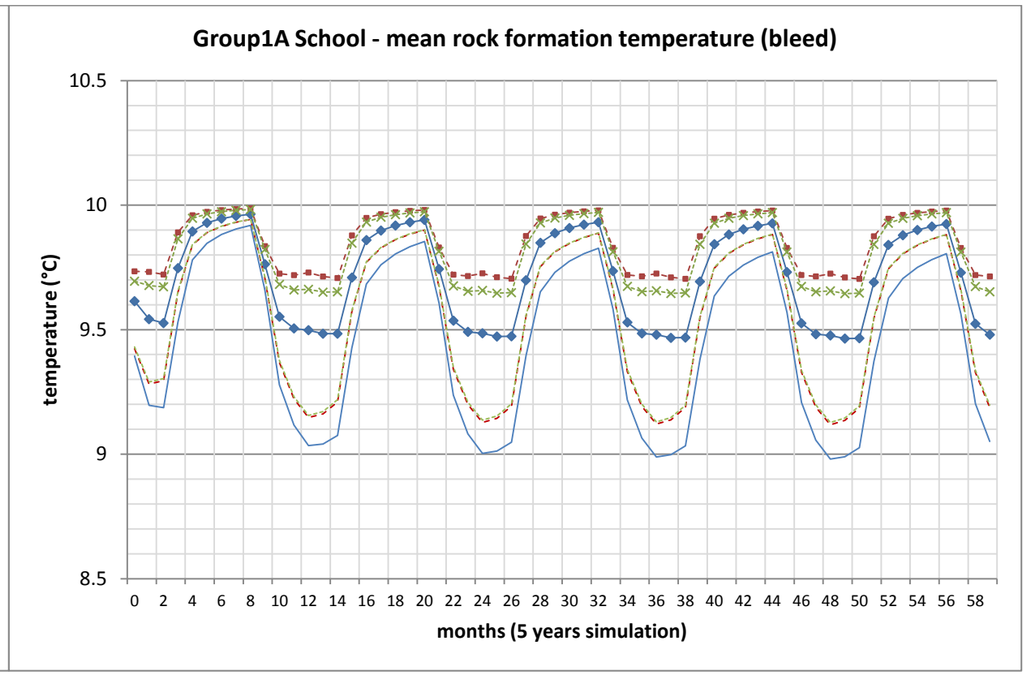
Group1A School - mean rock formation temperature (bleed)
temperature (°C)
10.5
10
9.5
9
8.5
0 2 4 6 8 10 12 14 16 18 20 22 24 26 28 30 32 34 36 38 40 42 44 46 48 50 52 54 56 58
months (5 years simulation)

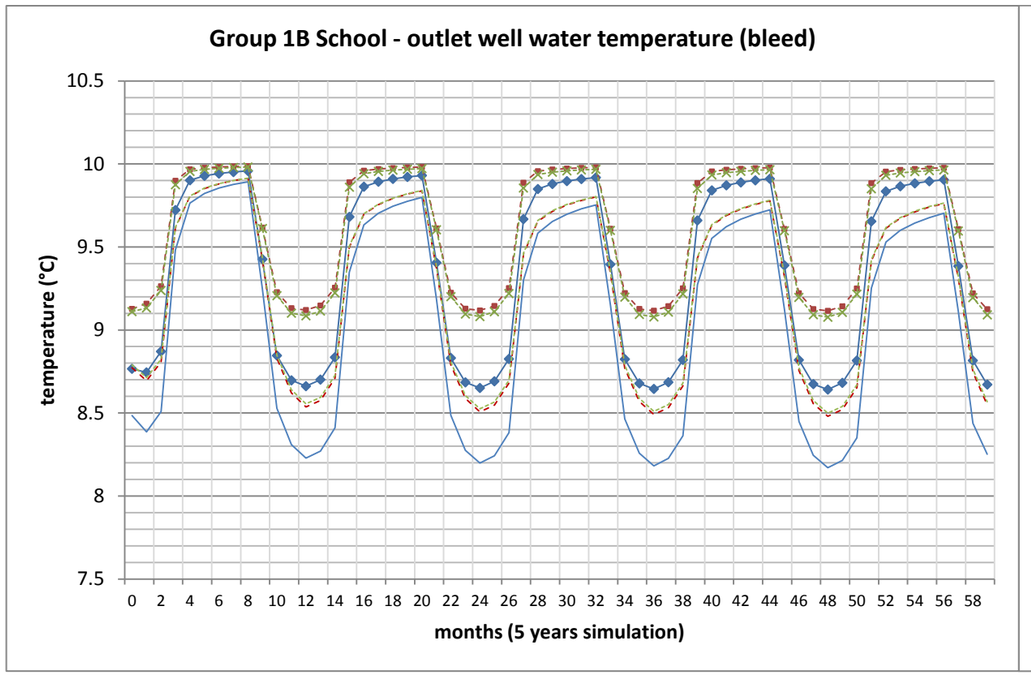
Group 1B School - outlet well water temperature (bleed)
temperature (°C)
10.5
10
9.5
9
8.5
8
7.5
0 2 4 6 8 10 12 14 16 18 20 22 24 26 28 30 32 34 36 38 40 42 44 46 48 50 52 54 56 58
months (5 years simulation)

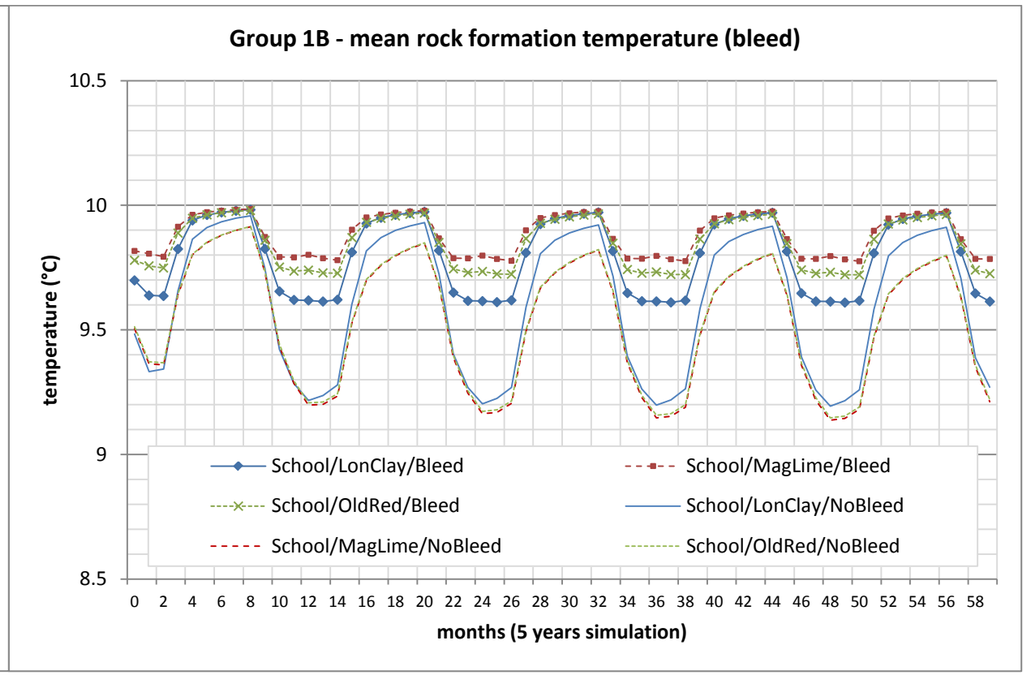
Group 1B - mean rock formation temperature (bleed)
temperature (°C)
10.5
10
9.5
9
8.5
0 2 4 6 8 10 12 14 16 18 20 22 24 26 28 30 32 34 36 38 40 42 44 46 48 50 52 54 56 58
months (5 years simulation)
School/LonClay/Bleed
School/MagLime/Bleed
School/OldRed/Bleed
School/LonClay/NoBleed
School/MagLime/NoBleed
School/OldRed/NoBleed

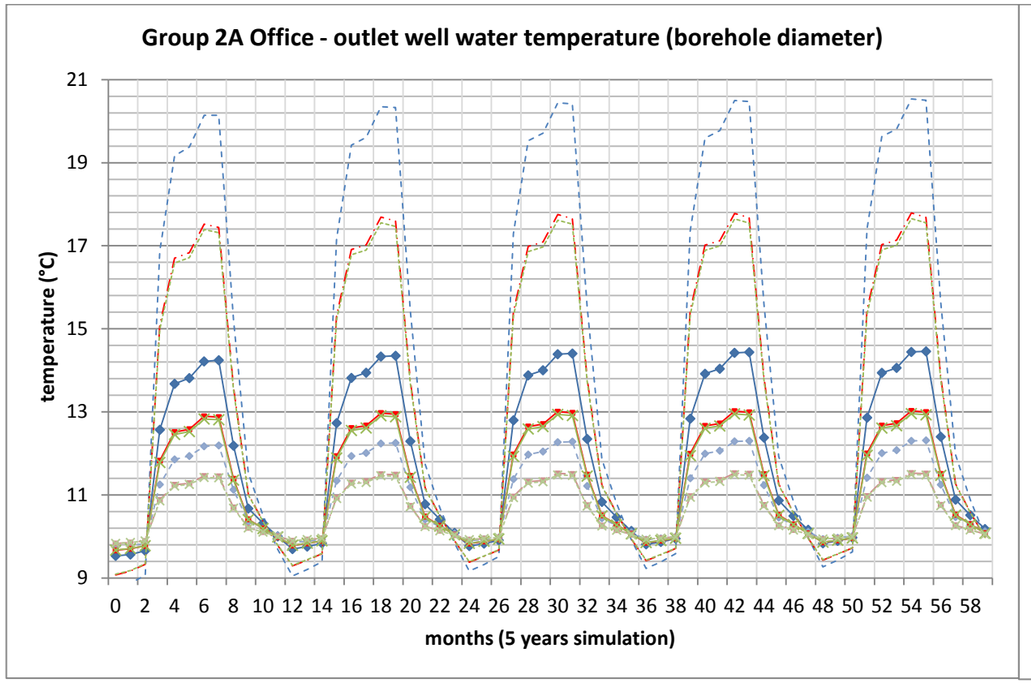
Group 2A Office - outlet well water temperature (borehole diameter)
temperature (°C)
21
19
17
15
13
11
9
0 2 4 6 8 10 12 14 16 18 20 22 24 26 28 30 32 34 36 38 40 42 44 46 48 50 52 54 56 58
months (5 years simulation)

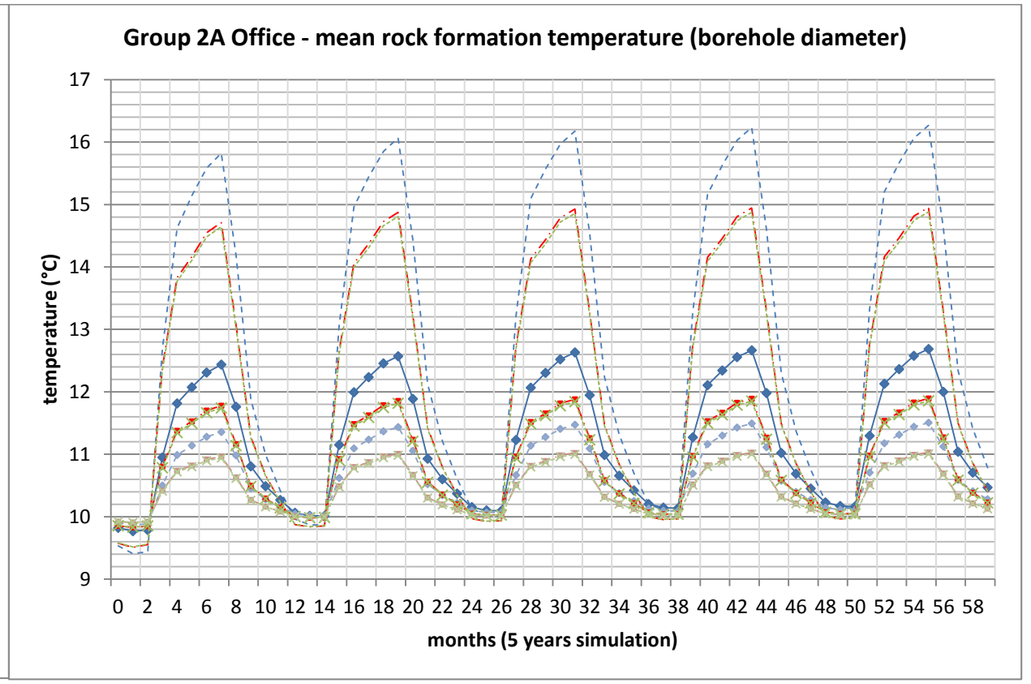
Group 2A Office - mean rock formation temperature (borehole diameter)
temperature (°C)
17
16
15
14
13
12
11
10
9
0 2 4 6 8 10 12 14 16 18 20 22 24 26 28 30 32 34 36 38 40 42 44 46 48 50 52 54 56 58
months (5 years simulation)

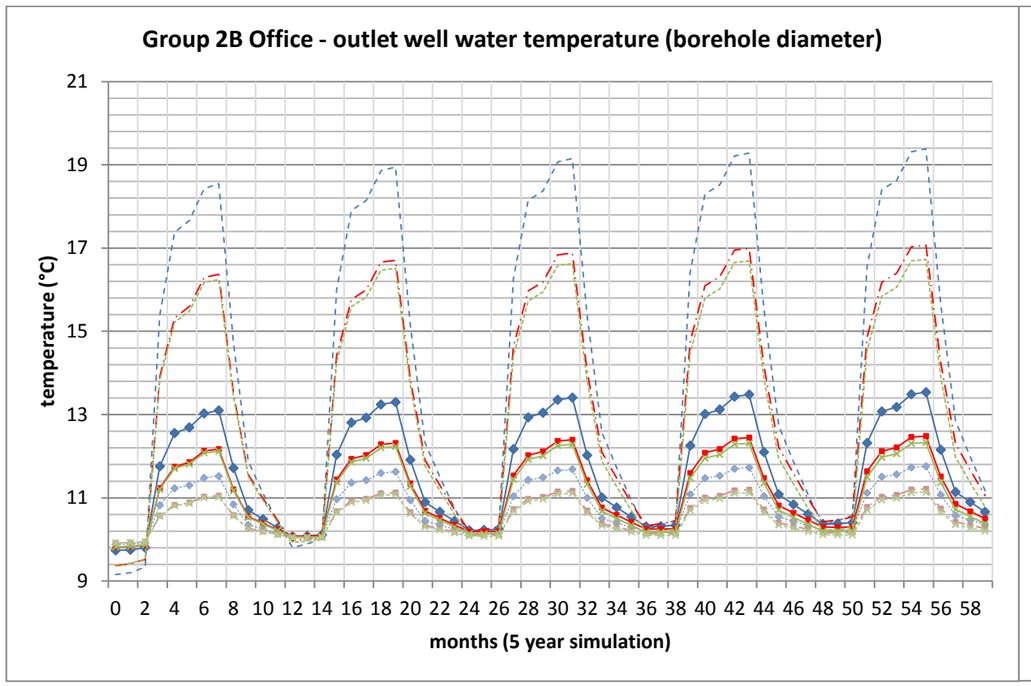
Group 2B Office - outlet well water temperature (borehole diameter)
temperature (°C)
21
19
17
15
13
11
9
0 2 4 6 8 10 12 14 16 18 20 22 24 26 28 30 32 34 36 38 40 42 44 46 48 50 52 54 56 58
months (5 year simulation)

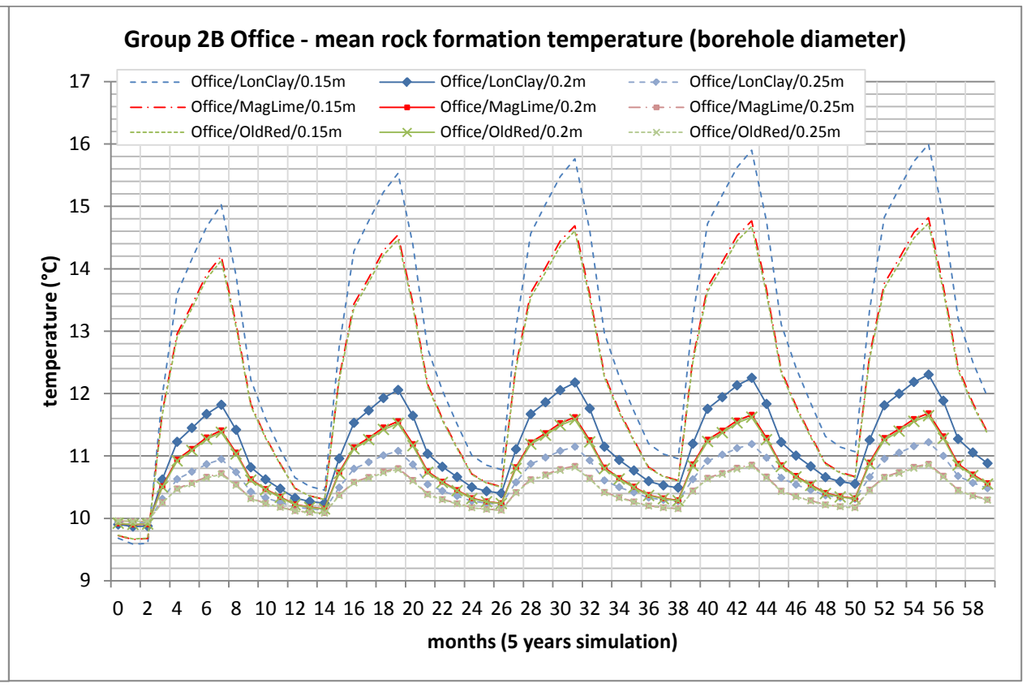
Group 2B Office - mean rock formation temperature (borehole diameter)
Office/LonClay/0.15m
Office/LonClay/0.2m
Office/LonClay/0.25m
Office/MagLime/0.15m
Office/MagLime/0.2m
Office/MagLime/0.25m
Office/OldRed/0.15m
Office/OldRed/0.2m
Office/OldRed/0.25m
temperature (°C)
17
16
15
14
13
12
11
10
9
0 2 4 6 8 10 12 14 16 18 20 22 24 26 28 30 32 34 36 38 40 42 44 46 48 50 52 54 56 58
months (5 years simulation)

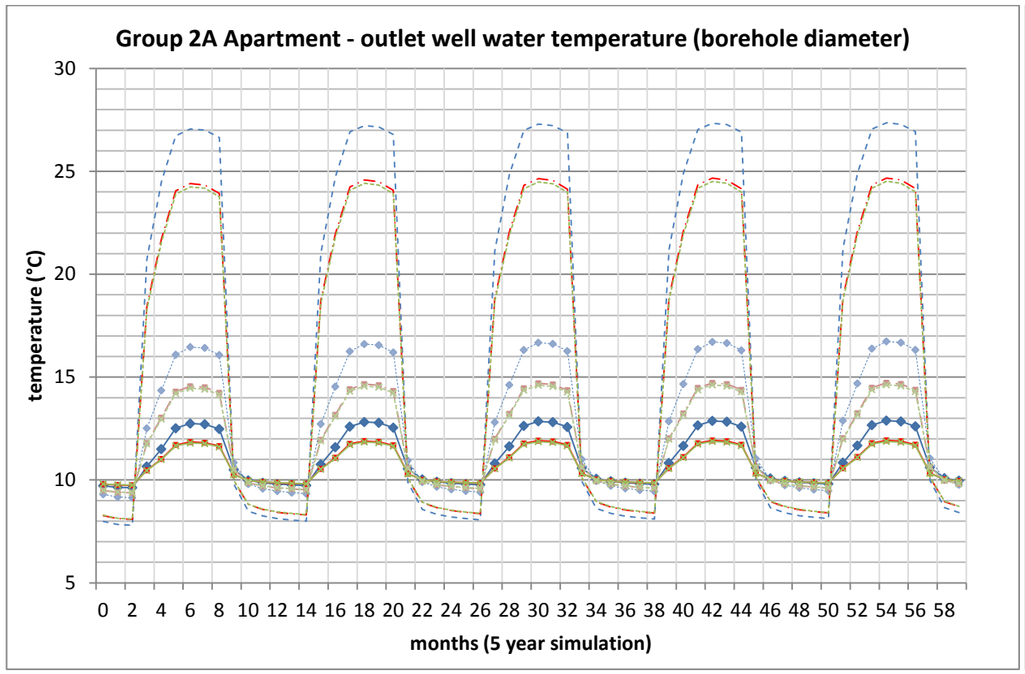
Group 2A Apartment - outlet well water temperature (borehole diameter)
temperature (°C)
30
25
20
15
10
5
0 2 4 6 8 10 12 14 16 18 20 22 24 26 28 30 32 34 36 38 40 42 44 46 48 50 52 54 56 58
months (5 year simulation)

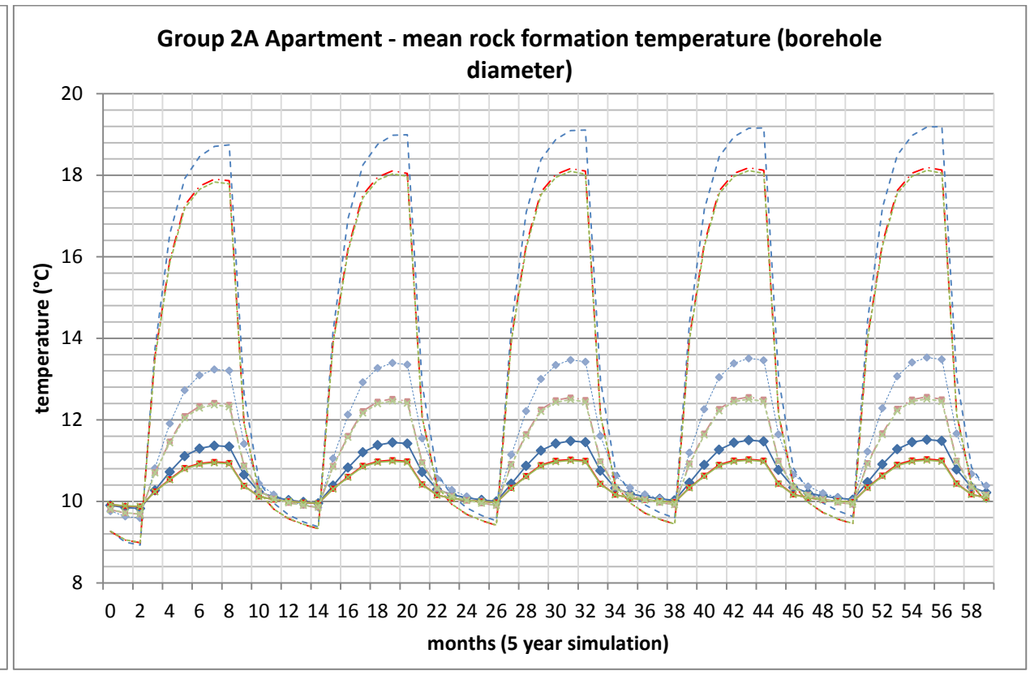
Group 2A Apartment - mean rock formation temperature (borehole diameter)
temperature (°C)
20
18
16
14
12
10
8
0 2 4 6 8 10 12 14 16 18 20 22 24 26 28 30 32 34 36 38 40 42 44 46 48 50 52 54 56 58
months (5 year simulation)

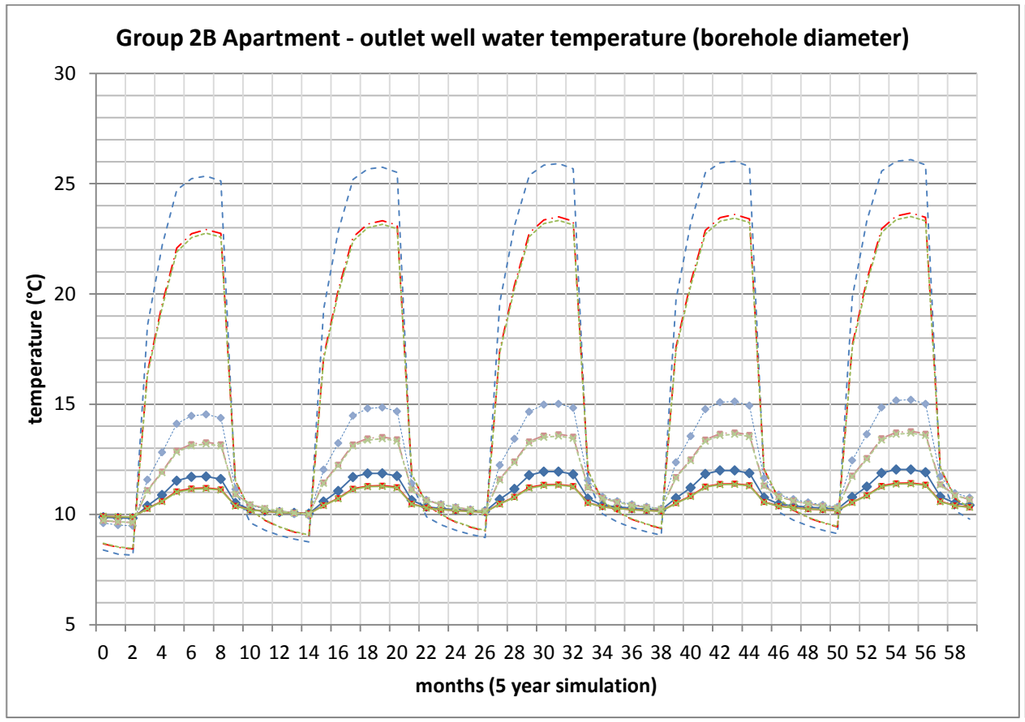
Group 2B Apartment - outlet well water temperature (borehole diameter)
temperature (°C)
30
25
20
15
10
5
0 2 4 6 8 10 12 14 16 18 20 22 24 26 28 30 32 34 36 38 40 42 44 46 48 50 52 54 56 58
months (5 year simulation)

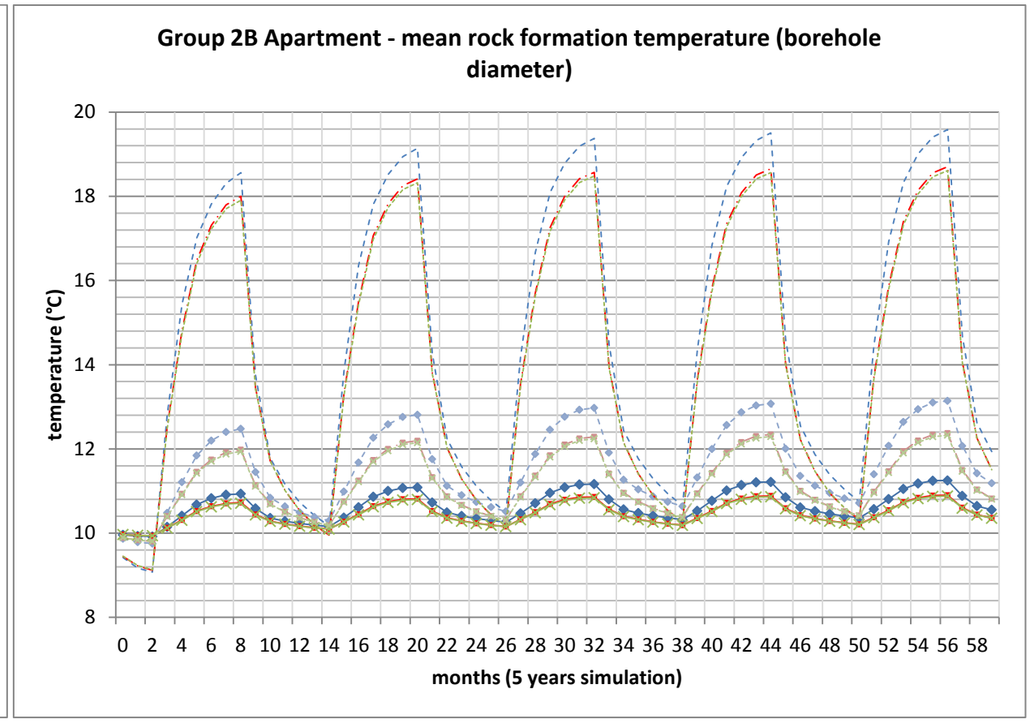
Group 2B Apartment - mean rock formation temperature (borehole diameter)
temperature (°C)
20
18
16
14
12
10
8
0 2 4 6 8 10 12 14 16 18 20 22 24 26 28 30 32 34 36 38 40 42 44 46 48 50 52 54 56 58
months (5 years simulation)

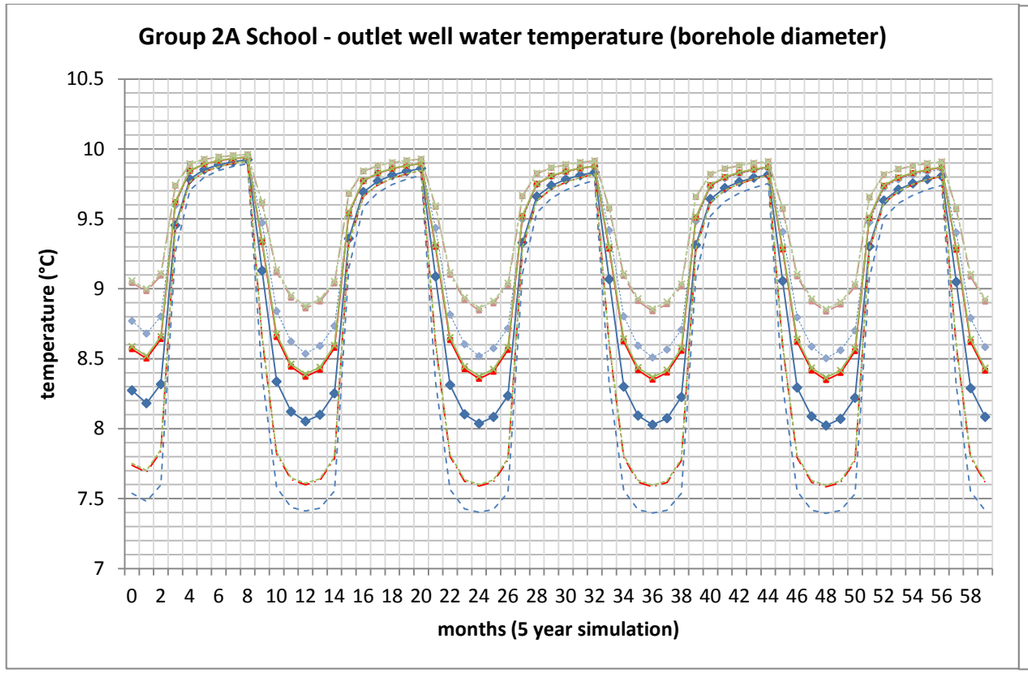
Group 2A School - outlet well water temperature (borehole diameter)
temperature (°C)
10.5
10
9.5
9
8.5
8
7.5
7
0 2 4 6 8 10 12 14 16 18 20 22 24 26 28 30 32 34 36 38 40 42 44 46 48 50 52 54 56 58
months (5 year simulation)

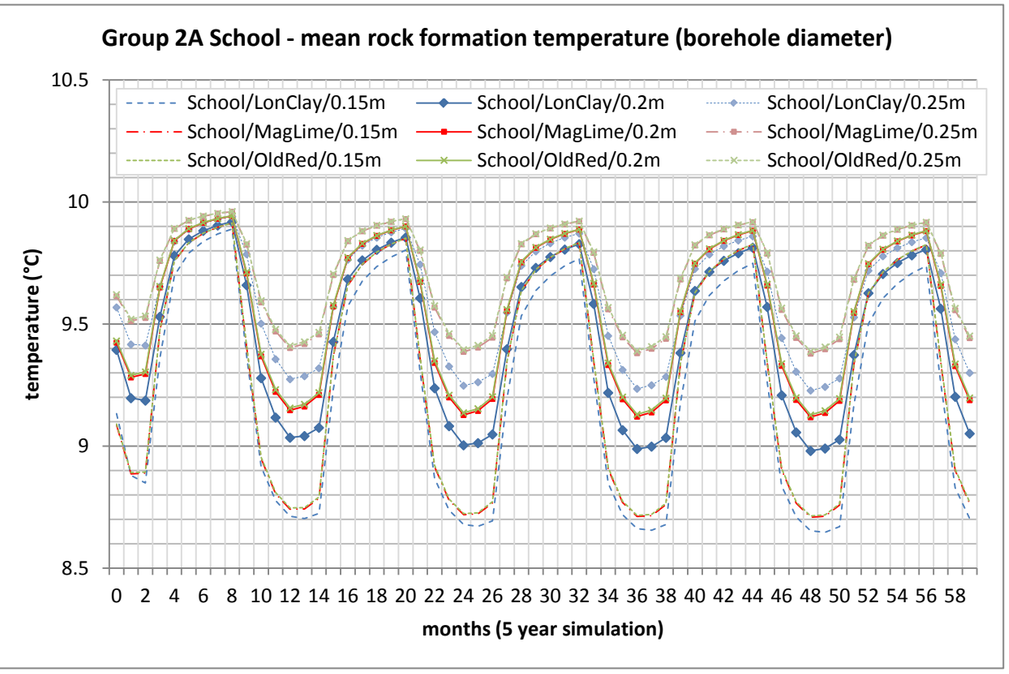
Group 2A School - mean rock formation temperature (borehole diameter)
School/LonClay/0.15m
School/LonClay/0.2m
School/LonClay/0.25m
School/MagLime/0.15m
School/MagLime/0.2m
School/MagLime/0.25m
School/OldRed/0.15m
School/OldRed/0.2m
School/OldRed/0.25m
temperature (°C)
10.5
10
9.5
9
8.5
0 2 4 6 8 10 12 14 16 18 20 22 24 26 28 30 32 34 36 38 40 42 44 46 48 50 52 54 56 58
months (5 year simulation)

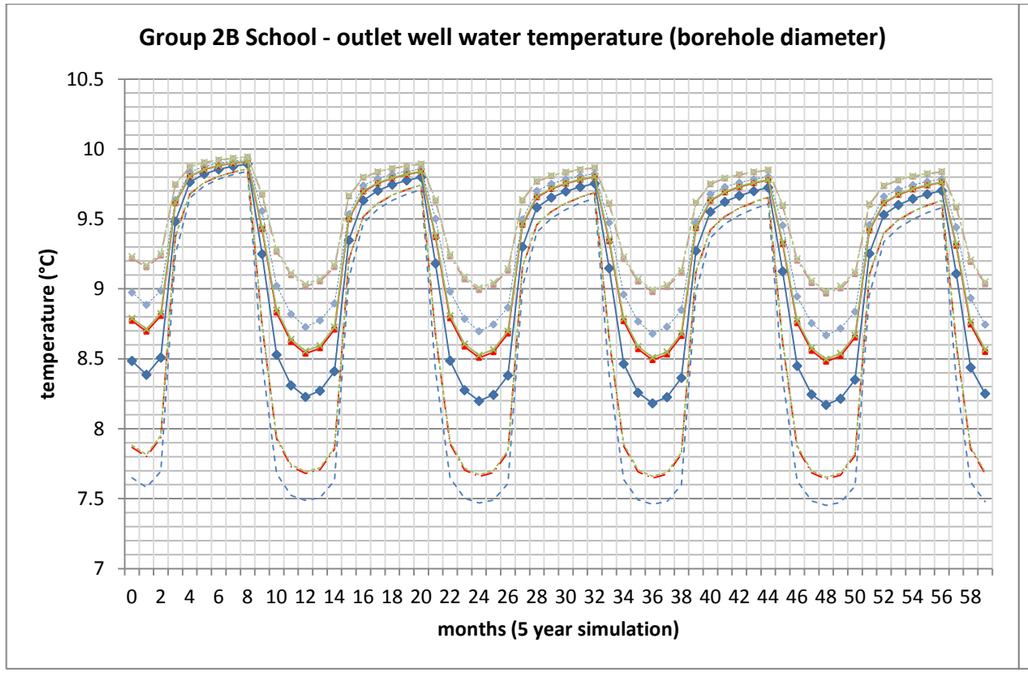
Group 2B School - outlet well water temperature (borehole diameter)
temperature (°C)
10.5
10
9.5
9
8.5
8
7.5
7
0 2 4 6 8 10 12 14 16 18 20 22 24 26 28 30 32 34 36 38 40 42 44 46 48 50 52 54 56 58
months (5 year simulation)

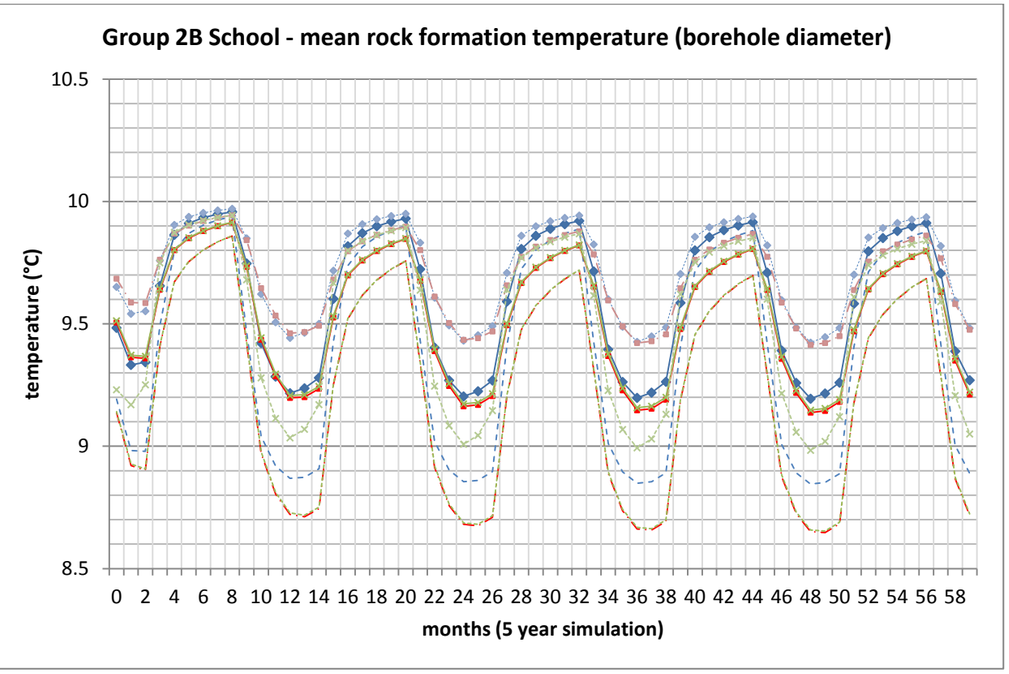
Group 2B School - mean rock formation temperature (borehole diameter)
temperature (°C)
10.5
10
9.5
9
8.5
0 2 4 6 8 10 12 14 16 18 20 22 24 26 28 30 32 34 36 38 40 42 44 46 48 50 52 54 56 58
months (5 year simulation)

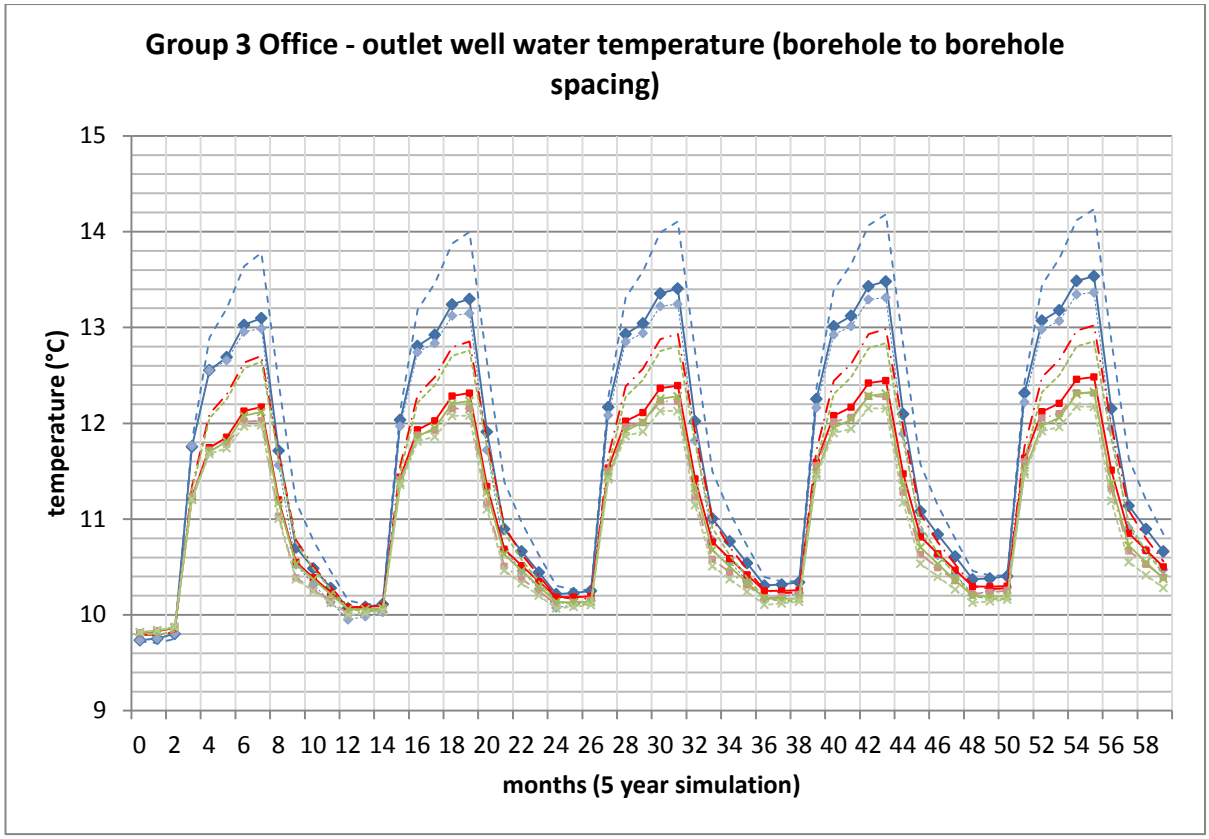
Group 3 Office - outlet well water temperature (borehole to borehole spacing)
temperature (°C)
15
14
13
12
11
10
9
0 2 4 6 8 10 12 14 16 18 20 22 24 26 28 30 32 34 36 38 40 42 44 46 48 50 52 54 56 58
months (5 year simulation)

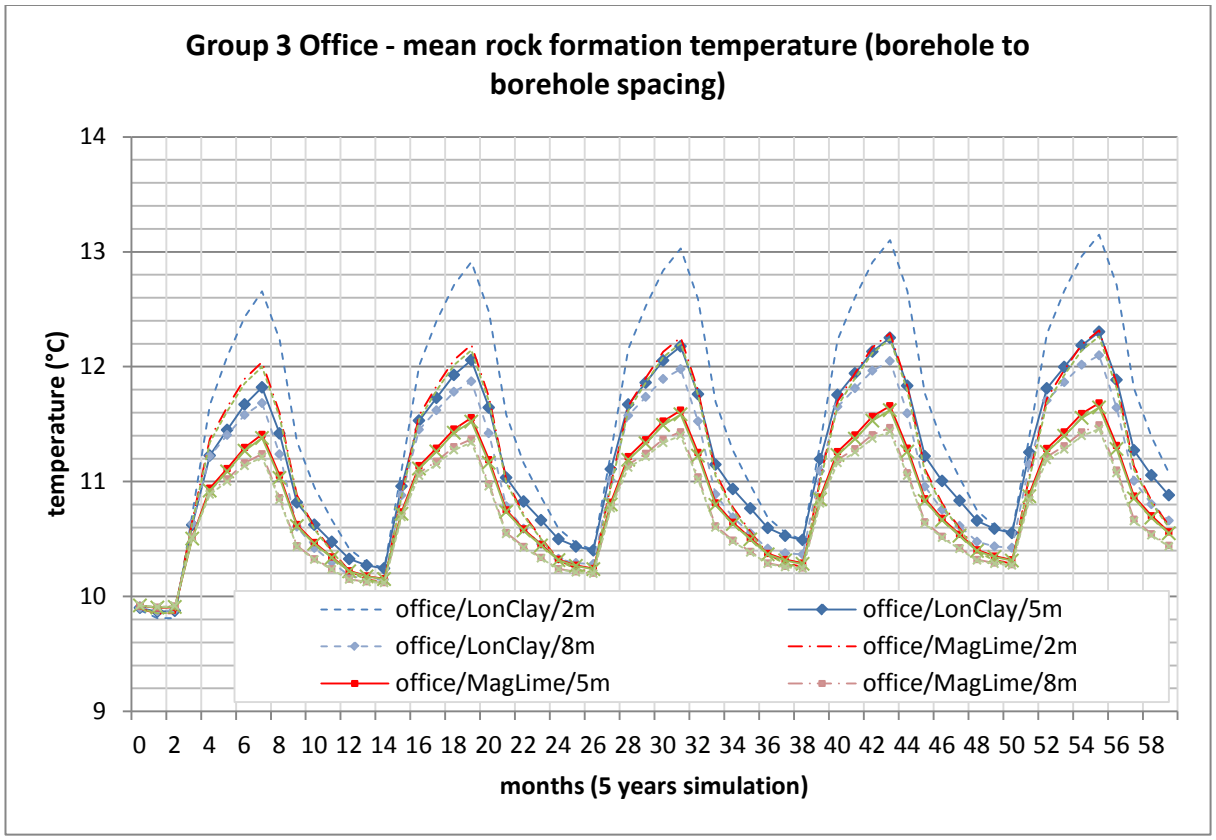
Group 3 Office - mean rock formation temperature (borehole to borehole spacing)
temperature (°C)
14
13
12
11
10
9
0 2 4 6 8 10 12 14 16 18 20 22 24 26 28 30 32 34 36 38 40 42 44 46 48 50 52 54 56 58
months (5 years simulation)
office/LonClay/2m
office/LonClay/5m
office/LonClay/8m
office/MagLime/2m
office/MagLime/5m
office/MagLime/8m

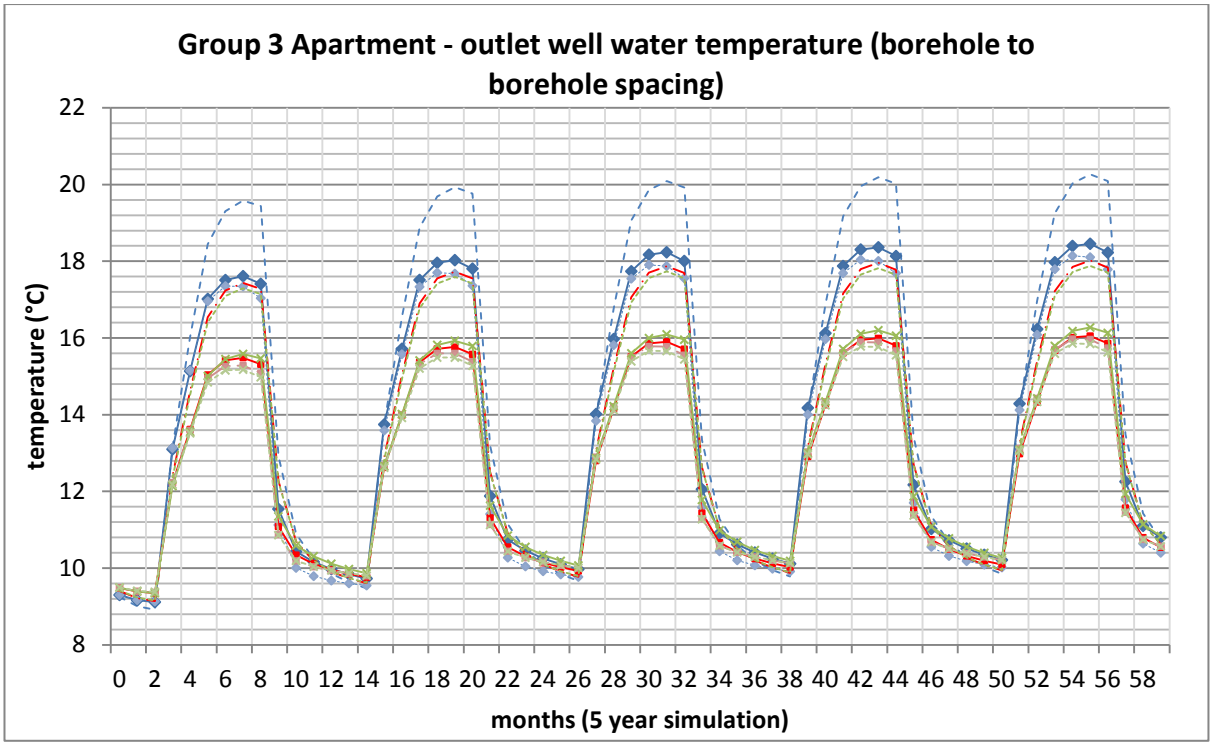
Group 3 Apartment - outlet well water temperature (borehole to borehole spacing)
temperature (°C)
22
20
18
16
14
12
10
8
0 2 4 6 8 10 12 14 16 18 20 22 24 26 28 30 32 34 36 38 40 42 44 46 48 50 52 54 56 58
months (5 year simulation)

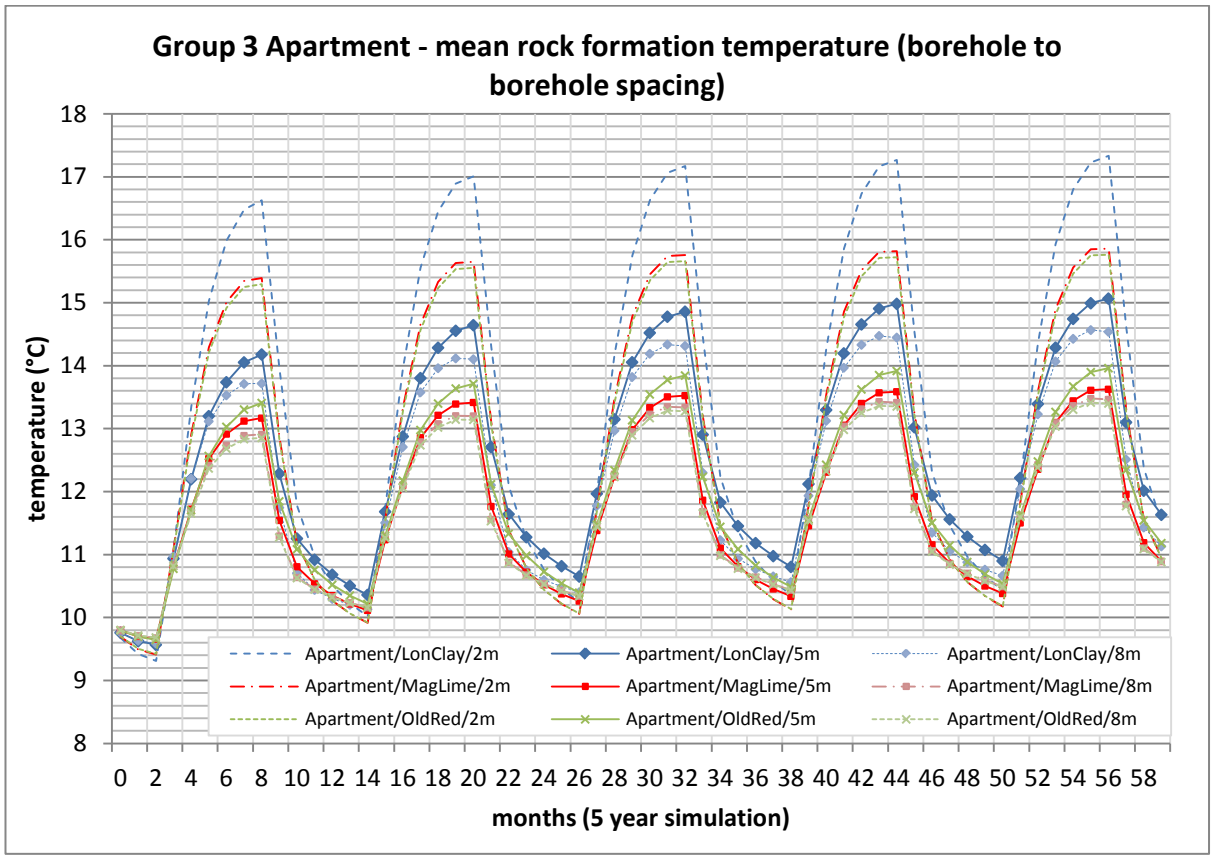
Group 3 Apartment - mean rock formation temperature (borehole to borehole spacing)
temperature (°C)
18
17
16
15
14
13
12
11
10
9
8
0 2 4 6 8 10 12 14 16 18 20 22 24 26 28 30 32 34 36 38 40 42 44 46 48 50 52 54 56 58
months (5 year simulation)
Apartment/LonClay/2m
Apartment/LonClay/5m
Apartment/LonClay/8m
Apartment/MagLime/2m
Apartment/MagLime/5m
Apartment/MagLime/8m
Apartment/OldRed/2m
Apartment/OldRed/5m
Apartment/OldRed/8m

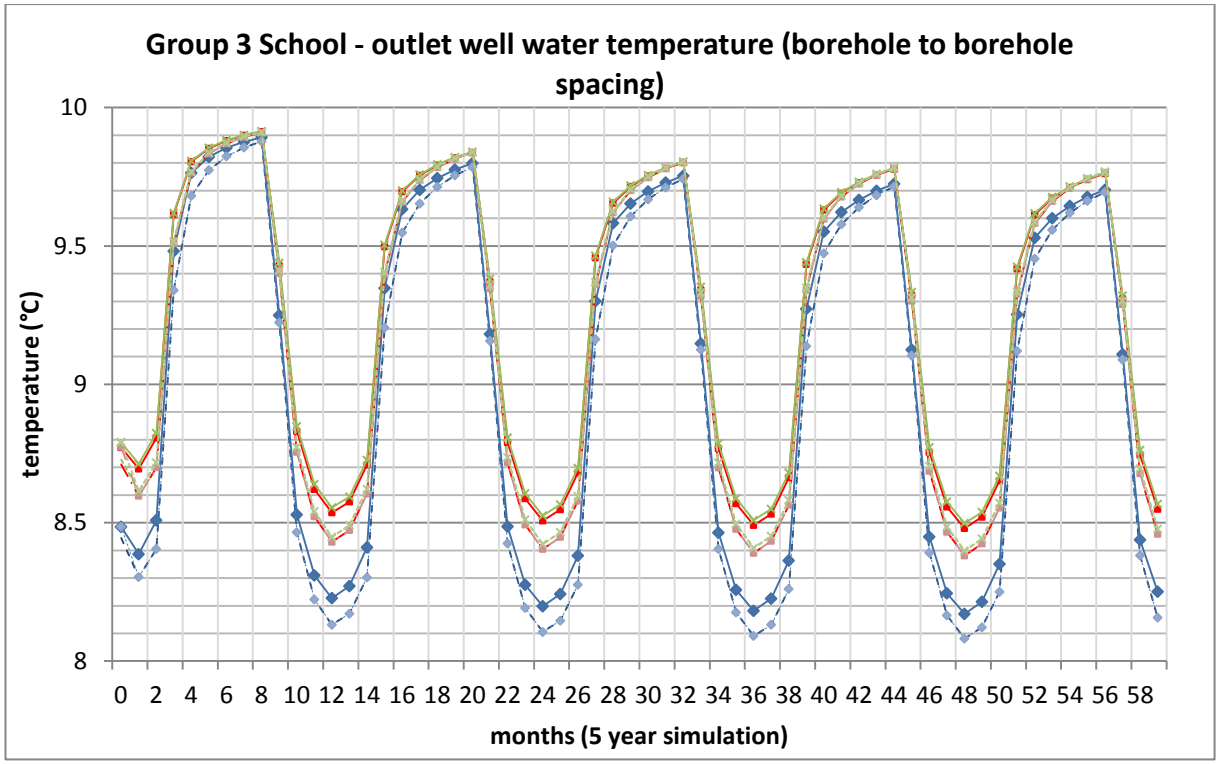
Group 3 School - outlet well water temperature (borehole to borehole spacing)
temperature (°C)
10
9.5
9
8.5
8
0 2 4 6 8 10 12 14 16 18 20 22 24 26 28 30 32 34 36 38 40 42 44 46 48 50 52 54 56 58
months (5 year simulation)

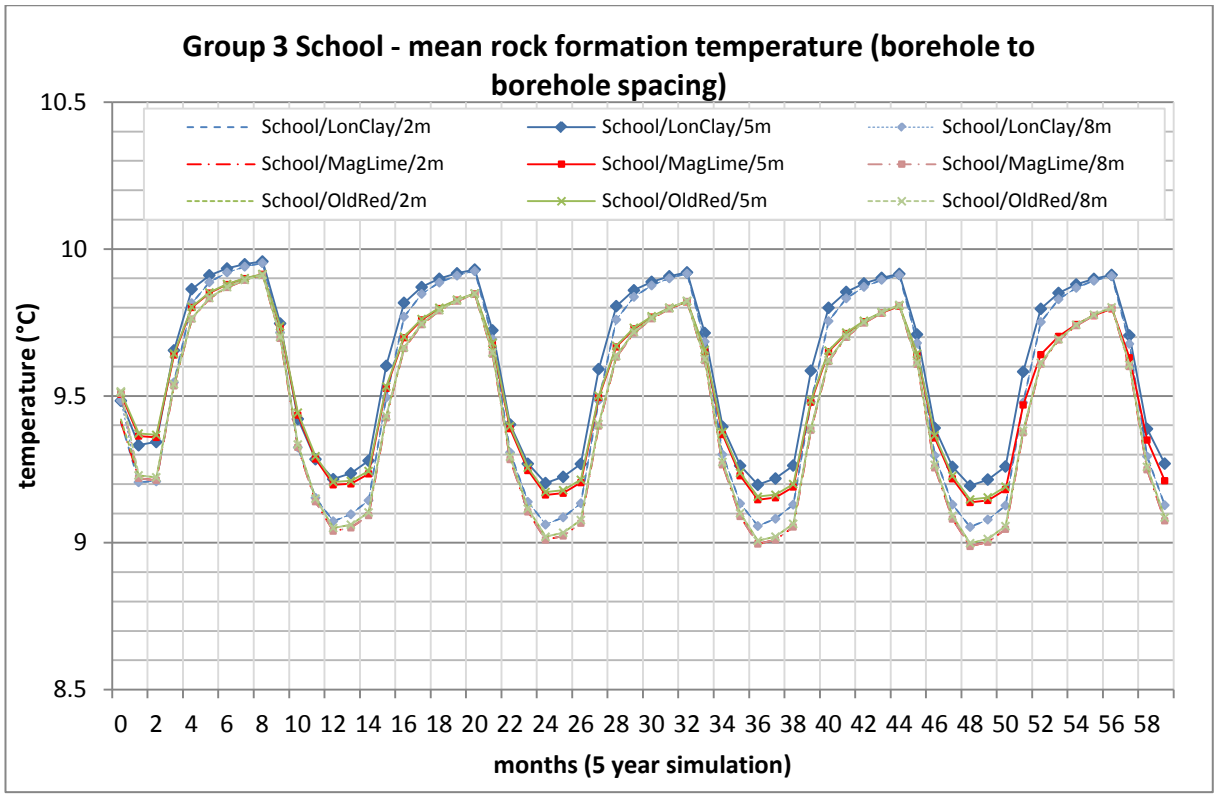
Group 3 School - mean rock formation temperature (borehole to borehole spacing)
School/LonClay/2m
School/LonClay/5m
School/LonClay/8m
School/MagLime/2m
School/MagLime/5m
School/MagLime/8m
School/OldRed/2m
School/OldRed/5m
School/OldRed/8m
temperature (°C)
10.5
10
9.5
9
8.5
0 2 4 6 8 10 12 14 16 18 20 22 24 26 28 30 32 34 36 38 40 42 44 46 48 50 52 54 56 58
months (5 year simulation)

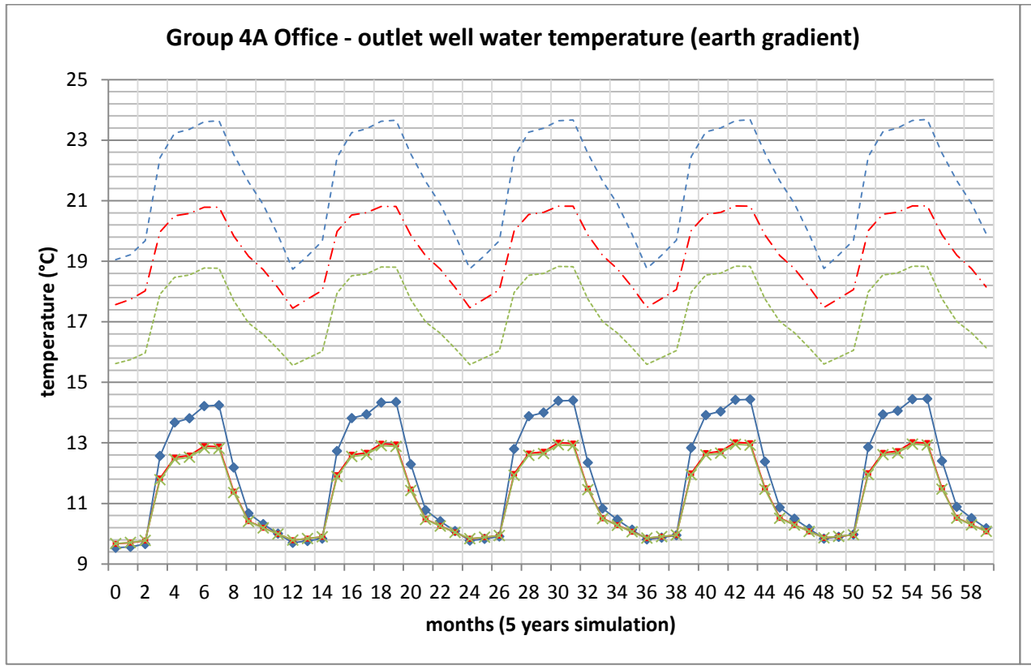
Group 4A Office - outlet well water temperature (earth gradient)
temperature (°C)
months (5 years simulation)

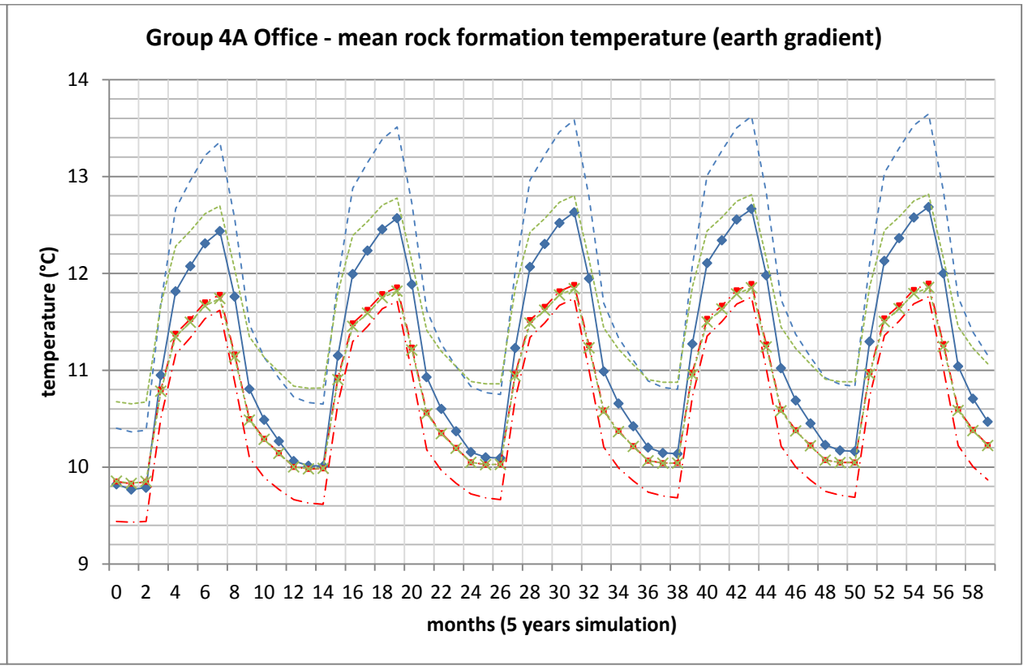
Group 4A Office - mean rock formation temperature (earth gradient)
temperature (°C)
months (5 years simulation)

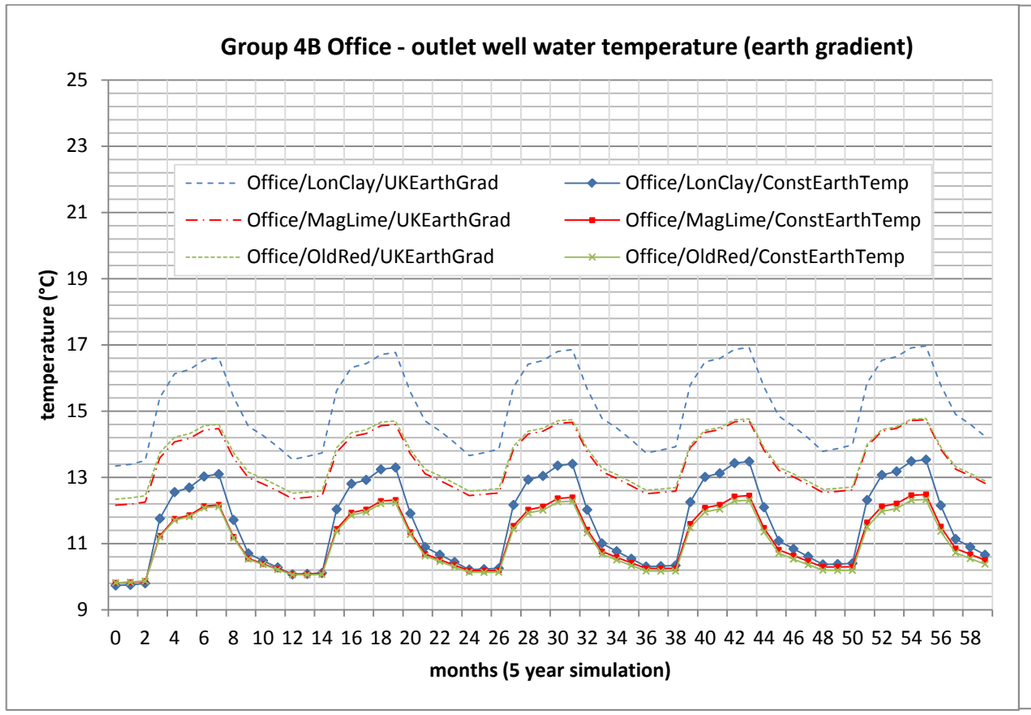
Group 4B Office - outlet well water temperature (earth gradient)
Office/LonClay/UKEarthGrad
Office/LonClay/ConstEarthTemp
Office/MagLime/UKEarthGrad
Office/MagLime/ConstEarthTemp
Office/OldRed/UKEarthGrad
Office/OldRed/ConstEarthTemp
temperature (°C)
months (5 year simulation)

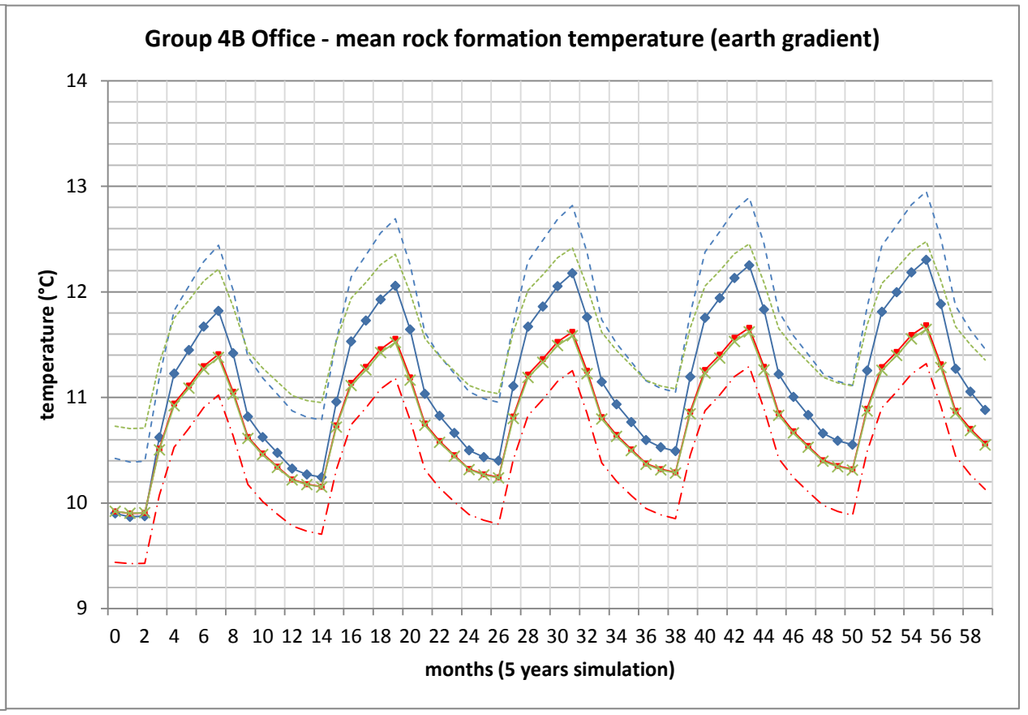
Group 4B Office - mean rock formation temperature (earth gradient)
temperature (°C)
months (5 years simulation)

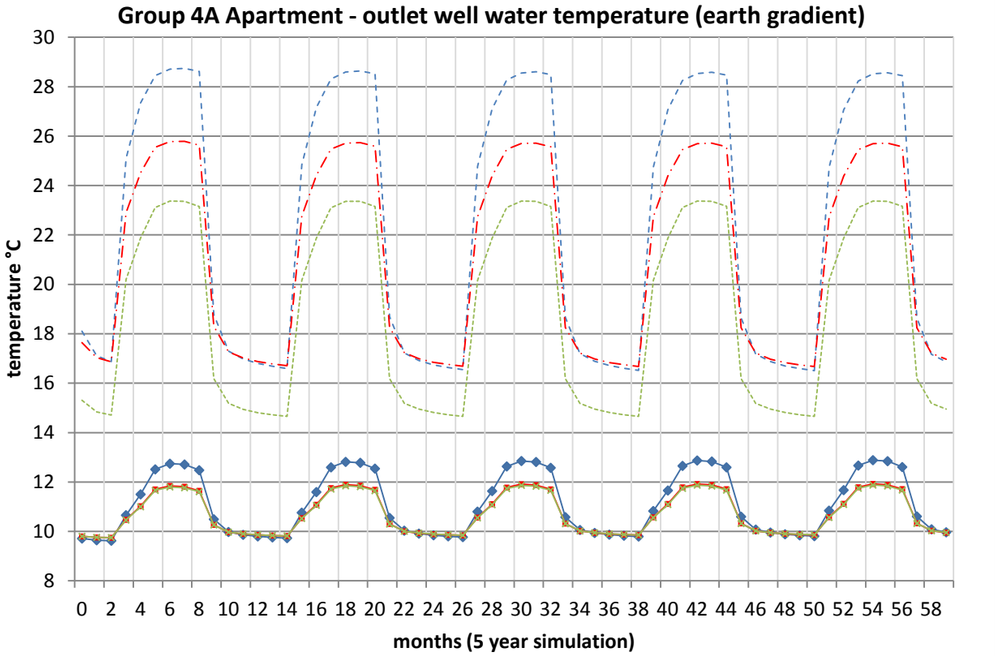
Group 4A Apartment - outlet well water temperature (earth gradient)
temperature °C
months (5 year simulation)

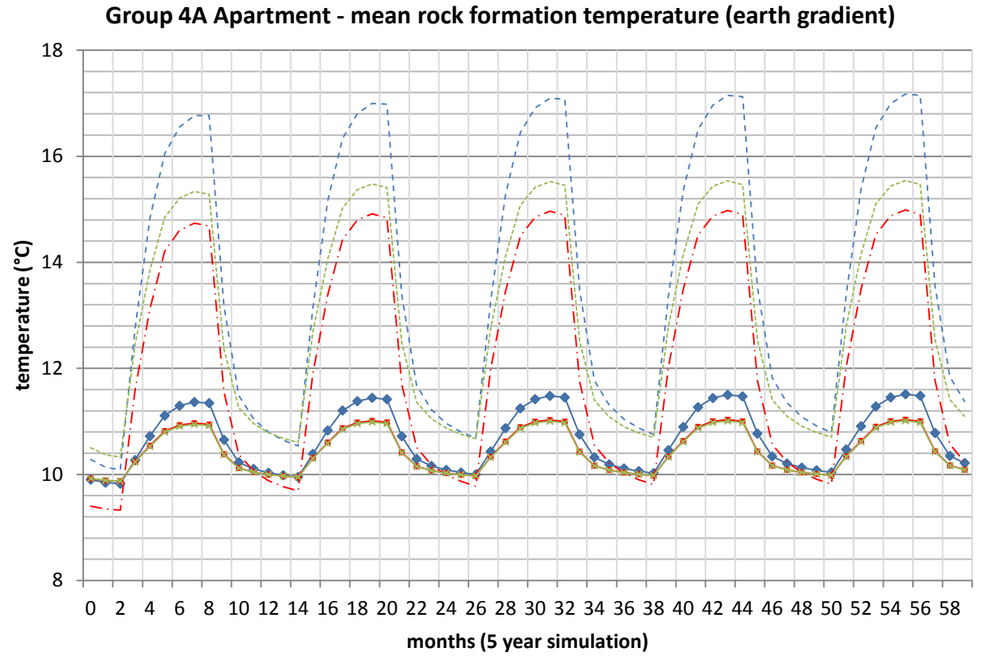
Group 4A Apartment - mean rock formation temperature (earth gradient)
temperature (°C)
months (5 year simulation)

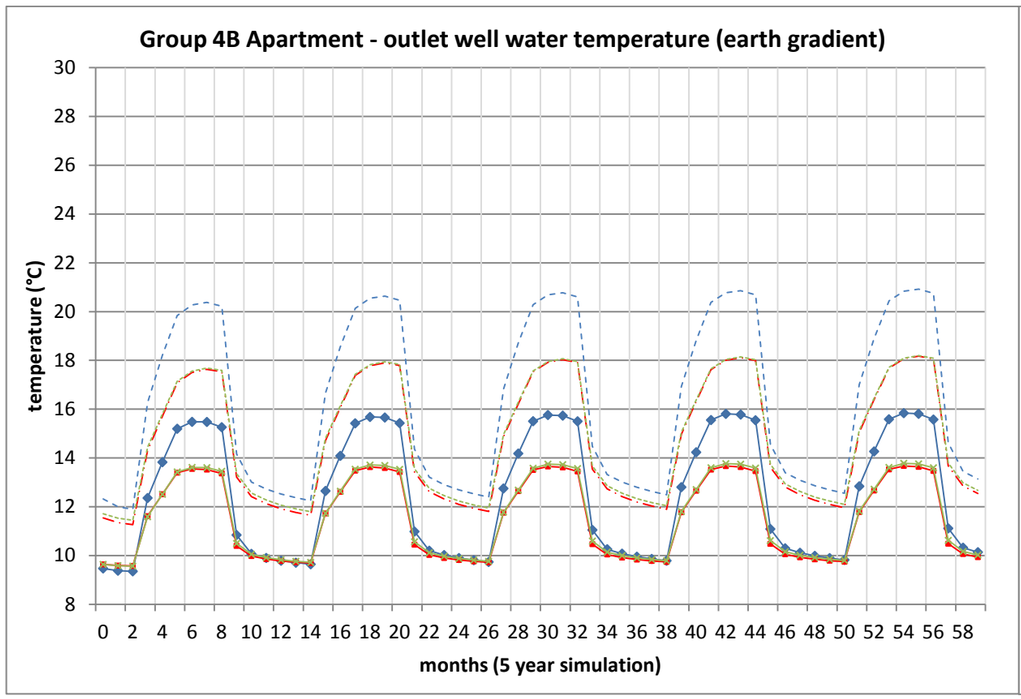
Group 4B Apartment - outlet well water temperature (earth gradient)
temperature (°C)
months (5 year simulation)

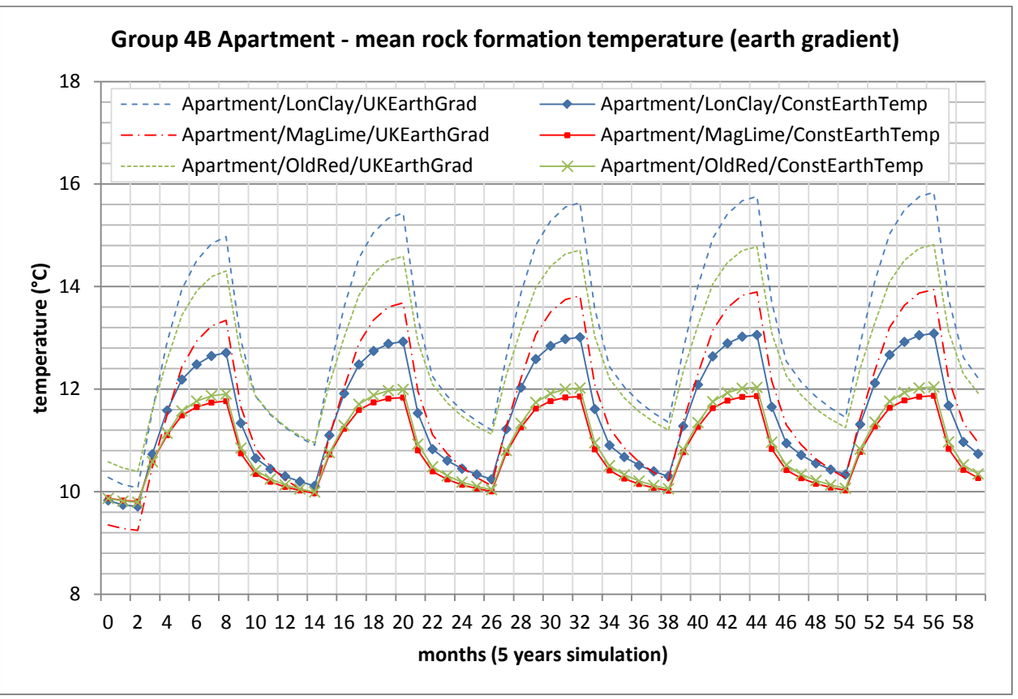
Group 4B Apartment - mean rock formation temperature (earth gradient)
Apartment/LonClay/UKEarthGrad
Apartment/LonClay/ConstEarthTemp
Apartment/MagLime/UKEarthGrad
Apartment/MagLime/ConstEarthTemp
Apartment/OldRed/UKEarthGrad
Apartment/OldRed/ConstEarthTemp
temperature (°C)
months (5 years simulation)

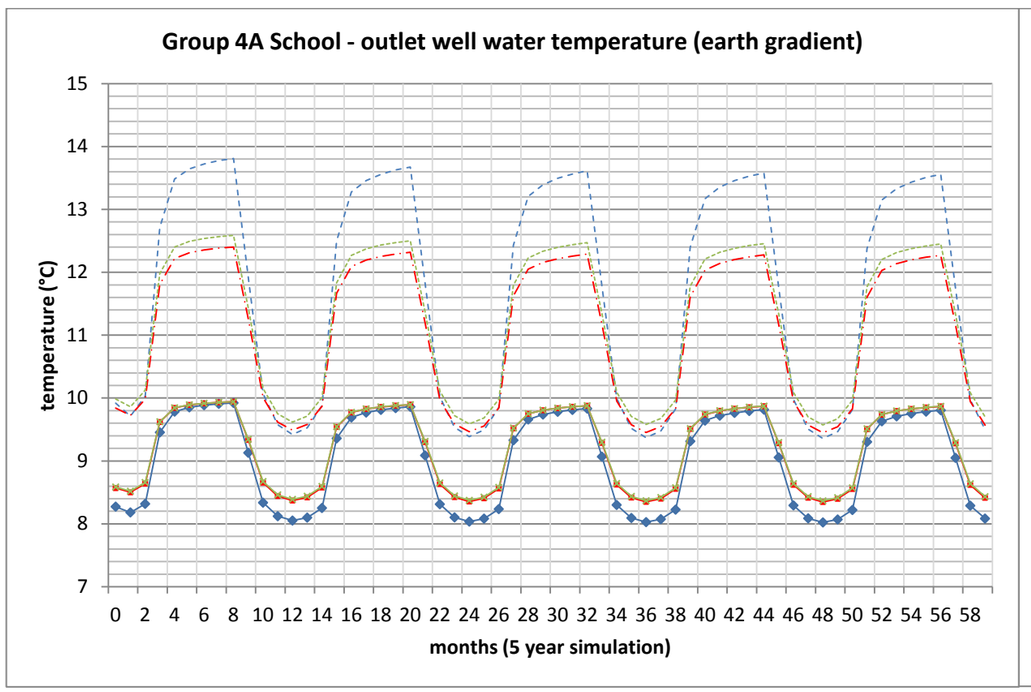
Group 4A School - outlet well water temperature (earth gradient)
temperature (°C)
15
14
13
12
11
10
9
8
7
0 2 4 6 8 10 12 14 16 18 20 22 24 26 28 30 32 34 36 38 40 42 44 46 48 50 52 54 56 58
months (5 year simulation)

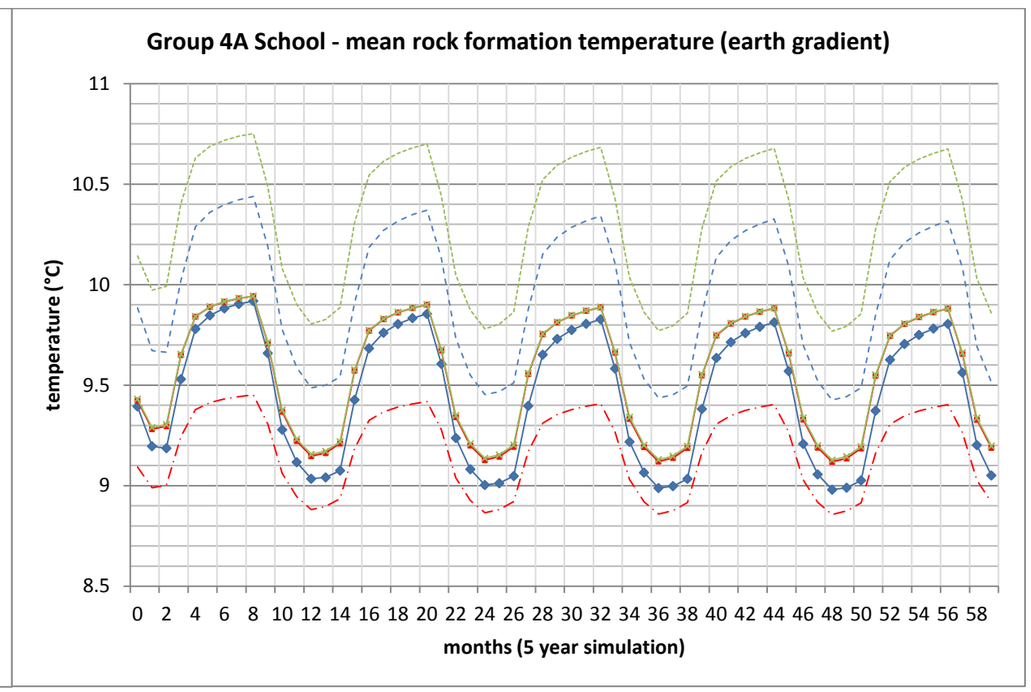
Group 4A School - mean rock formation temperature (earth gradient)
temperature (°C)
11
10.5
10
9.5
9
8.5
0 2 4 6 8 10 12 14 16 18 20 22 24 26 28 30 32 34 36 38 40 42 44 46 48 50 52 54 56 58
months (5 year simulation)

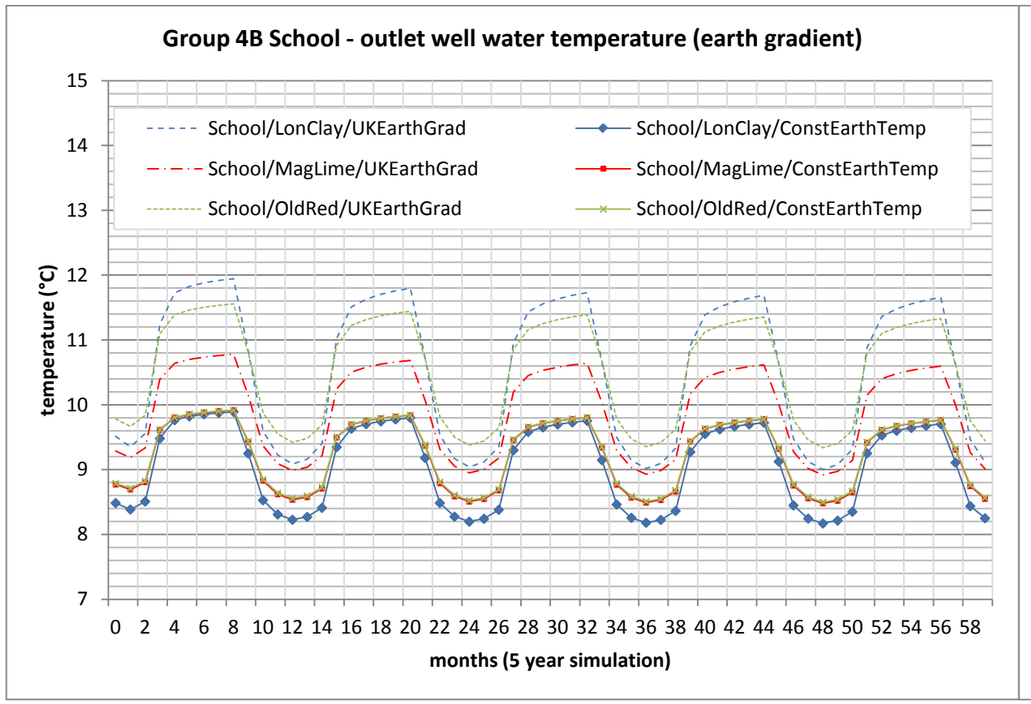
Group 4B School - outlet well water temperature (earth gradient)
School/LonClay/UKEarthGrad
School/LonClay/ConstEarthTemp
School/MagLime/UKEarthGrad
School/MagLime/ConstEarthTemp
School/OldRed/UKEarthGrad
School/OldRed/ConstEarthTemp
temperature (°C)
15
14
13
12
11
10
9
8
7
0 2 4 6 8 10 12 14 16 18 20 22 24 26 28 30 32 34 36 38 40 42 44 46 48 50 52 54 56 58
months (5 year simulation)

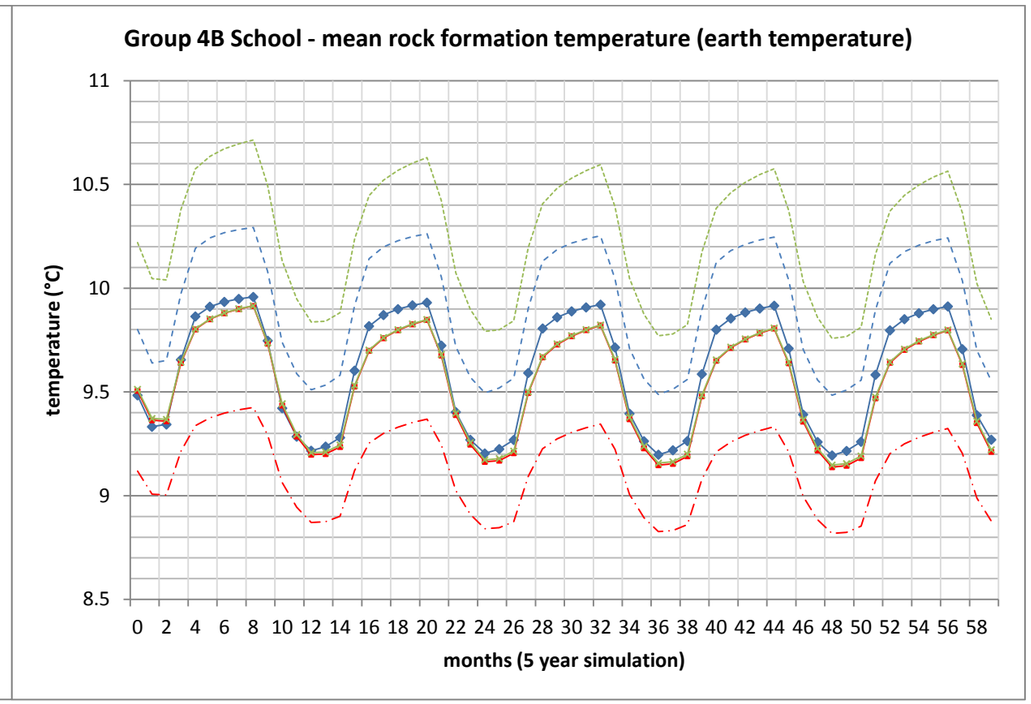
Group 4B School - mean rock formation temperature (earth temperature)
temperature (°C)
11
10.5
10
9.5
9
8.5
0 2 4 6 8 10 12 14 16 18 20 22 24 26 28 30 32 34 36 38 40 42 44 46 48 50 52 54 56 58
months (5 year simulation)

Appendix D - Related publications

Conference paper

- Ng, B., Underwood, C. & Walker, S. (2009). 'Numerical modelling of multiple standing column wells for heating and cooling buildings', *Building Simulation 2009 Eleventh International IBPSA Conference*, Glasgow, Scotland, pp. 49-55.

Journal paper

- Ng, B., Underwood, C. & Walker, S. (2011) 'Standing Column Wells - Modelling the potential for applications in geothermal heating and cooling', HVAC&R Research, 17 (6), pp. 1089-1100.

Conference paper

Building Simulation 2009

Eleventh International IBPSA Conference
Glasgow, Scotland
July 27-30, 2009

NUMERICAL MODELLING OF MULTIPLE STANDING COLUMN WELLS FOR HEATING AND COOLING BUILDINGS

Bobo Mingsum Ng, Chris Underwood and Sara Walker
Northumbria University, Newcastle Upon Tyne, Newcastle, United Kingdom

ABSTRACT

A model for simulating clusters of standing column wells (SCWs) for use in geothermal heating and cooling systems is described in this paper. The model is three-dimensional, dynamic and solves the governing equations using a finite volume discretisation scheme with a fully implicit algorithm. The slower-acting field equations are solved using a wider time interval than that used for the faster-acting well equations and the two sets of equations are coupled through the field equation source terms. A groundwater bleed feature is incorporated. The model is applied to two evaluative test cases the first of which involves heating only and the second, heating and cooling. Results of the applications suggest that SCWs can deliver substantially higher rates of heat transfer than conventional closed loop borehole heat exchanger arrays especially when groundwater bleed is operational. An important practical consequence of this is that far less geotechnical drilling is needed when using SCWs than is the case with closed loop arrays.

INTRODUCTION

Geothermal energy is a reliable and stable source for providing space heating and cooling with relatively low electricity consumption and high energy efficiency, when compared with conventional heating and cooling systems.

Geothermal heating and cooling systems (GHCS) can be categorised in two general ways according to the design of the ground heat exchangers: Closed loop systems and open loop systems. The distinction between these systems lies in the fluid circulation arrangements. The fluid (fresh water or antifreeze solution) is re-circulated around the embedded heat exchangers in the closed loop case but abstracted as groundwater in the open loop case. The open loop method has the advantage of reduced ground works and thermal resistance.

Standing column wells (SCWs) (Figure 1) are technically derived from a single-well open loop, which re-circulates the groundwater from the well to the building through two open end columns placed concentrically. They have merit in applications where open loop groundwater yields are limited.

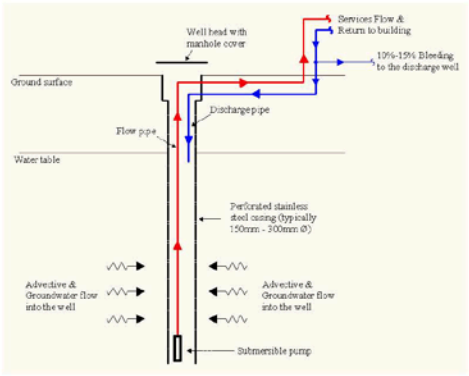

Figure 1 Typical standing column well (SCW) arrangement with bleed

Recent studies (Yavuzturk & Chiasson, 2002; Deng, Spitler & Rees, 2006) in the United States confirmed that SCWs allow a significant reduction in borehole depth requirement by comparing with the conventional closed loop system of single u-tube heat exchanger, due to the improved thermal heat transfer owing to the enhancement of the flow of groundwater into/out of the well by adopting open end columns.

In addition, the performance of SCWs can be improved by 'bleeding', i.e. part of the water from the system being bled (discharged) instead of fully recirculated to the annulus of the SCW to induce a flow of the groundwater and maintain the far field temperature in the well. A parametric study by Rees *et al.* (2004) showed that the bleed rate is one of the most significant parameters to affect SCW performance and offer reductions in borehole depth, capital cost and life cycle cost compared with the non-bleed case.

Orio, Johnson & Poor (2006) studied 10 years of performance of a SCW application in a New England school in the USA, which achieved a considerable saving in electricity use (about 1300MWh per year) after replacing the electricity heating system with a geothermal heating and cooling system (10 heat pumps coupled to 6 SCWs). The supply water temperature from the SCWs was measured after 10 years operation, and the data demonstrated that supply water temperature remained fairly constant and undisturbed with the outside air temperature directly. This is the key benefit of adopting the ground source rather than air source as a heat transfer medium to the heat pump and justifies the reliable and stable performance of geothermal systems.

Even though the merits of SCWs have been revealed, only a few studies (Oliver & Braud, 1981; Yuill & Mikler, 1995; Deng, 2004; Rees *et al.*, 2004; Deng, Rees & Spitler, 2005) concentrated on the SCW design. Most of these only considered either heating or cooling applications based on a single well applicable to North American applications, and little attention has been paid to UK applications.

Multiple boreholes arrangements are commonly used for large applications in conventional closed loop systems, but not often in SCW design. All existing SCW numerical models are merely capable of dealing with single well construction even though several multiple SCW arrangements have already appeared in North American non-residential building applications (Orio *et al.*, 2005).

The mild winters and cool summers experienced in the UK means that it should be possible to extract heat from the ground during winter and reject it back during summer to enhance the seasonal performance. In this work, a 3-dimensional numerical model is developed to explore the performance of small clusters of SCWs with/without bleed and to compare the results with what might be achieved using conventional closed loop methods based on typical UK common hydro-geological conditions.

PREVIOUS WORK

In earlier SCW designs, the well had an impermeable casing and hence the convection heat transfer surrounding the borehole wall due to natural groundwater movement was ignored in the energy transfer analysis.

Oliver & Braud (1981) analyzed the thermal performance of a completely cased borehole SCW design in the steady state. The temperature distribution in the pipes were solved analytically based on the temperature gradient across the earth, the annulus and the inner pipe (suction pipe) with pure conduction heat transfer through the pipe walls. It showed that the length of the ground heat exchangers can be reduced by increasing the thermal resistance (pipe insulation) of the inner pipe wall because of the reduction of short-circuit heat transfer between the inner pipe and the annulus.

Yuill and Mikler (1995) investigated the influence of natural ground water movement on the performance of standing column wells (referred as thermal well in this text), with an open well cased construction enhancing the flow of groundwater into/out of the well. The ratio of heat transfer to the SCW by conduction or convection (due to the groundwater movement) was obtained from a dimensionless term called the groundwater factor (*GF*). The outward and inward groundwater flow rates to the SCW was determined from the hydraulic gradient across the SCW and *GF*, according to the Darcy equation in cylindrical coordinates. The hydraulic head distributions along the SCW could only be measured experimentally, thus an 'equivalent thermal conductivity' was introduced to consider the impact of groundwater motion in an approximation of the water temperature inside the SCW. Therefore, the usability of this model is limited without drilling a test borehole to collect the hydraulic head conditions in advance.

Rees, *et al.* (2004) and Deng (2004) proposed a finite volume numerical model of SCW that is capable of dealing with the natural groundwater movement as well as the induced groundwater flow by bleed operation. A range from 5% to 15% was suggested to be most effective bleeding rate to enhance the SCW performance. Regarding to the groundwater flow analysis, the resistances of the groundwater flow along the borehole, dip tubes and the rocks were analysed by a nodal network. The borehole flux was calculated by the well borehole model according to thermal resistances and thermal mass analysis from the nodal network, and being passed onto a finite volume model (coupled by Darcy's flow equation and Bear's (1972) porous medium energy equation) to deal with the excitation to the aquifer surrounding the SCW. A one-dimensional numerical SCW model was developed by Deng, Rees and Spitler (2005) in order to reduce the computation power consumption of their previous model (Deng, 2004; Rees *et al.*, 2004). A tri-diagonal matrix algorithm (TDMA) method was adopted in the finite difference model to speed up the simulation time. The water inside the SCW was assumed to be a perfectly mixed single zone to calculate the mean water temperature in the well. The leaving water temperature from the well can be estimated from this mean value and corrected by a short-circuit correction to account for the short-circuit phenomena inside the well. The groundwater movement caused by pumping and buoyancy was taken into account in this model through the improved value of thermal conductivity, referred as 'enhanced thermal conductivity', similar as the 'equivalent thermal conductivity' in Yuill and Mikler's model (1995). The enhanced thermal conductivity can be worked out either from in-situ

experiments (numerically or physically), or the correlations based on the actual hydraulic and thermal properties of the rock from the site.

The heat transfer mechanism in SCWs involves not only pure conduction through from/to rock to/from the fluid wall, but also the advection in the surrounding rock and convection along the dip tubes and borehole walls. Therefore, the impact of the groundwater movement on the thermal and hydraulic heat transfer must be considered in the SCW model in order to achieve a reasonable approximation representing the real SCW situation especially during bleed operation.

The ratio of convective to conductive heat transfer in the borehole is expressed by Nusselt's number, which is determined from the characteristic of flow (Reynolds number) and the properties of the water (Prandtl number). The convective coefficient can be derived from the Nusselt number and reflected in the borehole and suction-pipe surface resistances to account for the heat transfer by both convection. Gnielinski's simplified correlations were used in this work for convention across the inner annulus and suction pipe surfaces (Holman, 1997) with Norris's (1971) correction for roughness at the annulus outer surface. Lu and Wang's (2008) correlation was used for convection at the suction pipe outer surface.

STANDING COLUMN WELL MODEL

Previous SCW models tended to ignore the energy transfer in the aquifer in the vertical direction (Yuill & Mikler, 1995; Deng, 2004; Rees *et al.*, 2004; Deng, Rees & Spitler, 2005) in order to simplify the structure of the PDEs or reduce the model computational cost. This work is intended to focus on multiple SCWs applications and hence, the energy equations are solved in 3 spatial dimensions with a fully implicit finite volume scheme.

The regional groundwater flow (such as local pumping or recharge from local rivers) and the seasonal water table movement are not considered in the model; only the local flows caused by well pumping are considered.

Field model

The field model coupled with two sets of partial differential equations (PDEs), the Darcy flow equation in saturated flow conditions and continuity energy equation in porous medium (Bear, 1972) to handle the thermal and hydraulic energy transport in the aquifer. These two equations are coupled with the Darcy's velocity. Homogeneity and isotropy are assumed throughout the field domain.

Head equation:

$$S\frac{\partial h}{\partial t} - F = K\nabla^2 h \qquad [1]$$

Where:
K = hydraulic conductivity (m/s);
S = specific storage;
F = source term (m^3s^{-1});
h = hydraulic head (m);
t = time (s).

Darcian flow:

$$u_x = -\frac{K}{n}\frac{\partial h}{\partial x} \qquad [2]$$

Where:
u_x = the velocity in the x direction
n = rock porosity
(and, likewise, u_y & u_z).

Energy:

$$n\rho_w c_{pw} + (1-n)\rho_s c_{ps}\frac{\partial T}{\partial t} - n\rho_w c_{pw}\nabla uT - k_{\text{eff}}\nabla^2 T = Q \qquad [3]$$

Where:
ρ = density (subscripts: w – water, s – rock, kgm^{-3});
c_p = spec. heat cap. (subscripts as above, $Jkg^{-1}K^{-1}$)
T = temperature (**°C**);
k_{eff} = effective thermal conductivity ($Wm^{-1}K^{-1}$);
Q = source term (Wm^{-3}).

The SCW model consists of two sub-models, the well model and field model to deal with the energy transport in the borehole and the surrounding field respectively. These two sub-models are coupled by the well annulus heat transfer and groundwater transfer rates both of which are 'connected' via the relevant field equations' source terms. The source terms in the head equation (F) and energy equation (Q) refers to the amount of groundwater abstracted to SCW (bleed rate) and heat added/ removed from the ground respectively. Hence, the data from the field model are employed by well model to update the borehole flux according to the new aquifer conditions and the bleed flow rates forced by the well pump are likewise imposed on the head field equation. The method makes use of the stiffness of the problem in

that the well equations act rapidly (timescale measured in minutes) whereas the field equations act slowly (timescale measured in days). Hence the well equations supply new values of F and Q to the field equations delayed by a short time interval (one hour) Figure 2 illustrates the algorithm.

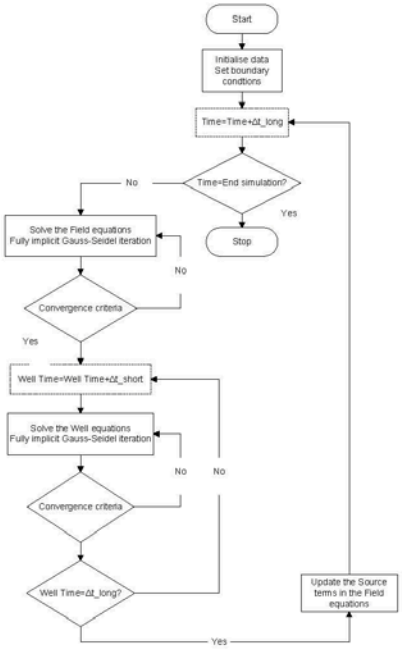

Figure 2 Flow chart of the computer algorithm of the SCW model

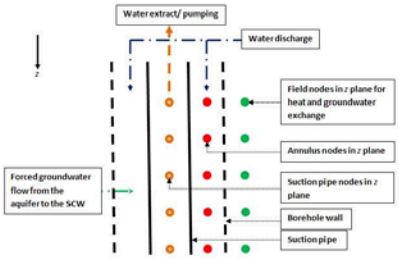

Figure 3 Cross section of the well model (the borehole and pipe wall resistances are omitted in this figure)

Well model

The well model is coupled to the field equations through the field equation source terms and is solved using a smaller time interval than that used to solve the field equations. In effect, each well is treated by the field equations as a line source/sink of finite depth. This decoupling means that the field equations can be solved independent of the standing column wells at the coarser time step appropriate to the field variables. The well equations are then solved iteratively at a shorter series of time steps within the coarser field time step and the source terms are then updated in the field equations. The advantage of this approach is that standing column wells of different types can be applied with other source types (e.g. closed loop heat exchangers) to form a fully flexible hybrid scheme is desired.

Water temperature in the annulus:

$$C_A \frac{\partial T_A}{\partial t} + c_{pw} \frac{\partial m_w T_A}{\partial z} - Q_A - Q_S = 0 \qquad \textbf{[4]}$$

Where:

C_A = annulus thermal capacity (JK^{-1});

m_w = water mass flow rate in the annulus (kgs^{-1});

T_A = annulus water temperature **(°C);**

Q_A = heat transfer (annulus to rock, W);

Q_S = heat transfer (annulus to suction pipe, W)

Water temperature in the suction pipe:

$$C \frac{\partial T_S}{\partial t} + m_w + m_b \; c_{pw} \frac{\partial T_S}{\partial z} + Q_S = 0 \qquad [5]$$

Where:

m_b = total bleed water flow rate (kg/s)

C_{SP} = heat capacity of the suction pipe water (J/K)

APPLICATION OF THE MODEL

The model was applied to two evaluative test cases:

- Heating only
- Heating and direct cooling

For evaluative purposes, a 4-well cluster was investigated consisting of 4 × 100m-deep standing column wells arranged on a 10m grid-spacing at the centre of a 50m × 50m × 120m (deep) domain.

For the numerical model settings, an initial meshing study considered uniform grid spacings of 0.25m – 3.0m and concluded that a 1m spacing would give the best balance between accuracy and computational cost. Checks were also conducted using the 1m x 1m x 1m grid size with classical line source theory (Ingersoll & Plass, 1948) for 3-day disturbance pulse inputs of first pumping rate and then heat. Model results at the first (1m) node from the disturbance were compared with line source theory results at a 1m radius with excellent agreement. Thus, a 1m grid spacing was adopted in the model. All PDEs being solved as an initial value problem and thus all temperature nodes were set at 10°C whereas all initial heads were set at zero since the model was derived to predict the head distribution due to pumping only (i.e. local groundwater flow effects were not considered). Details of the earth properties and SCW parameters can be found in tables 1 and 2.

The first test case consisted of applying a heating load and well mass flow rate using values within the range of those observed for a survey of some 35 standing column well installations carried out by Orio *et al.* (2005) in North America. This would enable results to be compared with the range of observed capacities of the surveyed wells. The surveyed wells consisted of a mix of residential and commercial installations (heating mainly in residential with some commercial applications used for cooling) with a mean specific rate of heat transfer of 275W/m and a mean overall well mass flow rate of 1.4kg/s. Two simulations were carried out; one with bleed (set at 10% of nominal well flow rate) and one without bleed. In the former case, a simple bleed control strategy was adopted in which bleed was applied at all times when there is a demand for heat. It is stressed that this exercise was merely an attempt to *verify* the results of the model with the results summarised by Orio *et al.* (2005) rather than to attempt a full and precise comparison (which would not in any case be possible due to the incompleteness of the data presented in Orio *et al.*'s survey). Figure 4 shows the simulated heating delivered by the 4 well cluster (and, superimposed, are the bounds of heat transfer rates reported by Orio *et al.* (2005) for the 35 installations in North America), and Figure 5 shows the simulated mean monthly temperatures over one year of well cluster operation with, and without, bleed operation. In Figure 4, the mean rock temperatures 1m away from the 4 wells are also plotted.

Table 1 The earth properties

Thermal conductivity of rock k (W/mK)	Hydraulic conductivity of rock K (m/s)	Specific heat capacity of rock c_{pr} (J/m^{3}K)	Porosity n
3.9	0.00001	1.86x10^6	0.275

Table 2 The standing column well setting

SCW diameter (m)	Total borehole length (m)	Pumping rate (L/s)	Bleed rate (%)
0.2	400m	1	10%

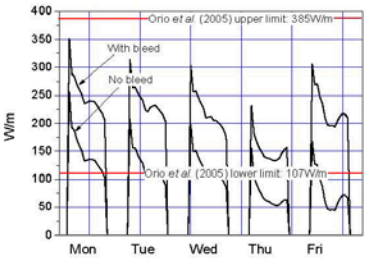

Figure 4 Simulated heating delivered by a cluster of 4 x 100m-deep SCWs operating at capacities within the range of that reported by Orio et al. (2005)

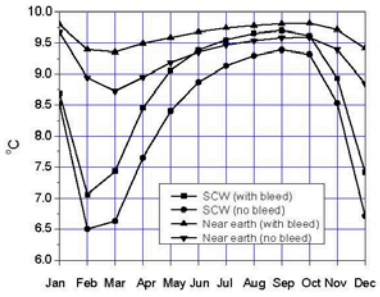

Figure 5 Mean well water temperatures and local rock temperatures for the 4 well cluster ('near earth' represents the earth temperature 1m from well centre)

The simulated isotherms and isobars abound the well cluster were found to be uniform as might be expected for the identical well specifications occupying a uniform grid pattern. For example, Figure 6 shows isobars on the *x-y* plane at half well depth.

The second test case consisted of a heating and direct cooling application using data for a heating and chilled ceiling application given by Underwood and Spitler (2007). In the latter work, a design analysis

of vertical closed loop borehole heat exchangers was carried out for a range of air conditioning system alternatives. It is thus possible to compare the response of the closed loop array performance with that of a standing column well cluster in the present exercise.

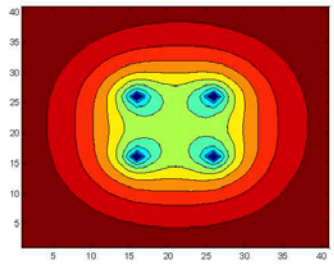

Figure 6 Simulated x-y isobars at half well depth for a cluster of 4 identical SCWs

Sample values...

Well centre	*-751Nm^{-2}*
Domain centre	*-362Nm^{-2}*
Between wells	*-353Nm^{-2}*
12,20	*-31Nm^{-2}*
6,20	*-13Nm^{-2}*
1,20	*-4Nm^{-2}*

The peak requirement of this application was 44kW (heat sourceed from the geothermal source) and 55kW (direct cooling heat rejected to the geothermal sink). The corresponding annual energy rates were 18,900kWh (heat sourced) and 41,400kWh (heat rejected to the geothermal loop). Thus the application is cooling-dominant. Again, the same 4-well cluster was applied as was used in the previous case and the simulated energy demands were applied to the well clusters first with conditional bleed rate of 10% of nominal well flow rate (bleed applied at all times a load exists) and then without any bleed. Results of the annual mean water loop temperatures and near rock temperatires are given in Figure 7.

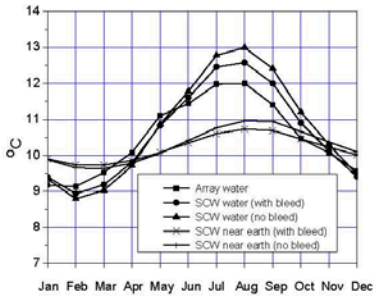

Figure 7 Comparsion of annual monthly mean water temperatures derived from a 2500m borefield and a 400m 4-well SCW cluster ('near earth' represents the earth condition at 1m from well centre)

DISCUSSION

For heating only, the 4 well cluster simulation resulted in per-metre well heat transfer rates that were between the limits observed in existing standing column well installations (Figure 4) and a significant increase in heat transfer is noted when groundwater bleed is used. The initial rock temperature at the start of simulation was 10°C and, precisely one year later, had declined to 9.3°C and 8.6°C for the bleed and no bleed cases respectively. This implies a gradual but significant decline in rock temperature for the heating only case over several years of operation resulting in a corresponding decline in heat pump coefficient of performance and, of greater seriousness, incapacity through the danger of freezing. A larger cohort (or greater depth) of standing column wells would, of course, reduce this decline.

For the heating and cooling case, an exemplar 4 well cluster competes well with a traditional closed loop borehole heat exchanger array in that, for a similar performance in annual monthly mean water temperatures, just 400m of standing column well is needed as opposed to 2500m of closed loop array. Figure 7 shows that the mean water temperatures of the well cluster with and without bleed and the mean water temperature of the closed loop are consistently within 1K of one another over an annual simulation period. Furthermore, the mean temperatures imply satisfactory operation in winter with (essentially, in the case of the SCWs) fresh water and that the summer temperatures are sufficient to enable direct cooling using either chilled ceilings or chilled beams. Underwood and Spitler (2007) found that this combination can deliver carbon emission savings due to heating and cooling energy use of greater than

60%. The major issue here is that the SCW cluster involves significantly less ground works than would be needed with the 50 × 56m deep borehole heat exchangers depicted in the closed loop solution obtained by Underwood and Spitler (2007). In this cooling-dominant example, the mean earth temperature change after one year was found to be negligible. However, further work is needed to investigate well cluster performance over extended time horizons.

CONCLUSION

This paper has described the development of a model for simulating clusters of standing column wells for use in geothermal heating and cooling systems. The model has been applied to two test cases the first involving heating only (i.e. heat extracted from the well system in winter) and the second involving heating in winter and direct cooling in summer (i.e. heat both extracted and rejected to the well system over an annual operational cycle). The well cluster was found to offer a high rate of heat transfer of, typically, up to 250W/m especially when groundwater is bled into the well system. When heating only, besides enhancing heat transfer, the decline in surrounding rock temperature can be minimised through the use of bleed. For applications involving both heating and cooling, standing column well clusters offer the potential for very substantial reductions in geotechnical drilling compared with conventional closed loop vertical borehole heat exchanger arrays. This offers significant opportunities for geothermal heating and cooling systems in regions with high water tables such as is frequently found in the United Kingdom.

Further work is currently underway to improve the computational efficiency of the model so that it can be used for longer time-horizon simulations. The detailed calculation of well pressure gradients is also being incorporated. Finally, a test site is currently being investigated with a view to validating the model.

REFERENCES

Bear, J. (1972) *Dynamics of Fluids in Porous Media, 764 pp*. Dover, Mineola, NY.

Deng, Z. (2004) *Modeling of standing column wells in ground source heat pump systems* PhD Thesis. Oklahoma State University.

Deng, Z., Rees, S. J. & Spitler, J. D. (2005) 'A Model for Annual Simulation of Standing Column Well Ground Heat Exchangers', *HVAC&R Research,* 11 (4), pp. 637-656.

Deng, Z., Spitler, J. D. & Rees, S. J. (2006) 'Performance Analysis of Standing Column Well Ground Heat Exchanger Systems', *ASHRAE Transactions 2006,* 112 (2), pp. 633-643.

Ingersoll, L. R. & Plass, H. J. (1948) 'Theory of the ground pipe heat source for the heat pump', *ASHVE Transactions,* 54, pp. 339-348.

Oliver, J. & Braud, H. (1981) 'Thermal exchange to earth with concentric well pipes', *Transactions of ASAE,* 24 (4), pp. 906-910.

Orio, C. D., Chiasson, A., Johnson, C. N., Deng, Z., Rees, S. J. & Spitler, J. D. (2005) 'A survey of standing column well installations in North America', *ASHRAE Transactions 2005,* 111 (2), pp. 109-121.

Orio, C. D., Johnson, C. N. & Poor, K. D. (2006) 'Geothermal standing column wells: Ten years in a New England school', *ASHRAE Transactions 2006,* 112 (2), pp. 57-64.

Rees, S. J., Spitler, J. D., Deng, Z., Orio, C. D. & Johnson, C. N. (2004) 'A Study of Geothermal Heat Pump and Standing Column Well Performance', *ASHRAE Transactions 2004,* 110 (1), pp. 3-13.

Underwood, C. P. & Spitler, J. D. (2007) 'Analysis of vertical ground loop heat exchangers applied to buildings in the UK', *Building services Engineering Research and Technology* 28 (2), pp. 133-60.

Yavuzturk, C. & Chiasson, A. D. (2002) 'Performance Analysis of U-Tube, Concentric Tube, and Standing Column Well Ground Heat Exchangers Using a System Simulation Approach', *ASHRAE Transactions: Symposia*, pp. 925-938.

Yuill, G. K. & Mikler, V. (1995) 'Analysis of the Effect of Induced Groundwater Flow on Heat Transfer from a Vertical Open-Hole Concentric-Tube Thermal Well', *ASHRAE Transactions 1995,* 101 (1), pp. 173-185.

Journal paper

Standing Column Wells – Modelling the Potential for Applications in Geothermal Heating and Cooling

Bobo M. Ng,*Chris P. Underwood, Sara L. Walker
School of built and natural environment, Northumbria University, Newcastle Upon Tyne, UK
** Correspondence author. E-mail: bobo.ng@northumbria.ac.uk*

Standing column wells (SCWs) have the potential to deliver much higher rates of heat transfer to geothermal heating and cooling systems in buildings via heat pumps than conventional vertical borehole heat exchange arrays. The development of a numerical model for clusters of standing column wells is described in this paper. The model is three-dimensional, dynamic and solves the governing equations using a finite volume discretization scheme with a fully implicit algorithm. The slower-acting field equations are solved using a wider time interval than that used for the faster-acting well equations and the two sets of equations are coupled through the field equation source terms. A groundwater bleed feature is incorporated. The model has been verified thermally and hydraulically using existing field data. Two test cases have been applied to reveal the advantages of using SCWs in UK conditions, competing with the conventional closed loop system of vertical bore hole heat exchangers. Results of the applications suggest that SCWs can deliver substantially higher rates of heat transfer than conventional closed loop borehole heat exchanger arrays especially when groundwater bleed is operational. With appropriate earth conditions in the UK, SCWs can deliver space heating and direct cooling for example chilled beam or chilled ceiling successfully to offer a huge saving on carbon emissions. Another important practical consequence of this is that far less geotechnical drilling is needed when using SCWs than is the case with closed loop arrays.

INTRODUCTION

Geothermal energy is a reliable and stable source for providing space heating and cooling in buildings with relatively low electricity consumption and high energy efficiency, when compared with conventional heating and cooling systems.

Geothermal energy is expected to make a significant contribution to the European Union's 80% carbon reduction target by 2050. In the UK, mild winters with typical mean annual air temperatures of 8 to

Bobo M. Ng, is a PhD student and Student Member ASHRAE. **Chris P. Underwood, PhD**, is a professor and Member ASHRAE. **Sara L. Walker, PhD**, is a principal lecturer.

11 °C (46.4 °F – 51.8°F), coupled with many sites bearing reasonably high water tables, create a good opportunity to exploit groundwater for use in geothermal systems for both heating and cooling buildings.

The world capacity of geothermal energy utilization reported by Lund (2010) was 48.49 GW (an increase of 58% over the previous five years (Lund, Freeston & Boyd, 2005)) with annual growth rate of 11.4%. Indirect geothermal energy utilising ground-source heat pumps is the largest application of geothermal energy amounting to 68.3% of the current world total (Lund, 2010) with the remainder being taken up by direct (natural) 'hot rocks' geothermal. The UK is reported to be one of the fastest growing countries in the use of indirect geothermal having increased its installed capacity from 10.2MW in 2005 to 186.2MW in 2010 (Lund, 2010). Thus, a continuing rapid growth in this technology in the UK is expected to continue in the coming years.

Numerous studies (Yavuzturk & Chiasson, 2002; Lund et al., 2004; Lund, Freeston & Boyd, 2005; Deng, Spitler & Rees, 2006) in the United States confirmed that SCWs allowed a significant reduction in borehole depth requirement compared with the conventional closed loop system consisting of arrays of single u-tube heat exchangers, because of the enhancement of the flow of groundwater into/out of the well by adopting open-ended columns (see Figure 1).

In addition, the performance of SCWs can be improved by 'bleeding', i.e. part of the water from the system being bled (discharged) instead of fully re-circulated to the annulus of the SCW to induce a flow of groundwater and maintain the far field temperature in the well. A parametric study by Rees et al. (2004) showed that the bleed rate was one of the most significant parameters to affect SCW performance and offer reductions in borehole depth, capital cost and life cycle cost compared with the non-bleed case.

Orio, Johnson & Poor (2006) studied 10 years of performance of a SCW application in a New England school in the USA, which achieved a considerable saving in electricity use (about 1300MWh per year) after replacing the electric heating system with a geothermal heating and cooling system (10 heat pumps coupled to 6 SCWs). The supply water temperature from the SCWs was measured after 10 years operation, and the data demonstrated that it remained fairly constant throughout this period. This is the key benefit of adopting the ground source rather than air source as a heat transfer medium to the heat pump and justifies the reliable and stable performance of geothermal systems.

Even though the merits of SCWs have been revealed, only a few studies (Oliver & Braud, 1981; Yuill & Mikler, 1995; Deng, 2004; Rees et al., 2004; Deng, Rees & Spitler, 2005) focused on the SCW design. Most of these only considered either heating or cooling applications based on a single well applicable to North American applications, and little attention has been paid to UK applications. Multiple borehole arrangements are commonly used for large applications in conventional closed loop systems, but not often in SCW design. All existing SCW numerical models are merely capable of dealing with single well construction even though several multiple SCW arrangements have already appeared in North American non-residential building applications (Orio et al., 2005). The mild winters and cool summers experienced in the UK means that it should be possible to extract heat from the ground during winter and reject it back during summer to enhance the seasonal performance of SCWs. These are the key elements of novelty which form the basis of this work. Thus the aim of this work is to develop a detailed thermofluid model of a SCW cluster or array involving more than one well with the possibility of bleeding small amounts of groundwater from the array and to apply this model to heating and cooling demand profiles applicable to a typical commercial UK building. The objectives of the work are threefold:

- Develop a three-dimensional dynamic thermofluid model of the geological field and superimpose one or more detailed SCW well models onto the field model. Discretise the field equations using a finite volume scheme applicable to a problem involving fluid flow.
- Conduct simple verification tests on the completed model using existing field data derived from pumping tests and thermal response tests conducted at various UK sites.
- Apply the model to a range of typical UK commercial building applications involving winter heating and summer cooling and compare the results with those from a conventional closed loop geothermal array design.

SCW MODEL DEVELOPMENT

Structure of the model. For the purpose of managing certain operations (such as bleed flow) and installation arrangements in the numerical model in a more flexible way, a field model of the background geology is first developed and then a detailed well model is separately developed so that it can be superimposed on the field model.

The field problem consisting of the rock and groundwater flow in the earth was dealt with as a 'parent model' to that of the standing column well cluster. The 'child model' (or well model) was coupled to the field model equations through the source terms and was solved using a smaller time interval than that used to solve the field equations. In effect, each well was treated by the field equations as a line source/sink of finite depth. This decoupling meant that the field equations could be solved independent of the standing column wells at the coarser time step appropriate to the field variables. The well equations were then solved iteratively at a shorter series of time steps within the coarser field time step and the source terms were then updated in the field equations. The advantage of this approach is that standing column wells of different types can be applied with other source types (e.g. closed loop heat exchangers) to form a fully flexible hybrid scheme if desired. The computation time of the model from a standard computer (4G ram, 2.66 GHz processor, Window XP) is about 2.7 hours for a 3-well cluster and 1.9 hours for a 2-well cluster in a domain size of 50m*50m*160m(deep) for 1 year simulation. The graphic representation of the concept is shown in Figure 2.

Field model development. The field model consists of two partial differential equations (PDEs), the head diffusion equation in saturated flow conditions and energy equation in porous medium (Bear, 1972) to describe the thermal and hydraulic energy transport in the aquifer. These two equations are coupled with Darcy's equation which relates flow velocity to head via the hydraulic conductivity property of the rock. Homogeneity and isotropy are assumed throughout the field domain in the present work.

The SCW system requires relatively low discharge and suction flow rate to balance the pumping cost and heat transfer performance, which imposes a low velocity flow profile of water in the well and, hence, it is sufficient to apply Darcy's law in this work to predict the fluid flow in the earth.

Head equation

$$S\frac{\partial h}{\partial t} - F = K\nabla^2 h \qquad (1)$$

where:

K = hydraulic conductivity (ms^{-1});

S = specific storage;

F = source term (m^3s^{-1});

h = hydraulic head (m);

t = time (s).

Darcy Flow equation

$$u_x = -\frac{K}{n}\frac{\partial h}{\partial x} \qquad (2)$$

where:

u_x = the velocity in the x direction (ms^{-1});

n = rock porosity

(and, likewise, u_y & u_z).

Energy equation

$$\left(n\rho_w c_{pw} + (1-n)\rho_s c_{ps}\right)\frac{\partial T}{\partial t} - n\rho_w c_{pw}\nabla uT - k_{eff}\nabla^2 T = Q \qquad (3)$$

where:

ρ = density (subscripts: w – water, s – rock, kgm^{-3});

c_p = specific heat capacity (subscripts as above, $Jkg^{-1}K^{-1}$)

T = temperature (K);

k_{eff} = effective thermal conductivity ($Wm^{-1}K^{-1}$);

Q = source term (Wm^{-3}).

Numerical approaches analysis. The performance of several numerical solution schemes with different combinations of numerical approaches were investigated. The best combination was identified and used as a basis for superimposing a 'child model' of the standing column well cluster. The best combination was largely governed by accuracy and computational efficiency considerations.

Two discretization techniques (finite-difference (FD) and finite-volume (FV)) and two time derivative solution schemes (implicit and explicit approaches) were examined. Furthermore, a two-dimensional finite element (FE) approach based on a commercial software (Matlab PDE toolbox) was investigated.

In order to compare the various numerical options described above, a one layer confined aquifer in cube shape, 100m x 100m x 100m (328ft x 328ft x 328ft) in 3-dimensions and 100m x 100m (328ft x 328ft) in 2-dimensions was considered with a fully penetrated well located in the middle of the domain. All boundaries were considered as no flow boundaries (i.e. general groundwater flow was not considered – only that caused by pumping was considered). The line source concept was utilized to describe the pumping action from the well, i.e. the structure of SCW was omitted. A control case was generated using the line source theory-based method of Barry, Parlange & Li (Barry, Parlange & Li, 2000) applied to the practical hydrogeology test case of Morel-Seytoux & Daly (Morel-Seytoux & Daly, 1975). The response of the various model formulations was compared with the control case based on a unit pulse alternatively applied to heat input and pumped water flow rate each of 10h duration. Grid dependency checks were carried out at grid spacings of 0.3, 0.4, 0.6 and 1.2m (11.8, 15.7, 23.6, 47.2 inches) as was a variety of tests at alternative time intervals. The following summarises the findings of the various comparisons:

Preliminary results suggested the computation cost of both explicit model formulations to be substantially higher than all other implicit options. These model formulations were therefore discarded from further studies.

A grid spacing of 0.6m (23.6inches) was found to result in lowest root-mean-square error values of 0.032 (implicit finite difference), 0.024 (implicit finite volume) and 0.029 (finite element with 2062 unstructured triangular elements). The results were broadly comparable for both head and energy disturbances at this grid spacing.

Time intervals of up to 12h had minimal impact on energy predictions but the limit for head predictions was found to be 600s. Therefore the latter value was used.

Comparative results at these setting are summarised in figures 4 and 5.

Though the finite element model provided slightly better computational efficiency this model formulation lacked flexibility for well model superimposition and was thus discarded. The slight performance advantage in terms of root mean square errors of the implicit finite volume model over implicit finite difference justified the selection of this model type with the grid and time interval settings mentioned above as the final model choice.

Well model development-Concept of well model. The well equations are summarised as follows. Figures 6-7 illustrate the overall solution algorithm and the field/well interactions for the coupled field and SCW in 3D.

The ratio of convective to conductive heat transfer in the borehole was expressed by the Nusselt number, which was determined from the characteristic of flow (Reynolds number) and the properties of the water (Prandtl number). The convective coefficient can be derived from the Nusselt number and reflected in the borehole and suction-pipe surface resistances to account for the heat transfer by both mechanisms. Gnielinski's simplified correlations (Holman, 1997) were used in this work for convection across the inner annulus and suction pipe surfaces with Norris's (Norris, 1971) correction for roughness at the annulus outer surface. Lu and Wang's (Lu & Wang, 2008) correlation was used for convection at the suction pipe outer surface.

Energy balance in the annulus

$$C_A \frac{\partial T_A}{\partial t} + c_{pw} \frac{\partial m_A T_A}{\partial z} - Q_A - Q_S = 0 \qquad (4)$$

where:

C_A = annulus thermal capacity (JK^{-1});

m_a = water mass flow rate in the annulus (kgs^{-1});

T_A = annulus water temperature (°C)

Q_A = heat transfer (annulus to rock, W);

Q_S = heat transfer (annulus to suction pipe, W)

Energy balance in the suction pipe

$$C_{sp} \frac{\partial T_s}{\partial t} + m_{sp} c_{pw} \frac{\partial T_s}{\partial z} + Q_s = 0 \qquad (5)$$

where:

m_{sp} = total bleed water flow rate (kgs^{-1})

C_{SP} = heat capacity of the suction pipe water (JK^{-1})

$$m_{sp} = \frac{\sum m_w}{\partial z} \qquad (6)$$

where:

m_w = bleed water flow rate at each dz level due to the pressure difference occurred between the standing column well and earth (kgs^{-1})

MODEL VERIFICATION

Three alternative model verification tests were carried out using experimental data obtained from a variety of field tests. The first test made use of results from a short-time thermal response test in order to evaluate the energy prediction behaviour of the model. The second made use of data from a short-time pumping test in order to evaluate head predictions and the third test made use of longer term field data from a single SCW installation in order to evaluate the complete model behaviour. The performance of the model was determined by comparing the numerical predictions with the experimental measurements.

Model verification with thermal response test data. A thermal response test (TRT) was carried out in June 2007 on a test borehole heat exchanger at a site in the centre of Gateshead, Tyne & Wear. The geology consisted of Coal Measures comprising mudstone, sandstone and coal seams.

A heat source of 3kW (10.24 Btu/hr) was applied onto a 52m (171 ft) deep U-tube collector for 68.8 hours to interpret the effective ground thermal conductivity and borehole thermal resistance based on the line 'sink' assumption as represented in Equation (7). Thermal parameters evaluated from this method are only valid for values of time of t > 5rb2/a (i.e. t > 300 minutes in this case).

$$\Delta T = \frac{Q}{4\pi k_{eff} H}\ln(t) + \frac{Q}{4\pi k_{eff} H}\left[\ln\left(\frac{4a}{r_b^2}\right) - \gamma\right] + \frac{Q}{H}R_b \qquad (7)$$

where:

H	=	borehole collector depth (m)	= 52m (171 ft)
λ	=	ground thermal conductivity ($W\ m^{-1}K^{-1}$)	
a	=	ground thermal diffusivity ($m^2\ s^{-1}$)	$=\lambda/S_c$
S_c	=	specific heat capacity of subsurface ($J\ K^{-1}m^{-3}$)	
P	=	heat power input (W)	
r_b	=	borehole radius	= 82.5mm (3.25 inches)
γ	=	euler's constant	= 0.5772
R_b	=	borehole thermal resistance ($km\ W^{-1}$)	

t = time (s)

Results from the thermal response test are as follows and these values were used in the model:

Thermal conductivity = 4.16 W $m^{-1}K^{-1}$ (2.41 Btu $hr^{-1}ft^{-1}°F^{-1}$)

Borehole thermal resistances = 0.127 Km W^{-1} (0.22 hr ft °F Btu^{-1})

Measured inlet water temperatures from the TRT were employed as an input to the model, to predict the outlet water temperature from the U-tube. The actual outlet water measurements were used to compare with the predicted outlet water temperature from the model. The boundary condition of the formation was based on the actual borehole temperature profile which was measured by a downhole temperature dipper at 5 m intervals prior to the thermal response test (the downhole measurements were carried out one week after the test U-tube was filled with clean fresh water).

This TRT data was measured from a closed loop system whereas the model described here was developed for standing column wells. Thus, for the purpose of this model test comparison only, the standing column well model was replaced with a simple steady state heat transfer expression (equation 8) for the closed loop u-tube and its grout. The earth temperature at every unit depth was calculated by the field model and the simplified model was used to predict the u-tube response. The borehole thermal resistance was interpreted from Equation (7) by assuming a volume heat capacity appropriate to the formation observed from the drill log. The simple expression (equation 8) was considered suitable for this purpose because the borehole resistance term tends to be mainly influential during the first few hours of a transient response test only (e.g. Kavanaugh et al. 2001) whereas for the longer term response, the formation thermal conductivity is dominant. Since the ultimate SCW model described in this work will mainly be used for performance over long time horizons (several years) this simplification was considered acceptable for the purposes of the simple comparison test considered here.

$$Q = \frac{L}{R}\Delta T_{LM} \quad (8)$$

where

Q = heat transfer to the ground (W)

L = length of the bore (closed – loop pipe) (m)

R = effective thermal resistance of the ground (Km W^{-1})

ΔT_{LM} = Log mean temperature difference between the ground temperature and the water temperature in the closed loop

Results of the model predicted outlet water temperature and measured outlet water temperature are shown in Figure 8. The largest absolute error is -0.96K (i.e. a percentage error of 6.3%) observed early in the transient, but the error declined towards zero (a percentage error of 0.02%) at the end of the test (Figure 9). The root mean square error of the model disregarding the first 300 minutes is 0.16.

The small errors obtained verify that the SCW model is able to reliably predict the thermal response of the ground at least over the short term though it is acknowledged that further work is needed to verify model performance over the much longer time horizons of relevance to building energy transfers. In addition, the results also indicated the quality of input thermal parameters make a great impact on the accuracy of the model, and hence employing appropriate experiments to acquire accurate parameters is crucial for successful model construction. and model simulation success. Deng's parameters study (2004) confirmed that hydraulic conductivity and thermal conductivity should be the two most influential parameters in this type of model.

Model verification using data from a pumping test. Results from a pumping test carried out in December 2006 on a site near Belfast city centre were used to verify the head prediction capability of the model. The site geology consisted mainly of red sandstone and was water-bearing. A 200mm (7.87 inches) diameter water well was constructed to a depth of 108m (354 ft) and pumped at a constant rate of 3 ls-1 (1.89×10-7 gpm) for a period of just under 3 days. The aquifer hydraulic conductivity was obtained using both the Theis and Cooper and Jacob methods (see for example (Freeze & Cherry, 1979)) both of which gave very similar results. The hydraulic conductivity was thus found to be 6.04 x 10-7 ms-1 (1.279 gal day-1 ft-2)

A comparison of measured and predicted hydraulic drawdown based on this pumping test is shown in Figure 10. The root mean square error of the model is 0.42. A maximum percentage error of 7.2% occurs at the initial stage of the drawdown test reducing to 0.7% later in the test and averaging at 2.0% for the

complete test. Thus the model yields a good prediction based on a short term test though, again, further work is needed to evaluate performance over the longer term.

Model verification using operational data from a SCW installation

The space heating and cooling in Haverhill library in Massachusetts is provided by a SCW installation (Deng, 2004). Two wells were initially installed in 1994, but only one well was active before June 1996. Two wells were added additionally after 1996 due to the expansion of the library. Each of the boreholes was 457m (1500ft) deep and the diameter was 0.1524m (6 inches). Only one of the wells was active at the time of monitoring.

As there was no drawdown test data available, geological information provided by the U.S. Geological Survey was used. This indicated that Ordovician and Cambrian sedimentary rocks are found in Haverhill region and hence the following properties were applied.

K	Hydraulic conductivity ($m\ s^{-1}$)	1.00×10^{-5}	($21.18\ gal\ day^{-1}\ ft^{-2}$)
n	Porosity	0.025	
S	Specific storage (m^{-1})	1.00×10^{-5}	($3.28 \times 10^{-5}\ ft^{-1}$)
k_{eff}	Thermal conductivity ($W\ m^{-1}K^{-1}$)	3.9	($2.26\ Btu\ hr^{-1}ft^{-1}F^{-1}$)
ρ	Density ($kg\ m^{-3}$)	2200	($137\ lb/ft^3$)
c_p	Specific heat capacity ($J\ kg^{-1}K^{-1}$)	1000	($0.24\ Btu\ lbm^{-1}\ F^{-1}$)

The measured inlet and outlet water temperatures were the key variables for this validation. The hourly inlet water temperatures were applied to the model as an input to the annulus space and the outlet water temperatures from the suction pipe were predicted by the model (with the SCW 'child model' fully participating) and compared with the measured outlet water temperatures. The initial conditions before the experiment were not known and hence inaccurate predictions to a certain extent at the initial period might be expected from the model. Deng (Deng, 2004) compared her model results with Haverhill experiment data but including a set of self-generated initial conditions to obtain a better agreement with the data. Results of measured and predicted outlet water temperatures during a 2,400 hour period together with the corresponding absolute errors between the two are plotted in figures 11 and 12.

A good fit between the predicted and observed outlet water temperatures is demonstrated in Figure 11. The largest absolute error of 0.78°C (33.4 °F) was observed immediately after the simulation started (the

2nd hour); this is attributable to the unknown initial ground conditions on the site. The magnitude of errors improved later in the simulation and the overall standard error (root mean square error) was 0.268K. This reasonably low error result revealed a good level of accuracy by the model. In addition, about 95% of the predicted values from SCW model were within ±0.4°C (32.7 °F) throughout the entire verification test period (Figure 12).

MODEL APPLICATIONS

The model has been applied to two application case studies. The first of these (case 1) compares the performance of a variety of SCW cluster options compared with a conventional vertical borehole heat exchange array for an example building. Details of the example building and the conventional array design can be found in Underwood and Spitler (2007). Additionally, a sensitivity test case (case 2) is carried out in order to identify the SCW cluster performance associated with variations in typical earth property conditions in the UK. The earth properties described in Younger and Milne's work (1997) related to the Penrith and St Bees aquifers in Cumbria, UK, representing an example of commonly found hydogeological properties to be found in UK conditions and likely to be helpful to SCW applications.

Heating and direct cooling application, closed loop array Vs SCW (case 1). The peak requirement of heating and direct cooling (by means of chilled ceilings) in a commercial building described by Underwood and Spitler (Underwood & Spitler, 2007) is 44kW (heat sourced from the geothermal source by a heat pump) (150.13×103 Btu/hr) and 55kW (cooling, directly rejected to the geothermal sink) (187.67×103 Btu/hr). The corresponding annual energy rates are 18,900kWh (heat sourced) (644.89×106 Btu) and 41,400kWh (heat rejected) (141.26×106 Btu). In this application case study, the annual conventional array performance is compared with 4 SCW clustering options. These are: 4 SCWs with no bleed; 4 SCWs with 10% (on nominal circulating well flow) continuous bleed; 6 SCWs with 10% continuous bleed and 8 SCWs with 10% continuous bleed. In all cases, the SCWs are set out on a 5m spacing grid pattern. Results of annual mean water circulating temperatures for all cases are shown in Figure 13. Also shown is the mean ground temperature surrounding the SCW cluster (for the 6 well option only) at mid depth (50m below surface) (164 ft). The design parameters that were used for all SCW options are summarised in tables 1 and 2.

Earth properties sensitivity test (case 2). For the sensitivity case, the extreme values (highest and lowest) of the rock thermal conductivity, specific heat capacity, hydraulic conductivity and storativity for a site in Cumbria (Younger & Milne, 1997) was used in the model to form what are referred to as 'base case' (typical conditions) 'good earth' (most favourable) and 'bad earth' (least favourable). Simulations of the 6 SCW cluster option (with bleed) considered in case 1 were then repeated in order to identify the likely impact of earth thermal property variability. The properties used are summarised in Table 3 (taken from Younger & Milne (Younger & Milne, 1997)). Results are plotted in Figure 14.

DISCUSSIONS

A good agreement between the numerical solutions and practical earth response data (both thermal and hydraulic) through the verification exercises verified the field model is accurate enough to predict the reactions from the earth due to the heat pump operation. The precision of the whole SCW model was verified with a set of real SCW operation data and a good agreement was obtained. All of these tests demonstrated performance of the model over the short term.

Regarding the model application, the mean temperatures from the 6 SCW cluster in case 1 imply an operation in winter which compares favourably with a conventional 'U-tube' geothermal array. It is evident from the example case considered that increased SCW array sizes about 6 x 100m (6 × 328 ft) would bring little additional performance benefit. Underwood and Spitler (2007) found that this combination can deliver carbon emission savings due to heating and cooling energy use of greater than 60%. The major issue here is that the 6 x 100m (6 × 328 ft) deep SCW cluster involves significantly less ground works than would be needed with the 50 × 56m deep borehole heat exchangers depicted in the closed loop solution obtained by Underwood and Spitler (2007). In this case, the mean earth temperature change after one year was found to be negligible. In terms of capital cost, the conventional closed loop system is still the most favourable option in UK at present, typically costing £35 – £40 per m of borehole depth (£11 - £12 per foot), while well costs (including PVC well screens and submersible pumps) typically cost £70 - £150 pounds per m (£21 - £46 per foot) in the UK. This would suggest little difference in installation costs between the two technologies due to the reduced sizes need for a SCW installation.

When considering the sensitivity to the earth properties, Figure 14 illustrates that the mean water temperature in this cooling dominant application during the cooling and heating seasons might vary by up

to 1K between the 'good' and 'bad' earth cases. Again, it is important to note that the water temperature provided by a SCW system in both cases is sufficiently low enough in summer for direct cooling and thus can offer large savings in carbon emissions. The temperature conditions are also high enough in winter to avoid freezing. However, the impact of earth properties is sufficiently significant to necessitate the need to evaluate conditions on a site-by-site basis.

CONCLUSION

This paper has described the development of a model for simulating clusters of standing column wells for use in geothermal heating and cooling systems. The model has been verified using a variety of existing measured data revealing good model behaviour over the short time horizon. There is a need to do further work on the long term response of multiple SCWs and, to this end, a test site consisting of two adjacent SCWs is currently being planned on the Northumbria University campus with a view to a more extensive and long-term validation test of the model. Further work is needed to measure the response of SCW clusters over extended time horizons (at least 2-3 years) and the sensitivity of the well spacing in order to give further confidence in the model behaviour and, thus, develop it as a potential design tool. The results shown that the computation time needed to simulate SCW clusters increases sharply as the number of SCWs increases, and thus further work is needed to explore ways of reducing the iterative demands associated with bringing each SCW to a balanced state at each time step. Two application case studies have been applied to the model to reveal the benefits of using a SCW cluster in UK conditions. For applications involving both heating and cooling, SCW clusters offer the potential for very substantial reductions in geotechnical drilling compared with conventional closed loop vertical borehole heat exchanger arrays. In the example considered in this work, the SCW array size is just 25% of the conventional borehole heat exchange array alternative. This offers significant installation cost benefit for geothermal heating and cooling systems in regions with high water tables such as is frequently found in the United Kingdom.

REFERENCES

Barry, D. A., Parlange, J. Y. & Li, L. (2000) 'Approximation for the exponential integral (Theis well function)', *Journal of Hydrology*, 227 (1-4), pp. 287-291.

Bear, J. (1972) *Dynamics of fluids in porous media*. Dover, Mineola, NY.

Deng, Z. (2004) *Modeling of standing column wells in ground source heat pump systems*. PhD Thesis. Oklahoma State University.

Deng, Z., Rees, S. J. & Spitler, J. D. (2005) 'A model for annual simulation of standing column well ground heat exchangers', *HVAC&R Research,* 11 (4), pp. 637-656.

Deng, Z., Spitler, J. D. & Rees, S. J. (2006) 'Performance analysis of standing column well ground heat exchanger systems', *ASHRAE Transactions 2006,* 112 (2), pp. 633-643.

Freeze, R. A. & Cherry, J. A. (1979) *Groundwater*. Prentice Hall, Inc.

Holman, J. P. (1997) *Heat transfer*. McGraw-Hill, New York.

Kavanaugh, S. (2010) Determining ground resistance: ground heatr exchangers. *ASHRAE Journal 52* (8), 72-75.

Lu, G. & Wang, J. (2008) 'Experimental investigation on heat transfer characteristics of water in a narrow annulu', *Applied Thermal Engineering,* 28, pp. 8-13.

Lund, J. (2010) 'Direct Utilization of Geothermal Energy', *Energies,* 3 (8), pp. 1443-1471.

Lund, J. W., Freeston, D. H. & Boyd, T. L. (2005) 'Direct application of geothermal energy: 2005 Worldwide review', *Geothermics,* 34 (6), pp. 691-727.

Lund, J. W., Sanner, B., Rybach, L., Curtis, R. & Hellström, G. (2004) 'Geothermal (Ground-source) heat pumps a world overview', *Geo-heat Centre Quarterly Bulletin,* 25 (3).

Morel-Seytoux, H. J. & Daly, C. J. (1975) 'A discrete kernel generator for stream-aquifer studies', *Water Resources Reserach,* 11 (2), pp. 253-260.

Norris, R. H. (1971) 'Some simple approximate heat transfer correlations for turbulent flow in ducts with rough faces', *ASME Augmentation of Convective Heat and Mas Transfer*, pp. 16-26.

Oliver, J. & Braud, H. (1981) 'Thermal exchange to earth with concentric well pipes', *Transactions of ASAE,* 24 (4), pp. 906-910.

Orio, C. D., Chiasson, A., Johnson, C. N., Deng, Z., Rees, S. J. & Spitler, J. D. (2005) 'A survey of standing column well installations in North America', *ASHRAE Transactions 2005,* 111 (2), pp. 109-121.

Orio, C. D., Johnson, C. N. & Poor, K. D. (2006) 'Geothermal standing column wells: Ten years in a New England school', *ASHRAE Transactions 2006,* 112 (2), pp. 57-64.

Rees, S. J., Spitler, J. D., Deng, Z., Orio, C. D. & Johnson, C. N. (2004) 'A study of geothermal heat pump and standing column well performance', *ASHRAE Transactions 2004,* 110 (1), pp. 3-13.

Underwood, C. P. & Spitler, J. D. (2007) 'Analysis of vertical ground loop heat exchangers aplied to buildings in the UK', *Building Services Engineering Research and Technology,* 28 (2), pp. 133-160.

Yavuzturk, C. & Chiasson, A. D. (2002) 'Performance analysis of U-tube, concentric tube, and standing column well ground heat exchangers using a system simulation approach', *ASHRAE Transactions: Symposia*, pp. 925-938.

Younger, P. L. & Milne, C. A. (1997) 'Hydrostratigraphy and hydrogeochemistry of the Vale of Eden, Cumbria, UK', *PROCEEDINGS-YORKSHIRE GEOLOGICAL SOCIETY,* 51, pp. 349-366.

Yuill, G. K. & Mikler, V. (1995) 'Analysis of the effect of induced groundwater flow on heat transfer from a vertical open-hole concentric-tube thermal well', *ASHRAE Transactions 1995,* 101 (1), pp. 173-185.

Table 1 Thermal property parameters (case 1)

Thermal conductivity of rock k		Hydraulic conductivity of rock K		Specific heat capacity of rock c_{ps}		Porosity N
$W\ m^{-1}K^{-1}$	$Btu\ hr^{-1}ft^{-1}F^{-1}$	$m\ s^{-1}$	$gal\ day^{-1}ft^{-2}$	$J\ m^{-3}K^{-1}$	$Btu\ ft^{-3}F^{-1}$	
3.9	2.26	1×10^{-5}	21.18	1.86×10^{6}	27.71	0.275

Table 2 Standing column well design parameters (case 1)

SCW diameter		Total borehole length		Pumping rate		Bleed rate
mm	in	m	ft	$L\ s^{-1}$	gpm	%
200	7.87	400	1310	1	15.85	10

Table 3 Earth properties adopted in the sensitivity test (case 2)

	Thermal conductivity of rock k		Hydraulic conductivity of rock K		Specific heat capacity of rock c_{ps}		Storativity S
	$W\ m^{-1}K^{-1}$	$Btu\ hr^{-1}ft^{-1}F^{-1}$	$m\ s^{-1}$	$gal\ day^{-1}ft^{-2}$	$J\ m^{-3}K^{-1}$	$Btu\ ft^{-3}F^{-1}$	
Good scenario	4.3	2.49	1.16×10^{-4}	245.6	5.00×10^{6}		0.045
Base case	3.9	2.26	1×10^{-5}	21.18	1.86×10^{6}		0.0014
Bad scenario	2.5	1.45	3.47×10^{-6}	7.349	1.00×10^{6}		1.40×10^{-9}

Figures

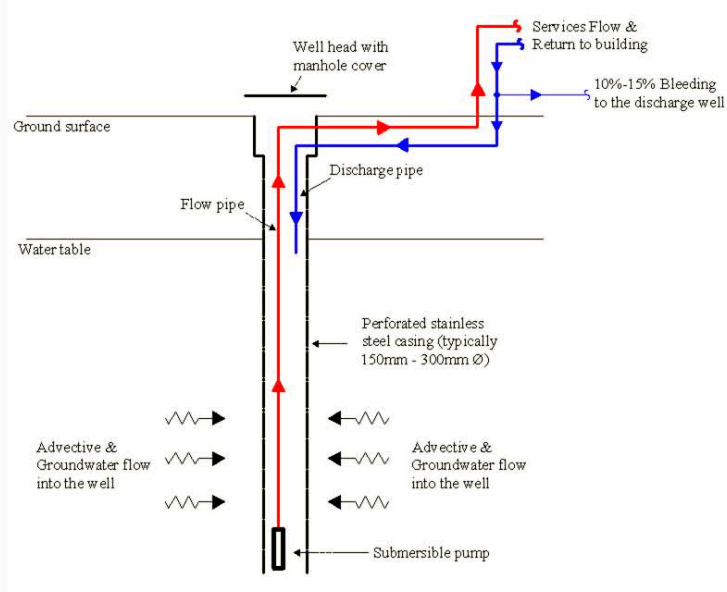

Figure 1 Construction of standing column well (SCW) system

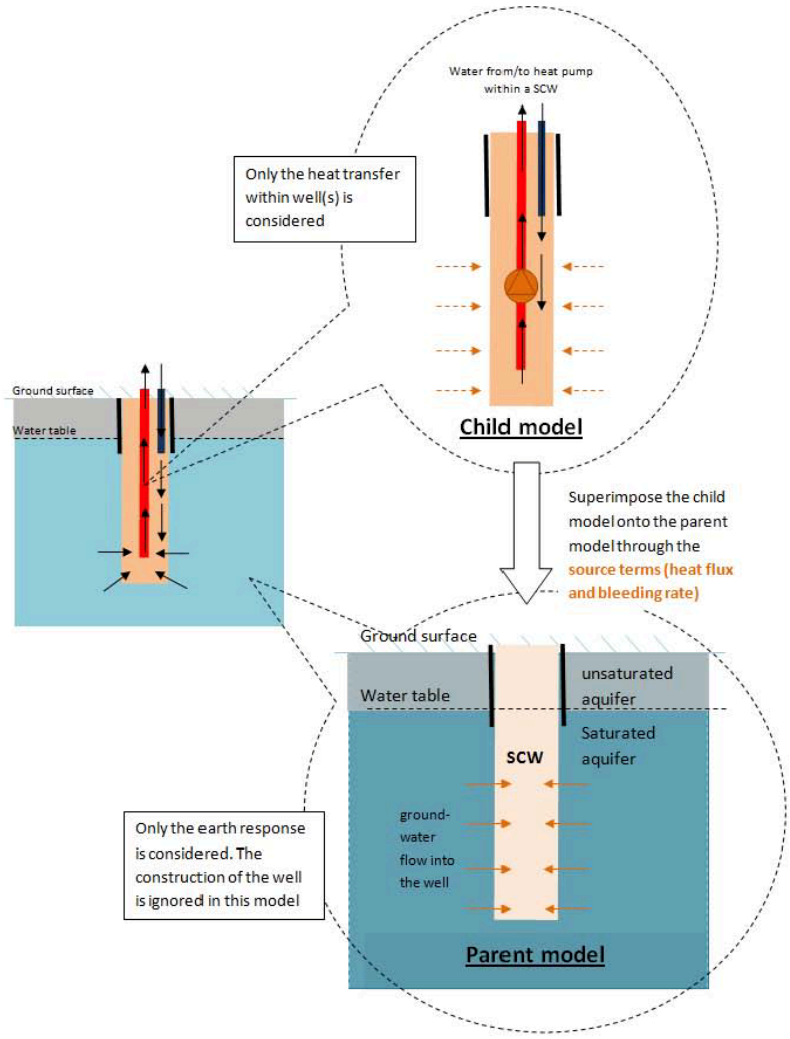

Figure 2 Decoupling concept of the model

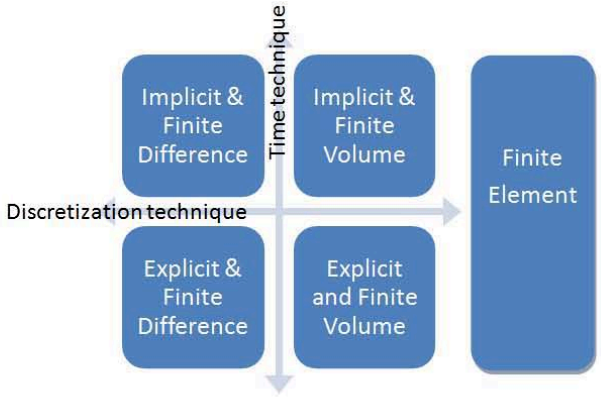

Figure 3 Combination of numerical approaches

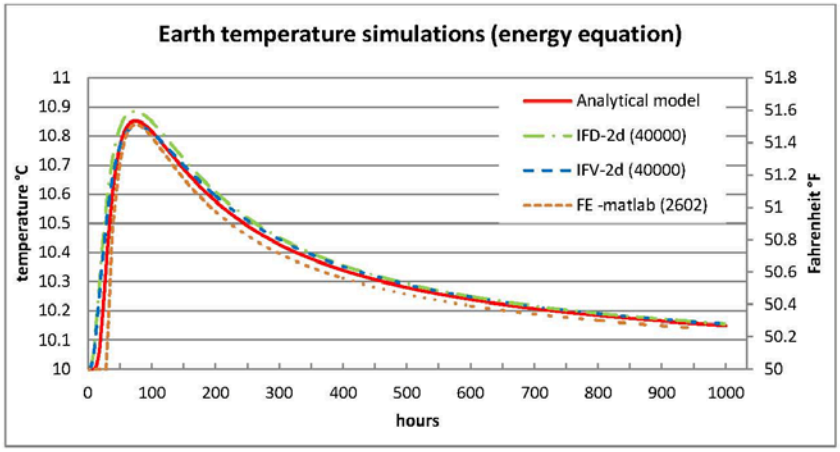

Figure 4 Earth temperature simulation by FE, IFD (refined) and IFV (refined) models.

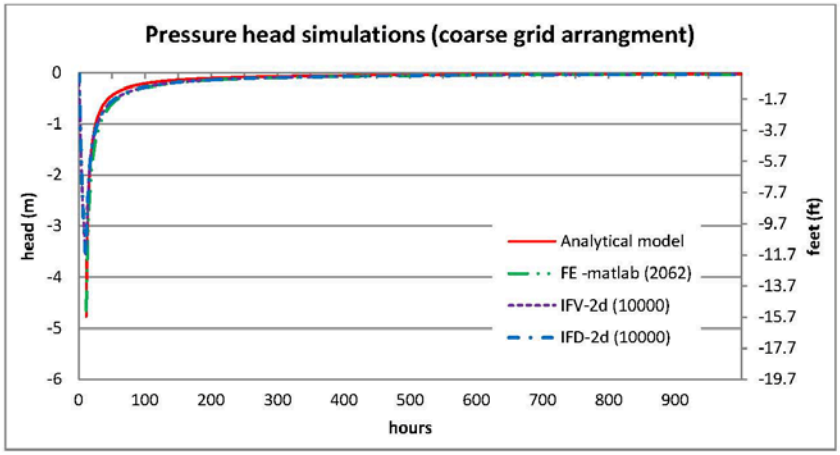

Figure 5 Hydraulic drawdown and recovery simulations by FE, IFD and IFV (grid refined) models

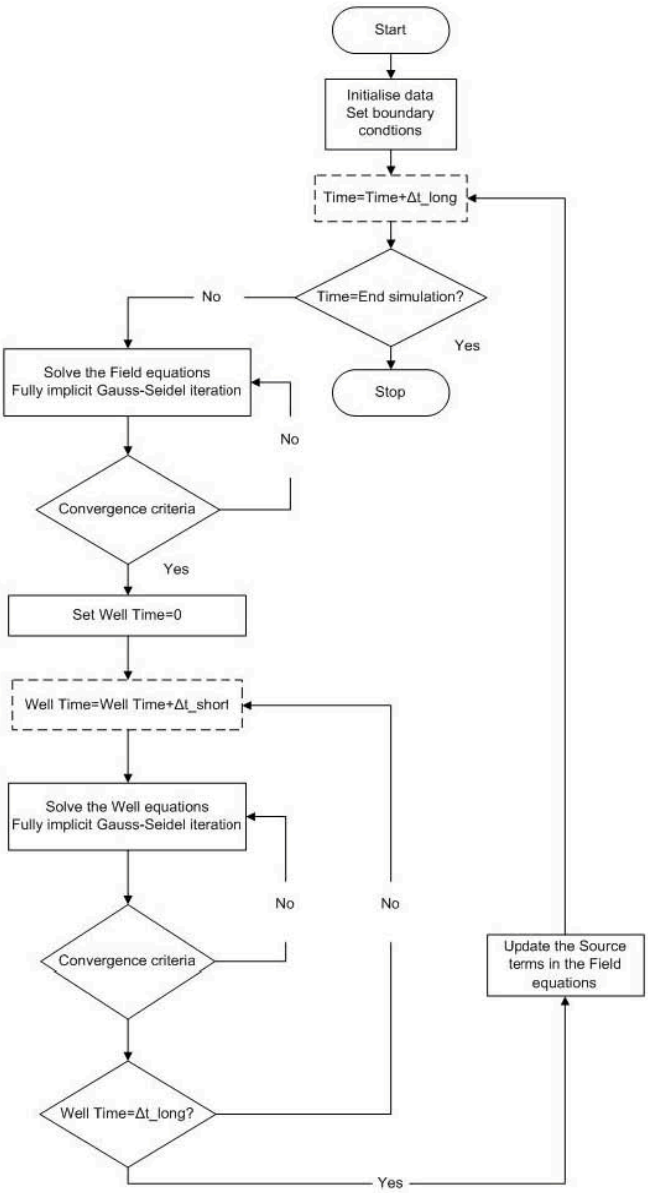

Figure 6 Flow chart of the computer algorithm of SCW model

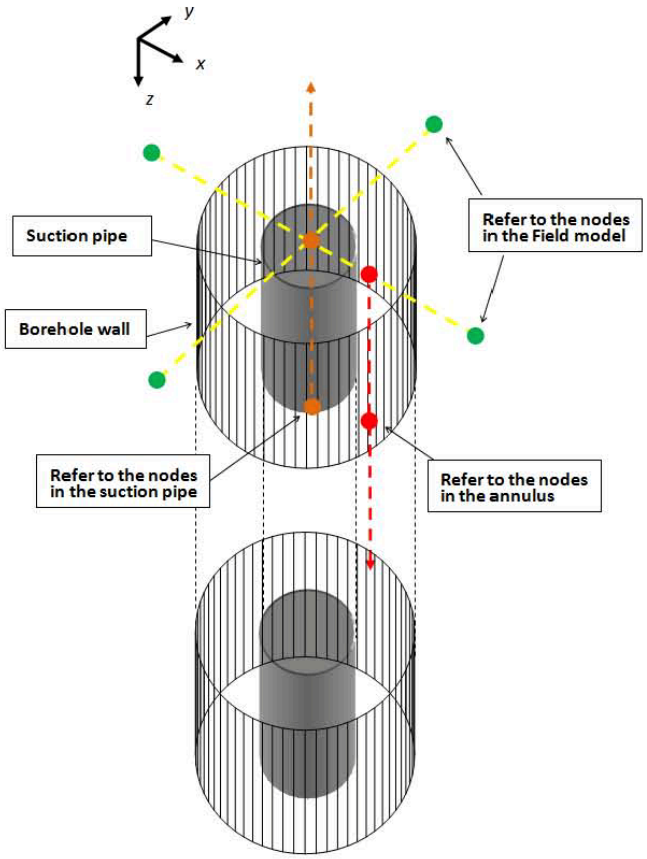

Figure 7 3D representation of the well model

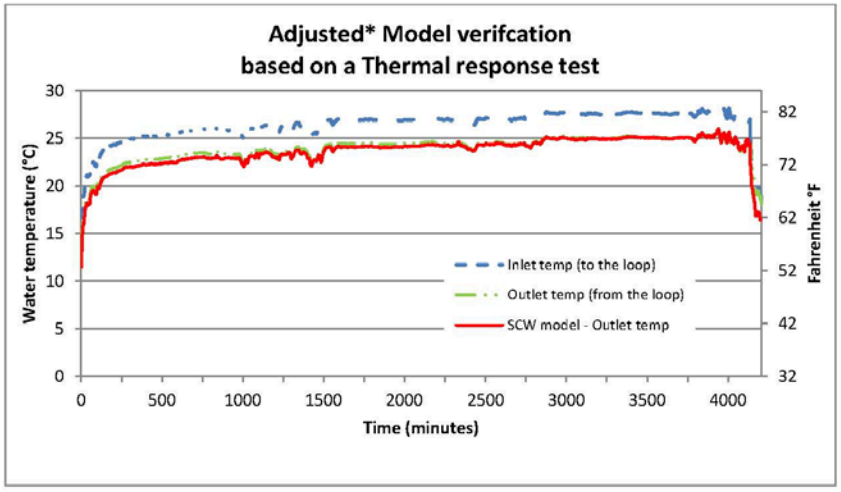

Figure 8 Thermal response test results

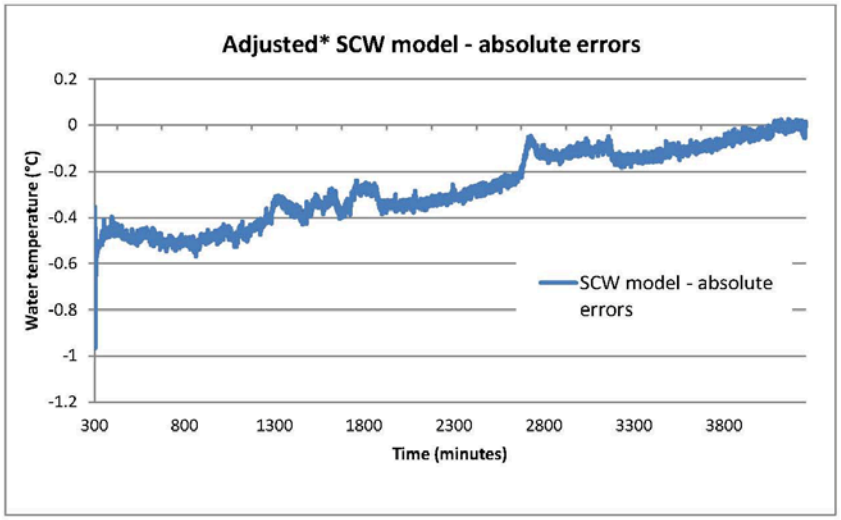

Figure 9 Absolute errors based on a thermal response test.

**Part of the model (the well model) was replaced with a simple vertical borehole heat exchanger model for the purposes of this test comparison.*

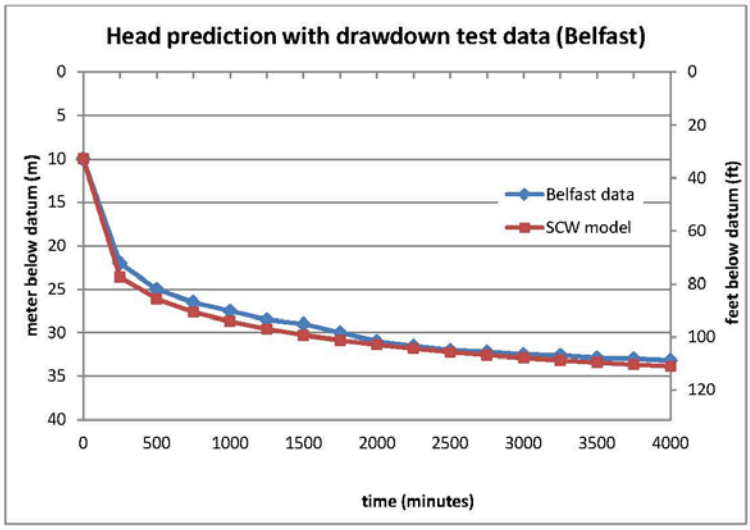

Figure 10 Model comparison with drawdown test data from Belfast

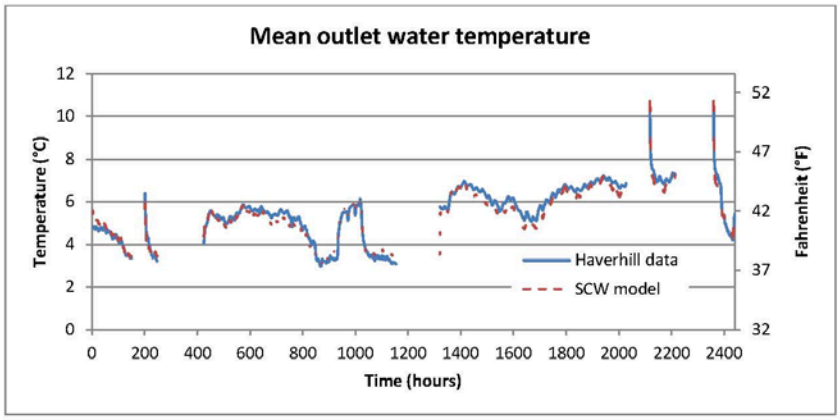

Figure 11 Model comparison with Haverhill SCW data

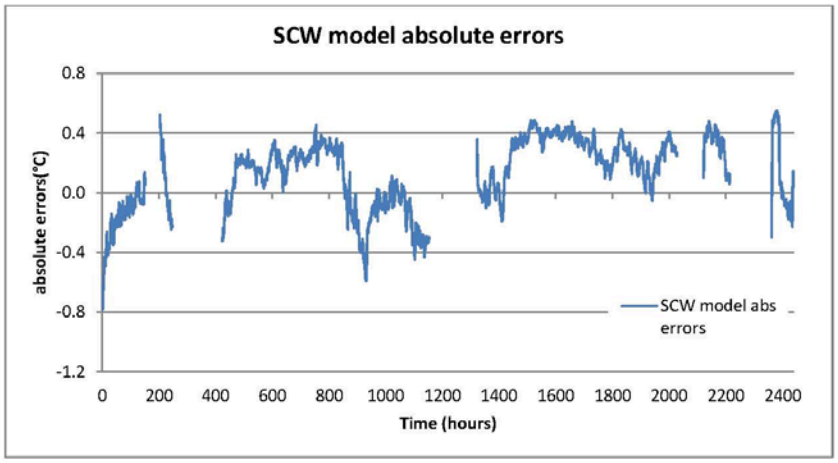

Figure 12 Absolute errors of SCW model and Haverhill data

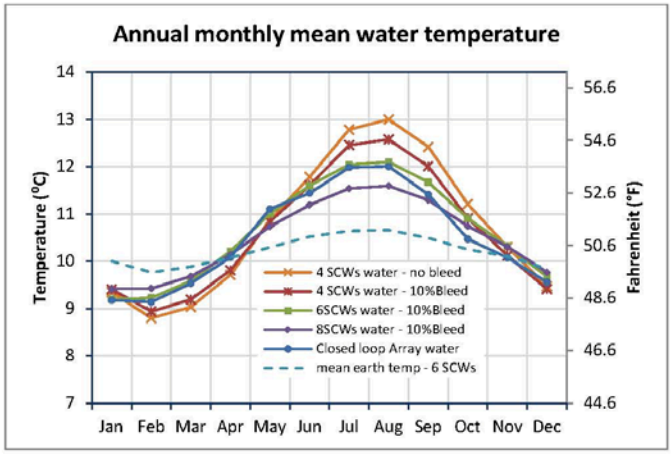

Figure 13 Comparison of annual monthly mean water temperatures derived from a 2800m borefield array closed loop (50-Well,each 56m deep), 400m (4-well) SCW, 600m (6-well) SCW and 800m (8-well) SCW cluster system

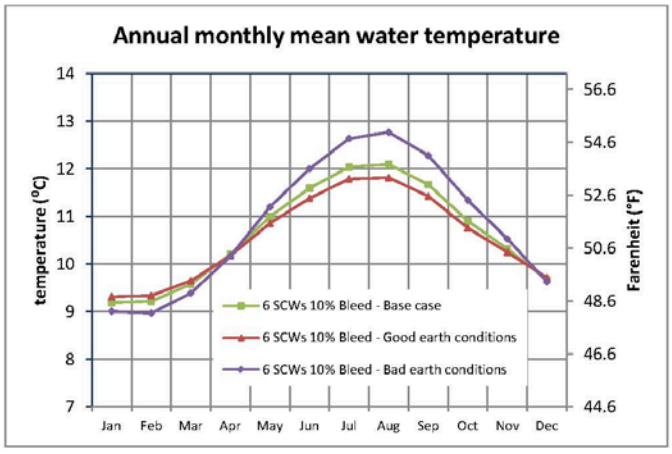

Figure 14 Comparison of annual monthly mean water temperatures derived from the 6 SCW cluster system under different earth properties